Astrocyte control of neurotransmitter signalling

Narges Bazargani

A thesis submitted to University College London for the degree of Doctor of Philosophy

Department of Neuroscience, Physiology and Pharmacology

University College London

July 2016

Abstract

Astrocytes interact with, and regulate the activity of, neurons by various mechanisms. They can release molecules known as gliotransmitters which act on neuronal receptors, or they can regulate the concentration of neurotransmitters in the extracellular space through the expression of transporters. In this thesis I describe experiments on hippocampal astrocytes and neurons that examine both of these mechanisms.

By recording glutamate transporter currents in astrocytes and NMDA-evoked currents in pyramidal neurons, I demonstrate that a relatively understudied G protein coupled receptor present in astrocytes, GPCR37L1, decreases the activity of astrocyte glutamate transporters and decreases neuronal NMDA receptor activity, presumably by regulating the release of modulatory molecules from astrocytes. In ischaemia, expression of GPCR37L1 and addition of an analogue of its agonist, prosaposin, are neuroprotective. This presumably reflects the smaller NMDA receptor-evoked Ca^{2+} entry occurring when GPR37L1 is active, and may also reflect decreased release of glutamate by reversal of glutamate transporters.

A similar approach is used to show that the modulatory neurotransmitter noradrenaline reduces glutamate uptake currents in astrocytes. This action of noradrenaline is blocked by buffering intracellular calcium concentration in astrocytes and by blocking adrenergic receptors that lower the concentration of cyclic AMP.

Furthermore, I demonstrate that the intracellular protein nischarin, shown previously by the Attwell and Kittler groups to interact with astrocyte GLT-1 glutamate transporters, decreases astrocyte glutamate transport.

Lastly, I provide evidence for a role of astrocyte calcium signalling in maintaining the firing frequency of inhibitory interneurons in hippocampus. I also assessed the involvement of calcium concentration rises in astrocytes in regulating excitatory neurotransmission and the effect of noradrenaline on synaptic transmission to pyramidal cells.

Overall, I demonstrate signalling mechanisms that regulate glutamate uptake by astrocytes (via GPCR37L1, nischarin, and adrenergic receptors), and how astrocytes modulate excitatory neurotransmission (presumably through the release of gliotransmitters) or maintain inhibitory transmission (through Ca^{2+} signalling).

Statement of the candidate's contribution to this thesis

I, Narges Bazargani, confirm that the work presented in this thesis is the result of my own planning and research. The experiments in this thesis can be divided into two broad categories (see below) and the contribution of collaborators to the relevant figures is described below. Figure production and writing were performed entirely by Narges Bazargani (with normal supervisorial input from Professor David Attwell).

(1) Electrophysiology in brain slices and cultures

All electrophysiological experiments were conducted solely by Narges Bazargani without any assistance.

(2) Immunohistochemistry

In chapter 3, antibody labelling experiments were conducted by Dr. Sarah Jolly from the Richardson Lab. These include: (i) the experiments describing the expression pattern of GPRC37L1 (Fig. 3.1, done by Dr. Jolly); (ii) analysis of gap junctional coupling in astrocytes (Fig. 3.3), for which Narges Bazargani conducted patch clamp recordings from GPCR37L1 positive and negative astrocytes in brain slices with an internal solution including biocytin, while immunolabelling of the slices against biocytin and GFP, and imaging, were conducted by Dr. Jolly; (iii) the analysis of cell death during ischaemia, for which Narges Bazargani incubated brain slices in control or ischaemic solutions in the presence of propidium iodide (PI) to label cell death, while the subsequent immunohistochemistry for NeuN and GFAP, and the quantification of cell death, were done by Dr. Jolly. In chapter 4, for the experiments involving immunolabelling against adrenoceptors, Narges Bazargani received assistance from an undergraduate student, Ms. Florence Ip, who she was supervising for a BSc project. In chapter 5, data for figure 5.2 was provided by the Kittler Lab. In chapter 6, data for figure 6.5 was collected with Dr. Fergus O'Farrell.

Signed (candidate)
Narges Bazargani Date

Signed (supervisor)
Professor David Attwell Date

Acknowledgements

First, I would like to thank my supervisor Professor David Attwell for his outstanding help and support throughout my PhD, and during the preparation of this thesis. He has provided daily support and intellectual advice whenever I needed it and has been a real source of inspiration as a scientific leader.

I also extend my gratitude to my second supervisor Professor Alasdair Gibb, who has been extremely generous with his time and has always answered my many questions at all times. I would also want to thank my previous supervisor at UCL, Professor Sarah-Jayne Blakemore, without whose encouragement and support I would never have applied to secure a prestigious studentship from the Wellcome Trust to do my PhD.

I would also like to thank my collaborators Professor William Richardson and Dr. Sarah Jolly for inviting me to work with them on the functional role of GPCR37L1 in astrocytes (described in chapter 3). Similarly, I thank Professor Josef Kittler and Dr. Swati Gupta for inviting me to work with them on investigating the role of nischarin in cultured astrocytes (described in chapter 5).

My colleagues and friends at the Attwell Lab have helped me enormously with the day-to-day challenges of doing experiments and have thought me various techniques. In particular, I want to thank Christian Madry and Nicola Hamilton-Whitaker for teaching me all the dos and don'ts of patch-clamp electrophysiology. I also thank Vasiliki Kyrargyri and Lorena Arancibia-Carcamo for teaching me techniques in molecular biology and also helping me with confocal imaging, and Anusha Mishra for inspiring conversations on topics related to astrocytes.

My time at UCL has been a happy one which would not have been possible without lovely friends and colleagues from past and present: Eleni Kougioumtzidou, Aude Marzo, Elisabeth Engl, Anna Krasnow, Fergus O'Farrell, Marc Ford, Renaud Jolivet, Catherine Hall, Julia Harris, Ross Nortley, in addition to the other amazing Attwell Lab crew mentioned above.

Last but not least, I must thank my mother and father for their loving support without which I would never have been able to pursue a life in research in the United Kingdom.

The work presented in this thesis was supported by the Wellcome Trust.

Table of Contents

Chapter 1: Introduction

Chapter 2: Materials and Methods

Chapter 3: Neuroprotective role of a glial specific GPCR

Chapter 4: Regulation of glial glutamate uptake by noradrenaline

Chapter 5: Regulation of the glutamate transporter GLT-1 by the intracellular protein nischarin

Chapter 6: The role of astrocyte calcium in basal and noradrenaline mediated synaptic transmission

List of figures

Chapter 3:

Chapter 4:

Chapter 5:

Chapter 6:

Chapter 1:

Introduction

In the central nervous system, astrocytes are powerful regulators of ionic homeostasis, transmitter synthesis and removal, metabolism, neuronal spiking, synaptic plasticity, and blood flow. The discovery that astrocytes respond to factors released from neurons, and to alterations of the composition of the extracellular fluid, with transient elevations of calcium concentration, which enables them to communicate to neurons, has revolutionized the field. There is, however, controversy over whether this astrocyte-to-neuron communication is mainly through the release of "gliotransmitters" from astrocytes, or through changing the concentrations of extracellular molecules by means of their transporters. In this chapter, I will review how the recent literature has changed our understanding of how astrocytes interact with neurons, by focusing on two major fields: (i) the functional consequences of astrocyte calcium signalling for neuronal activity and (ii) the role of glutamate transporters, in astrocytes, in regulating excitatory synaptic transmission, and how the activity of these transporters may be modulated by different factors. This review, part of which has been published as Bazargani & Attwell (2016), will provide the essential background to the work described in this thesis on astrocyte receptors and the modulation of neuronal function (in chapters 3 and 6) and on modulation of astrocyte glutamate transport (in chapters 3, 4 and 5).

1.1 Astrocyte structure and identification

In the late nineteenth century, glial cells were discovered by Golgi and Ramón y Cajal by using potassium dichromate/silver staining of brain tissue (for a review, see Kimelberg, 2004). These newly identified cells showed morphological heterogeneity and were later subdivided into the macroglia (including astrocytes and oligodendrocytes) and microglia.

Astrocytes are abundant cells in the central nervous system (CNS), with a distinct "bushy and star-shaped" morphology and multiple processes. They form contacts with other astrocytes through gap junctional connexins, which allow electrical communication and chemical diffusion within a large interconnected network of astrocytes (Anders, 2014). Another distinct characteristic of astrocyte morphology is their endfeet, which are bulbous endings of processes that wrap around brain capillaries and contribute to the maintenance of the blood-brain barrier, BBB (see Nico & Ribatti, 2012 for a review). The endfeet also regulate brain water homeostasis of (see Mack & Wolburg, 2013 for a review), and glucose transport into the brain parenchyma (see Prebil *et al.*, 2011 for a review). Thanks to these distinct morphological properties, filling the cells with dyes and observing dye spread through gap junctions can be used to identify astrocytes, by confirming their cell morphology and gap junctional coupling, both *in vitro* and *in vivo* (Anders *et al.*, 2014; Nimmerjahn & Helmchen, 2012). However, there is regional heterogeneity in astrocyte morphology as the radial Bergmann glia and retinal Müller cells, which are considered as honorary astrocytes, have a distinct non-stellate morphology (Kettenmann and Ransom, 2005).

Astrocytes are also commonly identified with antibodies which target some of their highly expressed proteins. Common examples include antibodies to glial

fibrillary acidic protein (GFAP), glutamine synthetase (GS), the calcium binding protein S100β, and the astrocyte-specific glutamate transporters GLAST and GLT-1 (Kettenmann and Ransom, 2005; Kimelberg 2004).

In conjunction with these biochemical markers, the electrophysiological properties of astrocytes are often used as cell-identifying criteria. Astrocytes are electrically non-excitable cells, despite expressing a low density of voltage-gated sodium channels (Schaller et al., 1995), the function of which is not well understood in astrocytes. They have a characteristic linear or "passive" (i.e. time-independent) relationship between applied voltage and membrane current, which is dominated by the potassium conductance of the cell (Salánki, 2013).

1.2 The major functions of astrocytes

In this section, the key functions of astrocytes will be discussed briefly, with emphasis being put on two aspects that are most relevant to the work described in this thesis: (i) the role of astrocyte calcium in modulating neuronal activity (section 1.2.6, relevant to chapters 4 and 6), and (ii) the clearance of the excitatory neurotransmitter glutamate by glial transporters (section 1.2.7, relevant to chapters 3, 4 and 5).

1.2.1 K^+ buffering and ion homeostasis

The intra- and extracellular concentrations of ions can change rapidly following neuronal activity - during the action potential an influx of sodium (Na^+) depolarises the cells, and a slower-activating potassium (K^+) efflux then hyperpolarises the cells. As a result, the extracellular concentration of potassium, $[K^+]_o$, can increase by almost 1 mM from its resting concentration (~3 mM) following a single action potential (Adelman & Fitzhugh, 1975), while intense activation within

a network can increase this level up to 12 mM: a level which if surpassed would have pathological effects resulting from neuronal depolarization (Heinemann & Lux, 1977; Connors *et al.*, 1982; Hansen, 1985). When Na^+/K^+ pumping is abolished in ischaemia, $[K^+]_o$ can rise as high as 80 mM in the cortex (Heinemann & Lux, 1977).

Astrocytes play a crucial role in dispersing the activity-evoked accumulation of potassium and keeping the $[K^+]_o$ level around its normal resting value (~3 mM) in order to avoid excess depolarisation. They achieve this, in part, by removing K^+ via ion channels and redistributing it via gap junctions through the astrocytic network from areas with high $[K^+]_o$ to areas with normal $[K^+]_o$, a process known as K^+ spatial buffering (Orkand, Nicholls & Kuffler, 1966; Orkand, 1986). They also remove K^+ with their Na^+/K^+ pump (see Amédée *et al.*, 1997 for a review).

1.2.2 Neurotransmitter synthesis: the glutamate-glutamine cycle

Astrocytes also play a central role in the synthesis of glutamate and GABA, which are the major excitatory and inhibitory transmitters in the CNS (Roberts & Frankel, 1950; Florey, 1954; Watkins, 2000). Following its release at synapses, glutamate is taken up by both neuronal and glial glutamate transporters (see section 1.2.7 for an extensive review of this topic). Once inside the cell, the enzyme glutamine synthetase converts glutamate (and ammonia and ATP) into glutamine (and ADP and phosphate: Bradford, Ward, Thomas, 1978; Hamberger, 1979; Liaw, Kuo & Eisenberg, 1995). Interestingly, glutamine synthetase is highly expressed in the processes of astrocytes which wrap synapses (Derouiche & Frotscher, 1991), implying that astrocyte processes are ideally positioned to remove and store glutamate (as glutamine) immediately following its release.

Astrocytes can release the stored glutamine via transporters, into the extracellular space, when needed. Extracellular glutamine can then be taken up by transporters in neuronal presynaptic terminals and converted back to glutamate (Billups *et al*., 2013). This conversion is carried out by the glutaminase enzyme (Westergaard *et al*., 1995; Yudkoff, 1989). In inhibitory GABAergic presynaptic terminals, the enzyme glutamate decarboxylase (GAD) catalyzes the decarboxylation of glutamate to GABA and CO_2 (Pinal & Tobin, 1998).

Although the majority of glutamate is thought to be produced from astrocyte-derived glutamine, a smaller fraction of it can also be made from pyruvate in neurons (following the metabolism of glucose or lactate, Hassel & Brathe, 2000; see the next section 1.2.3).

1.2.3 Control of glucose and lactate metabolism

At their endfeet, astrocytes are specialised to transport glucose from the blood by expressing a high density of glucose transporters GLUT-1 (see review by Abbott, 2002). The sodium-dependent uptake of glucose by astrocytes is activity-dependent, such that glutamate release following neuronal activation stimulates the uptake of glucose from blood at the endfeet (Pellerin & Magistretti, 1994). This process is facilitated by synaptically released glutamate-evoked calcium (Ca^{2+}) changes inside astrocytes which help to insert more glucose transporters at the endfeet (Loaiza, Porras & Barros, 2003). Upon its uptake, glucose can be stored as glycogen, or converted to pyruvate and lactate, in the glycolytic pathway (for a recent review see Barros, 2013).

Glycolysis is an energy producing process that releases two adenosine triphosphate (ATP) molecules per glucose. This released energy can be harnessed by the sodium-potassium pump (Na-K-ATPase) to extrude Na^+ which enters the cell to

power the uptake of glutamate. In fact, there is a metabolic "coupling" between the neural activity and glucose uptake by nearby astrocytes, such that stronger neuronal activity evokes more glucose entry (Pellerin & Magistretti, 1994).

The end product of glycolysis is either pyruvate, which enters mitochondria to generate ATP from the citric acid cycle and oxidative phosphorylation, or lactate, which is produced from pyruvate by lactate dehydrogenase. Lactate can be released from astrocytes via monocarboxylate transporters, and then be taken up by monocarboxylate transporters (MCTs) in neurons: a process termed the astrocyte-neuron lactate shuttle (Pellerin & Magistretti, 1994). Subsequently, it can serve as an energy source for neurons both *in vitro* (Schurr *et al.*, 1988) and *in vivo* (Wyss *et al.*, 2011), by being converted back to pyruvate and entering mitochondria. Thus, astrocytes may function as key sources of energy for the energy-demanding neurons.

1.2.4 Regulation of blood flow

Apart from inserting glucose transporters, Ca^{2+} changes in astrocytes are thought to release messengers from astrocytes at their endfeet to regulate the energy supply to the brain according to the activity of synapses (for a review see Attwell *et al.*, 2010). These messengers include arachidonic acid derivatives (such as prostaglandins, epoxyeicosatrienoic acids (EETs) and 20-hydroxyeicosatetraenoic acid (20-HETE)) that modify the contraction of the vascular smooth muscle (Zonta *et al.*, 2003; Mulligan & MacVicar, 2004; Gordon *et al.*, 2008).

The mechanisms underlying neuronal activity-driven release of vasoactive messengers from astrocyte endfeet, to control blood flow, are controversial. It is thought that either vasoactive messengers (NO or arachidonic acid derivatives) are generated in astrocyte processes near synapses and then diffuse to the nearest vessel,

or alternatively perhaps a $[Ca^{2+}]_i$ wave generated by either (i) Ca^{2+}- induced Ca^{2+} release from stores mediated by ryanodine receptors (Pankratov & Lalo, 2015) or (ii) Ca^{2+}-induced ATP release (Bowser & Khakh, 2007) may transmit the signal to dilate the vessel from the astrocyte's synapse-wrapping processes to its endfeet.

1.2.5 pH detection and respiration

Peripheral chemoreceptors are ideally located within the carotid and aortic bodies to detect the main driving factor for respiration, the blood level of carbon dioxide (CO_2) (Teschemacher, Gourine & Kasparov, 2015). A centrally acting sensor is, however, needed as well, since peripheral chemosensation lacks the sensitivity to detect neuronally evoked changes in CNS levels of oxygen (O_2) and CO_2 (Angelova *et al.*, 2015).

Despite debate over the identity of the CNS chemosensors, some have suggested that the CNS response to an altered partial pressure of CO_2 is the main drive to increase respiration (Heeringa *et al.*, 1979). Support for this hypothesis came from studies in which respiration was largely preserved in animals with severed peripheral sensors (Davenport *et al.*, 1947; Curran *et al.*, 2000).

Brain stem astrocytes have been nominated as key regulators of CNS chemosensation (Holleran, Babbie & Erlichman, 2001; Gourine *et al.*, 2010; Angelova *et al.*, 2015). These astrocytes can detect and respond to PCO_2 and pH changes (independent of neuronal activity) by changing their intracellular levels of Ca^{2+}. In fact, it has been shown that a decrease in pH evokes a Ca^{2+} dependent release of ATP from brainstem astrocytes which activates the local retrotrapezoid nucleus (RTN) chemoreceptor neurones, and triggers a robust respiratory response *in vivo* (Gourine *et al.*, 2010; Angelova *et al.*, 2015).

1.2.6 Modulation of neuronal activity

Many key functions of astrocytes have been linked to astrocyte calcium signalling, including glucose uptake from the blood (see section 1.2.3, Loaiza, Porras & Barros, 2003), regulation of blood flow (see section 1.2.4, Gordon *et al.*, 2008; Attwell *et al.*, 2010), and the control of respiration (see section 1.2.5, Gourine *et al.*, 2010; Angelova *et al.*, 2015). Astrocytes can respond to neuronal activity by elevating their intracellular Ca^{2+} levels, $[Ca^{2+}]_i$, which would allow them to signal back to neurons via Ca^{2+}-dependent release of molecules known as gliotransmitters (see Shigetomi, Patel, Khakh, 2016; Bazargani & Attwell, 2016 for recent reviews). The field of astrocyte Ca^{2+} signalling, however, has not been spared from controversies. Since several of the phenomena studied in this thesis involve Ca^{2+} signalling, in this section, I will provide an in-depth analysis of the history of the field, the challenges to the idea that astrocyte Ca^{2+} signalling is important, and recent findings that resolve some of the previous contradictions.

1.2.6.1 Astrocyte calcium signalling - early evidence

In 1990, glutamate was discovered to evoke a calcium concentration rise in astrocytes in culture (Corner-Bell et al., 1990). This was later confirmed in brain slices and *in vivo* (Dani, Chernjavsky & Smith, 1992; Porter & McCarthy, 1996; Newman & Zahs, 1997; Wang et al., 2006). These $[Ca^{2+}]_i$ elevations were not only shown to occur in the soma and processes of a single astrocyte, but were also capable of spreading through the network of gap junctionally coupled astrocytes (Hirase et al., 2004; Nimmerjahn et al., 2004).

Following their initial discovery, it was demonstrated that elevations in $[Ca^{2+}]_i$, in astrocytes, in turn, induce a $[Ca^{2+}]_i$ rise in adjacent neurons (Parpura et al., 1994;

Nedergaard 1994). In fact, astrocytes can use a repertoire of molecules to signal back to neurons. These molecules, known as gliotransmitters, include glutamate (Parpura et al., 1994; Pasti et al., 1997; Bezzi et al., 1998; Parri et al., 2001; Fellin et al., 2004; Angulo et al., 2004; Kang et al., 1998), ATP (Newman 2001; Newman 2003; Pryazhnikov & Khiroug 2008), D-serine (Yang et al., 2003; Mothet et al., 2005; Henneberger et al., 2010), and GABA (Liu et al., 2000; Kozlov et al., 2006).

The functional consequences of gliotransmission are diverse. Glutamate release has been shown to regulate neuronal excitability and synchronize action potential firing (Angulo et al., 2004; Perea & Araque, 2005; D'Ascenzo et al., 2007). Release of D-serine, a co-agonist at neuronal NMDA receptors, from astrocytes modulates synaptic plasticity (Pascual et al., 2005; Zhang et al., 2003; Serrano et al., 2006; Yang et al., 2003; Henneberger et al., 2010): a phenomenon relevant to some experiments carried out in chapter 3. Furthermore, astrocytic release of glutamate, GABA, and of ATP (which is converted to adenosine by extracellular ecto-ATPases), can all regulate the probability of presynaptic vesicle release (Kang et al., 1998; Araque et al., 1998; Fiacco & McCarthy, 2004; Jourdain et al., 2007; Perea & Araque, 2007). It has even been suggested that astrocytes are likely to have played a crucial role in human evolution, as transplantation of human astrocytes (which display faster Ca^{2+} events) into the rodent brain has been shown to enhance synaptic plasticity (Oberheim et al., 2009; Han et al., 2013).

Thus, these findings shaped a dogma which defined astrocyte Ca^{2+} signalling as a key regulator of complex neuronal functions, which had previously been thought of as solely generated by neurons.

1.2.6.2 Astrocyte calcium signalling: challenges to the dogma

Despite these findings which proposed astrocyte Ca^{2+}-dependent gliotransmission as a route by which neuronal activity can be regulated, controversies were raised over the mechanisms by which $[Ca^{2+}]_i$ is raised in astrocytes, the time course of that elevation, and the mechanisms by which gliotransmitters are released. These controversies will be reviewed here, as they are relevant to some of the experiments in this thesis.

G_q-coupled metabotropic glutamate receptors type 1 and 5 (mGluR1/5), which release Ca^{2+} from internal stores through an IP_3-dependent pathway, were suggested to generate astrocyte Ca^{2+} signaling in response to synaptically released glutamate in young rodents (Porter & McCarthy 1996; Pasti, Volterra, Pozzan & Carmignoto, 1997; Parri, Gould, & Crunelli, 2001; Zonta *et al.*, 2003). This is because mGluR antagonists (in particular selective antagonists against mGluR1/5) blocked these $[Ca^{2+}]_i$ transients in astrocytes (Zonta *et al.*, 2003; Porter & McCarthy1996; Takano *et al.*, 2006). However, there are two caveats here: (i) neurons also express mGluR5 (Cahoy *et al.*, 2008), and (ii) astrocyte expression of mGluR5 decreases as astrocytes mature (when assessed at the mRNA level: Sun *et al.*, 2013). These findings question the relevance of glutamate-mediated Ca^{2+} signalling in astrocytes, especially in mature adult cells. However, it should be noted that mRNA extraction from older, more ramified astrocytes may be less easy, decreasing their apparent expression of mGluRs, and also mRNA level may not necessarily predict the total mGluR protein level. Arguing that mGluR5 expression really decreases with age, however, is the observation that the agonist ACPD failed to evoke $[Ca^{2+}]_i$ rise in adult astrocytes (Sun *et al.*, 2013).

The signaling pathway downstream of mGluRs (or other G_q-coupled receptors) involved in Ca^{2+} release from intracellular stores has similarly been criticized. Firstly,

it was shown that astrocyte processes close to synapses lack intracellular calcium stores (Patrushev *et al*., 2013), which questions their ability to respond to synaptic transmitter release with Ca^{2+} release from stores. Secondly, knocking-out the type 2 receptor for IP_3 (which is the main IP_3 receptor expressed in astrocytes, Zhang *et al.*, 2014) had no effect on neuronal excitability (Petravicz, Fiacco & McCarthy, 2008), synaptic plasticity (Agulhon, Fiacco & McCarthy, 2010), neurovascular coupling (Bonder & McCarthy, 2014; Nizar *et al.*, 2013) or various behavioural assays (Petravicz, Boyt & McCarthy, 2014). Similarly, evoking a $[Ca^{2+}]_i$ rise by applying exogenous molecules (which activate a "designer receptor exclusively activated by a designer drug", or DREADD), which targeted receptors that were exclusively expressed in astrocytes, had no effect on neuronal $[Ca^{2+}]_i$ or excitability, nor on excitatory synaptic currents (Fiacco *et al.*, 2007; Bonder & McCarthy, 2014). Thus, these data challenged the notion that astrocyte $[Ca^{2+}]_i$ transients, driven by IP_3-evoked Ca^{2+} release from internal stores, release gliotransmitters that have a major influence on neuronal function. To further complicate matters, raising $[Ca^{2+}]_i$ with a G_q-coupled receptor failed to evoke gliotransmitter release even when uncaging of calcium within astrocytes did (Wang *et al.*, 2013), and different G_q-coupled receptors can have a very different efficacy for evoking gliotransmitter release (Shigetomi, Bowser, Sofroniew & Khakh, 2008), suggesting that the subcellular localization of receptors with respect to internal calcium stores may be a crucial determinant of gliotransmitter release.

The mode of gliotransmitter release downstream of $[Ca^{2+}]_i$ transients, has also been a controversial area of research. There is no consensus yet over whether the release of gliotransmitters is mediated by exocytosis (Bezzi *et* al., 2004; Jourdain *et* al., 2007; Lalo *et al*.,2014) or through ion channels (this will be discussed in section 1.2.6.3; Wang *et* al., 2013; Lee *et* al., 2010; Takano *et* al., 2005). Exocytosis of

glutamate and GABA would require the appropriate vesicular transporters to be present in astrocytes. However, the presence of these transporters has been disputed on the basis of a lack of overlap of transporter labelling with astrocyte markers in immunolabelling studies, and a lack of their mRNA expression (Li *et al.*, 2013; Zhang *et al.*, 2014), despite the apparent confirmation of their presence by others (Bezzi *et al.*, 2004). Findings from RNA-sequencing data should be, however, treated with caution as tissue extraction from astrocyte processes may be more difficult (especially in more ramified adult astrocytes).

Exocytosis also requires the formation of a SNARE (soluble NSF attachment protein receptor) complex, which mediates Ca^{2+}-dependent vesicular release. Although some SNARE complex proteins are more highly expressed in astrocytes (SNAP-23, VAMP3; Zhang *et al.*, 2014), there is no exclusively astrocytic component that could be deleted to prevent transmitter exocytosis from astrocytes. Despite this, some have tried to inhibit exocytosis from astrocytes by expressing the cytosolic portion of the SNARE domain of synaptobrevin 2 (dnSNARE) in astrocytes (Pascual *et al.*, 2005). This was shown to alter synaptic transmission and plasticity (Pascual *et al.*, 2005) and to reduce the pressure to sleep (Halassa *et al.*, 2009) by suppressing the astrocyte release of ATP. However, importantly, a recent study has shown that this genetic modification of the SNARE domain of synaptobrevin 2 also occurs in some neurons at a lower level (Fujita *et al.*, 2014). Others have used SNARE-cleaving toxins inside astrocytes to show that gliotransmitter release is affected (Jourdain *et* al., 2007; Araque *et al.*, 2000), but these agents (or the dominant negative SNARE) may also affect trafficking to the surface membrane (Jurado *et al.*, 2013; Feldmann *et al.*, 2011) of ion channels that mediate transmitter release (see below) or alter other cellular processes such as autophagy (Moreau et al., 2014).

These controversies, over the receptors raising astrocyte $[Ca^{2+}]_i$, the involvement of internal calcium stores, and the mechanism (if any) by which astrocyte Ca^{2+} signalling releases transmitters, provided a major challenge to the idea that astrocytes play an important role in responding to, and regulating, neuronal activity.

1.2.6.3 Astrocyte calcium signalling: resolutions

A breakthrough in the quest for decoding the complexities of astrocyte Ca^{2+} signalling was made when some research groups combined two-photon fluorescence imaging (giving improved spatial resolution), with Ca^{2+}-sensing molecules such as Ca^{2+}-sensing dyes or genetically encoded calcium indicator (GECI) proteins. Results from such studies revealed different types of Ca^{2+} transient in different parts of the astrocyte (Nett, Oloff & McCarthy, 2002; Shigetomi *et al.*, 2010 & 2012; Di Castro *et al.*, 2011; Panatier *et al.*, 2011).

Shigetomi *et al.* (2010 & 2012) targeted a GECI to the membranes of astrocytes to show that spontaneously occurring $[Ca^{2+}]_i$ transients just below the cell membrane arise from the opening of TRPA1 (transient receptor potential ankyrin type 1) channels in the astrocyte. These TRPA-1 mediated $[Ca^{2+}]_i$ transients, in turn, promote the insertion of GABA transporters into the astrocyte membrane to regulate GABAergic transmission (Shigetomi *et al.*, 2012). By using Ca^{2+} sensing dyes, others revealed brief (~0.7 s), spatially localized (~4 μm) transients in astrocyte processes in response to spontaneous release of neurotransmitters, while action potentials triggered longer lasting (~3 s), spatially broader (~12 μm) events (Di Castro *et al.*, 2011). Importantly, the fast Ca^{2+} transients evoked in the processes of astrocytes response to single vesicular release were shown to regulate glutamatergic transmission in the hippocampus: introducing a Ca^{2+} chelator, BAPTA, into the astrocytes inhibited such

signalling (Di Castro *et al.*, 2011; Panatier *et al.*, 2011; in contrast to Sibille *et al.*, 2015). Despite the issue that the resting $[Ca^{2+}]_i$ is ill defined in these two studies (Di Castro *et al.*, 2011; Panatier *et al.*, 2011) because no Ca^{2+} was added to the internal solution, and the fact that the two sets of authors attributed the $[Ca^{2+}]_i$ rises in astrocytes and the subsequent effects on neurons to different neuro- and gliotransmitters (ATP and glutamate (Di Castro *et al.*, 2011), or glutamate and ATP or adenosine (Panatier *et al.*, 2011), respectively), these studies helped researchers in the field to recognise that $[Ca^{2+}]_i$ rises in the fine processes of astrocytes are key regulators of neurotransmission.

Further support for a regulatory role of astrocyte Ca^{2+} signalling came from Srinivasan *et al.* (2015), who challenged the earlier reports (Fiacco *et al.*, 2007; Petravicz *et al.*, 2008; Agulhon *et al.*, 2010; Bonder & McCarthy, 2014; Nizar *et al.*, 2013; Petravicz *et al.*, 2014) that had implied that there would be an abolition of astrocyte $[Ca^{2+}]_i$ transients when IP_3R2 was knocked out. Srinivasan *et al.* (2015) showed that although the majority of Ca^{2+} transients were abolished in the astrocyte soma (~90% block), a significant proportion of the transients were spared in the fine processes (~40%, Srinivasan *et al.*, 2015). The same authors used Ca^{2+} free external solution to confirm that Ca^{2+} entry from the extracellular space (presumably through TRPA1, Shigetomi *et al.*, 2012), was the source of most of the transients in the processes (while Ca^{2+} release from internal stores was the main source of the $[Ca^{2+}]_i$ transients at the soma). Consequently, previous conclusions (Fiacco *et al.*, 2007; Petravicz *et al.*, 2008; Agulhon *et al.*, 2010; Bonder & McCarthy, 2014; Nizar *et al.*, 2013; Petravicz *et al.*, 2014) based on knocking out IP_3R2 receptors and assuming that astrocyte Ca^{2+} signaling then has little functional effect on neurons (on the basis of a lack of somatic Ca^{2+} responses), require re-examination.

Other pathways that can increase $[Ca^{2+}]_i$ in astrocytes have also been suggested which could explain how astrocyte $[Ca^{2+}]_i$ is raised even in the absence of mGluR5 in adult mice (Sun *et al.*, 2013). For glutamate, the activation of $G_{\alpha i}$-coupled mGluR2/3 receptors (which lower the production of cAMP) has been suggested, surprisingly, to raise $[Ca^{2+}]_i$ in the processes of astrocytes (Haustein et al., 2014). These receptors, unlike mGluR1/5, are expressed throughout life (Sun *et al.*, 2013). The underlying mechanism may involve activation of Ca^{2+} release from stores, or Ca^{2+} entry to the cell, mediated by the G protein's $\beta\gamma$ subunits (Kajikawa *et al.*, 2001). In addition, glutamate (Schummers *et al.*, 2008) and GABA (Doengi et al., 2009) transporters have been suggested to raise astrocyte $[Ca^{2+}]_i$ in response to neuronal activity, probably by raising $[Na^+]_i$ and reversing the operation of Na^+/Ca^{2+} exchangers (Doengi et al., 2009). Astrocyte $[Ca^{2+}]_i$ is also regulated by neuromodulatory transmitters such as noradrenaline (via α_1 receptors; Duffy & MacVicar, 1995), the effects of which I will study in chapter 6 and acetylcholine (via muscarinic receptors; Shelton & McCarthy, 2000), which are released from wide-ranging axons with somata in the locus coeruleus and the nucleus basalis of Meynert, respectively. Recent work has shown that both noradrenaline and acetylcholine can evoke $[Ca^{2+}]_i$ elevation in astrocytes *in vivo* (Paukert *et al.*, 2014; Ding *et al.*, 2013 for noradrenaline; Chen *et al.*, 2012; Takata *et al.*, 2011 for acetylcholine). Importantly, the noradrenaline results were obtained in unanesthetized animals (Paukert *et al.*, 2014; Ding *et al.*, 2013) and thus were not compromised by the suppressive effect of anesthetics on astrocyte Ca^{2+} transients that has been reported (Thrane *et al.*, 2012).

The controversy over whether exocytosis mediates Ca^{2+}-dependent release of gliotransmitters from astrocytes was rendered less crucial with the discovery of ion channel mediated release of gliotransmitters. Both GABA and glutamate can be

released from astrocytes via Ca^{2+}-activated bestrophin-1 anion channels and, surprisingly, K^+-selective TREK two-pore domain channels (Lee *et al.*, 2010; Woo *et al.*, 2012; Park *et al.*, 2013). In addition, activating a proton permeable channelrhodopsin expressed in cerebellar astrocytes evokes glutamate release from the cells (Beppu *et al.*, 2014) suggesting that acidification of astrocytes could evoke gliotransmitter release. Furthermore, there is increasing awareness that changes in astrocyte $[Ca^{2+}]_i$ can have effects on neurons not only by releasing substances, but also through changes in the activity of transporters in the astrocyte membrane: a theme I will return to in chapter 3, 4, and 5. As previously mentioned, TRPA1-mediated $[Ca^{2+}]_i$ transients promote the insertion of GABA transporters into the astrocyte membrane and thus regulate GABAergic transmission (Shigetomi *et al.*, 2012). Similarly, G_q-coupled mGluRs increase glutamate uptake currents (Devaraju *et al.*, 2013) and membrane insertion of GLAST glutamate transporters (Mashimo *et al.*, 2010, see section 1.2.7.6 for further discussion).

Although our ability to decode astrocyte $[Ca^{2+}]_i$ transients and their downstream signalling in different neuronal networks is still far from complete, the discovery of astrocyte $[Ca^{2+}]_i$ transients has been a breakthrough in understanding the role of astrocytes in regulating neuronal function. In chapter 6 I will examine the role of astrocyte Ca^{2+} signalling in regulating the activity of hippocampal pyramidal neurons and show that $[Ca^{2+}]_i$ changes in astrocytes are crucial for maintaining the rate of inhibitory transmission.

1.2.7 Glutamate uptake in the plasma membrane

L-glutamate is the major excitatory neurotransmitter in the CNS (see Headley & Grillner, 1990 for a review), which plays an important role in learning, memory,

synapse formation and pruning, and cell death. Although the concentration of glutamate is within the high millimolar range inside the synaptic vesicles of the presynaptic terminal (at least 60 mM as estimated for purified synaptic vesicles, Burger *et al*., 1989), the resting extracellular level of glutamate does not exceed 3-10 μM as measured by microdialysis (Hamberger *et al*., 1983) and in the absence of damage by the microdialysis tube the resting level is probably below 0.1 μM (Cavelier & Attwell, 2005). Thus, the level of glutamate outside the cell must be precisely regulated. Sodium-dependent excitatory amino acid transporters in the plasma membrane are the main agents that mediate glutamate clearance in the brain (see Danbolt, 2001 for a review). In this section, the structure and function of these neuronal and glial glutamate transporters will be discussed in detail, as chapters 3-5 of the thesis involve work on these transporters. Glutamate transporters are also present in vesicular membranes and mitochondria, but they have a different structure and ionic dependence from the transporters in the plasma membrane (see reviews by Ozkan & Ueda, 1998; Sluse, 1996), and will not be discussed in this chapter.

1.2.7.1 Plasma membrane glutamate transporters: expression and localization

The excitatory amino acid transporters (EAATs) include five major subtypes (EAAT1-5), and the expression of each type is cell selective (Zhang *et al.*, 2014; Danbolt, 2001). Based on an mRNA database (Zhang *et al.*, 2014), Type 1 (EAAT1, or GLAST) and type 2 (EAAT2, or GLT-1) transporters are predominantly expressed in astrocytes, even though neurons and oligodendrocyte precursors also express these transporters at a lower level. In contrast, Type 3 transporter (EAAT3) mRNA is highly present in oligodendrocyte lineage cells, endothelial cells, and to a lower extent in neurons (Zhang *et al.*, 2014). EAAT4 is highly expressed in cerebellar neurons and

oligodendrocyte precursors (Zhang *et al.*, 2014; Tanak *et al.*, 1997). Unlike the other EAATs, EAAT5 mRNA expression is not detected in the CNS except in the retina (Arriza *et al.*, 1997). As the expression of EAAT4 and EAAT5 in the forebrain is negligible (or undetectable in the case of EAAT5), they will not be further discussed in this chapter.

At the protein level, GLT-1 expression dominates over that of GLAST in most of the CNS (Danbolt *et al.*, 1994; Haugeto *et al.*, 1996), except in the cerebellum (Lehre & Danbolt, 1998) and in the retina (Derouiche & Rauen, 1995) where GLAST is expressed more than GLT-1. When GLAST is genetically deleted in mice, glutamate clearance is only significantly reduced in the cerebellum and the retina (Lehre & Danbolt, 1998; Derouiche & Rauen, 1995) without showing any further developmental changes (Harada *et al.*, 1998; Watase *et al.*, 1998). In contrast, deletion of GLT-1 abolishes about 95% of the total glutamate uptake in the brain (Tanaka *et al.*, 1997), and the mice develop epilepsy and are more prone to die within the first month of birth. Although GLT-1 is predominantly expressed in astrocytes, its mRNA is also detected in neurons (Torp *et al.*, 1994) but antibody labelling against neuronal GLT-1 has been a challenge (see Chaudhry *et al.*, 1995; Danbolt, 2001). Nevertheless, combining antibody labelling and electron microscopy has suggested that about 10% of the total GLT-1 in the hippocampus is present in the CA3 hippocampal axonal terminals (Furness *et al.*, 2008).

Compared to GLT-1 and GLAST, the neuronal transporter (EAAT3) is apparently expressed at a lower level in the brain (Conti *et al.*, 1998). However, this low detection might be partly due to a lack of a selective antibody for this transporter. Despite this potential confounding factor, labelling for EAAT3 exhibits a strong cytoplasmic localization, which may suggest a pool of transporters that can be inserted

into the membrane when needed (Conti *et al.*, 1998). Moreover, EAAT3 labelling is only found in the soma and the dendrites of neurons, and not in axons (Shashidharan *et al.*, 1997).

1.2.7.2 Glutamate transporters: structure and function

All subtypes of glutamate transporters have a similar structure and share about half of their amino acid sequence (Arriza *et al.*, 1993; Utsunomiya-Tate *et al.*, 1996). In addition, they all have high affinities for L-glutamate (K_m=~20 µM; Roberts & Watkins, 1975; Barbour *et al.*, 1991; Klöckner *et al.*, 1994), and L- and D-aspartate (K_m=~6-17 µM, Klöckner *et al.*, 1994, Sutherland *et al.*, 1995), and L-cysteine (K_m=~20-110 µM, Bridges *et al.*, 1999), though these values vary significantly depending on the preparations used, see Danbolt (2001) for a review. In contrast, the affinity for D-glutamate is very low (K_m>1 mM, Klöckner *et al.*, 1994), as measured for brain slices or isolated cells. Apart from these high-affinity transporters, glutamate can also be taken up by the low-affinity neutral amino acid transporter (Km > 500 µM, Utsunomiya-Tate *et al.*, 1996), and the glutamate-cystine exchanger (Erecińska *et al.*, 1986), which have a different stoichiometry from the EAAT subtypes, and will not be discussed here.

All glutamate transporters depend on the electrochemical gradients of several ions to transport glutamate. More precisely, the driving forces for the glutamate transport cycle are the electrochemical gradients of sodium (Na^+), potassium (K^+) ions and protons (H^+), all of which are necessary for the cycle to complete (Brew & Attwell, 1987; Barbour *et al.*, 1988; Sarantis & Attwell, 1990; Szatkowski *et al.*, 1991; Billups *et al.*, 1996; Levy *et al.*, 1998). In fact, for every glutamate molecule transported into the cell, three Na^+ ions, and one H^+ ion are transported into the cell by binding to the

carrier protein, while a K^+ ion is exported from the cell in order to complete the cycle (Billups *et al.*, 1996; Levy *et al.*, 1998; Zerangue & Kavanaugh, 1996). Thus, glutamate uptake results in two net positive charges being added to the cell and thus is referred to as an electrogenic process.

To make matters more complex, the transport of glutamate also activates an anion conductance (carried by chloride anions, Cl^-) (Sarantis *et al.*, 1988; Billups *et al.*, 1996). In fact glutamate transporters function as an anion channel upon Na^+ and glutamate binding to the carrier protein, yet this anion conductance is independent of the direction of the glutamate transport cycle (Fairman *et al.*, 1995; Billups *et al.*, 1996).

Glutamate uptake is a crucial step in terminating the synaptic actions of glutamate. As mentioned earlier, the concentration of glutamate is in the nanomolar to low micromolar range in the extracellular space (Hamberger *et al.*, 1983; Cavelier & Attwell, 2005), as opposed to at high millimolar levels inside the presynaptic vesicles (Burger *et al.*, 1989) and the cytosol (Jabaudon *et al.*, 1999). Once released into the synapse, the glutamate concentration rises to ~1 mM, but the glutamate is cleared quickly (Wadiche *et al.*, 1995; Auger & Attwell, 2000), initially by diffusion out of the synaptic cleft and then by uptake into astrocytes. In fact, the rate constant for glutamate binding to the transporter is in the ~ 1 $msec^{-1}$ range and completion of glutamate uptake cycle only takes about 70ms (Wadiche *et al.*, 1995; Auger & Attwell, 2000).

Efficient removal of glutamate is important not only to terminate synaptic transmission but also because it protects the brain against excitotoxicity. A high concentration of glutamate can induce cell damage and death (Olney and Sharpe 1969), mainly via depolarisation-evoked calcium entry via the activation of

postsynaptic NMDA receptors (Goldberg *et al*., 1987; Johnson & Ascher, 1987; Rossi, Oshima & Attwell, 2000). Furthermore, inhibition of glutamate transport potentiates glutamate-evoked neurotoxicity (Robinson et al., 1993).

1.2.7.3 Reverse vs. forward glutamate uptake

As mentioned previously, for every glutamate molecule to be transported into the cell, three Na^+ and one H^+ are transported, while a K^+ ion is transported out. This mode of transport is referred to as forward transport (Billups *et al.*, 1996; Levy *et al.*, 1998; Zerangue & Kavanaugh, 1996). Glutamate transport is, however, dependent not only on the concentration of the glutamate, but also on the electrochemical gradients of the main ions involved. In ischaemia, when a failure of ion pumping leads to $[Na^+]_i$ rising, $[Na^+]_o$ falling, and $[K^+]_o$ rising, glutamate transporters are likely to reverse their transport direction (Szatkowski, Barbour & Attwell, 1990). This means that, instead of transporting glutamate into the cell, the glutamate is now released from the cytosolic side to the extracellular space, a process termed reverse transport or reversed uptake (Rossi *et al*., 2000).

Reversal of glutamate uptake is an important contributor to cell death and toxicity following ischaemia or other severe insults (which I will study in chapter 3). In early ischaemia, the slowing of the sodium pump caused by a loss of energy supply leads to neuronal depolarisation and increased exocytotic release of glutamate (Dawson *et al*., 2000). In severe ischaemia, complete cessation of operation of the sodium pump, and the resulting large depolarisation of cells and ion concentration changes mentioned above, lead to a reversal of glutamate transporters, which further increases the extracellular glutamate concentration to a level of hundreds of micromolar (Rossi, Oshima & Attwell, 2000; for a recent review see Krzyżanowska,

Pomierny, Filip & Pera, 2014). Although both glial and neuronal glutamate transporters are expected to reverse in ischaemia, experiments on mice lacking the main glial transporter GLT-1 (Hamann *et al*., 2002) have suggested that reversal of these transporters contributes much less to the elevation of extracellular glutamate concentration than does reversal of neuronal glutamate transporters (Gebhardt *et al*., 2002; see also Dawson *et al*., 2000).

Thus glutamate transporters play a key role not only in maintaining the extracellular level of glutamate below toxic levels in normal conditions, but also in raising it to a level that damages neurons in ischaemia.

1.2.7.4 Heteroexchange

Although glutamate transporters normally maintain the extracellular level of L-glutamate below toxic levels (Hamberger *et al*., 1983; Burger *et al*., 1989), under experimental conditions these same transporters may release cellular glutamate. For instance, although inhibition of glutamate uptake elevates the levels of glutamate in the extracellular space (Jabaudon *et al*., 1999), it has been shown that some glutamate transport inhibitors can be transported into the cell, thus inducing the release of glutamate by heteroexchange. Examples of these inhibitors, which are termed ‘’transported’’ inhibitors, include threo-beta-hydroxy-aspartate (TBHA, Arriza et al., 1994) and L-trans pyrrolidine-2,4-dicarboxylic acid (PDC, Volterra et al., 1996), both of which can cause a release of glutamate upon being transported inside the cells. In contrast, ‘’non-transported’’ inhibitors (such as dihydrokainate, DHK, Arriza et al., 1994; DL-TBOA, Shimamoto et al.,1998; L-trans-2,3-PDC, and L-antiendo-3,4-MPDC, Koch et al.,1999) do not cause this heteroexchange.

Heteroexchange is, however, not limited to the transported inhibitors. All transported glutamate analogues will also evoke the heteroexchange process upon being taken up. In fact, heteroexchange has been suggested to occur via presynaptic GLT-1 for D-aspartate (Zhou et al., 2014), and in cell lines expressing GLT-1 for D-aspartate, L-aspartate, L-glutamate and L-cysteate (Dunlop, 2001). It is, however, not known whether the rates of uptake and heteroexchange are different (Zhou et al., 2014).

1.2.7.5 Measuring glutamate uptake

As mentioned previously, glutamate transporters have high affinities for L-glutamate, and L- and D-aspartate, but a very low affinity for D-glutamate (Roberts & Watkins, 1975; Barbour *et al.*, 1991; Klöckner *et al.*, 1994). Unlike glutamate, however, D-aspartate does not act on glutamate receptors (such as NMDA, AMPA or metabotropic glutamate receptors, Klöckner *et al.*, 1994). Thus, D-aspartate can be used as a selective substrate to study the rate of glutamate uptake mediated by the transporters. In contrast, L-aspartate does activate NMDA receptors and can be metabolized by endogenous enzymes such as aspartate aminotransferase (Bender, Woodbury & White, 1997). Thus, D-aspartate (a non-metabolizable analog of L-aspartate) is preferentially used to study glutamate uptake (Szatkowski, Barbour & Attwell, 1991; Bender, Woodbury & White, 1997).

The transport of glutamate (or D-aspartate), as discussed previously, is an electrogenic process, which means two net positive charges are added to the cell for the transport of every glutamate molecule (Billups *et al.*, 1996; Levy *et al.*, 1998; Zerangue & Kavanaugh, 1996). The entry of this net positive charge allows measurement of transport as an uptake current in whole-cell voltage clamp recordings.

This is because, in voltage clamp mode, when the membrane voltage is kept at a set level, ionic current changes are measured as the amount of current that needs to be injected to balance the current going across the cell membrane at the set voltage (see Franciolini (1986) for a review). Thus, a glutamate transporter current can be recorded from astrocytes, patch-clamped near their resting potential, by applying D-aspartate.

Furthermore, the magnitude of the glutamate uptake current is voltage dependent, being largest at negative potentials and reduced at more positive potentials (Brew & Attwell, 1987; Wadiche *et al.*, 1995; Levy *et al.*, 1998). Importantly, the glutamate uptake current always remains inward even at positive potentials, which emphasizes the independence of the uptake current from the chloride ion conductance which is present in the transporter (Brew & Attwell, 1987; Levy *et al.*, 1998). As a result, to better detect the uptake current in astrocytes, it is ideal to voltage-clamp the cells at their negative resting potentials (>-80 mV): a strategy employed later in this thesis.

As D-aspartate may lead to an efflux of intracellular glutamate (or D-aspartate) through heteroexchange (Volterra et al., 1996; Dunlop, 2001; Zhou et al., 2014), it is important to include in the extracellular solution glutamate receptor blockers and an action potential blocker, to counter the effects of any glutamate efflux through heteroexchange. It is also better to use non-transported inhibitors of glutamate uptake (such as DHK, DL-TBOA, or TFB-TBOA) when possible, which do not cause problems via heteroexchange.

1.2.7.6 Regulation of glutamate transporters by extracellular ligands

There is evidence that a change in the expression level of glutamate transporters may contribute to various pathological conditions. For example,

experiments on Alzheimer's patients' brain tissue (Li *et al.*, 1997), and cerebral ischaemia experiments on rat brain (Levy *et al.*, 1995), have shown a reduction in the expression of GLT-1. Furthermore, a causal role for glutamate transporters in epilepsy has been suggested following the knockdown of GLT-1 (Rothstein *et al.*, 1996; Tanaka *et al.*, 1997). Thus, developing an understanding of signalling molecules that can affect the expression and activity of glutamate transporters is of clinical importance. My experiments in chapters 3-5 contribute to this.

1.2.7.6.1 Glutamate-mediated signalling can regulate glutamate transporters

Extracellular glutamate and the signalling mechanisms activated upon its release at synapse can shape the spatial localisation and the density of glutamate transporters near the synapse. A recent study by Murphy-Royal *et al*. (2015) has shown that GLT-1 is highly expressed near glutamatergic synapses, where it can change the extracellular level of glutamate to regulate excitatory transmission. This dense expression was the result of glutamate binding to the GLT-1 which decreased the surface diffusion rate of the transporters, thus leading to their clustering near the synapse (Murphy-Royal *et al.*, 2015).

Glutamate receptors present on the astrocyte plasma membrane may also regulate the density of glutamate transporters. Astrocytes express both ionotropic (Lalo *et al.*, 2006 & 2011) and metabotropic glutamate receptors, mGluRs (see a review by Bradley & Challiss, 2012). Thus, conceivably, the entry of Na^+ and Ca^{2+} (through AMPA and NMDA receptors), or the release of Ca^{2+} downstream of mGluR1/5 G_q-mediated signalling, may change trafficking to the surface membrane of glutamate transporters. Indeed, there is support for a regulatory role of Ca^{2+} transients in astrocytes in regulating transporter surface density: Shigetomi *et al.*

(2012) have shown that intracellular Ca^{2+} events in the astrocytes processes regulate the insertion of GABA transporters into the plasma membrane of astrocytes. Similarly, signalling downstream of G_q-coupled mGluRs has been shown to increase glutamate uptake currents in hippocampal astrocytes (Devaraju *et al*., 2013) and membrane insertion of GLAST glutamate transporters in the cerebellum (Mashimo *et al*., 2010). However, a decrease in surface expression of GLT-1 has also been reported following protein kinase C (PKC) activation (Kalandadze *et al*., 2002), which can be activated downstream of Gq-mediated signalling (Hubbard & Hepler, 2006). Thus, understanding the effect of astrocyte calcium signalling on glutamate transporters needs further examination.

Astrocytes also express the canonical G_i signaling pathway that is activated by mGluR2 and mGluR3. The activation of this signalling pathway not only inhibits cyclic AMP production, but also increases the intracellular level of Ca^{2+} in astrocytes (Haustein et al., 2014), an effect that may be mediated by the βγ subunits activating IP_3-dependent release of Ca^{2+} from internal stores. Interestingly, there are suggestions that changes in the level of cAMP (downstream of G_i or G_s signalling) may also affect the expression of glutamate transporters. In cultured astrocytes, addition of the cAMP analogue dbcAMP, upregulates the transport of glutamate (Gochenauer & Robinson, 2001; Hughes *et al*., 2004). Therefore, it appears that either an increase or a decrease in the level of cAMP may affect activity of glutamate transporters.

Glutamate transporters themselves have been suggested to be capable of increasing astrocyte $[Ca^{2+}]_i$ in response to neuronal activity (Schummers *et al*., 2008). This may be mediated by reversed operation of Na^+/Ca^{2+} exchangers (Doengi *et al*., 2009), following an uptake-evoked rise of $[Na^+]_i$.

Finally, as previously mentioned, the rate of glutamate uptake depends mainly on the electrochemical gradient of Na^+ ions (Brew & Attwell, 1987; Barbour *et al.*, 1988; Sarantis & Attwell, 1990; Szatkowski *et al.*, 1991; Billups *et al.*, 1996; Levy *et al.*, 1998). Thus, a surge in Na^+ entry following fast opening of AMPA receptors may in fact decrease the drive for glutamate uptake.

1.2.7.6.2 Noradrenaline-mediated signalling can regulate glutamate transporters

Apart from glutamate, neuromodulatory neurotransmitters such as noradrenaline (Paukert *et al.*, 2014; Ding *et al.*, 2013) and acetylcholine (Shelton & McCarthy, 2000) can also increase astrocyte $[Ca^{2+}]_i$, which may conceivably affect glutamate transporters.

Noradrenaline has a repertoire of receptors that can mediate its complex actions. These adrenoceptors (ARs) belong to the G-protein-coupled receptor family, and are divided into three sub-categories (i.e. α_1, α_2, and β) depending on the G protein that they couple to. Stimulation of α_1-ARs (which are coupled to G_q-proteins) releases calcium from internal stores via an inositol trisphosphate (IP_3)-dependent pathway, while activating α_2-ARs (which are coupled to G_i/G_o-proteins) decreases the intracellular concentration of cAMP ($[cAMP]_i$) by inhibiting adenylyl cyclase (an enzyme which catalyzes the conversion of ATP to cAMP; for a review see Hertz et al., 2004). Conversely, the activation of β-ARs (which are coupled to G_s-proteins) stimulates the production of cAMP by activating adenylyl cyclase (Hertz et al., 2004).

The functional consequences of noradrenaline signalling to astrocytes may include modulating the clearance of glutamate from the synapse. Data from astrocyte cultures suggest that noradrenaline evokes an increase in glutamate uptake by activating G_q-coupled α_1-ARs (Fahrig, 1993). Further support for this came from a

microdialysis study *in vivo* in which glutamate clearance was enhanced by an α_1-ARs agonist (Alexander et al., 1997). Results from another group, however, suggested that noradrenaline evokes an increase in glutamate uptake by acting on β-receptors in astrocyte cultures (Hansson & Rönnbäck, 1991). All these previous studies used radiotracing, and therefore, confirmation using a more direct method of the effects of noradrenaline on glutamate uptake is needed. I will investigate this issue in chapter 4 of the thesis.

1.2.7.6.3 The role of an understudied G protein coupled receptor in glutamate uptake

Understanding the expression and function of cell-type specific receptors may help to unravel the functional heterogeneity of the cells in the brain, and assist in developing new drug targets. Of special interest are over a hundred GPCRs that are still classified as orphans (i.e. they have no known endogenous ligand: Stockert and Devi, 2015).

In a search for new molecular markers, the Richardson Lab, at UCL, conducted a visual screen of the Allen Brain Atlas *in situ* hybridization database of gene expression patterns in the postnatal mouse brain, to look for potential glial markers. Their search revealed a glial selective pattern of expression for two orphan receptors, GPCR37 and GPCR37like-1 (unpublished work).

Both of these receptors belong to the Class A rhodopsin-like receptor subfamily of GPCRs, and were first identified as a result of their homology with the endothelin type B receptor gene, yet they do not bind endothelin or related peptides (Leng et al. 1999; Valdenaire et al. 1998). GPCR37 and GPCR37L1 share more than 40% of their amino acid sequence (Meyer et al., 2013). However, they are expressed in mutually exclusive populations of cells; while GPCR37 is expressed in mature

oligodendrocytes and a subpopulation of neurons, GPCR37L1 is in a subset of astrocytes and oligodendrocyte precursor cells (unpublished work). This glial specific pattern of expression may suggest a different specific function for GPCR37L1.

It has been suggested that GPCR37 is a substrate for Parkin (which is an ubiquitin ligase, mutations in which are associated with Parkinsonism: Mandillo et al., 2013; Yang et al., 2003; Imai et al., 2001). GPR37 is also thought to downregulate CNS myelination (Yang et al. 2016). In contrast, not much is known about the functional importance of GPCR37L1.

Recently, prosaposin (a polypeptide) was identified as a potential ligand for both GPR37 and GPR37L1 (Meyer et al. 2013). Following its release from the Golgi apparatus, prosaposin is either targeted to the lysosome as a monomer, or it can be secreted into the extracellular space as an oligomer (Yuan & Morales, 2011). It has been shown that prosaposin expression and release is enhanced following conditions of cellular stress such as ischaemia (Costain et al. 2010; Hiraiwa et al. 2003; Yokota et al. 2001). Prosaposin, as well as prosaptide (an active cleavage product of prosaposin), are thought to exert neuroprotective and glioprotective properties during oxidative stress (Meyer et al. 2014; Morita et al. 2001; Sano et al. 1994), through the activation of GPCR37 and GPCR37L1 (Meyer et al. 2014). This conclusion is, however, controversial as a recent study has suggested that GPCR37L1 is constitutively active and that its activity is regulated by proteolytic cleavage near the N-terminus (Coleman et al. 2016; Smith 2015), not by prosaposin (or prosaptide, as suggested by Meyer et al. 2014). It is, therefore, unclear whether the activation of GPCR37L1 is triggered by binding of an extracellular ligand (like prosaposin) or by post-translational modification.

The functional specificity of these two receptors in their respective cell subtypes is still understudied, in particular for GPCR37L1. In chapter 3, I demonstrate that the expression and activation of GPCR37L1 regulates glutamate uptake in astrocytes and also modulate neuronal excitatory transmission.

1.2.7.7 Regulation of glutamate transporters by endogenous proteins and signalling pathways

Although changes in the expression and function of glutamate transporters have been linked to various pathological conditions such as ischaemic stroke, Alzheimer's disease, and other neurodegenerative disorders (Li *et al.*, 1997; Levy *et al.*, 1995), the mechanisms by which glutamate transport is regulated inside the cell are poorly understood.

Intracellular proteins can interact with, and modulate the activity and surface levels of, glutamate transporters. It has been reported that the phosphorylation and activation of Akt and its downstream target, mTOR, following the release of growth factors (Figiel *et al.*, 2003), increased GLT1 (EAAT2) expression in cultured astrocytes (Wu *et al.*, 2010). However, the regulation of GLT-1 (EAAT2) may differ between its two isoforms, EAAT2a and EAAT2b, which are generated by the gene EAAT2. These two isoforms contain different sequences at their C termini due to alternative RNA splicing. This difference determines the surface expression and trafficking of the transporter. While EAAT2a is predominantly localised inside vesicles ready to be inserted into the plasma membrane, EAAT2b is localised predominantly to the plasma membrane. In fact, the addition of a postsynaptic density-95/Discs large/zona occludens-1 (PDZ) ligand at the cytoplasmic C terminus of GLT-1 is required for its localisation to the cell membrane (Underhill *et al.*, 2015). The

interaction of PDZ with EAAT2b is dependent on intracellular signalling pathways. In fact, it has been shown that the activation of the CaMKII pathway phosphorylates the PDZ protein and decreases EAAT2b surface expression, without affecting the distribution of EAAT2a (Underhill *et al.*, 2015).

Furthermore, internalisation of glutamate transporters is accelerated following the transport of substrates like glutamate or D-aspartate, or transported inhibitors like PDC (Ibáñez *et al.*, 2016). This is thought to be dependent on the binding of the adaptor protein β-arrestin and ubiquitin ligase Nedd4-2 with the C terminus of GLT-1, and a subsequent internalization of the ubiquitinated transporter (Ibáñez *et al.*, 2016).

Glutamate transporter associated proteins (GTRAPs) can also interact with the C terminus of glutamate transporters to either enhance glutamate uptake by increasing the surface of EAAT4 in cerebellar Purkinje cells (by GTRAP41 and 48, Jackson *et al.*, 2001), or reducing the binding affinity of neuronal EAAC1 for glutamate (by GTRAP3-18, Lin *et al.*, 2001). It is, however, not known whether GTRAPs can also modulate the activity, or surface expression of, GLT-1.

Another protein that has been shown to regulate the internalisation of GLT-1 is nischarin (unpublished data from the Kittler Lab). Nischarin is a mouse homologue of the human imidazoline receptor (Piletz *et al.*, 2003; Zhang & Abdel-Rahman, 2006) that may act as a membrane-associated mediator of receptor signaling. There are three classes of imidazoline receptor, I1, I2 and I3, all of which are important cardiovascular drug targets (see chapter 5). Nischarin is proposed as a homologue of the I1 receptor, which may act as a membrane-associated mediator of receptor signaling involved in sympatho-inhibitory actions of imidazolines (see Head & Mayorov for a recent review

2006). In contrast, the I2 receptor is targeted by imidazoline adrenergic molecules (e.g. clonidine but not catecholamines) while the I3 receptor regulates insulin secretion.

Nischarin, which belongs to the super family of Rab and Rac GTPases, contains an N-terminal PHOX domain, has been shown to target GLT-1 to the endosome. This internalisation is dependent on phosphatidyl inositol-3-phosphate (PI3P) signalling (Alahari *et al*., 2000; Kuijl *et al*., 2013). Although nischarin mRNA is highly expressed in most cells (Zhang et al., 2014), not much is known regarding its function in the brain except that nischarin expression increases following neuroinflammation in the rat brain (Wu *et al*., 2013), and that it may play a role in neuronal migration (Ding *et al*., 2013).

More recently, nischarin was discovered to directly bind to GLT-1 (unpublished data resulting from yeast 2 hybrid screen by Hélène Marie in the Attwell and Kittler Labs). In addition, the overexpression of nischarin was shown by the Kittler lab to decrease the surface expression of GLT-1. Therefore, in chapter 5, I will examine the functional consequences of nischarin expression for glutamate uptake in astrocytes.

7.5 Overarching hypotheses and conclusions of this thesis

The overarching hypothesis of this thesis is that astrocytes actively modulate neuronal signal transmission. In the thesis I have described experiments on hippocampal astrocytes and neurons that examine the interaction between these cells mediated either by the release from astrocytes of molecules known as gliotransmitters which act on neuronal receptors, or by changes in the extracellular level of glutamate produced by modulation of the rate of glutamate transport in astrocytes.

I demonstrate that a relatively understudied G protein coupled receptor present in astrocytes, GPCR37L1, decreases the activity of astrocyte glutamate transporters and decreases neuronal NMDA receptor activity, presumably by regulating the release of modulatory molecules from astrocytes. In ischaemia, expression of GPCR37L1 and addition of an analogue of its agonist, prosaposin, are neuroprotective. It would be of interest to study the release of prosaposin under conditions such as stress or other pathological conditions, to see if prosaposin can similarly affect glutamate uptake in astrocytes, and postsynaptic neuronal NMDA responses.

A discovery that the neuromodulatory neurotransmitter noradrenaline reduces glutamate uptake currents in astrocytes, in chapter 4, challenges the previous thin body of literature. Noradrenaline is a key regulator of astrocyte calcium signalling (Paukert *et al*., 2014), and my results show that noradrenaline-mediated reduction of glutamate uptake is, at least partly, calcium-dependent, and that astrocyte calcium signalling acts as a key regulator of the spontaneous firing of inhibitory interneurons in hippocampus. Thus, it is plausible that the reduction in glutamate uptake by noradrenaline, and the subsequent rise in the extracellular glutamate level, can increase the activity of a certain class of interneurons which may reduce excess excitatory transmission to increase the precision of transmission - a possible mechanism for the phenomenon of attention. If true, then studying such modulation of attention by glutamate uptake during development will be of utmost interest, to see whether changes in nischarin level contribute to this.

Chapter 2:

Materials and Methods

This chapter explains the general methods used for experiments throughout the thesis. Further details of the specific methods used are provided in each results chapter. Experiments were carried out on hippocampal slices from rats and transgenic mice, and also on cultures prepared from embryonic hippocampal tissue from transgenic mice as described below.

2.1 Animals

For experiments in chapter 3, GPCR37L1 knock-out mice at postnatal day 14-16 were obtained from the Richardson Lab. In these mice, a LacZ-neomycin cassette was inserted by homologous recombination into the first exon of the *Gpr37l1* gene, thereby causing a deletion of part of the molecule and a loss of function of the gene. Homozygous mice ($GPR37L1^{-/-}$) and their control wild-type ($GPR37L1^{+/+}$) littermates were obtained by crossing the heterozygous mice ($GPR37L1^{+/-}$).

GPCR37L1-GFP transgenic mice at postnatal day 14-16 were also obtained from the Richardson Lab. They were generated using a bacterial artificial chromosome (BAC). The targeting vector contained the floxed GFP gene, driven by the GPCR37L1 promoter and followed by a 4x polyA stop sequence (GPR37L1-LoxP-GFP-4XpA-LoxP-DTA, the diphtheria toxin fragment A, DTA, is not expressed in the absence of Cre), and was inserted by homologous recombination immediately before the open reading frame of the *Gpr37l1* sequence. This led to the appearance of GFP-positive cells (which expressed the GPCR37L1 protein) and GFP-negative cells (which did not express the GPCR37L1 protein).

For experiments in chapters 4 and 6, Sprague-Dawley rats at postnatal day 12 were obtained from the UCL animal facility.

For experiments in chapter 5, embryonic hippocampal cultures were obtained from the Kittler lab on their tenth day *in vitro*. Cultures were prepared from nischarin WT or KO mice embryos at 16 days post-fertilization. A *Nisch* knockout mouse line was generated by the Wellcome Trust Sanger Institute and obtained from the Harwell Mary Lyon Centre. The *Nisch* transgenic line was generated by inserting a L1L2_Bact_P cassette encoding an engrailed1 splice acceptor sequence, a LacZ reporter and a neomycin resistance gene between exons 4 and 5 thus disrupting *Nisch* transcription. Homozygous mice ($Nisch^{-/-}$) and their control wild-type ($Nisch^{+/+}$) littermates were obtained by crossing the heterozygous mice ($Nisch^{+/-}$).

2.2 Hippocampal slice preparation

For experiments in chapter 3, hippocampal slices (270 μm thick) were prepared from the GPCR37L1 knockout mice ($GPCR37L1^{-/-}$) and their wild-type littermates ($GPCR37L1^{+/+}$), or alternatively from the transgenic mice with cells that were GFP-positive (i.e. expressing GPCR37L1) or GFP-negative (i.e. without GPCR37L1 expression, see above and section 3.3.1), age P14-16. Animals were killed by cervical dislocation, followed by decapitation. The head was immediately immersed in ice-cold slicing solution containing (in mM): 87 NaCl, 25 $NaHCO_3$, 25 glucose, 75 sucrose, 2.5 KCl, 1.25 NaH_2PO_4, 0.5 $CaCl_2$, 7 $MgCl_2$, 1 kynurenic acid (to block glutamate receptors during the slicing process), pH 7.2-7.4 (bubbled with 95% O_2 / 5% CO_2), osmolarity ~ 330-340 mOsm. Dissection of hippocampus was carried out as described by Bischofberger et al. (2006), which involved separating the two hemispheres through the corpus callosum then laying each hemisphere on its cut

sagittal surface, then making a cut oriented anterior to posterior at about 10^{o} to the ventral surface (referred to as the ‘’magic cut’’, for full details see Bischofberger *et al.,* 2006). Hippocampal slices were cut using a Vibratome. The slices were then transferred to a heated chamber at 30^{o}C for 40 min, and subsequently removed and allowed to reach room temperature (RT) for a further 20 min prior to recording.

For experiments in chapters 4 and 6, Sprague-Dawley rats, age P12, were used for the preparation of hippocampal slices. The slicing procedure was similar to the one described for chapter 3 with the exception that the slices were 300μm thick, and were collected and stored in a chamber containing slicing solution at RT for a minimum of one hour prior to recording, in order to allow slice recovery.

2.3 Recording Solutions

2.3.1 Extracellular solutions

Brain slices were perfused with solutions mimicking cerebrospinal fluid (artificial cerebrospinal fluid, aCSF) which contained HEPES-based buffer (in chapters 3, 4, and 5) or bicarbonate-based buffer (in chapter 6). HEPES-based extracellular solution contained (in mM): 140 NaCl, 10 HEPES, 10 glucose, 2.5 KCl, 2 $CaCl_2$, 1 NaH_2PO_4, 1 $MgCl_2$, pH 7.4 with NaOH, osmolarity 300 mOsm (bubbled with 100% O_2). Bicarbonate-based extracellular solution contained (in mM): 124 NaCl, 26 $NaHCO_3$, 10 glucose, 2.5 KCl, 2 $CaCl_2$, 1 NaH_2PO_4, 1 $MgCl_2$, pH 7.2-7.4 (bubbled with 95% O_2/5% CO_2). For experiments in chapters 3, 4, and 5, the solution was perfused at a flow rate of 3-4 ml/min through the recording chamber by the use of gravity perfusion using syringes (60ml) that were connected to individual tubes, which merged into a single outlet prior to reaching the bath. These experiments were done at RT. For experiments in chapter 6, however, the solution was perfused through

the recording chamber by a peristaltic pump at a flow rate of 2-3 ml/min, and passed through a heating block where its temperature was adjusted to 32-35°C (by manually increasing or decreasing the current flow through a series of resistors attached to the heating block according to the thermometer reading in the recording chamber).

2.3.1.1 Drugs added to the extracellular solution

For experiments in chapter 3, in order to record glutamate receptor currents from CA1 pyramidal neurons (in Figs. 3.7 & 3.8), voltage clamp recordings were made at -30 mV, including the -14mV junction potential (see section 2.7.2) for the caesium gluconate internal solution. Kainate (3 μM to activate AMPA/kainate receptors) was applied in the presence of D-AP5 (50 μM, Tocris) to block the NMDARs. Alternatively, N-methyl D-aspartate (NMDA, 5 μM) was applied to activate NMDARs, in the presence of NBQX (10 μM, Sigma). An action potential blocker (tetrodotoxin, TTX, 400 nM, Tocris) and postsynaptic $GABA_A$ receptor blocker (picrotoxin 100 μM, Sigma) were also present throughout the experiments. For experiments in Figs. 3.7 and 3.8, responses to NMDA (5 μM), were recorded in the presence of TTX (150 nM, even 100 nM TTX is sufficient to block action potentials, Trombley & Westbrook, 1991) and picrotoxin (100 μM). In some experiments, prosaptide TX 14(a) (10 μM, AnaSpec) was used as an agonist for GPCR37L1 (Meyer et al., 2012), mimicking its endogenous agonist prosaposin.

In chapters 3, 4 and 5, to record the glutamate uptake current from astrocytes, voltage clamp recordings were made at a potential close to the cell's resting potential (typically around -90 mV). The aCSF was supplemented with a selection of blockers that were present throughout the experiment. These include: TTX (150 nM, Tocris), a $GABA_A$ receptor blocker (bicuculline 10 μM, Sigma), the NMDA receptor blockers

(D-AP5 50 μM, Tocris; (+)MK-801 10 μM, Sigma; 5,7-DCK 10 μM, Sigma), the AMPA and kainate receptor blocker (NBQX 10 μM, Sigma), and the inwardly rectifying potassium channel blocker (barium chloride 200 μM, Sigma). In addition to these blockers, D-aspartate (200 μM, Sigma) was used as a glutamate substitute to evoke the transporter current. A non-transported glial glutamate transporter blocker, TFB-TBOA (10 μM, Tocris) was used in some experiments to block the glutamate transporter current in the presence of D-aspartate. Two different approaches were taken following the application of D-aspartate: either a solution containing both D-aspartate and a non-transported glial glutamate transporter blocker, TFB-TBOA (10 μM) was applied to block the D-aspartate-evoked current (in chapters 3 and 5). Alternatively, the solution containing D-aspartate was simply removed (in chapters 3, 4 and 5). The size of the uptake current was subsequently calculated as the inward current recorded in D-aspartate minus the average of the baseline currents measured before and after D-aspartate application. All experiments in chapters 3 and 5 were performed with me blinded to the genotype of the mice studied.

For the ischaemia experiments in chapter 3, hippocampal slices were incubated at 37°C in an ischaemic solution in which glucose was replaced with 7 mM sucrose, and oxygen was removed by equilibrating solutions with 5% CO_2 and 95% N_2. In addition, 2 mM iodoacetate and 25 μM antimycin were added to the ischaemic solution to block ATP generation by glycolysis and oxidative phosphorylation, respectively (Allen, Káradóttir, Attwell, 2005). Control slices were incubated in aCSF, gassed as usual with 5% CO2, 95% O2, and were incubated for 30 min at 37^{o}C. Propidium iodide (PI, 7.5 μM) was added to both solutions to label dead cells. After 30 min incubation in ischaemia or control solution, slices were fixed for 1 hour in 4% paraformaldehyde, and then rinsed three times in PBS (20 min each). Subsequently,

immunohistochemistry for astrocytes and neurons was performed (see section 2.7). These experiments were done in pairs such that the brains from one GPCR37L1$^{+/+}$ mouse and one GPCR37L1$^{-/-}$ mouse were dissected, and one hemisphere from each of the animals was mounted in the slicer simultaneously. The slices from both mice were then incubated in a recovering chamber for 1hr at ~33^{o}C (see section 2.1.1) before being incubated in either ischaemia or control solutions as mentioned above. This procedure minimizes any unintended bias in the treatment of the two genotypes. The slices were later coded so that the experimenter was blinded as to the genotype when carrying out immunohistochemistry.

For the experiments in chapter 4, glutamate uptake in hippocampal astrocytes was measured as described above for chapter 3. In addition the effect of bath perfusion of DL-noradrenaline (2 μM) on the peak D-aspartate-evoked current was monitored in the presence and absence of adrenergic receptor blockers. These include the α_1-adrenoceptor blocker, terazosin (1 μM) and the α_2-adrenoceptor blocker, atipamezol (1 μM). Ascorbic acid (500 μM) was included to block oxidation of noradrenaline (Hugh *et al.*, 1987).

For the experiments in chapter 5, glutamate uptake was measured (as described above) in cultured astrocytes prepared from Nisch$^{+/+}$ and Nisch$^{-/-}$ mice embryonic hippocampal tissue. Glutamate uptake in hippocampal astrocytes was measured as described above for chapter 3. All experiments in this chapter were performed with the experimenter blinded to the genotype of the mice studied.

For the experiments in chapter 6, the effects of bath perfusion of DL-noradrenaline (5 or 20 μM) on postsynaptic excitatory and inhibitory currents were measured in CA1 pyramidal neurons, when changes in the intracellular concentration of calcium (Ca^{2+}) were buffered with different concentration of chelators (1 mM

EGTA, or 30 mM BAPTA) in nearby astrocytes. The recipes of the intracellular solutions used for this are given below (see section 2.3.2). In some experiments, TTX (400 nM) was used to assess the action potential dependence of the effect of 20 μM noradrenaline on inhibitory transmission. Unlike for the experiments in chapter 4, ascorbic acid was not added to inhibit oxidation of noradrenaline in this chapter. This is because ascorbic acid may affect the levels of Ca^{2+} in astrocytes, as it has been shown to block T-type calcium channels (Parsey & Matteson, 1993; Todorovic & Jevtovic-Todorovic, 2011). TTX (100 nM; to block action potentials), was also present in some experiments as indicated in the figure captions.

2.3.2 Intracellular solution

Whole-cell patch clamping experiments in neurons (in chapters 3 and 6) were performed using a caesium-gluconate based solution containing (in mM): 130 caesium-gluconate, 4 NaCl, 10 HEPES, 10 Na_2phosphocreatine, 0.1 $CaCl_2$, 1 EGTA, 2 QX-314 (to block voltage-gated sodium channels and improve voltage control), 2 MgATP, and 0.5 Na_2GTP (pH 7.1–7.2 adjusted with CsOH, and osmolarity ~ 285 mOsm). Alexa Fluor 488 (20 μM) was added to each aliquot of internal daily.

For recordings from astrocytes in chapters 3, 4 and 5 I used a potassium-gluconate based solution containing (in mM): 130 K-gluconate, 4 NaCl, 10 HEPES, 1 $CaCl_2$, 10 EGTA, 2 MgATP, 0.5 Na_2GTP (pH 7.1–7.2 adjusted with KOH, and osmolarity ~ 285 mOsm). Alexa Fluor 594 (20 μM), or Alexa Fluor 488 (20 μM), was added to each aliquot of internal daily. For recordings from astrocytes in chapter 6, I used a slightly different potassium-gluconate based solution containing a lower concentration of EGTA to allow changes in $[Ca^{2+}]_i$ to occur. This solution contained (in mM): 130 K-gluconate, 4 NaCl, 10 HEPES, 10 Na_2phophocreatine, 0.15 $CaCl_2$, 1

EGTA, 2 MgATP, 0.5 Na_2GTP (pH 7.1–7.2 adjusted with KOH, and osmolarity ~ 285 mOsm). Alexa Fluor 488 or 594 (20 μM) was added to each aliquot of internal daily.

For some of the recordings in chapter 3, dialysis of biocytin into the network of astrocytes via the patch pipette was used to assess the extent of gap-junction coupling in the network of astrocytes. The potassium-gluconate based solution used for these experiments contained (in mM): 130 K-gluconate, 4 NaCl, 10 HEPES, 10 Na_2phosphocreatine, 0.15 $CaCl_2$, 1 EGTA, 2 MgATP, 0.5 Na_2GTP, biocytin 3.33 mg/ml (pH 7.1–7.2 adjusted with KOH, and osmolarity ~ 285 mOsm)

For some of the recordings in chapters 4 and 6, in order to examine the effect of intracellular cAMP concentration changes in astrocytes on NA-evoked changes in glutamate uptake, 1mM cAMP (in chapter 4), or 5mM cAMP (for chapter 6), both of which are saturating levels, was added to the internal solution on the day of the experiment.

To examine the effects of intracellular calcium concentration changes in astrocytes on noradrenaline-evoked changes in glutamate uptake (chapter 4), or on excitatory and inhibitory postsynaptic currents (EPSCs and IPSCs) in adjacent pyramidal neurons (in chapter 6), the faster calcium chelating agent, BAPTA (30 mM), was employed in the internal solution instead of 10 mM EGTA. The internal solution containing BAPTA (tetra-potassium salt) was similar but with the $CaCl_2$ and EGTA replaced with (in mM) 3 $CaCl_2$ and 30 BAPTA (so that the free $[Ca^{2+}]_i$ was ~20 nM in both the control and the BAPTA internal solutions, calculated using MaxChelator: http://maxchelator.stanford.edu/webmaxc/webmaxcE.htm) and with osmolarity differences compensated by lowering the K-gluconate concentration. Osmolarity measurements showed that K_4-BAPTA does not dissociate completely so that correspondingly less compensation of osmolarity was needed. The solution contained

(mM) 67 K-gluconate, 2 NaCl, 3 $CaCl_2$, 10 HEPES, 30 K_4-BAPTA, 2 $MgCl_2$, 2 Na_2ATP, 0.5 Na_2GTP, 10 Na_2 phosphocreatine and 0.04 Alexa Fluor 488, with pH set to 7.1 using KOH.

2.4 Cell identification and dye filling

Neurons and astrocytes were selected for patch-clamping on the basis of the shape and size of their soma (neurons were selected in the CA1 pyramidal layer, and astrocytes in the stratum radiatum). Diffusion of an Alexa Fluor 488 dye into the pyramidal neuron's soma and apical dendrites confirmed the cell identity. Similarly, the diffusion of an Alexa Fluor 594 / or 488 into astrocytic (star-shaped) processes, and into other nearby astrocytes (to which the patch-clamped cell was gap junctionally coupled) further confirmed the glial cell identity (see Fig. 6.2 in chapter 6 as an example of a neuron filled with Alexa 488 and the network of astrocytes around the neuron filled with Alexa 594). Astrocytes typically had a resting potential around -90 mV. To further characterize the properties of the patch-clamped cells, I applied voltage steps in 20 mV increments (from around −130 to -10 mV, 200 ms duration, for astrocytes; and from -100 to +20 mV for neurons, in voltage-clamp mode, using pClamp 10.2, Axon Instruments). The presence of a large voltage-gated sodium current further confirmed the identity of pyramidal neurons, while a passive current-voltage relation was used as a criterion for the identification of astrocytes.

2.5 Sequence of recordings made

For recording from astrocytes (in chapter 3, 4 and 5), whole-cell patch-clamp recordings were made from single astrocytes in the stratum radiatum of the hippocampal formation in brain slices (chapters 3 & 4), or in cultures (chapter 5). In

these chapters, following the confirmation of astrocyte identity (see section 2.4), membrane current was recorded from the astrocytes.

Dual whole-cell patch-clamp recordings, in chapter 6, were made from CA1 pyramidal neurons and their nearby astrocytes in the stratum radiatum. In each case, a gigaseal was achieved on an astrocyte in the stratum radiatum, and subsequently a nearby CA1 pyramidal neuron was whole-cell patch clamped (see section 2.4 on patch clamp techniques). The initial 2 minutes of recording were ignored while the holding current reached a stable level, and then 5 mins of baseline data were recorded from the neuron. Whole-cell recording mode was then achieved in the astrocyte, and the effects of astrocyte dialysis with the internal solution (with or without BAPTA) were recorded.

2.6 Patch-clamp set-up

2.6.1 Mechanical and optical set-up

The whole-cell patch-clamping experiments in all chapters were performed with an Olympus BX51WI upright microscope, with a fixed stage and microscope-moving table. The CA1 region and its associated stratum radiatum was found using a 5x objective, and then a 40x water-immersion objective (both Olympus) together with differential interference contrast (DIC) optics was used to choose cells (i.e. CA1 pyramidal neurons in the pyramidal layer, or astrocytes in the stratum radiatum) for patch-clamp recording. For chapter 5, cultured astrocytes throughout the dish were chosen for recordings. The microscope was equipped with a xenon/mercury arc lamp and a filter cube for viewing Alexa Fluor 488-filled cells (excitation wavelength 495 nm, 470-490 nm dichroic, and emission wavelength above 519 nm), or Alexa Fluor 594-filled cells (excitation wavelength 590 nm, 594 nm dichroic, and emission

wavelength above 617 nm). A video camera (COHU, 2700 series) was attached to the microscope so that cells could also be visualized using a TV monitor.

2.6.2 Recording electrodes

Patch pipettes were made from thick-walled filament-containing borosilicate glass capillaries (outer diameter 1.5 mm, inner diameter 0.86 mm, type GC150F-10 from Harvard Apparatus) using a four-step horizontal puller (Sutter Instruments P-97). For recording from neurons, pipettes with 4-6 MΩ resistance were filled with the intracellular solution given in section 2.3.2, while for recording from astrocytes, pipettes with 6-8 MΩ resistance were filled with the intracellular solution given in section 2.3.2.

The recording electrode was inserted into the pipette holder of a patch-clamp headstage (Axopatch CV-7B, Axon Instruments), which was controlled by an electrical micro manipulator (SM5, Luigs and Neumann) attached to the pipette holder. A silver wire coated with silver chloride (AgCl) was present inside the pipette electrode that was in contact with the intracellular solution. Similarly, an AgCl coated pellet was used as a bath electrode. The extracellular and intracellular solutions (see section 2.3, above) contained chloride ions which allow a reversible exchange of chloride ions: $Ag + Cl^- \Leftrightarrow AgCl + e^-$

To ensure that this ionic exchange occurs at all times, both the silver wire and bath electrode were regularly chlorided by placing them in a solution containing chloride ions (10% bleach, NaOCl).

2.6.3 Stimulating electrodes

For field excitatory postsynaptic recordings in chapter 3, low resistance

stimulating electrodes (~1-2 MΩ) were used, which were filled with HEPES-based aCSF as described in section 2.3.1, and inserted into a pipette holder which was controlled by an electrical micro-manipulator (SM1, Luigs and Neumann). A silver wire, coated with silver chloride in the same way as above (section 2.6.2), was inserted into the pipette. The silver wire was connected to the cathode of an isolated stimulating box (Model DS2, Digimeter Ltd.). The anode of the stimulating box was connected to a silver pellet bath electrode, also coated with silver chloride. Voltage steps in 20V increments (from 0-100V), applied close to the CA3 pyramidal region, evoked field excitatory postsynaptic currents (fEPSCs), which were recorded using a pipette filled with a HEPES-based aCSF, in the layer of the CA1 pyramidal neurons' apical dendrites.

2.6.4 Data collection

Patch-clamp recordings were made with a Multiclamp 700B amplifier, and signals were sampled at 50 kHz, filtered at 10 kHz, and digitized at 0.5-10 kHz (Digidata 1440A), depending on the experiment, using pClamp 10.2. Data were also stored using Axoscope, sampling at 1 kHz (filtered at 500Hz). Currents were analysed using Clampfit 10.2 software (Axon instrument). Series resistance and access resistance were also monitored throughout, as described below.

2.7 Patch-clamp recording

2.7.1 Whole-cell configuration

All recordings were performed in the whole-cell configuration (Hamill et al., 1981; Edwards et al., 1989). Voltage clamp mode (section 2.4.3, below) was used to obtain whole-cell configuration and record synaptic currents in all chapters.

Additionally, current clamp mode (in chapter 3) was also used to record the frequency of action potentials evoked by current injection.

After a neuron or an astrocyte was selected, the patch pipette was lowered into the bath. A 50 msec, -10 mV voltage step was delivered at 5 Hz to monitor the pipette resistance before and after contacting the cell membrane. Positive pressure was applied to the pipette (through a 1 ml syringe) while it was lowered in the slice, to prevent the pipette tip becoming blocked. Once a contact was made between the patch pipette and the cell soma, gentle suction was applied to form a high resistance seal (resistance >1 GΩ) between the cell membrane and the tip of the patch pipette, thus achieving cell-attached mode. At this point, the holding potential (including the junction potential) was set to -74 mV for neurons, or -90 mV for astrocytes (close to the cells' resting membrane potential), and the pipette capacitance was compensated (i.e. a signal is added to the current trace that effectively subtracts the current generated by charging of the pipette capacitance). Subsequently, further gentle suction was applied to break through the piece of membrane at the tip of the pipette, thus achieving the whole-cell configuration and gaining diffusive and electrical access to the cell's interior.

2.7.2 Liquid junction potential and its compensation

Because of the different ionic composition inside the pipette solution and the aCSF in the bath, a potential difference (i.e. the junction potential) occurs at the end of the electrode when it enters the bath. This potential difference, however, is not present in whole-cell configuration when the pipette solution has diffused into the cell (Fenwick et al., 1982). The junction potential depends on the diffusion coefficients of the anions and cations present in each solution, which are determined by the molecular

weight and charge of ions, both of which affect ion mobility. The principal ions responsible for generating the junction potential in my experiments were K^+(or Cs^+), Na^+, Cl^- and gluconate. K^+(or Cs^+) ions diffuse out of the patch electrode into the bath more quickly ($D_K = 1.99x10^{-9}$ m^2 s^{-1}) than Na^+ ions diffuse inside the patch electrode ($D_{Na} = 1.36x10^{-9}$ m^2 s^{-1}), and gluconate ions diffuse out more slowly ($D_{gluconate} = 1.06x10^{-9}$ m^2 s^{-1}) than Cl^- ions diffuse in ($D_{Cl} = 1.99x10^{-9}$ m^2 s^{-1}) (Robinson and Stokes, 1965). This leaves the patch electrode potential more negative than the bath potential.

The junction potential can be measured experimentally using an agar bridge (containing 4 M NaCl) to connect the bath solution to a reference electrode. This avoids changes in the reference electrode potential following a change in the external solution. When zero current is applied, the junction potential is the difference between the voltage value obtained when both the patch electrode and bath contained the same solution (both internal solution, so there is no junction potential) and the value obtained when the bath solution was that used for experiments (aCSF). For the gluconate-containing solutions mentioned above (given in section 2.2), the junction potential was -14 mV. Thus all the voltage values for any voltage clamp recordings were corrected subsequently (i.e. -14 mV was added to all voltages measured with the patch-clamp).

2.7.3 The electrical circuit for whole-cell voltage clamp recording

Electrically excitable and non-excitable cells respond to chemical signals through changes in their membrane potential. Therefore, circuit equivalents can serve as an appropriate analogy to conceptualize the properties of brain cells. For instance, the lipid bilayer of the cell membrane serves as an electrical insulator while the intracellular and extracellular solutions act as conductors of current. This arrangement

of intra- and extracellular solutions (conductors) surrounding the lipid bilayer (insulator) defines a capacitor, C, that can store charge (Q, measured in Coulombs) proportional to the applied voltage and the membrane's capacity to store charge. Thus, this relation can be defined by the following equation: $Q = CV$

Capacitance is proportional to the membrane surface area; the more membrane, the more charge can be stored. One important property related to this is that the time required for charging the membrane capacitance through the resistance of the pipette is the rate-limiting step in changing the membrane voltage. This prevent instantaneous changes in voltage when patch-clamping, and also affects the conduction of electrical signals such that an action potential travelling along an axon is subject to a delay in propagation due to the time needed for charging the cell membrane, therefore limiting the speed of action potential propagation. Current can also flow across the cell membrane via ion channels at a rate $I_{ionic} = V/R_m$, where R_m is the membrane resistance.

The current flowing through a capacitor (C) is proportional to the rate of change of voltage with time (dV/dt):

$$I = dQ/dt = CdV/dt \quad (2.1)$$

2.7.4 Series resistance

The resistance between the cell and the pipette, in the whole-cell patch-clamp configuration, is referred to as the pipette resistance (or series resistance, R_s). A lower series resistance achieves a better electrical and diffusion pathway from the pipette into the cell, which is essential for the exchange of molecules between the pipette and the cell and for better voltage clamp control. As a result of this resistance between the pipette and the cell, the current flowing between the pipette and the cytoplasm will

face a voltage drop across the pipette tip (the larger the series resistance, the bigger the voltage drop). This change in voltage, or voltage error, can be calculated from the following equation:

$$V_{error}=IR_s \quad (2.2)$$

The apparent membrane potential is the sum of the real membrane potential, in the soma, plus the voltage drop across R_s. The higher the series resistance or the larger the current, the larger the voltage drop. Therefore, series resistance is commonly compensated for electronically to minimise such voltage errors. What this means is that a positive feedback circuit is used to add to the command potential a voltage that is proportional to the current flowing. This increases the voltage applied to the pipette when the current flow and the voltage error are greatest, driving extra current through the electrode, which is exactly what would happen if the electrode had a lower resistance. In my experiments, varying amount of compensation was applied (typically between 30-60% for astrocytes, and 50-70% for neurons).

For all the experiments, the pipette series resistance was typically < 20 MΩ following compensation. This resistance was monitored throughout the experiment, and those recordings in which the resistance changed by more than 20% were excluded.

The pipette series resistance can be measured by analysing the current response to a voltage step. However, this depends on the spatial structure of the cell. For instance, in a spatially compact cell, in the whole-cell configuration, the membrane acts as a capacitor and resistor connected in parallel, and the pipette series resistance is in series with these. The current flow (I) through this circuit in response to a voltage step (V_s) is (Tessier-Lavigne et al., 1988):

$$I(t)=\left(\frac{V_s}{R_m+R_s}\right)\cdot\left(1+\frac{R_m\cdot e^{-t/\tau}}{R_s}\right) \quad (2.3)$$

where t is the time after the onset of the voltage step, R_m is the membrane resistance, R_s is the series resistance, and the decay time constant of the current transient, is:

$$\tau = C_m\cdot\frac{R_s\cdot R_m}{R_s+R_m} \quad (2.4)$$

At t = 0 (the onset of the voltage step), the capacitor is uncharged and the voltage across it is zero. So, once the voltage step is applied, the voltage across the series resistance (i.e. excluding the voltage drop) is initially the applied voltage step, and the intial fast onset of the current allows calculation of the series resistance as (from equation 2.3 at t=0):

$$R_s = \frac{V_s}{I(t=0)} \quad (2.5)$$

At steady state (t = ∞), the capacitor is fully charged and no current flows through it. From equation 2.3 at t = ∞, and the membrane resistance at t = ∞ will be:

$$R_m = \frac{V_s}{I(t=\infty)} - R_s \quad (2.6)$$

Substituting R_s from equation at t=0 gives:

$$R_m = V_s\cdot\frac{I(t=0)-I(t=\infty)}{I(t=0)\cdot I(t=\infty)} \quad (2.7)$$

The membrane capacitance can be calculated by rearranging equation 2.4 to give:

$$C_m = \tau\cdot\frac{R_s+R_m}{R_s\cdot R_m} \quad (2.8)$$

Substituting R_s from equation 2.5 and R_m from equation 2.7 gives:

$$C_m = \tau\cdot\frac{I(t=0)^2}{V_s\cdot\left(I(t=0)-I(t=\infty)\right)} \quad (2.9)$$

The time constant, τ, was obtained by fitting the current transient with a single exponential using Clampfit. For cells with complex morphology, however, the resistance of the processes or dendrites makes the cell non-uniform in voltage, and the capacity current decays as the sum of 2 or more exponentials. Indeed it has been shown that voltage control at the CA1 pyramidal dendrites is poor when patch-clamped at the soma (Major 1993). This is expected to be an even bigger problem for astrocytes which exist in a spatially distributed network with gap-junctional coupling to other astrocytes (giving them a large apparent capacitance and a large conductance at rest which gives them a very low membrane resistance, ~1-5 MΩ). Thus holding the membrane voltage of a patch-clamped astrocyte soma away from the resting potential of astrocytes is not likely to alter the voltage of a substantial area of the astrocytic network. As a result, in all experiments involving membrane current recording from astrocytes, the voltage was set close to the resting potential.

2.7.5 The electrical circuit for whole-cell current clamp recording

Voltage changes in a whole-cell patch clamped neuron can be monitored in current clamp mode. In this configuration, injection of a step of current, I, into a cell will generate a voltage, V, change in the cell with a charging curve composed of one exponential component described by the membrane time constant, τ_m, being given by:

$$V = I\,(1 - e^{-t/\tau}) \text{ where } \tau_m = R_m \,.\, C_m \qquad (2.10)$$

Again R_m is the membrane resistance (given by equation 2.6) and C_m is the membrane capacitance (given by equation 2.8).

In current clamp, unlike voltage clamp, voltage error (as described in section 2.6.4) as a result of pipette series resistance only affects the recorded voltage, and not the voltage change that is actually "seen" by the cell. Therefore, the error induced by

the series resistance can be corrected for using a circuit which adds the dropped voltage, calculated from the series resistance of the cell (measured in voltage clamp) and the injected current.

2.7.6 Effects of the cell capacitance

The combination of the series resistance and the cell capacitance filters signals when patch-clamping. To change the cell voltage, current needs to flow through the series resistance, which generates a voltage drop that limits the speed of charging of the capacitance. This effectively creates a low-pass RC filter with a time constant τ as given in equation 2.4; this effect of cell capacitance in whole-cell mode is compensated for electronically (as part of the process for compensating the series resistance, described in section 2.6.4) by adding a transient component to the command potential. Similarly, in current clamp mode, the amplifier electronically reduces the effective value of the pipette capacitance by injecting a transient current into the headstage input to charge and discharge the pipette capacitance during signal changes (page 33, Multiclamp 700B manual) in order for a voltage change to be measured more accurately.

2.8 Labelling of cells

2.8.1 Immunohistochemistry

For the ischaemia experiments in chapter 3, hippocampal slices (270 μm) were prepared (as described in section 2.1) and, following the incubation period for the ischaemic experiments, slices were fixed in 4% PFA and transfered to the Richardson lab for immunolabelling. Slices were then blocked with 1x PBS containing 10% foetal bovine serum (FBS) and 0.1% Triton-X100 for 1 hour at RT and subsequently

incubated with the primary antibody at an appropriate dilution in 1x PBS with 5% FBS and 0.1% Triton-X100 at 4˚C overnight (ON). On the next day, slices were incubated with secondary antibodies (Alexa-conjugated secondary antibodies coupled to the fluorophores 488, 568 or 647, Thermo Fisher) for 2 hours at RT. The list of primary antibodies used in this study was as follow: mouse Neun, mouse, 1/200 dilution, Millipore; guinea pig Sox10, 1/2000 dilution, a gift from the Wegner Lab; rabbit PDGFRα, 1/500 dilution, Cell Signalling; chicken GFAP, 1/1000 dilution, Abcam; mouse S100β, 1/500 dilution, Sigma).

For the experiments involving the dialysis of biocytin within the network of astrocytes in chapter 3, hippocampal slices (270 μm) were prepared (as described in section 2.2) and, following a dialysis period of 20 min, the patch pipette was carefully removed to allow the membrane to seal. Slices were then fixed in 4% PFA for 1 hour at RT and then rinsed 4 times in 1x PBS. At this stage, the slices were given to Sarah Jolly in the Richardson Lab for staining of biocytin and image analysis. This involved incubating the slices with the anti-GFP antibody diluted in the blocking medium overnight at 4˚C. The following day, slices were rinsed 3x 10 minutes in PBS and endogenous peroxidases were inactivated by incubating the slices in 3% H_2O_2 (Sigma) in PBS. The slices were extensively rinsed 4 times in PBS and incubated with the secondary antibody (anti-rat 488 Alexa-antibody) in PBS with 10% FBS and 0.1% Triton-x100 for 5 hours at RT. The Avidin/Biotinylated enzyme complex (Vector Labs, PK-6100) was then incubated for 40 min at RT with the slices (longer times resulted in high background). The fluorescent tyramide was then added to the slices for 10 minutes at RT (Cyanine 5 – tyramide diluted 1/100 into the Amplification diluent, TSA™ Plus Fluorescein System, Perkin Elmer). Finally the slices were washed in 1x PBS, counterstained with Hoechst and mounted with the Dako

fluorescence mounting medium.

For the experiments in chapter 4, Sprague-Dawley rats at postnatal day 12 were used and dissection of the brain tissue was performed as described in 2.2. Each hemisphere was then stored in 4% PFA overnight at 4°C. Hippocampal slices (50 μm thick) were cut the next day in ice-cold solution containing PBS containing 0.2M glycine, and were then washed in PBS before blocking non-specific labelling with 10% normal goat serum in PBS containing 0.5% Triton, 0.2M glycine, 1% bovine serum albumin (BSA) on a shaker at RT for 1 hour. All primary and secondary antibody incubations were diluted in PBS. Slices were simultaneously incubated with primary antibodies against glial fibrillary acidic protein (GFAP) (monoclonal chicken, diluted 1:2000, AbCam, Ab4674) and against one adrenoceptor (AR) subtype: α1A-AR (monoclonal rabbit, diluted 1:100, Alomone Labs), α1B-AR (monoclonal rabbit, diluted 1:100, Alomone Labs), α2A-AR (monoclonal rabbit, 1:200 as suggested by Alomone Labs), or β1-AR (monoclonal rabbit, diluted 1:400 as suggested by Alomone Labs) at 4°C overnight, while shaking. Primary labelling was followed by 3 x 15 minutes washes in PBS before applying Alexa Fluor 647-conjugated donkey anti-chicken (diluted 1:2000, Molecular Probes) and Alexa Fluor 488-conjugated goat anti-rabbit (diluted 1:1000, Molecular Probes) at 4°C for 4 hours in the dark, while shaking. Slices were then washed 3 x 15 minutes in PBS and counterstained with 4',6-diamidino-2-phenylindole (DAPI) in PBS at RT for 15 minutes. After staining, slices were mounted on slides using DAKO Fluorescent mounting medium (DAKO North America, Inc). Four independent sets of immunolabelling experiments were performed to check reproducibility (see section 2.8.2 for further discussion).

2.8.2 In situ hybridisation coupled with immunohistochemistry (conducted by Dr. Jolly)

For experiments in Fig. 3.1, coronal brain slices (15 µm) were cut on a cryostat, collected on Superfrost Plus microscope slides (VWR International) and left to dry for 1 hour at RT. Sections were hybridized at 65˚C overnight with the digoxigenin (DIG)-labelled antisense RNA probe (1:1000) diluted in pre-warmed hybridization buffer (DEPC-treated deionized water with 50% (v/v) deionized formamide, 200 mM NaCl, 5 mM EDTA, 10 mM Tris-HCl pH 7.5, 5 mM NaH_2PO_4, 5 mM Na_2HPO_4, 0.01 mg/ml yeast tRNA, 1× Denhardt's solution, and 10% w/v dextran sulphate). Slices were washed three times for 20 min at 65˚C with a washing solution (150 mM NaCl, 15 mM $Na_3C_3H_5O(COO)_3$ (= 1x saline sodium citrate), 50% (v/v) formamide and 0.1% (v/v) Tween-20), followed by two washes of 15 min at RT in MABT (100 mM maleic acid, 150 mM NaCl, 0.1% (v/v) Tween-20, pH 7.5). Slices were subsequently blocked for 1 hour at RT with a blocking solution (MABT with 2% blocking reagent and 10% heat-inactivated sheep serum) and then incubated overnight at 4˚C with the anti-DIG antibody conjugated with alkaline phosphatase (AP) (Roche Diagnostics, 1:1500 in blocking solution). Next, the slices were washed with MABT for 10 min three times at RT, followed by two washes of 5 min in 0.1 M Tris-HCl pH 8.2. Immediately before use, the Fast Red solution (Roche) was prepared by dissolving the tablets in 0.1 M Tris pH 8.2, and then filtered through a 0.22 µm filter. Slices were incubated with Fast Red for 2 to 3 hours at 37˚C. Finally, the slices were washed three times with 1x PBS and immunohistochemistry staining was performed.

For antibody labelling, slices were blocked with PBS containing 10% foetal bovine serum (FBS) and 0.1% Triton-X100 for 1 hour at RT. Subsequently, these slices were incubated with the primary antibody at an appropriate dilution in PBS with

5% FBS and 0.1% Triton-X100 at 4˚C overnight (ON). The next day, slices were incubated with secondary antibodies (Alexa-conjugated secondary antibodies coupled to the fluorophores 488, 568 or 647, Thermo Fisher) for 2 hours at RT. The list of primary antibodies used in this study was as follows: mouse NeuN, 1/200 dilution, Millipore; guinea pig Sox10, 1/2000 dilution, a gift from the Wegner Lab; rabbit PDGFRα, 1/500 dilution, Cell Signalling; mouse GFAP, 1/500 dilution, Abcam; mouse S100β, 1/500 dilution, Sigma).

For each marker, different dilutions were used prior to choosing the final concentration. The specificity of the immunolabelling was established by omitting each of the primary antibodies in turn. A more thorough approach would be to assess the staining using positive controls (e.g. co-labelling with other markers that stain the cell/receptor of interest) and negative controls (e.g. using transgenic tissue or label regions where the cell or receptor of interest is not expressed).

2.9 Confocal imaging and set-up

For experiments in chapter 4, fixed slices were imaged with an inverted confocal laser scanning microscope (Leica TCS SPE for chapter 3 or Zeiss LSM 700 for chapter 4). Images were taken with x10, x20, or x63 oil DIC objectives. All imaging with multiple wavelengths was carried out with sequential scans, in order to minimise "bleed through" from one channel to another. The standard excitation and emission filters provided on the microscopes for visualizing Hoechst 33258, DAPI, Alexa Fluor 488, and Alexa Fluor 647 were used. Scanning areas of interest in slices was done in the x-y and z directions, and averaged 2-4 times depending on the signal. The gain and offset parameters and the size of the z-stack were kept fixed. Image analysis was with ImageJ (NIH) unless otherwise stated.

2.10 Statistics

Data are represented as mean ± sem. P values are from 2-tailed Student's t tests (either paired or unpaired), 2-way ANOVA, or Kolmogorov–Smirnov test, as appropriate. A normality test, the F-test, was applied prior to an unpaired t-test, to address whether the two sets of data fit a normal distribution. The type of t-test used is indicated in the appropriate figure legend. Data were corrected for multiple comparisons, when appropriate, using a procedure equivalent to the Holm-Bonferroni method (for N comparisons, the most significant p value is multiplied by N, the 2nd most significant by N-1, the 3rd most significant by N-2, etc.; corrected p values are significant if they are less than 0.05).

Chapter 3:

Neuroprotective role of a glial specific GPCR

3.1 Summary of this chapter

There is evidence for different functional subtypes of astrocytes (see Bayraktar *et al*., 2015 for a recent review), but progress in this area has been hampered by a lack of subtype-specific molecular markers. A screen of the Allen Brain Atlas gene expression database by the Richardson Lab at UCL resulted in the identification of *GPR37-like 1 (GPR37l1)* as an mRNA that is differentially expressed in different astrocytes. The *GPR37l1* gene encodes a G-protein coupled receptor, referred to as GPCR37L1. *GPR37l1* is first expressed in a subset of astrocytes and oligodendrocyte precursors (OPCs) in the brain at around postnatal day 8, and its expression continues throughout adulthood. In collaboration with the Richardson Lab, I characterised the electrophysiological properties of astrocytes expressing and lacking GPCR37L1. The results showed that GPCR37L1-positive and -negative astrocytes are interconnected within the same astroglial network, and have similar membrane properties. Importantly, I found that the expression of GPCR37L1, and its activation by its putative ligand, prosaptide, are neuroprotective in *in vitro* models of ischaemia. Investigating the mechanisms underlying this, I demonstrated that GPCR37L1 signalling both reduces neuronal NMDA receptor activity and inhibits activity of the glutamate transporters in astrocytes. Both of these effects can confer neuroprotection during ischaemia, as discussed below.

3.2 Introduction

Although some G protein coupled receptors (GPCRs) are widely expressed in most cells (such as α_1-adrenoceptors), some are cell-type specific. This latter group can serve as selective molecular markers. Despite a well-established selection of markers for different developmental stages of the oligodendrocyte cell lineage, there are relatively few reliable markers for astrocytes. Thus, an astrocyte-specific molecular marker would be particularly useful. In the search for new molecular markers, several researchers have studied gene transcription patterns in the major glial, neuronal and vascular brain cell populations (Cahoy et al. 2008; Doyle et al. 2008; Zhang et al. 2014). Similarly, the Richardson Lab, at UCL, conducted a visual screen of the Allen Brain Atlas *in situ* hybridization database of gene expression patterns in the postnatal mouse brain, to look for potential glial markers. Their search (unpublished) revealed a glial selective pattern of expression for *GPR37like-1 (GPR37L1),* with heterogeneous expression among astrocytes and oligodendrocyte precursor cells.

As described in chapter 1 (section 1.2.7.6.3), not much is known about the function of this receptor in the CNS, apart from a suggested role in cerebellar development, which involves an interaction with Sonic hedgehog signalling (Marazziti et al., 2013). The receptor can be activated by an endogenous ligand prosaposin (a polypeptide), which also activates the related receptor GPCR37 (Meyer et al. 2013). It has been shown that prosaposin expression and release are enhanced following conditions of cellular stress such as ischaemia (Costain et al. 2010; Hiraiwa et al. 2003; Yokota et al. 2001), and prosaposin, as well as prosaptide (an active cleavage product of prosaposin), are thought to promote cell survival (Meyer et al. 2014; Morita et al. 2001; Sano et al. 1994), through the activation of GPCR37 and

GPCR37L1 (Meyer et al., 2014). I therefore assessed the function of GPCR37L1 in astrocytes, in collaboration with a post-doc from the Richardson Lab, Dr. Sarah Jolly.

I provide evidence that: (i) GPCR37L1 expression does not change the basic membrane properties of astrocytes; (ii) GPCR37L1-positive and -negative astrocytes form gap junctions within the same interconnected networks; (iii) GPCR37L1 expression and signalling via its ligand (prosaptide) are neuroprotective in ischaemic brain slices; (iv) GPCR37L1-signalling by prosaptide reduces neuronal NMDA receptor activity; and (v) prosaptide signalling also inhibits the glutamate transporters in astrocytes. I suggest that the latter two effects could confer neuroprotection during ischaemia.

3.3 Methods

3.3.1 Animals

As described in chapter 2, GPCR37L1 knock-out mice and GPCR37L1-GFP transgenic mice were obtained from the Richardson Lab. In the latter mice, GFP-positive cells expressed the GPCR37L1 protein and GFP-negative cells did not express the GPCR37L1 protein.

3.3.2 Analysis of GPCR37L1 expression

In situ hybridization and immunohistochemistry experiments for Fig. 3.1 were carried out using coronal brain slices (15 μm). Digoxigenin (DIG)-labelled antisense RNA probe (1:1000 dilution), and primary antibodies [mouse NeuN (1:200 dilution), guinea pig Sox10 (1:2000 dilution), rabbit PDGFRα (1:500 dilution), mouse GFAP (1:500 dilution), and mouse S100β (1:500 dilution)] were used as described in detail in section 2.8.2.

3.3.3 Electrophysiology

3.3.3.1 Slice preparation

Hippocampal slices (270 μm thick) were prepared from the GPCR37L1 knockout mice ($GPCR37L1^{-/-}$) and their wild-type littermates ($GPCR37L1^{+/+}$), or alternatively from the transgenic mice with cells that were GFP-positive (i.e. expressing GPCR37L1) or GFP-negative (i.e. without GPCR37L1 expression), at postnatal day 14-16 (as described in section 2.2). Following the slicing procedure, the slices were then transferred to a heated chamber at 30°C for 40 min, and subsequently removed and allowed to reach RT for a further 20 min prior to recording.

3.3.3.2 Whole-cell patch clamp recording

Neurons and astrocytes were selected visually for patch-clamping, and after entering whole cell mode the diffusion of Alexa Fluor 488 into the somata and the apical dendrites of the pyramidal neurons, and of Alexa Fluor 488/594 into the astrocytic processes, confirmed the cells' identities. The presence of a large voltage-gated sodium current, or a passive current-voltage relation across all the voltage steps (section 2.4), further confirmed the identity of cells as being pyramidal neurons or astrocytes, respectively.

3.3.3.3 Extracellular solutions

In the recording chamber, slices were perfused with a solution that mimics the cerebrospinal fluid (artificial cerebrospinal fluid, aCSF) containing (in mM): 140 NaCl, 10 HEPES, 10 glucose, 2.5 KCl, 2 $CaCl_2$, 1 NaH_2PO_4, 1 $MgCl_2$, pH 7.4 with NaOH, osmolarity 300 mOsm (bubbled with 100% O_2). This solution was perfused through the recording chamber by the use of a gravity perfusion method (as described in section 2.3.1). The flow rate was set to ~3-4 ml/min. Electrophysiology experiments were carried out at RT. Prosaptide and / or pharmacological blockers of action potentials, GABA and glutamate receptors, and glutamate uptake were added as appropriate, as described in section 2.3.1.1. Glutamate uptake currents were evoked in pharmacologically isolated manner, as described in section 2.3.1.1. All experiments on wild-type versus knockout animals were performed with me being blind to the genotype of the mouse.

3.3.3.4 Intracellular solutions

Whole-cell patch clamp recordings were made from neurons using a caesium-

gluconate based solution (as described in section 2.3.2). A potassium gluconate based solution was used to record from astrocytes (as described in section 2.3.2).

3.3.3.5 Field excitatory postsynaptic currents recordings

Hippocampal slices were prepared (as described in section 3.3.3.1) from GPCR37L1$^{+/+}$ or the GPCR37L1$^{-/-}$ mice (at P14-16). The CA3 pyramidal axon initial segments were stimulated as described in section 2.6.3, which evoked field excitatory postsynaptic currents (fEPSCs, recorded in voltage clamp mode in area CA1).

3.3.3.6 Biocytin labelling

Hippocampal slices were prepared (as described in section 3.3.3.1) from transgenic GPCR37L1-GFP mice (at P14-16) and whole-cell patch clamp recordings were made from astrocytes in the stratum radiatum using an internal solution that included biocytin (see section 2.3.2 on intracellular solutions). Following the dialysis of biocytin for at least 20 min, the patch pipette was carefully removed to allow the membrane to seal. Slices were then fixed in 4% PFA for 1 hour at RT and then rinsed 4 times in PBS. At this stage, the slices were given to Dr. Jolly for staining against biocytin and image analysis (as described in 2.8.1).

3.3.4 Chemical ischaemia

Chemical ischaemia was performed as previously described by Hall *et al*. (2014). Hippocampal slices were prepared (as described in section 3.3.3.1) from GPCR37L1$^{+/+}$ or the GPCR37L1$^{-/-}$ mice (at P14-16). The slices were allowed to recover for 40 min before being incubated for 30 min at 37°C in (i) a control solution containing aCSF or (ii) an ischaemic solution, as described in section 2.3.1.1, before

being given to Dr. Jolly to perform immunolabelling against NeuN and GFAP (see section 2.8.1). A minimum of two brain slices were used per animal per condition. Four pictures were taken and PI-labelled cells were counted in both the stratum radiatum and the pyramidal layer of the hippocampus at standardised locations. The quantification of cell death was performed with the experimenters blind to the mouse genotype. The size of the z-stack was fixed at 25 µm with a z-step of 0.5 µm. The gain and the offset settings for the imaging were chosen for the first set of images and were then fixed for all the slices.

3.3.5 Statistical analysis

Statistical significance was determined with Origin Pro or Excel. All the values in the text and figures are means ± s.e.m. Further details of the statistical analysis are given in section 2.10.

3.4 Results

3.4.1 GPR37L1 is expressed in a subpopulation of astrocytes and oligodendrocyte precursor cells from the second postnatal week

The expression pattern of *GPR37L1* in the brain has not previously been clearly established. To determine the expression pattern of *GPR37L1*, Dr. Jolly combined in situ hybridization (ISH), using a probe against *GPR37L1* mRNA, with immunostaining for GFAP (an astrocyte marker), or PDGFRα (an OPC marker). Co-localisation of *GPR37L1* mRNA with an antibody against GFAP or PDGFRα showed that *GPR37L1* was expressed in a subset of astrocytes and a subset of OPCs in the cortex and the hippocampus (Fig. 3.1A). These results were further confirmed when *GPR37L1* mRNA co-localisation with another astrocyte marker, S100β, and an oligodendrocyte lineage marker (Sox10), were quantified. In fact, 22±2% of astrocytes and 63±4% of OPCs expressed this receptor in the cortex, while 33±2% of astrocytes and 75±2% of OPCs expressed this receptor in the hippocampus (Fig. 3.1B). In contrast, *GPR37L1* was not expressed in neurons, microglia, or mature myelinating oligodendrocytes (using immunolabelling markers NeuN, Iba-1 and CC1 respectively, data not shown).

Next, the expression pattern of *GPR37L1* during brain development was examined. While expression of *GPR37L1* was not detectable at birth (when measured at P1, Fig. 3.1C), its expression increased from the second postnatal week (see data at P8), and was maintained at 4 months. This suggests that GPCR37L1 may have a functional role from the period of synaptogenesis and myelination through to adulthood.

After the Richardson Lab discovered this novel marker for a subset of astrocytes and OPCs, I assessed the function of GPCR37L1 in hippocampal astrocytes.

3.4.2 GPCR37L1 expression does not alter the basic membrane properties of, and gap junction formation by, astrocytes

I initially assessed whether astrocytes expressing or lacking GPCR37L1 differed in their membrane resistance (Rm) and resting potential (Vrest). To do this, I conducted patch-clamp recordings from visually selected GFP-positive or GFP-negative astrocytes in slices from the GPCR37L1-GFP mouse, or alternatively from astrocytes in slices from the wild-type (WT) or the GPCR37L1 knockout (KO). I found that GFP-positive and GFP-negative cells had a similar membrane resistance (Fig. 3.2A, 5.2±1.4 MΩ for GFP-positive cells, n=9, and 5.3±1.5 MΩ for GFP-negative cells, n=6, unpaired t-test p=0.9), and resting potential (Fig. 3.2B, -94.8±1.5 mV for GFP-positive cells, and -94.9±1.4 mV for GFP-negative cells, t-test p=0.9). Similarly, deletion of the *GPR37L1* gene did not affect these basic membrane properties (Fig. 3.2C & D). The resistance was 5.4±0.6 MΩ for 25 astrocytes in the WT mouse, and 5.1±0.5 MΩ for 29 astrocytes in the KO mouse (unpaired t-test p=0.7), while the resting potential was -93.4±0.4 mV for the astrocytes in the WT, and -92.7±0.4 MΩ for the astrocytes in the KO (t-test p=0.2).

Next, I examined whether the expression of GPCR37L1 in a subset of astrocytes confers changes in their ability to form gap junctions within the astrocyte network. Specifically, do astrocytes that express GPCR37L1 form gap junctions with one another preferentially, or do they also form gap junctions with astrocytes lacking GPCR37L1? To answer this, I conducted voltage-clamp recordings from GFP-positive and -negative astrocytes in the stratum radiatum area of the hippocampus. I held them near their resting potential (typically around -93 mV) and dialysed the cells with biocytin (through the patch pipette). This method allowed biocytin to spread through the network of astrocytes and revealed the extent of their gap junctional coupling (an

approach used previously by Xu *et al.*, 2010). Dialysis of biocytin for a minimum of 20 min revealed that astrocytes form gap junctions with other astrocytes irrespective of their expression of GPCR37L1 (Fig. 3.3). Furthermore, the lack of a difference of input resistance between astrocytes expressing and lacking GPCR37L1 (Fig. 3.2A) argues against a major difference in the number of gap junctions made by the two classes of astrocyte (since a larger number of gap junctions will tend to lower the input resistance by allowing current flow to adjacent cells).

These experiments confirm that the expression of GPCR37L1 does not affect astrocyte basic membrane properties nor their gap junctional coupling.

3.4.3 GPCR37L1 expression and its activation are neuroprotective in ischaemia

Expression of GPCR37L1 in a subset of astrocytes (see Fig. 3.1) raises questions as to its functional importance. A recent study has identified prosaposin as an endogenous ligand for GPCR37 and GPCR37L1 (Meyer *et al.*, 2013). They also showed that prosaposin protects primary cultured astrocytes against oxidative stress. Curiously, others have reported that the expression of prosaposin is upregulated following kainic-acid induced neurotoxicity (Nabeka et al., 2014, 2015). Furthermore, prosaposin and its analogue, prosaptide, are reported to be neuroprotective in *in vivo* models of ischaemia (Lu *et al.*, 2000; Morita et al. 2001; Sano et al., 1994). These findings increase the possibility that the neuroprotective effects of prosaposin (or prosaptide) in neurotoxicity and ischaemia may involve signalling through GPCR37 and GPCR37L1. Therefore, I examined the effects of GPCR37L1 expression, and its activation following the addition of the prosaposin analogue prosaptide, on cell death in ischaemia.

Hippocampal slices from the WT and the KO animals were incubated for 30 min at 37°C in a solution containing aCSF (control) or in a solution that evoked ischaemic damage (with O_2 and glucose removed, and containing iodoacetate to block glycolysis and antimycin to block oxidative phosphorylation: Hall *et al.*, 2014). Both solutions contained propidium iodide (PI, 7.5 µM), which becomes fluorescent when it gains access to cells and binds to DNA/RNA, and which is commonly used to mark necrotic cell death in brain slices (Hall *et al.*, 2014; Vivar *et al.*, 2013). Slices were then fixed with 4% PFA for 1 hour prior to being transferred to the Richardson Lab for cell death quantification.

Cell death was detectable after 30 min of chemical ischaemia in the CA1 pyramidal layer (where nuclear PI staining colocalised with a neuronal marker, NeuN, Fig. 3.4A) and in the stratum radiatum (where PI staining was often surrounded by cytosolic GFAP staining in astrocytes, suggesting that many dead cells were astrocytes, data not shown in figure). The percentage of cell death was low for both the WT and the KO slices after 30 min in the control solution (3.2±1.6% of pyramidal layer neurons and 1.7±0.8% of stratum radiatum astrocytes in the WT, and 2.6±2.0% of neurons and 2.3±0.8% of astrocytes in the KO, in 12 slices from 6 animals for each genotype, showed nuclear PI staining). Ischaemia significantly increased cell death (Fig. 3.4B) and, to our surprise, the expression of GPCR37L1 was sufficient to significantly prevent cell death in the pyramidal cell layer during ischaemia (Fig. 3.4B, 13.6±1.1% PI staining in the WT compared to 21.3±2.9% in the KO, n=6, two-way ANOVA with Holm-Bonferroni correction for multiple comparisons p=0.016). There was, however, no difference in cell death in the stratum radiatum (16.0±1.6% PI staining in the WT compared to 17.3±2.9% in the KO, 12 slices from 6 animals for each genotype, data not shown in figure). This may be due to a different cell type (e.g.

mainly astrocytes) dying in the stratum radiatum in response to the chemical ischaemia protocol used in this experiment, or alternatively, due to quantification of cell death for the stratum radiatum being in more superficial layers of the slice, where cells are more unhealthy.

Furthermore, the addition of prosaptide (10 μM) significantly reduced cell death in the pyramidal layer of the WT (a 25.5% decrease was seen when comparing cell death in ischaemia with and without prosaptide, n=4, two-way ANOVA p=0.011, Fig. 3.4C). This concentration of prosaptide was chosen based on the observed electrophysiological responses seen in astrocytes (see sections 3.4.4.2 and 3.4.4.3). Prosaptide also decreased cell death in the pyramidal layer of the KO animals but to a lesser extent (20% decrease, n=4, two-way ANOVA p=0.008, Fig. 3.4C). There was, however, no difference in ischaemia-evoked cell death in the stratum radiatum in the presence of prosaptide in the WT or the KO (1.1% increase in cell death for the WT, p=0.6, and 0.9% increase for the KO, p=0.8, data not shown in figure).

Thus, the activation of GPCR37L1 in ischaemia in the absence of added prosaptide (presumably by the release of endogenous prosaposin), along with further stimulation of this receptor when prosaptide was present, are neuroprotective in the pyramidal layer of the hippocampus.

3.4.4 Mechanisms underlying the neuroprotective role of GPCR37L1

3.4.4.1 Assessment of neuronal membrane properties

Exposure to high levels of glutamate and consequent activation of NMDA and AMPA/KA receptors is excitotoxic in the brain (Olney and Sharpe 1969). Ischaemia releases glutamate through reversal of glutamate transporters, and inhibiting glutamate receptors largely blocks the ischaemia-evoked neuronal depolarisation and the NMDA

receptor-mediated calcium entry that evokes cell death (Rossi, Oshima & Attwell, 2000). Thus, an increase in cell survival during ischaemia in the WT (Fig. 3.4) might (among other possibilities) reflect either a lower extracellular glutamate level during ischaemia, or a decrease in glutamate receptor activation by a given level of glutamate.

Various factors may alter glutamate release and its postsynaptic effect at the CA3 to CA1 synapse. For instance, it is plausible that the CA3 neurons that form the Schaffer collateral terminals projecting to CA1 neurons have an altered threshold for action potential generation and glutamate release in the GPCR37L1 KO compared to the WT, which could lead to altered glutamate release and cell death during ischaemia. To assess any differences in the excitability of CA3 neurons in the presence and absence of GPCR37L1, I conducted whole-cell patch-clamp recordings from CA3 pyramidal neurons in hippocampal slices in current clamp mode, injected different current steps and assessed the voltage responses of the cells. This allowed comparison of the cells' firing likelihood and the latency to the 1st action potential, between the WT and the KO slices.

I found no difference in the excitability of CA3 pyramidal neurons between the WT and the GPCR37L1 KO, as measured by the latency to the first action potential evoked by depolarising current injected at the soma (t-test p=0.96, n=15 for the WT, and n=14 for the KO, Fig. 3.5A), nor was there a difference in the firing probability as a function of injected current magnitude (Kolmogorov-Smirnov test p=0.49, Fig. 3.5B), suggesting that synaptic input (or ischaemia-evoked depolarization) would not lead to an increased number of active presynaptic fibres impinging on CA1 pyramidal cells. CA3 neurons also had a similar membrane resistance (t-test p=0.39, Fig. 3.5C) and resting potential (t-test p=0.93, Fig. 3.5D). Furthermore, when recording the stimulation-evoked field excitatory postsynaptic currents (fEPSCs) generated by CA1

cells in response to Schaffer collateral stimulation (Fig. 3.6), the dependence of fEPSC amplitude on stimulus magnitude (between 0 and 100V, fEPSCs were normalised to the fEPSC produced by a 100V stimulus) was similar in the WT and the KO (Fig. 3.6, a Kolmogorov–Smirnov test showed no difference between the two curves, p=0.27, n=8 for the WT, and n=9 for the KO). These data suggest there is no difference in excitability of CA3 neurons or their axons between the WT and the GPCR37L1 KO.

An alternative explanation for more ischaemia-evoked neuronal death occurring in the GPCR37L1 KO (Fig. 3.4) could involve an increase in total glutamate receptor number in CA1 cells in the KO, which would lead to more depolarisation, calcium influx, and cell death following glutamate release in ischaemia. To test this, I recorded responses (Fig. 3.7A) to kainate (3 µM, in the presence of the NMDA receptor blocker, D-AP5) or to NMDA (5 µM, in the presence of the AMPA/KA receptor blocker NBQX) in CA1 pyramidal neurons voltage clamped at -30mV to promote magnesium unbinding from NMDA receptor channels. However, no difference was seen between the WT and the KO in the size of the current evoked by kainate or NMDA (responses were measured at a fixed time after starting the application of KA or NMDA). The mean currents evoked by kainate were 30±5 pA for the WT (n=14) and 26±3 pA for the KO (n=12) which were not significantly different (t-test p=0.52). The mean currents evoked by NMDA were 106±12 pA for the WT (n=12) and 97±10 pA for the KO (n=14) which were also not significantly different (t-test p=0.57, Fig. 3.7A & B). CA1 pyramidal neurons in the WT and KO also had similar membrane resistances (300±36 MΩ for the WT, n=14, and 300±32 MΩ for the KO, n=14, t-test p=0.9, Fig. 3.7C) and cell capacitances (68.0±4.0 pF for the WT, n=14, and 62.0±3.0 pF for the KO, n=14, t-test p=0.4, Fig. 3.7D).

These results suggest that the enhanced cell death seen during ischaemia in the KO cannot be explained by changes in presynaptic excitability or postsynaptic receptor number.

3.4.4.2 Prosaptide signalling through GPCR37L1 decreases neuronal NMDA responses

Prolonged application of NMDA evoked a slowly increasing inward current at least over 10 mins (Fig. 3.7A) suggesting a sensitization of the NMDA response with time. Similarly, repeated (x3) brief (~3 min, at 4 min intervals) application of NMDA (5 µM, Fig. 3.8A), resulted in a progressive increase in the magnitude of the response recorded in CA1 pyramidal neurons. In both the WT and the KO, the response to the second application of NMDA was always bigger, leading to a ratio > 1 when comparing the second to the initial response (Fig. 3.8B, mean ratio=1.5±0.1, one sample t-test, significantly greater than 1, p=0.025, n=4, for the WT; mean ratio=1.2±0.1, p=0.019, n=4, for the KO). The potentiation was not significantly similar between the WT and the KO (unpaired t-test, p=0.12).

NMDA receptor-mediated calcium entry is largely responsible for the neuronal death that occurs following ischaemia (Goldberg *et al*., 1987; Vornov & Coyle, 1991; Brassai *et al.* 2015; Robinson & Jackson, 2016). Thus, the increase in the NMDA receptor conductance (on prolonged or repeated application of NMDA, Fig. 3.7A & 3.8A), which may mimic NMDAR behaviour in ischaemia, may potentiate neuronal death. Although this potentiation of the NMDA response did not differ between the WT and the KO in normoxic conditions (Fig. 3.8B), in ischaemia prosaposin is released (Costain et al. 2010; Hiraiwa et al. 2003; Yokota et al. 2001) and therefore, this protocol of repeated NMDA application was used to examine the potential effect

of prosaposin-evoked GPCR37L1 signalling on the increase of the neuronal NMDA response. An effect of astrocyte GPCR37L1 on neuronal NMDA responses is plausible as astrocyte-mediated regulation of the size of NMDA receptor responses, mediated by Ca^{2+}-dependent gliotransmission, has already been reported at this synapse (Henneberger et al., 2010; Shigetomi *et al.*, 2013).

Therefore, I repeatedly applied NMDA in the absence and then in the presence of the prosaposin analogue, prosaptide (10 μM, which was bath applied prior to, and throughout, the second application of 5 μM NMDA). Surprisingly, application of prosaptide during the second application of NMDA, blocked the potentiation of the NMDA current in the WT (Fig. 3.8C, mean ratio=0.79±0.14, one sample t-test not significantly different from 1, p=0.2, n=8), without affecting the NMDA potentiation response in the KO (Fig. 3.8C, mean ratio=1.48±0.12, one sample t-test significantly different from 1, p=0.016, n=5). Thus the ratio in the KO was not significantly different with or without prosaptide applied with the second application of NMDA (p=0.15). In contrast, in the WT the ratio was significantly less with prosaptide applied (Fig. 3.8B) than in its absence (Fig. 3.8C, p=0.009).

These results suggest that GPCR37L1-mediated signalling in astrocytes decreases the neuronal NMDA receptor response during prolonged activation of the NMDA receptors. This is important as it provides a likely neuroprotective mechanism when both glutamate and prosaposin are released during ischaemia. A reduction in cell death in the WT or with prosaptide added (Fig. 3.4B & C) is consistent with endogenous prosaposin release (or the addition of prosaptide) activating GPCR37L1-mediated signalling, which in turn reduces NMDA receptor-mediated calcium entry and cell death. Possible mechanisms of this effect are considered in the discussion below.

3.4.4.3 Assessment of glutamate uptake in astrocytes

In addition to the analysis above of how prosaposin and GPCR37L1 affect NMDARs, I also investigated how astrocyte GPCR37L1 might affect the glutamate level reached in ischaemia. Under physiological conditions, neuronal and glial transporters rapidly take up synaptically released glutamate from the extracellular space (Schousboe 1981; Robinson & Jackson, 2016). Thus, any inhibition of the rapid clearance of glutamate by the glial or neuronal transporters could elevate the extracellular level of glutamate, while a reduction of the glutamate transport rate might decrease the extracellular glutamate concentration reached in ischaemia when glutamate transporters reverse and release glutamate (Rossi *et al*., 2000; but note that glial transporters appear to play a small role in this phenomenon: Hamann *et al*., 2002). Such a reduction in glutamate release would tend to reduce NMDAR-mediated cell death in ischaemia (Robinson & Jackson, 2016; Vornov & Coyle, 1991; Brassai *et al.* 2015).

I compared the magnitude of the glutamate transporter current evoked by D-aspartate (i.e. reflecting glutamate uptake) in the WT and the KO hippocampal astrocytes. To do this, astrocytes in the stratum radiatum were whole-cell voltage clamped (near their resting potential) and responses to D-aspartate (200 μM, a substrate for glutamate transporters that has little effect on glutamate receptors, Gundersen et al. 1995) were recorded in the presence and absence of the glutamate transporter blocker, TFB-TBOA (10 μM, see Fig. 3.10A). Blockers for ionotropic glutamate and GABA receptors, voltage-gated sodium channels and inwardly rectifying potassium channels were also present throughout the experiment to isolate the transporter current and to block any effects (on neurons or glia) of glutamate

release through hetero-exchange (see section 2.3.1.1 in this chapter for more information).

The size of the glutamate uptake current was similar in GPCR37L1 KO astrocytes and in WT astrocytes (Fig. 3.10B, mean current=-44±4 pA for the WT, n=16; and -45±4 pA for the KO, n=23, unpaired t-test p=0.97). The glial glutamate transporter blocker, TFB-TBOA, which blocks both GLT-1 and GLAST transporters (Shimamoto *et al*., 2004), blocked the D-aspartate evoked current in both the WT and the KO, confirming that the current is generated by glutamate transporters (Fig. 3.10C, mean percentage block=90±7% for the WT, and 98±6% for the KO, not significantly different, unpaired t-test p=0.4).

These results suggest that the removal of glutamate by astrocytes, under non-ischaemic conditions, are not different in WT and KO animals. However, the possibility remains that there is no tonic activation of GPCR37L1 under normal conditions, and that it could modulate glutamate transport when prosaposin is released in ischaemia (Costain *et al*., 2010; Hiraiwa *et al*., 2003). I examine this possibility in the next section.

3.4.4.4 Prosaptide signalling via GPCR37L1 inhibits glutamate transport

In early ischaemia, the slowing of the sodium pump caused by a loss of energy supply leads to neuronal depolarisation and increased exocytotic release of glutamate (Dawson *et al*., 2000). In severe ischaemia, complete cessation of operation of the sodium pump and the resulting large depolarisation of cells leads to a reversal of glutamate transporters, which further increases the extracellular glutamate concentration to a level of hundreds of micromolar (Rossi, Oshima & Attwell, 2000; for a recent review see Krzyżanowska *et* al., 2014). Although both glial and neuronal

glutamate transporters are expected to reverse in ischaemia, experiments on mice lacking the main glial transporter GLT-1 (Hamann *et al*., 2002) have suggested that reversal of these transporters contributes much less to the elevation of extracellular glutamate concentration than does reversal of neuronal glutamate transporters (Gebhardt *et al*., 2002). Nevertheless, modulation of glial glutamate transporters could modulate glutamate dynamics in ischaemia and thus modulate neuronal death.

It is known that the expression and release of prosaposin are upregulated following ischaemia (Costain *et al*., 2010; Hiraiwa *et al*., 2003) and that both prosaposin and its analogue, prosaptide, exert neuroprotective effects in ischaemia (see Fig. 3.4; but also Lu *et al*., 2000; Morita *et al*., 2001; Sano *et al*., 1994). Importantly, results from this chapter suggest that GPCR37L1-mediated signalling provides neuroprotection during ischaemia (see Fig. 3.4B & C). Therefore, I investigated the effect of prosaptide on the D-aspartate (200μM) evoked glutamate transporter current, to test whether it modulates the uptake current in the presence of GPCR37L1 (i.e. in the WT) compared to its absence (in the KO).

Surprisingly, the results showed that the addition of prosaptide (10μM), at the peak of the current evoked by D-aspartate, significantly reduced the uptake current in the WT without affecting the current in the KO (Fig. 3.11B & C, mean inhibition= 31±3% for the WT, n=8, and -2±6% for the KO, n=8, significantly, different, t-test p=0.00003). Importantly, prosaptide failed to generate any current, in both the WT and the KO, in the absence of D-aspartate (Fig. 3.9C), showing that the outward current generated by prosaptide in the presence of D-aspartate reflects a suppression of uptake and not an effect on the baseline membrane current. The mean current generated by prosaptide was -1±2 pA for the WT (n=3, not significantly different from

zero, p=0.5), and 0.2±1.0 for the KO (n=4, not significantly different from zero, p=0.9).

This inhibition of astrocyte glutamate transporters by prosaptide in the WT might, in principle, play a neuroprotective role during ischaemia. If glial glutamate transporters can reverse in severe ischaemia (but see Hamann *et al*., 2002), and contribute to the release of glutamate (Rossi, Oshima & Attwell, 2000; Krzyżanowska, Pomierny, Filip & Pera, 2014), inhibition by prosaposin of glutamate transport (when operating in the reversal mode) would reduce glutamate release and excitotoxicity.

3.5 Discussion

Identification of GPCR37L1 by the Richardson Lab at UCL as a glial selective marker (unpublished), and the recent discovery of its endogenous ligand, prosaposin (Meyer *et al.*, 2013), call for an investigation into the functional importance of GPCR37L1 expressing cells. In this chapter, I have investigated the role of GPCR37L1 in astrocytes in the hippocampus.

Analysis of the expression pattern of *GPR37L1* revealed that a subgroup of astrocytes in the cortex (~22%) and in the hippocampus (~33%) express this receptor. In addition, the majority of OPCs express this receptor (~66% in the cortex and ~75% in the hippocampus, see Fig. 3.1A&B). These cells were identified using colocalisation of *GPR37l1* mRNA with antibodies commonly used to mark astrocytes (GFAP and S100β), or OPCs (Pdgfrα and Sox10). The apparently lower expression level of GPCR37L1 in astrocytes (compared to OPCs), however, is likely an underestimation. This is because (unlike for the OPC markers used), in the absence of a commercially available nuclear marker for astrocytes, quantification of colocalisation between a cytoplasmic marker of astrocytes (S100β) and mRNA

staining (which outlines the nuclei) is a challenge. This often led to the rejection of potential astrocytes due to ambiguity over whether the nuclear *in situ* labelling and the cytoplasmic S100β labelling were in the same cell.

Expression of *GPR37L1* is developmentally regulated. While there was no detectable staining at birth (measured at P1, Fig. 3.1C), *GPR37L1* mRNA expression was high during the second postnatal week (measured at P8), and this expression was maintained in adulthood (measured at 4 months). Similarly, the expression of prosaposin follows the same developmental trajectory, with no expression at birth, and high expression starting at P3-P7 (Morishita et al., 2014).

I used an array of detailed electrophysiological tests to investigate the functional importance of GPCR37L1 in hippocampal astrocytes residing in the stratum radiatum.

3.5.1 In search of a phenotype - GPCR37L1 confers neuroprotection in ischaemia

I assessed the basic membrane properties of astrocytes in brain slices prepared from: (i) mice expressing GFP under the promoter of *GPR37l1* promoter, which allowed direct comparison between cells expressing GPCR37L1 (GFP positive) and those that did not (GFP negative); and (ii) mice with global *Gpr37L1* gene deletion and their littermate wild-types. There was no apparent difference in the astrocyte membrane properties (i.e. membrane resistance and resting potential) in either of the two groups (see Fig. 3.2).

This lack of change in basic membrane properties probably suggests that the GPCR37L1 expressing astrocytes are likely to form an interconnected network with those that do not express this receptor. This is because deletion of the *GPR37l1* gene in less than half of all the astrocytes should have altered their input resistance had it

conferred changes in gap junctional coupling, since gap junctional coupling is thought to greatly lower the astrocyte input resistance (Meme *et al*., 2009). This was confirmed when I examined gap junctional coupling (using biocytin dialysis) in the GFP-positive and negative astrocytes (Fig. 3.3). Therefore, I conclude that the expression of GPCR37L1 does not affect astrocytes' basic membrane properties nor their gap junctional coupling.

A clue for a function of GPCR37L1 came from a recent study that identified prosaposin as an endogenous ligand for GPCR37 and GPCR37L1. It was claimed that prosaposin's action on GPCR37 and GPCR37L1 is glioprotective (as measured by cell death) against oxidative stress, in transfected HEK-293T cells and primary astrocyte cultures (Meyer *et al.*, 2013). Moreover, it has been reported that prosaposin expression is upregulated following glutamate-evoked excitoxocity (Nabeka *et al.*, 2014). This upregulation is likely to be a protective mechanism as prosaposin (or its analogue prosaptide) is reported to reduce learning disability (Sano *et al.*, 1994; Morita *et al.*, 2001), brain infarct area (Lu *et al.*, 2000), and neuronal death (Nabeka *et al.*, 2015), in *in vivo* rodent models of ischaemia. Thus, it is plausible that the neuroprotective effects of prosaposin (or prosaptide) in ischaemia involve activation of GPCR37L1. This, however, has not been tested before. Therefore, I examined the effects of GPCR37L1 expression, and its activation by prosaptide TX 14(a), on cell survival in brain slices subjected to chemical ischaemia (Hall *et al.*, 2014).

Curiously, the expression of GPCR37L1 alone (i.e. with no added prosaptide) was sufficient to significantly rescue cell death in the pyramidal layer of the WT compared to the KO (Fig. 3.4B). This suggests that prosaposin is released in the brain slices during ischaemia, which is plausible as prosaposin expression is detected in abundance in the hippocampal tissue of the mouse brain (Yoneshige *et al*., 2009) and

its expression is reported to increase following ischaemia (Nabeka *et al.*, 2014). In contrast to reports suggesting a glioprotective role for GPCR37L1 in HEK cells and primary astrocyte cultures following oxidative stress (Meyer *et al.*, 2013), we did not observe any difference in cell death within the astrocyte-rich stratum radiatum (see section 3.4.3). However, the addition of prosaptide caused a significant improvement in cell survival in the pyramidal layer of WT hippocampal slices (Fig. 3.4C). Thus, although it is neuroprotective, endogenous prosaposin release (in Fig. 3.4B) is not high enough in ischaemia to have a maximal protective effect, as the addition of extra prosaptide to activate GPCR37L1 further alleviated cell death (Fig. 3.4C).

Prosaptide also decreased cell death in the pyramidal layer of the KO slices but to a lesser extent (Fig. 3.4C). This suggests that the neuroprotective effects of prosaposin may partly rely on the effect of prosaposin/prosaptide on other receptors, such as GPR37 (as also reported by Meyer et al. 2013).

These results, for the first time, link the previous knowledge of a neuroprotective role for prosaposin during ischaemia with the activity of the newly characterized receptor GPCR37L1.

3.5.2 In search of a mechanism for the neuroprotective effects of GPCR37L1 in ischaemia

Exposure to high levels of glutamate is excitotoxic in the brain (Olney and Sharpe 1969). Also, NMDAR-mediated calcium entry is the major cause of neuronal damage following glutamate release by reversal of glutamate transporters in ischaemia (Goldberg *et al.*, 1987; Rossi, Oshima & Attwell, 2000). Therefore, a decrease in survival of CA1 pyramidal neurons during ischaemia in the GPCR37L1 KO (Fig. 3.4)

may reflect a change in extracellular glutamate levels or in the Ca^{2+} entry that a given level of glutamate produces.

Various factors can alter the extracellular levels of glutamate around CA1 pyramidal cells. Here, I revisit each of these factors (which were examined in the results section) and assess the plausibility of them contributing to cell survival in the WT during ischaemia.

First, it has been shown that excess glutamatergic input from CA3 pyramidal neurons to the CA1 dendritic region is a key contributor to the damage caused by ischaemia, since removal of this input is neuroprotective (Benveniste et al., 1989). Therefore, it is plausible that the Schaffer collateral terminals (the axons that originate from CA3 neurons) may have a lower threshold for glutamate release in the GPCR37L1 KO compared to WT, which would lead to an increased extracellular level of glutamate and excitotoxicity during ischaemia. Analysis of the excitability of CA3 neurons (i.e. their firing likelihood and latency to the first action potential, Fig. 3.5), and their stimulation threshold for glutamate release (Fig. 3.6), however, revealed no difference between the WT and KO.

An alternative mechanism leading to a decrease in cell survival in the KO during ischaemia (Fig. 3.4) may involve an increase in the number or conductance of the postsynaptic glutamate receptors. This is because glutamate receptor mediated depolarisation and calcium entry (in particular through NMDARs) is the major cause of neuronal damage in ischaemia (Goldberg *et al.*, 1987; Vornov & Coyle, 1991; Rossi, Oshima & Attwell, 2000; Brassai *et al.* 2015; Robinson & Jackson, 2016). Therefore, an increase in the number/or conductance of glutamate receptors could enhance cell death during ischaemia. However, no difference was seen between the kainate-evoked current (in the presence of D-AP5), and NMDA-evoked current (in the

presence of NBQX) in the WT and the GPCR37L1 KO CA1 pyramidal neurons (Fig. 3.7A). Although NBQX shows greater selectivity for AMPA over kainate receptors (Chittajallu *et al*., 1999), the lack of a difference between the kainate-evoked current argues against any significant change in the density of any of postsynaptic glutamate receptors between the WT and the GPCR37L1 KO. The neurons also had similar membrane properties in both genotypes (Fig. 3.7B&C).

A profound genotype-dependent difference in the excitatory behaviour of the neurons in the hippocampus under physiological conditions would, perhaps, have manifested itself in a more profound and distinct phenotype. For instance, it has been shown that a change in glutamate release and clearance correlates with poorer cognitive performance in mice (Hunsberger *et al*., 2015). However, unpublished data from the Richardson lab suggest that the GPCR37L1 KO mice do not have a gross phenotype and are normal when tested on some behavioural tests (including motor learning, and exploratory behaviour in the open fields). Therefore, a lack of change in basic neuronal or astrocyte membrane properties seems unsurprising.

3.5.3 GPCR37L1 signalling decreases neuronal NMDAR responses

Despite the lack of an apparent change in the currents mediated by AMPARs and NMDARs, I observed a slow increase in the conductance of the NMDA receptors upon repeated application of NMDA. In both the WT and the KO, the response to the second application of NMDA was always bigger (Fig. 3.8A), leading to a ratio > 1 when comparing the second to the initial response, perhaps due to increased insertion of a vesicular pool of glutamate receptors into the plasma membrane or a potentiation of the response of a fixed number of receptors. The implications of this increased NMDA-evoked response following repeated application of NMDA in physiological

conditions are unknown, but this increase (in Fig. 3.8A) may also be expected to occur during the prolonged glutamate release that occurs in ischaemia.

It has been shown that GPCR-mediated signalling in astrocytes can regulate neuronal excitatory transmission presynaptically (Di Castro *et al.*, 2011; Panatier *et al.*, 2011), and postsynaptic NMDAR-mediated long-term potentiation (Henneberger *et al.*, 2010; Shigetomi *et al.*, 2013). I therefore examined a potential effect of prosaptide-evoked GPCR37L1 signalling in astrocytes on postsynaptic neuronal NMDA responses.

During repeated application of NMDA I found surprisingly, that the presence of prosaptide during the second application of NMDA inhibited the potentiation of the NMDA current that would normally occur in the WT (Fig. 3.8C), without affecting the potentiation that occurred in the KO (Fig. 3.8C). These results suggest that GPCR37L1-mediated signalling in astrocytes decreases the neuronal NMDA response. Thus, an increase in endogenous prosaposin release (or the addition of prosaptide) during ischaemia may activate GPCR37L1-mediated signalling (presumably within astrocytes), which in turn would reduce NMDAR-mediated calcium entry and cell death. The mechanisms by which the activation of GPCR37L1 in astrocytes might lead to a reduction of the neuronal NMDA response could involve decrease in the release of D-serine (Henneberger *et* al., 2010) or TNF-α (Stellwagen & Malenka, 2006) from astrocytes. This will be further discussed in chapter 7.

As a caveat, there are, however, some OPCs in the hippocampus which receive glutamatergic input from the pyramidal neurons (Bergles *et al*., 2000), so, it is possible that GPCR37L1 expressing OPCs (see Fig. 3.1) also signal to neurons to reduce their NMDAR-mediated responses.

3.5.4 The effect of GPCR37L1 signalling on glutamate uptake in astrocytes

Any dysfunction in the clearance of glutamate by glial or neuronal transporters could elevate extracellular levels of glutamate and contribute to cell death in ischaemia (Robinson & Jackson, 2016) via activation of NMDA receptors (Vornov & Coyle, 1991; Brassai *et al.* 2015). Therefore, I compared the magnitude of the glutamate uptake current (measured as the current evoked by the glutamate analogue, D-aspartate) in WT and GPCR37L1 KO hippocampal astrocytes. This current was similar under physiological conditions, and in the absence of prosaptide (Fig. 3.10B). Surprisingly, however, the addition of prosaptide (10μM), significantly reduced the uptake current in the WT without affecting the current in the KO (Fig. 3.11B & C).

If glial glutamate transporters do reverse in severe ischaemia and contribute significantly to the release of glutamate (which has been questioned early in ischaemia by the work of Hamann *et al.*, 2002), then inhibition of glial glutamate transporters that are operating in the reversal mode may be another mechanism (in addition to reducing activation of NMDARs) by which prosaptide-evoked GPCR37L1 signalling exerts its neuroprotective effect during ischaemia.

The results from this chapter are encouraging in proposing a role for astrocytes in protecting neurons during excitotoxic conditions. Activation of the glial-specific GPCR37L1 appears to play a key role in this neuroprotection. In chapter 7, I will speculate on the mechanisms by which signalling downstream of GPCR37L1 in astrocytes may confer neuroprotection via neuronal NMDA receptors.

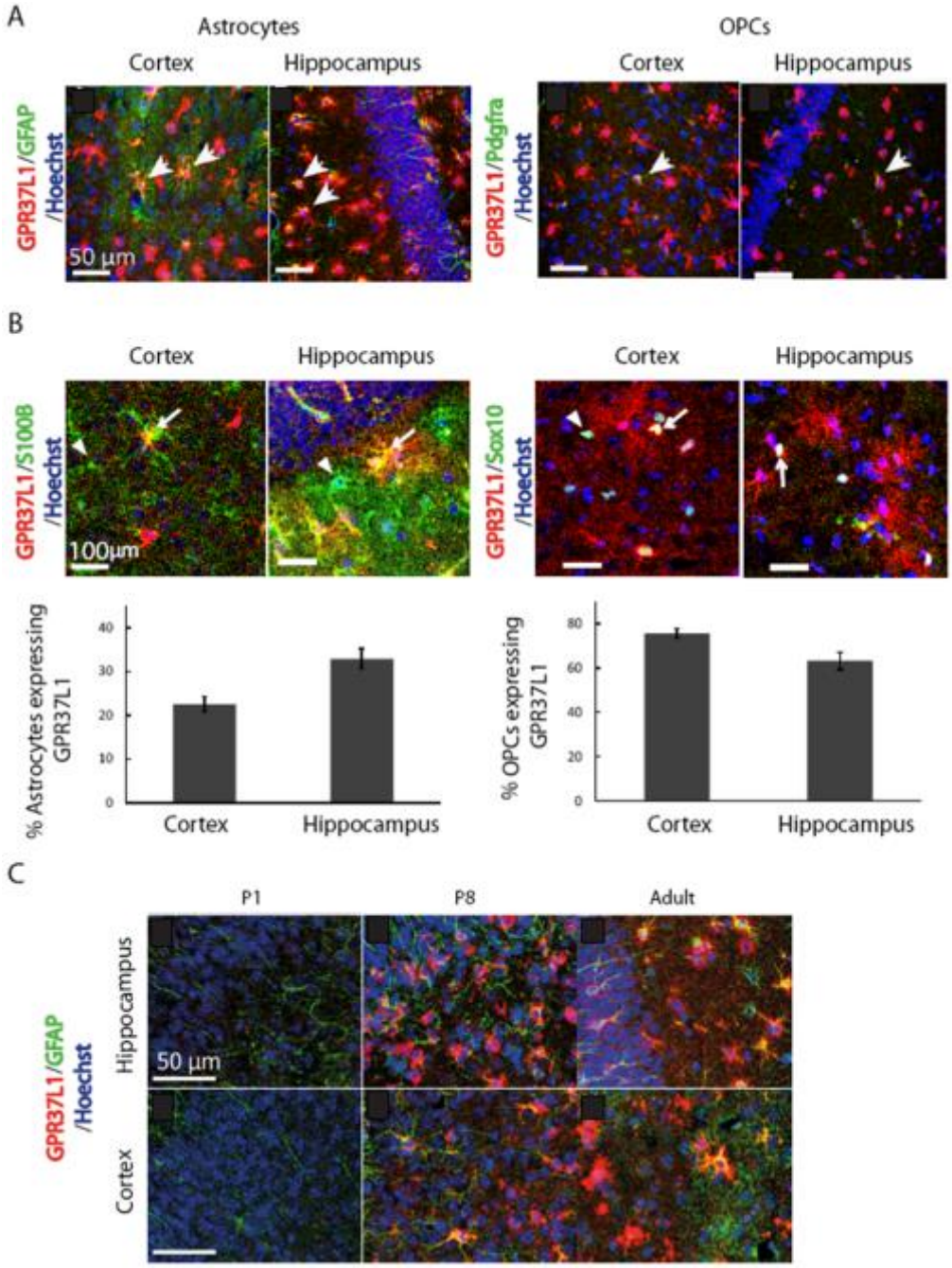

Figure 3.1: GPR37L1 expressed in a sub-population of astrocytes and of OPs
A. Cells expressing *GPR37l1* transcripts were distributed throughout all regions of the adult forebrain especially in the cortex, and hippocampus. Confocal images of fluorescent in situ hybridization showed expression of *GPR37l1* in GFAP-positive astrocytes and PDGFRα-positive OPCs (colocalisation of the red signal for *GPR37l1* mRNA and the green signal for GFAP/PDGFRα antibodies is marked by arrows). **B**. Top: S100β-positive astrocytes and Sox10-positive OPCs that express GPR37L1 in the cortex and in the hippocampus (arrows: GPR37L1-positive astrocytes or OPCs, arrowheads: GPR37L1-negative cells). Bottom: proportion of cells expressing GPCR37L1 (means ± s.e.m.). **C**. Expression of *GPR37l1* at different post-natal times (P1, P8, and adults at 4 months) in astrocytes by *in situ* hybridization followed by immunostaining for GFAP. *GPR37l1* expression was not detected at P1, and its expression had increased at P8, and was similar to P8 in adults. Scale bars: 50 µm.

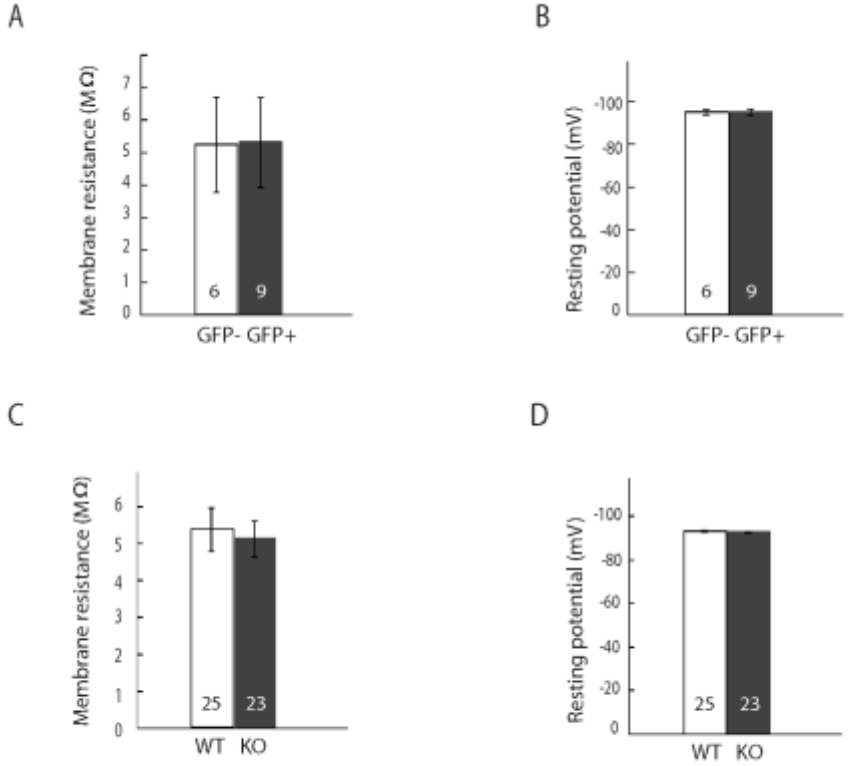

Figure 3.2: Expression of GPCR37L1 does not affect the basic membrane properties of astrocytes

Astrocytes in hippocampal slices from GPCR37L1-GFP mice (**A & B**) and from WT and GPCR37L1 KO mice (**C & D**), were patch-clamped near their resting potential. Membrane resistance and resting potential were compared between astrocytes that expressed or lacked GPCR37L1 (in the GFP-expressing mouse), and between astrocytes in WT or KO mice. The expression, or the deletion, of GPCR37L1, did not change the basic membrane properties of astrocytes. Data shown are the mean ± s.e.m.

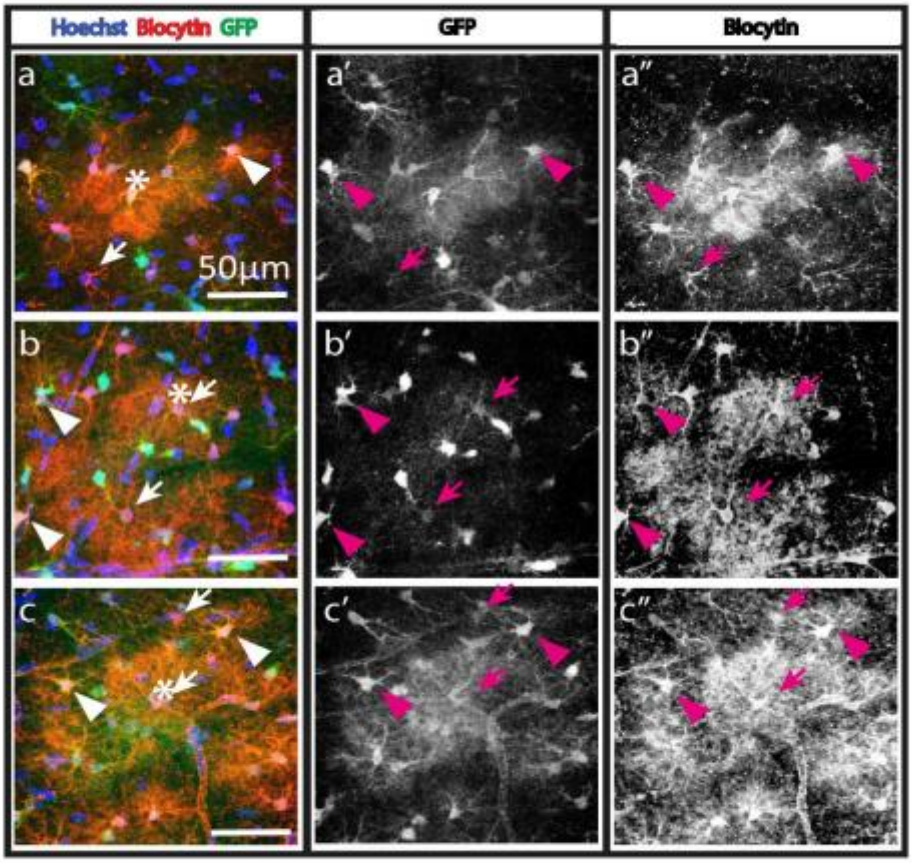

Figure 3.3: Astrocytes expressing and lacking GPCR37L1 form gap junctions

Astrocytes in hippocampal slices of GPCR37L1-GFP mice were patch-clamped near their resting potential and biocytin was loaded into the cells through the patch pipette. Three examples of astrocytes loaded with biocytin and those astrocytes they are coupled to are shown (**a, b, c**). Staining of GFP (with antibody: **a'**, **b'** and **c'**) and biocytin (**a''**, **b''**, **c''**) showed the presence of biocytin in both GFP-positive and GFP-negative cells. Star: probable patch-clamped astrocyte, arrows: GPCR37L1-negative astrocytes, arrowheads: GPCR37L1-positive astrocytes. Scale bars: 50 µm.

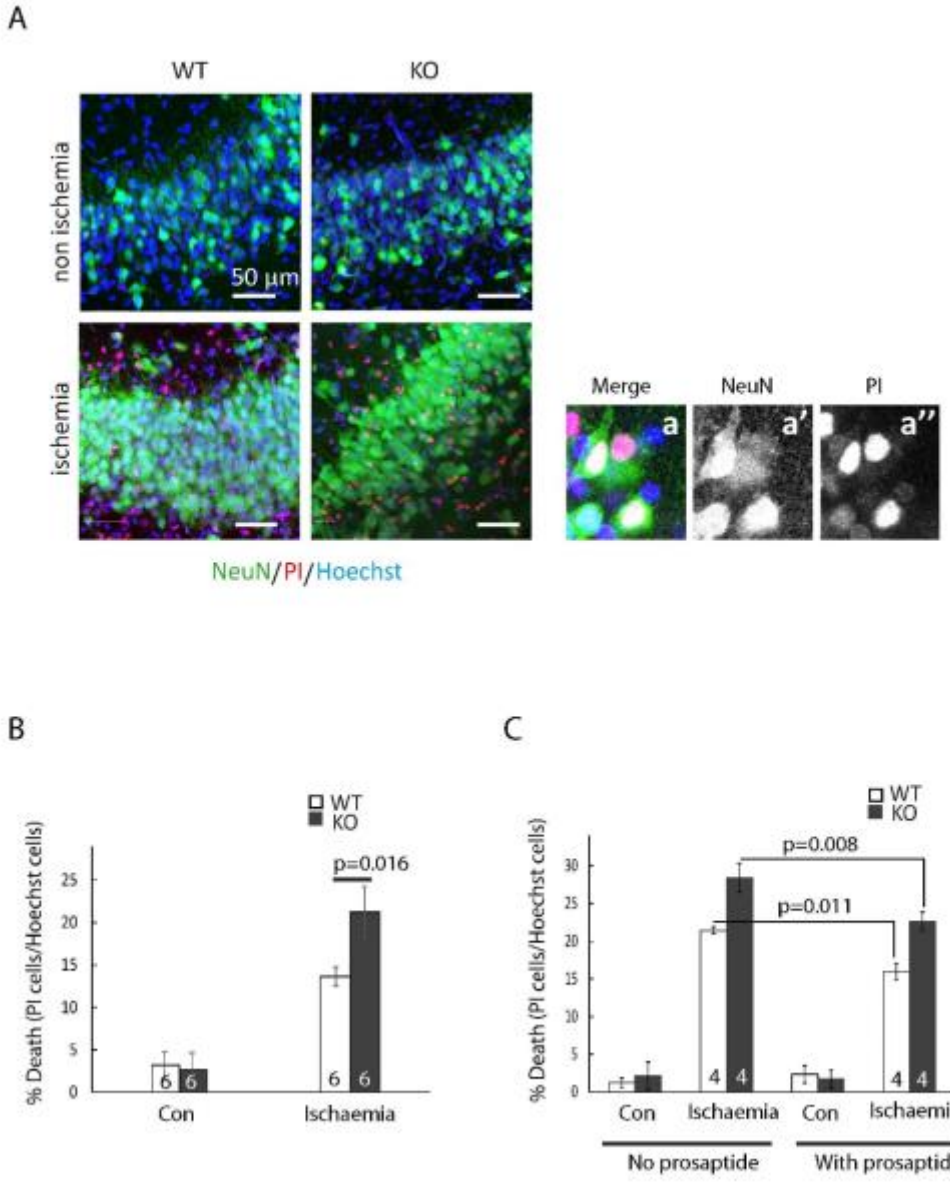

Figure 3.4: Role of GPCR37L1 during chemical ischaemia

A. Hippocampal slices from WT and GPCR37L1 KO mice were incubated for 30 min in control or ischaemic solution containing propidium iodide (PI) and were subsequently labelled for NeuN and Hoechst. Scale bars: 50 µm. **a.** A higher magnification image of pyramidal neurons showing colocalization in the merged image (**a**) of NeuN (**a'**) and PI (**a''**). **B**. Percentage of dead cells in control or ischaemia in GPCR37L1$^{+/+}$ and GPCR37L1$^{-/-}$ littermates. Data shown are the mean ± s.e.m. of six independent experiments. (**C**) Percentage of dead cells following incubation in control solution (Con), ischaemia solution alone, or control and ischaemia solution containing prosaptide (10 µM). Data shown are the mean ± s.e.m of four independent experiments. P values have been adjusted for multiple comparison by Holm-Bonferroni correction.

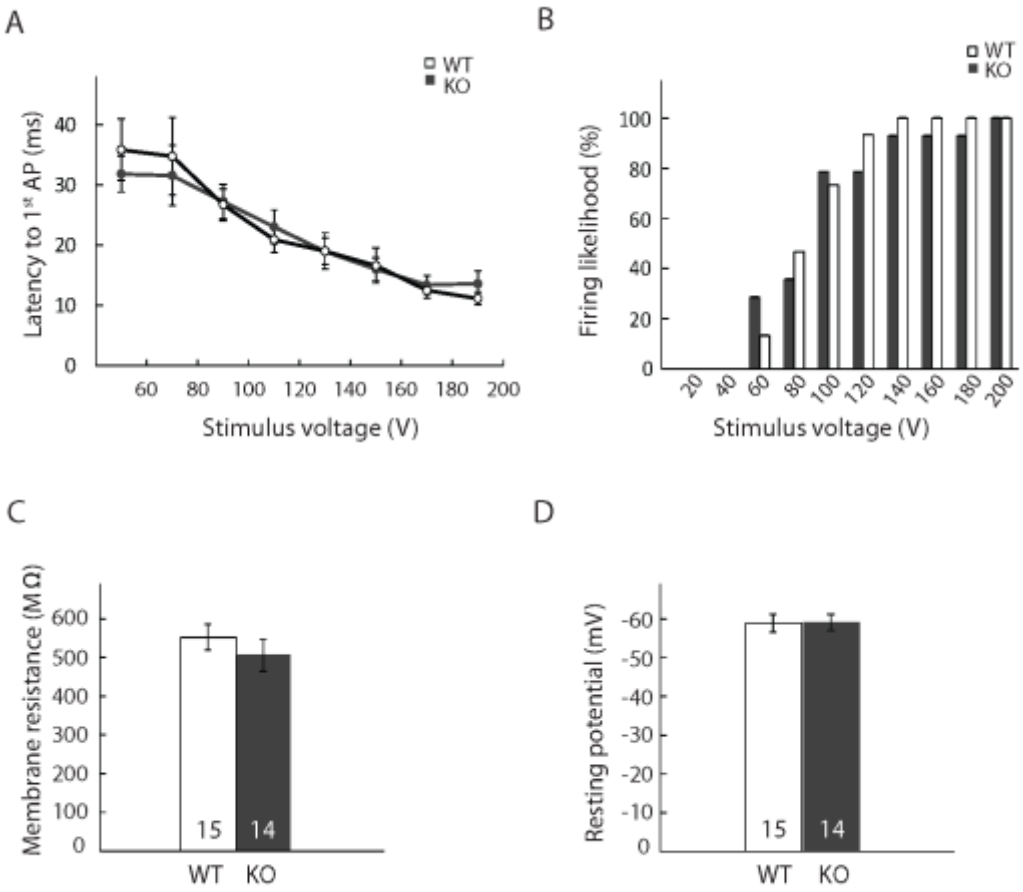

Figure 3.5: CA3 neuronal membrane properties are unchanged

CA3 pyramidal neurons exhibited similar excitability in hippocampal slices prepared from the WT and GPCR37L1 KO mice. Current clamp recordings from CA3 pyramidal neurons showed that the latency to the first action potential (**A**), the firing likelihood (percentage of stimuli evoking an action potential, **B**), the membrane resistance (**C**), and the resting potential (**D**) were similar in the WT and KO. Data shown are the mean ± s.e.m. in 15 slices for the WT and 14 slices for the GPCR37L1 KO.

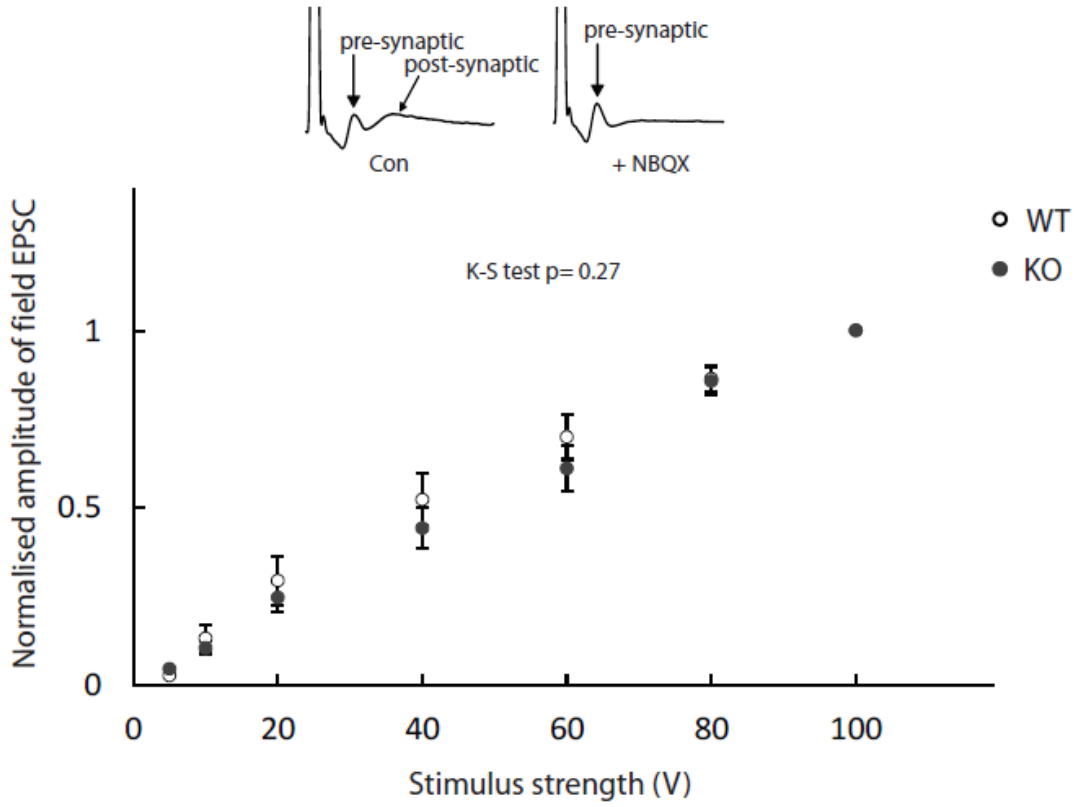

Figure 3.6: The stimulus-response curve for field EPSCs at the CA3-CA1 synapse is similar for WT and GPCR37L1 KO slices.

Hippocampal slices were prepared from WT and GPCR37L1 KO mice at P14-16. Thick-walled electrodes, filled with HEPES-based aCSF were used to evoke field excitatory postsynaptic currents (fEPSCs), which were recorded using another glass pipette filled with the same aCSF solution. fEPSCs were evoked by applying stimuli in steps of 20V from 0-100V. The responses show an early biphasic response which reflects the passage of the presynaptic action potential along the Schaffer collaterals, followed by a postsynaptic signal that is blocked by the AMPA/KA blocker NBQX (see inset: this is seen as an apparently outward current when measured in voltage-clamp as a charge passes from the extracellular space into the dendrites at synapses). The amplitudes of the responses were normalised to the maximal response (recorded at 100V) for each slice. The normalised amplitude of the fEPSCs was similar in the slices prepared from the WT (n=8) and those from the KO (n=9). A Kolmogorov–Smirnov test showed no difference between the two curves (p=0.27).

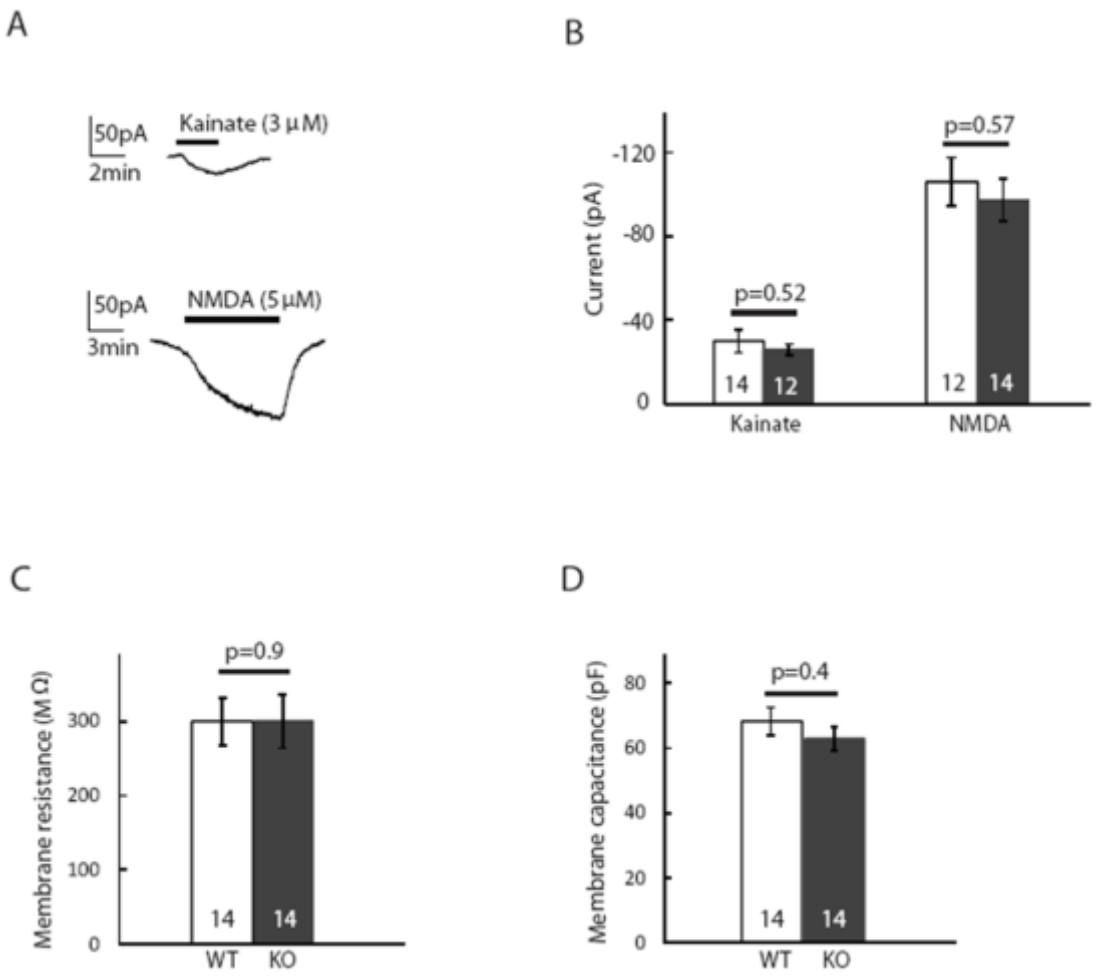

Figure 3.7: Properties of CA1 pyramidal neurons

Voltage clamp recordings were made from CA1 pyramidal neurons in hippocampal slices prepared from the WT and GPCR37L1 KO mice at P14-16. **A**. The amplitude of the currents evoked by bath application of (i) the AMPA/KA receptor agonist, kainate (3 µM, in the presence of the NMDAR blocker, D-AP5, 50 µM), or (ii) the NMDA receptor agonist, NMDA (5 µM, in the presence of the AMPA/KA blocker, NBQX 10 µM), were recorded. **B**. There was no difference in the amplitude of the AMPA/KA (n=14 for the WT and n=12 for the KO) or NMDA (n=12 for WT and n=14 for KO) receptor mediated currents between the two genotypes. **C & D**. GPCR37L1$^{+/+}$ and GPCR37L1$^{-/-}$ CA1 pyramidal neurons also displayed a similar cell membrane resistance (**C**) and capacitance (**D**). All recordings were made in the presence of TTX (150 nM) and picrotoxin (100 µM). Data shown are the mean ± s.e.m.

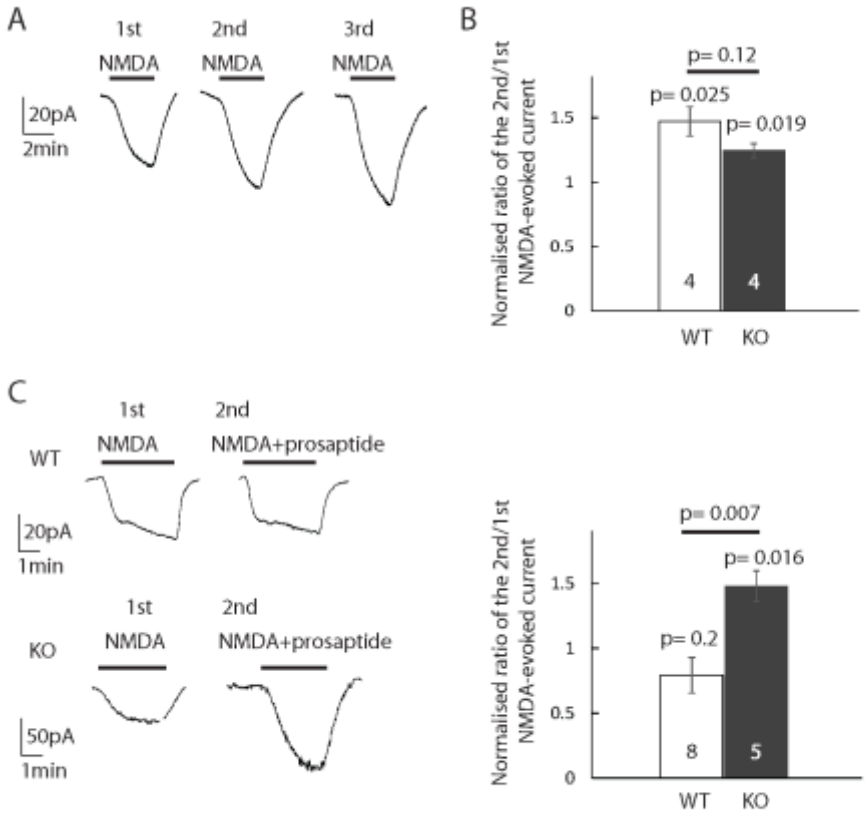

Figure 3.8: Potentiation of the NMDA-evoked response depends on the activation of the GPCR37L1

A. Repeated (x3) brief (~3 min, at 4 min intervals) application of NMDA (5 μM) resulted in a sequential increase in the magnitude of the response recorded in CA1 pyramidal neurons. **B**. In both the WT and the KO, the response to the second application of NMDA was always bigger, leading to a ratio > 1 when comparing the second to the initial response (n=4 for each genotype). **C**. Similar to **A** but NMDA was repeatedly applied in the absence (labelled 1st) and then in the presence of prosaptide (10 μM, labelled 2nd, n=8 for WT and n=5 for the KO). **D**. Prosaptide inhibited the potentiation of the NMDA current in the WT (ratio ~1) without affecting the potentiation of the NMDA response in the KO (ratio > 1). All recordings were made in the presence of TTX (150 nM) and picrotoxin (100 μM). Data shown are the mean ± s.e.m.

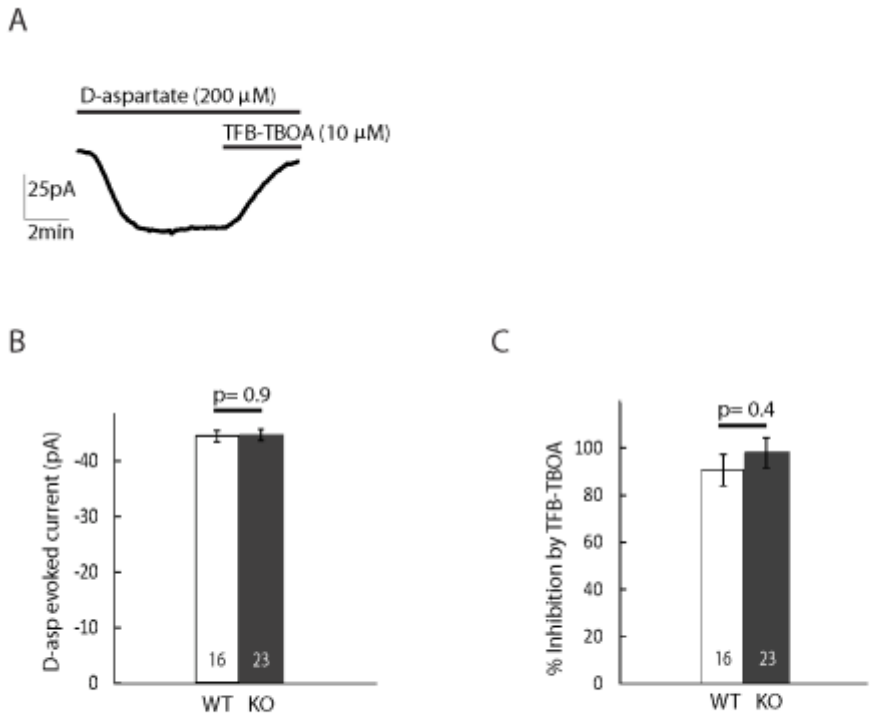

Figure 3.9: Glutamate uptake currents in astrocytes

(**A**) A sample trace showing the D-aspartate (200 µM)-evoked current, and its inhibition by the glial glutamate transporter blocker, TFB-TBOA (10 µM). **B**. Quantification of the glutamate uptake current (proportional to the rate of D-aspartate uptake) in astrocytes revealed no difference between the WT and the GPCR37L1 KO. **C**. The D-aspartate (200 µM)-evoked current was inhibited by the glutamate transporter blocker, TFB-TBOA (10 µM), thus proving that the current recorded reflects the glutamate uptake current in astrocytes. Blockers of NMDA receptors (10 µM D-AP5, 10 µM MK-801, 10 µM 5,7-DCK), AMPA/KA receptors (10 µM NBQX), $GABA_A$ receptors (10 µM bicuculline), voltage-gated sodium channels (150 nM TTX), and inwardly rectifying potassium channels (200 µM, barium chloride) were also present throughout the experiment. Data shown are the mean ± s.e.m.

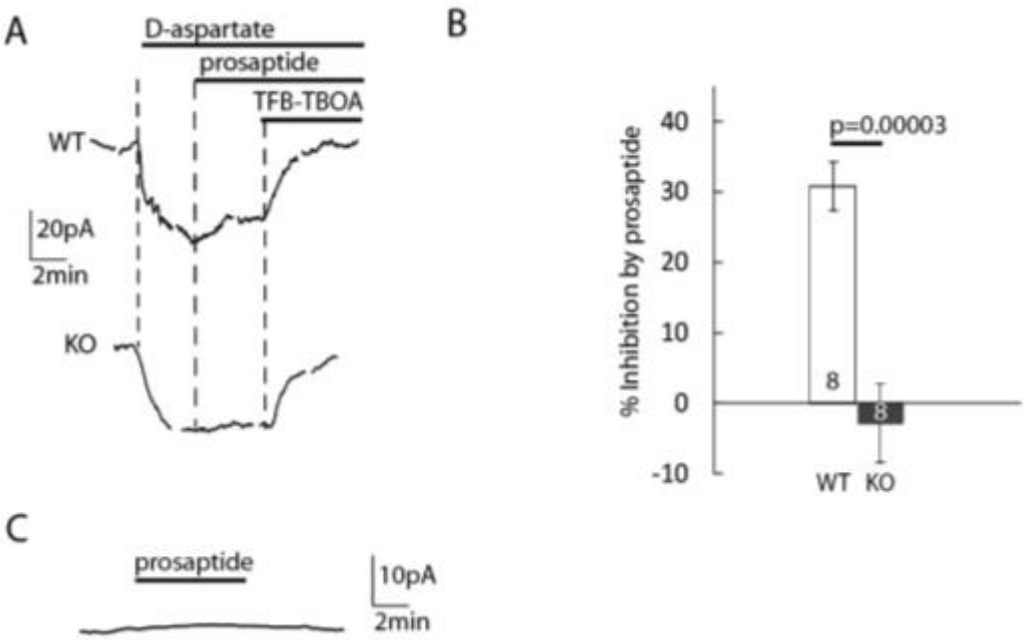

Figure 3.10: Activation of GPCR37L1 inhibits glutamate transport in astrocytes.

A. A sample trace showing the 200 µM D-aspartate-evoked current is inhibited partially by the application of prosaptide (10 µM) in the WT only. **B**. Quantification of this inhibition of the D-aspartate evoked current by prosaptide is presented for the WT and the KO. **C**. Prosaptide does not evoke a current in the absence of D-aspartate (for quantification, see text). Blockers of NMDA receptors (10 µM D-AP5, 10 µM MK-801, 10 µM 5,7-DCK), AMPA receptors (10 µM disodium NBQX), GABAA receptors (10 µM bicuculline), voltage-gated sodium channels (150 nM TTX), and inwardly rectifying potassium channels (200 µM, barium chloride) were also present throughout the experiment. Data shown are the mean ± s.e.m.

Chapter 4:

Regulation of glial glutamate uptake by noradrenaline

4.1 Summary of this chapter

Noradrenaline plays an important role in regulating astrocyte functions such as metabolism of glycogen and generating calcium concentration elevations in response to incoming visual stimuli. The possible role of noradrenaline in regulating glutamate clearance by astrocytes has, however, not been well studied. In this chapter, I will report my findings on the effect of noradrenaline on glutamate uptake in hippocampal astrocytes. My results from immunolabelling and electrophysiological experiments provide evidence for: (i) expression of adrenoceptor subtypes on the astrocyte membrane, and (ii) inhibition of glutamate uptake in astrocytes by noradrenaline. Furthermore, I will show that the noradrenaline-evoked inhibition of glutamate uptake depends on changes in the intracellular concentrations of both calcium (Ca^{2+}) and cyclic adenosine monophosphate (cAMP) in astrocytes.

4.2 Introduction

Noradrenaline is a neuromodulatory transmitter that can regulate the activity of neurons and glial cells all across the brain. Such global reach is made possible by long axons which originate from a collection of cells in the locus coeruleus (Descarries & Saucier, 1972), which provide noradrenergic input to most of the cortex (Levitt & Moore, 1978).

Release of noradrenaline in the brain has been associated with important behaviours. These include stimulation of wakefulness and arousal (Berridge *et al.*,

1993; Berridge & Waterhouse, 2003), attention and sensory processing (McLean & Waterhouse, 1994), and stimulation of the stress response (see Glavin, 1985, for a review). Noradrenaline depletion has also been linked to various psychological and neurological conditions in the central nervous system (see, Thase & Denko, 2008; Marien *et al*., 2004; for reviews).

Astrocytes and noradrenergic neurons have a mutually beneficial relationship. By releasing lactate, astrocytes stimulate action potential production by locus coeruleus noradrenergic neurons (Tang *et al*., 2014). In turn, noradrenaline can stimulate oxidative metabolism (Subbarao & Hertz, 1990), glycogen turnover (Hutchinson *et al*., 2011), the release of neurotrophic factors (Day *et al*., 2014), production of proinflammatory mediators (Hinojosa *et al*., 2013), and an increase in intracellular calcium concentration in astrocytes (Duffy & MacVicar, 1995; Schnell *et al*., 2016; Ding et al., 2014; Paukert et al., 2014). This rise of $[Ca^{2+}]_i$ has been shown to gate the astrocytes' calcium responsiveness to sensory stimuli (see section 1.2.6 for a detailed discussion of astrocyte Ca^{2+} signalling). These complex effects of noradrenaline are mediated by three receptor subtypes (i.e. α_1, α_2, and β, see section 1.2.7.6.2 for more details).

The functional consequences of noradrenaline signalling to astrocytes may include modulating the clearance of glutamate from the synapse. Data from astrocyte cultures suggest that noradrenaline evokes an increase in glutamate uptake by activating G_q-coupled α_1-adrenoceptors (α_1-ARs, Fahrig, 1993). Further support for this came from a microdialysis study *in vivo* in which glutamate clearance was enhanced by an α_1-AR agonist (Alexander et al., 1997). Results from another group, however, suggested that noradrenaline evokes an increase in glutamate uptake by acting on β-receptors in astrocyte cultures (Hansson & Rönnbäck, 1991). There are,

however, concerns with these reports from cultured astrocytes as follows. (i) The glutamate uptake experiments by Fahrig (1993) and Hansson & Rönnbäck (1991) did not voltage clamp the cells, and changes of membrane potential can modulate glutamate uptake (Brew & Attwell, 1987). (ii) They did not include blockers of glutamate receptors and activation of these receptors by glutamate (either applied to evoke uptake, or released by heteroexchange when D-aspartate is applied to evoke uptake) may raise extracellular concentration of potassium which also attenuates the uptake rate (Barbour *et al*., 1988). (iii) Hansson & Rönnbäck (1991) reported an effect of a β-receptor agonist on glutamate uptake, but not on D-aspartate uptake, despite many reports which have shown that D-aspartate and glutamate are transported at a similar rate by glutamate transporters (e.g. Barbour *et al*., 1991, or see section 1.2.7.2 for more detailed discussion).

Therefore, the aim of this project was to identify the presence, and spatial distributions, of AR subtypes on hippocampal astrocytes in brain slices, and to define the effect of noradrenaline receptor signalling on astrocyte glutamate uptake.

4.3 Methods

4.3.1 Hippocampal slice preparation

Hippocampal slices from 12-day-postnatal Sprague-Dawley rats were prepared for electrophysiological recordings as described in section 2.2.

4.3.2 Extracellular solutions

Brain slices were perfused with solutions mimicking cerebrospinal fluid (artificial cerebrospinal fluid, aCSF) which contained HEPES-based buffer (as described in section 2.3.1). Glutamate uptake current was recorded (as described in section 2.3.1.1) from astrocytes in the stratum radiatum by voltage clamping the cells at a potential close to the cell's resting potential (typically around -90 mV). D-aspartate (200 μM) was used as a glutamate substitute to evoke the transporter current.

In order to examine the effect of noradrenaline-mediated signalling on glutamate uptake, DL-noradrenaline (2 μM) was applied when the D-aspartate-evoked current had reached its peak in either the presence or absence of adrenergic receptor blockers. These blockers include the α_1-adrenoceptor blocker terazosin (1 μM), and the α_2-adrenoceptor blocker atipamezol (1 μM). Ascorbic acid (500 μM) was included to block oxidation of noradrenaline (Hugh *et al.*, 1987).

4.3.3 Intracellular solutions

For whole-cell patch-clamp recordings from astrocytes, a potassium-gluconate based solution was used, as described in section 2.3.2.

In some experiments, intracellular calcium concentration changes were abolished inside astrocytes by introducing the fast calcium-chelating agent BAPTA (30 mM) via the internal solution (instead of 10 mM EGTA: in this solution, the

concentration of K-gluconate was adjusted to keep the osmolarity ~ 285 mOsm, and 0.025 mM $CaCl_2$ was added [larger than that in the EGTA-containing internal solution] to ensure that the free calcium concentration was similar [~20 nM], calculated from www.stanford.edu/~cpatton/webmaxcS.htm).

In addition, in some experiments, 1 mM cAMP was added to the internal solution on the day of the experiment.

4.3.4 Immunohistochemistry

This was carried out as described in section 2.8.1.

In control experiments, brain slices were incubated with only the anti-GFAP primary antibody (i.e. omitting the primary antibody for AR) and both secondary antibodies. The lack of AR labelling seen in these conditions supported the idea that the AR antibody staining was specific. The list of primary antibodies include: chicken glial fibrillary acidic protein (GFAP, 1:2000 dilution), rabbit α1A-AR (1:100 dilution), rabbit α1B-AR (1:100 dilution), rabbit α2A-AR (1:200 dilution) and rabbit β1-AR (1:400 dilution).

4.3.5 Confocal imaging and analysis

Confocal imaging was performed as in section 2.9. To quantify the spatial localization of adrenergic receptors in astrocytes, each astrocyte was divided into four compartments (using the GFAP signal as a guide to demarcate the morphological structure of astrocytes): the soma (i.e. the region surrounding the cell nucleus), proximal processes (i.e. processes before the first branching point), distal processes (i.e. processes after the first branching point), and endfeet (the areas associated with a blood vessel, Fig. 4.1). Thus, by summing the signal intensity over the individual

compartments, the percentage of total adrenoceptor expression was calculated for each compartment. To account for the possibility that AR labelling in astrocytes may include "non-astrocyte" AR labelling (especially as labelling was assessed in maximum intensity projection images which may include non-astrocyte labelling of neurons above and below the astrocyte), the mean AR signal intensity of non-astrocyte areas (defined by a lack of GFAP labelling) was measured and compared to the mean signal across all the compartments of an astrocyte.

Within each astrocytic compartment, the average intensity of AR labelling per μm^2 of surface area was also measured. Estimates of the cell surface area were made by assuming that the soma corresponded to a sphere, while astrocyte processes were cylinders. Thus, the radius of the soma, the radius of each astrocytic process, and the length of each astrocytic process were measured manually. Analysis of receptor density was done for all the compartments except for the endfeet which had more complex surface areas.

4.3.6 Statistical analysis

Data are represented as mean ± s.e.m. All P values are from 2-tailed Student's t tests and have been corrected for multiple comparisons by using a Holm-Bonferroni correction for Figs. 4.2, 4.3, 4.4 and 4.5.

4.4 Results

4.4.1 Spatial expression of adrenoceptors in hippocampal astrocytes

Double staining with antibodies against astrocyte-specific GFAP and each of the ARs (i.e. α_{1A}, α_{1B}, α_{2A} and β_1) confirmed the expression of all these subtypes of adrenoceptors in astrocytes. The result for each AR subtype will be discussed below.

4.4.1.1 α_{1A}-adrenoceptors

α_{1A}-ARs showed strong antibody labelling in astrocytes (Fig. 4.2A), with the highest expression in astrocyte processes (Fig. 4.2C, 39.5±5.3% of the total signal across the compartments was in the proximal processes in 5 cells (which had an average of 6 proximal processes), and 37.0±7.8% was in the distal processes in 5 cells (which had an average of 7 distal processes)). In comparison, the soma showed only 18.7±1.9% of the total signal intensity (n=5 cells, unpaired t-test p=0.019 when compared to the proximal processes, and p=0.051, when compared to the distal processes). The expression in the soma was, however, significantly greater than in the astrocytic endfeet (7.8±2.2% of the total, 3 endfeet on 3 cells, p= 0.02). The results suggest that the majority of astrocyte α_{1A}-ARs are localized in the cell's proximal processes.

Importantly, the antibody signal intensity was significantly lower within the non-astrocytic areas (i.e. background parts of the image that lacked GFAP expression) compared to the mean signal across the astrocyte compartments (unpaired t-test, p=0.0012, n=5, comparing the mean signal within the astrocyte compartments with the mean signal from the selected non-astrocyte regions), thus suggesting a stronger expression of α_{1A}-AR in astrocytes than in the neuropil. However, there was significantly more α_{1A}-AR expression in the non-astrocytic regions compared to the

negative control sample (with no α_{1A}-AR primary antibody present, unpaired t-test p=0.02, n=5 pairs of images, Fig. 4.2B & D), suggesting that some $\alpha 1_A$-ARs are found in other cell types (presumably neurons) in the glial rich stratum radiatum region of the hippocampus.

Analysis of α_{1A}-AR density (i.e. signal normalised to astrocyte surface membrane area) within each compartment showed a fairly homogenous pattern of expression (Fig. 4.2E). There was no significant difference between the receptor density in the membrane of the somata and the processes per square micron (mean receptor density in arbitrary units: 168±30 for soma, 224±40 for proximal processes, and 212±53 for distal processes, n=5 cells; unpaired t-test p>0.5 for comparing either of the proximal or distal processes' receptor density with the soma). Thus, although the total signal intensity was higher in the proximal processes compared to the soma (Fig. 4.2C), analysis of receptor density per membrane area shows that α_{1A}-ARs are distributed fairly uniformly in the membrane of different astrocyte compartments (Fig. 4.2E), so the larger total signal in the proximal processes reflects this compartment having a larger membrane area.

4.4.1.2 α_{1B}-adrenoceptors

Antibody staining against the α_{1B}-ARs (which is the most highly expressed $\alpha 1$ subtype in astrocytes: Zhang *et al.*, 2014) revealed the greatest expression in the processes (Fig. 4.3A & B, 39.1±6.0% of the total signal was in the proximal processes in 5 cells (which had an average of 4 proximal processes), and 32.0±9.5% was in the distal processes in 5 cells (which had an average of 4 distal processes)). In comparison, the soma showed 17.5±3.1% of the total signal intensity (n=5 cells, unpaired t-test p=0.038 when compared to the proximal processes, and p=0.36 when compared to the

distal processes). There was also a considerable expression of α_{1B}-AR in endfeet (28.5±23.8% of the total, 2 endfeet on 2 cells), although there was a large standard error, which could be attributed to the small sample size.

Similar to α_{1A}-AR staining, the labelling for α_{1B}-ARs showed specificity for astrocytes when compared to the non-astrocyte areas (Fig. 4.3C, p=0.0004, for 5 cells comparing the mean signal within the astrocyte compartments with the mean signal from the selected non-astrocyte regions). There was, however, significantly more α_{1B}-AR expression in the non-astrocytic regions compared to the negative control sample (i.e. Fig. 4.2B) when no α_{1B}-AR primary antibody was present (unpaired t-test p=0.0005, n=5 pairs of images, Fig. 4.3C) indicating that α_{1B}-ARs are also present in other cell types in the stratum radiatum region of the hippocampus (presumably neurons).

Analysis of α_{1B}-AR density (per astrocyte membrane area) within each compartment also exhibited a fairly homogenous expression across astrocytes. There was no significant difference in the receptor density between soma and astrocyte processes (mean receptor density in arbitrary units: 243±63 for soma, 360±63 for proximal processes, and 304±74 for distal processes; n=5 cells, unpaired t-test p>0.4 for comparing either of the process compartments with the soma). Thus, although the total signal intensity was higher in the proximal processes compared to the soma (Fig. 4.3B), analysis of receptor density per membrane area shows that α_{1B}-ARs are uniformly distributed in the membrane of different astrocyte compartments (Fig. 4.3D), so the larger total signal in the proximal processes reflects this compartment having a larger membrane area.

4.4.1.3 α_{2A}- adrenoceptors

Antibody labelling against α_{2A}-AR revealed a higher expression level of this receptor in the processes of astrocytes (Fig. 4.4A & B, 43.4±7.1% of the total astrocyte signal across the compartments was in the proximal processes in 5 cells (which had an average of 5 proximal processes), and 32.1±9.0% was in the distal processes in 5 cells (which had an average of 7 proximal processes)). In comparison, the soma showed 17.2±2.9% of the total signal intensity (n=5 cells, unpaired t-test p=0.03 when compared to the proximal processes, and p=0.3 when compared to the distal processes). The expression of α_{2A}-AR at the endfeet was low (18.2±7.8%, 2 endfeet on 2 cells), though this might not be representative due to the small sample.

The expression of α_{2A}-ARs in astrocytes was significantly greater than in non-astrocyte background regions (Fig. 4.4C, unpaired t-test, p=0.0004, for 5 cells comparing the total signal within the astrocyte compartments with the total signal from the selected non-astrocyte regions). In spite of this, the expression of α_{2A}-ARs was significantly higher in the non-astrocytic regions compared to the negative control sample (i.e. Fig. 4.2B) when no α_{2A}-AR primary antibody was present (unpaired t-test p=0.00003, n=5 pairs of images, Fig. 4.4C) indicating that α_{2A}-ARs are also present in other cell types in the stratum radiatum region of the hippocampus.

Despite the seemingly higher expression of α_{2A}-AR in proximal processes compared to soma (see Fig. 4.4B), analysis of receptor density per area of astrocyte membrane revealed that, in fact, α_{2A}-AR are present at a higher density in the distal processes compared to the soma (mean receptor density in arbitrary units: 99±15 for the soma, and 158±13 for the distal processes, n=5 cells, unpaired t-test p=0.039), with no difference between the proximal processes and the soma (mean receptor density: 123±21 for the proximal processes, unpaired t-test p=0.3). Thus, in spite of a stronger

total signal intensity in the proximal processes (Fig. 4.4B), the results from the receptor density analysis suggest that the α_{2A}-AR density is in fact higher in the distal processes (Fig. 4.4D).

4.4.1.4 β_1-adrenoceptors

Labelling for β_1-AR did not show a convincing colocalisation with the astrocyte marker, GFAP (Fig. 4.5A), despite evidence for its expression in astrocytes (Zhang *et al.,* 2016). This is likely due to a lack of specificity, or a suboptimal concentration, of the antibody.

4.4.1.5 Summary of AR labelling

Overall, results from these experiments suggest a fairly homogeneous distribution of α_1-adrenoceptors (the activation of which can increase the intracellular level of Ca^{2+}) across different regions of the astrocytes. For α_{2A}-adrenoceptors only (the activation of which decreases the intracellular levels of cAMP) there was a higher concentration of receptors in distal finer processes of astrocytes relative to other cellular locations.

4.4.2 Noradrenaline inhibits glutamate uptake

I compared the magnitude of the glutamate transporter current evoked by D-aspartate (a substrate for glutamate transporters that has little effect on glutamate receptors, Gundersen et al. 1995, see section 1.2.7. for more details) in the absence and presence of noradrenaline. To do this, astrocytes in the stratum radiatum were whole-cell voltage clamped (near their resting potential) and responses to D-aspartate (200 μM) were recorded. Once the peak D-aspartate-evoked current was achieved,

noradrenaline (2 μM) was added to the solution containing D-aspartate to assess the effect of noradrenaline on glutamate uptake.

As reported in chapter 3 for mouse, D-aspartate evoked an inward uptake current (-168±23 pA in 10 rat astrocytes, Fig. 4.6B). Adding noradrenaline (2 μM) on top of the D-aspartate gave an additional outward current shift (quantified below) which was not seen in the absence of D-aspartate (noradrenaline alone evoked a baseline current shift of -1.8±1.5 pA in 3 cells, which was not significantly different from zero, p=0.7, Fig. 4.6C). Thus, noradrenaline appears to reduce the D-aspartate evoked uptake current. The reduction was significant: 55±7% in 10 cells (p= 0.0006, Fig. 4.6D).

However, it has been reported that noradrenaline can stimulate the sodium pump (Lee & Phillis, 1977), the operation of which causes an outward current because 3 Na^+ are pumped out for each 2 K^+ that are pumped in (Hamada *et al.*, 2003). Now when D-aspartate is applied, the activation of glutamate transporters will load the cell with co-transported Na^+ (see section 1.2.7.2), perhaps causing a rise of $[Na^+]_i$ that will activate the sodium pump. Thus, a potential alternative explanation for my data, showing that noradrenaline evokes an outward current in the presence of D-aspartate but not in its absence, is that noradrenaline is stimulating the sodium pump (which may be barely active in the absence of D-aspartate). To test this, I examined the effect of noradrenaline on the baseline current in the presence of a high intracellular concentration of sodium ($[Na^+]_i$, 30 mM, which was added to the internal solution), which is known to activate the sodium pump (Glitsch *et al.*, 1989). Importantly, noradrenaline failed to generate any current in the presence of a high concentration of sodium. The mean current generated by noradrenaline was 0.1±1.3 pA (Fig. 4.6E, n=8, not significantly different from zero, p=0.9). In contrast, noradrenaline inhibited the

D-aspartate evoked current even with high $[Na^+]_i$ in a subset of recordings (Fig. 4.6F, a 35±10% decrease was seen when comparing the peak current evoked by D-aspartate in the presence of noradrenaline with the peak current evoked by D-aspartate alone, n=4, p=0.017). This inhibition was not significantly different from that seen with low $[Na^+]_i$ (p=0.13).

These results provide evidence for inhibition of the D-aspartate evoked uptake current by noradrenaline.

4.4.3 Mechanisms of the noradrenaline-mediated inhibition of glutamate uptake

4.4.3.1 The effects of intracellular calcium signalling

Noradrenaline has three receptor subtypes through which it can potentially exert its inhibitory action on the glutamate uptake current in hippocampal astrocytes (as seen in Fig. 4.6). Activation of α_1-ARs can release calcium from internal stores, while activation of the other two subtypes (α_2-ARs and β-ARs) changes the intracellular concentration of cAMP. Therefore, I first assessed whether the inhibition of glutamate uptake by noradrenaline is mediated through its action on α_1-ARs.

To do this, I reduced calcium concentration elevations that would normally occur inside the astrocyte ($[Ca^{2+}]_i$) downstream of G_q-coupled signalling, by dialyzing into the astrocytes (via the patch pipette) the fast calcium chelator, BAPTA. This protocol should allow me to assess whether the noradrenaline mediated inhibition of the D-aspartate evoked current occurs through its action on α_1-ARs.

Interestingly, introducing BAPTA (30 mM) into astrocytes had no significant effect on the D-aspartate uptake current (-142±29 pA, n=4 with BAPTA, compared with -168±23, n=10 with EGTA, p=0.54). However, having BAPTA in the pipette largely abolished the inhibition of the D-aspartate evoked current that was evoked by

noradrenaline (Fig. 4.7A & B): a 12±4% decrease of the D-aspartate-evoked uptake current was generated by noradrenaline in 4 cells, compared with the 55±7% described above with 10 mM EGTA in the cell (significantly different, p=0.0039).

If activation of α_1-ARs and a subsequent downstream $[Ca^{2+}]_i$ elevation are necessary to inhibit glutamate uptake in astrocytes, blocking the activity of α_1-ARs should mimic the effects seen when BAPTA is present (Fig. 4.7). Therefore, to test this, I applied a potent selective α_1-AR blocker terazosin (1 μM, present throughout the experiment) while patch-clamp recordings were made from astrocytes and current changes were recorded in response to D-aspartate alone or with noradrenaline.

Terazosin had no significant effect on the D-aspartate uptake current (-115±36 pA, n=4 with terazosin, compared with -168±23, n=10 without the drug, p=0.24). However, terazosin almost completely abolished the inhibition of the D-aspartate evoked current by noradrenaline (Fig. 4.8A & B); a 1±1% decrease of the D-aspartate-evoked uptake current was generated by noradrenaline in 4 cells, compared with the 55±7% described above with noradrenaline in the absence of α_1-AR blocker (significantly different, p= 0.0008).

These experiments provide evidence that elevations in the intracellular concentration of calcium inhibit glutamate uptake in astrocytes, and this inhibition is mediated by the activation of α_1-adrenergic receptors. Thus, these results challenge the reports from studies in cultured astrocytes which claim that noradrenaline enhances glutamate uptake (Fahrig, 1993; Hansson & Rönnbäck, 1991).

4.4.3.2 The effects of intracellular cAMP signalling

Apart from α_1-ARs, astrocytes also express α_2-ARs and β-ARs, the activation of which decreases or increases the intracellular concentration of cAMP, respectively.

Therefore, I assessed whether the inhibition of glutamate uptake by noradrenaline may also involve changes in the intracellular concentration of cAMP.

To do this, I supplemented the internal solution inside the patch pipette with a large concentration of cAMP (1 mM) which was dialyzed into the astrocytes throughout the experiment. This protocol allows me to assess whether the noradrenaline-evoked inhibition of the D-aspartate evoked current occurs through a reduction or an increase in $[cAMP]_i$.

Introducing cAMP (1 mM) inside the astrocyte had no significant effect on the D-aspartate evoked uptake current (-186±64 pA, n=5 with cAMP, compared with -168±23, n=10 without cAMP, p=0.74). However, surprisingly, including cAMP in the pipette largely reduced the inhibition of the D-aspartate evoked current that was previously evoked by noradrenaline (Fig. 4.9A & B): a 18±6% decrease of the D-aspartate-evoked uptake current was generated by noradrenaline in 5 cells, compared with the 55±7% described above with noradrenaline in the absence of high $[cAMP]_i$ (significantly different, p= 0.0033).

This finding suggests that maintaining a high concentration of cAMP inside the cell interferes with the inhibitory effects of noradrenaline on glutamate uptake suggesting that a fall of $[cAMP]_i$ is needed for the inhibition to occur. Therefore, blocking the activity of α_2-ARs, which decrease $[cAMP]_i$, might mimic the effects seen with high levels of cAMP (Fig. 4.9). To test this, I applied a potent selective α_2-AR blocker atipamezole (1 μM, present throughout the experiment) while patch-clamp recordings were made from astrocytes and current changes were recorded in response to D-aspartate alone and then with superimposed noradrenaline.

Atipamezole had no significant effect on the D-aspartate uptake current (-128±77 pA, n=3 with atipamezole, compared with -168±23 pA, n=10 without the

drug, p=0.49). However, the inhibition of the D-aspartate evoked current that was evoked by noradrenaline (Fig. 4.6) was largely abolished when the α_2-AR blocker atipamezole was present (Fig. 4.10A & B): a 18±3% decrease of the D-aspartate-evoked uptake current was generated by noradrenaline in 3 cells, compared with the 55±7% described above with noradrenaline in the absence of α_2-AR blocker (significantly different, p= 0.013).

These experiments provide evidence that a reduction in the intracellular concentration of cAMP via α_2-ARs, as well as an increase in the concentration of calcium mediated via α_1-ARs, are involved in the inhibition by noradrenaline of glutamate transporter activity in hippocampal astrocytes.

4.5 Discussion

4.5.1 Analysis of adrenoceptor expression across astrocyte compartments

Adrenoceptors (ARs) are expressed in various cell types throughout the brain, including in astrocytes (Sutin & Shao, 1992; Hertz *et al*., 2010; Zhang *et al*., 2014 and 2016). Quantification of mRNA expression from isolated cell lines prepared from mice or adult rats suggest that α_1-ARs are highly expressed in astrocytes, neurons, and oligodendrocyte lineage cells, while α_2-ARs and β-ARs are present in astrocytes, neurons and microglia (Zhang *et al*., 2014 and 2016).

Understanding the distribution of ARs across different astrocytic regions is important as recent research suggests functional variations between different compartments. It has been shown that intracellular calcium changes inside fine processes of the astrocytes that wrap the synapse have the ability to regulate neuronal activity (Di Castro *et al.*, 2011; Panatier *et al.*, 2011). Moreover, the origin (Srinivasan *et al*., 2015) and speed (Di Castro *et al.*, 2011) of astrocyte calcium events are different between the soma (which shows widespread and slow calcium changes, that depend mainly on the release of calcium from internal stores via an IP_3-dependent pathway) and the processes (which show focal fast calcium changes, that depend more on calcium entry from extracellular space apart from release from internal stores): for a detailed review see Bazargani & Attwell (2016).

Furthermore, analysis of adrenergic evoked Ca^{2+} signals in astrocytes has revealed that α_1-ARs (which release calcium from internal stores) mediate startle- or movement-evoked coordinated [Ca^{2+}] increases in the network of astrocytes in awake behaving animals (Ding *et al.*, 2013; Paukert *et al.*, 2014), which tune their responsiveness to incoming visual stimuli (Paukert *et al.*, 2014). Importantly, Srinivasan *et al*. (2015) have recently shown that blocking α_1-ARs completely

abolishes the startle-evoked [Ca^{2+}] increase in the soma, while it only partially blocks the calcium changes in the processes, suggesting that calcium entry from the extracellular space, in conjunction with its release from internal stores, may mediate [Ca^{2+}] changes in the astrocyte processes (see section 1.2.6.3 for more details).

I, therefore, analyzed the receptor expression and density per surface area of the astrocyte for each adrenoceptor subtype within the stratum radiatum region of the hippocampus in brain slices prepared from young rats (P12) to assess whether there is a distinct AR subtype distribution across different compartments of astrocytes (i.e. in the soma, proximal and distal processes, and where possible, the endfeet).

Analysis of the antibody signal intensity for α_{1A}-ARs showed selectivity for astrocytes compared to non-astrocyte regions (Fig. 4.2C), and expression was highest in the proximal processes (Fig. 4.2 A & B). Although the total signal intensity was higher in the proximal processes compared to the soma (Fig. 4.2C), analysis of receptor density per membrane area showed that α_{1A}-ARs were distributed fairly uniformly in the membrane of different astrocyte compartments (Fig. 4.2E), so the larger total signal in the proximal processes reflects this compartment having a larger membrane area.

These results were similar for the α_{1B} subtype (which is the most highly expressed subtype in astrocytes, Zhang *et al*., 2014, and 2016) such that: (i) receptor staining showed specificity for astrocytes compared to non-astrocyte regions (Fig. 4.3C), and (ii) despite a higher total signal intensity within the proximal processes compared to the soma (Fig. 4.3B), the distribution per membrane area revealed a fairly homogenous result across all astrocyte regions (Fig. 4.3D). Thus, the larger total signal in the proximal processes reflects this compartment having a larger membrane area. I

did not investigate the expression of α_{1D}-ARs, as they are not expressed in astrocytes (Zhang *et al.*, 2014, and 2016).

These results suggest that the G_q-coupled α_{1A}- and α_{1B}-ARs are highly expressed in astrocytes within the stratum radiatum, and that these receptors are equally distributed per membrane area across all astrocyte regions.

Analysis of expression of α_{2A}-ARs (which are highly expressed in astrocytes unlike the other two subtypes, α_{2B}-AR and α_{2C}-AR, Zhang *et al.*, 2016) revealed that: (i) receptor staining showed specificity for astrocytes compared to non-astrocyte regions (Fig. 4.4C), and (ii) despite the higher total expression of α_{2A}-AR in the proximal processes (based on the receptor's signal intensity results, Fig. 4.4A & B), analysis of receptor density showed that in fact α_{2A}-AR distribution per membrane area was similar between the somata and the proximal processes while it was significantly higher in the distal processes (Fig. 4.4D).

The antibody to β_1-AR did not produce convincing staining (Fig. 4.5A & B), despite evidence for expression of this receptor in astrocytes (Aoki, 1992; Junker *et al.*, 2002; Zhang *et al.*, 2014, and 2016). This is likely due to lack of specificity of the antibody used. Thus, further quantification of the β_1-AR distribution in astrocytes was not performed.

Overall, results from the antibody labelling experiments provide evidence for selective staining for α_1- and α_2-ARs in hippocampal astrocytes. Furthermore, the results show that the G_q-coupled α_{1A}- and α_{1B}-ARs are equally distributed per membrane area across different compartments of astrocytes, while G_i-coupled α_{2A}-ARs show a stronger expression per membrane area within the distal processes (which are closer to synapses where elevations of $[Ca^{2+}]_i$ have been shown to regulate

excitatory transmission, Di Castro *et al.*, 2011; Panatier *et al.*, 2011), than in the soma and the proximal processes of astrocytes.

4.5.2 Noradrenaline inhibition of glutamate uptake in hippocampal astrocytes

In culture, noradrenaline has been claimed to increase glutamate uptake in astrocytes through the activation of α_1-ARs (Fahrig, 1993) or β-receptors (Hansson & Rönnbäck, 1991). There are, however, concerns with these reports from cultured astrocytes as the cells were not voltage clamped, the experiments did not include blockers of glutamate receptors (see section 4.2 for a discussion of the concerns with these findings from cultured astrocyte).

Interestingly, noradrenaline significantly inhibited the current evoked by D-aspartate in astrocytes in the stratum radiatum region of the hippocampus (Fig. 4.6). This result opposes the findings in cultured astrocytes reported by Fahrig (1993) and Hansson & Rönnbäck (1992). Apart from not using appropriate blockers when measuring glutamate uptake (as discussed in 4.2), further questions arise about the work from these two groups. First, pre-incubation of the cultures with a high concentration of noradrenaline (100 μM) for a short period (2 mins) before the addition of glutamate reportedly enhanced glutamate uptake (Fahrig, 1993) while longer incubation periods (> 5 mins) decreased the uptake or failed to show an increase. Furthermore, the high concentration of noradrenaline used by Fahrig (1993, 100 μM) compared to a more physiological concentrations used in this chapter (2 μM) may also explain the difference seen for the effect of noradrenaline on glutamate uptake. This is important as noradrenaline can have diverse effect on synaptic plasticity when used at a high (8.75 μM) compared to a low (0.33 μM) concentration (Salgado *et al.*, 2012). Another issue with the findings from cultured astrocytes by Hansson & Rönnbäck

(1991) is that they reported a β-AR mediated stimulation of glutamate uptake, without seeing any effect on D-aspartate uptake. This is also unexpected as D-aspartate and glutamate are taken up through the same mechanism, and the glutamate transporters have only a slightly higher affinity for D-aspartate compared to glutamate (e.g. Barbour *et al*., 1991, or see section 1.2.7.2 for detailed discussion).

Inhibition of glutamate transporters by noradrenaline (as seen in Fig. 4.6), and a resulting rise in the extracellular concentration of glutamate, may have two consequences:

(i) The decreased removal of glutamate may enhance excitatory transmission. Indeed, activation of α_1-ARs (Williams *et al*., 2014) has been associated with an increase in excitatory postsynaptic currents in brain slices.

(ii) Elevated levels of extracellular glutamate may dampen excitatory transmission by desensitizing the postsynaptic glutamate receptors. Activation of α_1-ARs (Salgado *et al*., 2012) or α_2-ARs (Yuen *et al*., 2014) has been associated with a decrease in excitatory postsynaptic currents in brain slices.

4.5.3 The mechanism underlying noradrenaline inhibition of glutamate uptake

I initially assessed the contribution of astrocyte $[Ca^{2+}]_i$ (presumably raised by α_1-ARs) to the noradrenaline-evoked inhibition of glutamate transporters. A change in intracellular calcium concentration is a plausible mechanism by which the activity of glutamate transporters may be regulated. This is because noradrenaline-evoked $[Ca^{2+}]_i$ elevations (as reported by Duffy & MacVicar, 1995; Paukert *et al*., 2014; Ding *et al*., 2013) might lead to the insertion into, or removal from the plasma membrane of glutamate transporters. In fact, it has been reported that $[Ca^{2+}]_i$ elevations in astrocytes lead to the insertion of the GABA transporter GAT-3 into the astrocyte

membrane (Shigetomi *et al.*, 2011). Similarly, signalling downstream of G_q-coupled mGluRs has been shown to increase glutamate uptake currents in the hippocampus (Devaraju *et al.*, 2013) and membrane insertion of GLAST glutamate transporters in the cerebellum (Mashimo *et al.*, 2010). However, a decrease in surface expression of GLT-1 has also been reported following protein kinase C (PKC) activation (Kalandadze *et al.*, 2002), which can be activated downstream of Gq-mediated signalling (Hubbard & Hepler, 2006). Thus, the effects of calcium signalling on neurotransmitter transporters are complex.

Interestingly, abolishing calcium concentration elevations inside astrocytes using the chelating agent BAPTA (via the patch pipette), largely inhibited the reduction of glutamate uptake by noradrenaline (Fig. 4.7). Thus, it appears that a rise in astrocyte $[Ca^{2+}]_i$, presumably via α_1-AR activation, is essential for the inhibitory effects of noradrenaline on the glutamate transporter current. Reassuringly, this result was confirmed when α_1-AR activation was inhibited by a potent selective blocker terazosin (Fig. 4.8).

These experiments, therefore, provide evidence that elevations in intracellular concentrations of calcium downstream of α_1-ARs decrease the activity of glutamate transporters in astrocytes. This finding is in line with reports by Kalandadze *et al*. (2002) who reported a decrease in surface expression of GLT-1 downstream of protein kinase C (PKC) activation in neuronal-glial co-cultures. Curiously, PKC is reported to have an opposite effect on the neuronal glutamate transporter EAAC1 (Davis *et al.*, 1998). This suggests that the glial transporters (GLT-1 and GLAST) may be differentially modulated compared to neuronal transporters.

Next, I examined the role of astrocyte $[cAMP]_i$ in the NA-evoked inhibition of glutamate transporters. An effect of cAMP on glutamate uptake is plausible because

the activation of α_2-ARs (which decrease $[cAMP]_i$, Yuen *et al*., 2014) and β-ARs (which increase $[cAMP]_i$, Salgado *et al*., 2012) have been associated with changes in glutamate excitatory postsynaptic transmission (as previously discussed in section 4.5.2). In addition, elevations in $[cAMP]_i$ following the activation of adenosine A_{2A} receptors have been reported to decrease glutamate uptake in cultured astrocytes (Matos *et al*., 2012).

Surprisingly, the addition of a high concentration of cAMP (1 mM) to the intracellular milieu of the astrocytes (via the patch pipette), largely abolished the inhibition of the transporter current evoked by D-aspartate by noradrenaline (Fig. 4.9). Thus, a concentration rise in cAMP inside the cell interferes with the inhibitory effects of noradrenaline on glutamate uptake (presumably by preventing a reduction of $[cAMP]_i$ downstream of α_2-AR activation). In support of this finding, blocking the activity of α_2-ARs with the potent selective α_2-AR blocker atipamezole also blocked the inhibition of the D-aspartate evoked current by noradrenaline (Fig. 4.10).

The results from these experiments are in agreement with the report by Matos *et al*. (2012), that an elevation in $[cAMP]_i$ following activation of adenosine A_{2A} receptors decreased glutamate uptake. However, the findings here provide the extra mechanistic insight that both a reduction in the intracellular concentration of cAMP (via α_2-ARs), and an increase in the concentration of calcium (via α_1-ARs), are needed to inhibit glutamate transporters in hippocampal astrocytes.

It is possible that the activation of either α_1-ARs or α_2-ARs may lead to changes in both the intracellular calcium and the cAMP concentrations. For example, some reports suggest that the activation of α_1-ARs can decrease the intracellular cAMP accumulation, in addition to its conventional role of elevating calcium (Barrett *et al*., 1993). Moreover, activating α_2-ARs not only reduces $[cAMP]_i$ but also

stimulates phospholipase C (a membrane-bound enzyme that is activated via G_q-coupled proteins) to stimulate IP_3-depenedent release of calcium from internal stores (Chabre *et al*., 1994; see also Zhu & Birnbaumer, 1996). At present it is unclear how Ca^{2+} and cAMP signalling synergise to regulate glutamate transport, but such synergy has been shown previously shown in mitochondria where calcium (Glancy *et al*., 2013) and cAMP (Acin-Perez *et al*., 2009) can both regulate oxidative phosphorylation and stimulate ATP production. Application of α_1-ARs and α_2-ARs antagonists (or alternatively selective agonists) while patch-clamping astrocytes, in combination with calcium imaging, can help to decipher how these two receptor subtypes may contribute to reducing glutamate uptake in astrocytes.

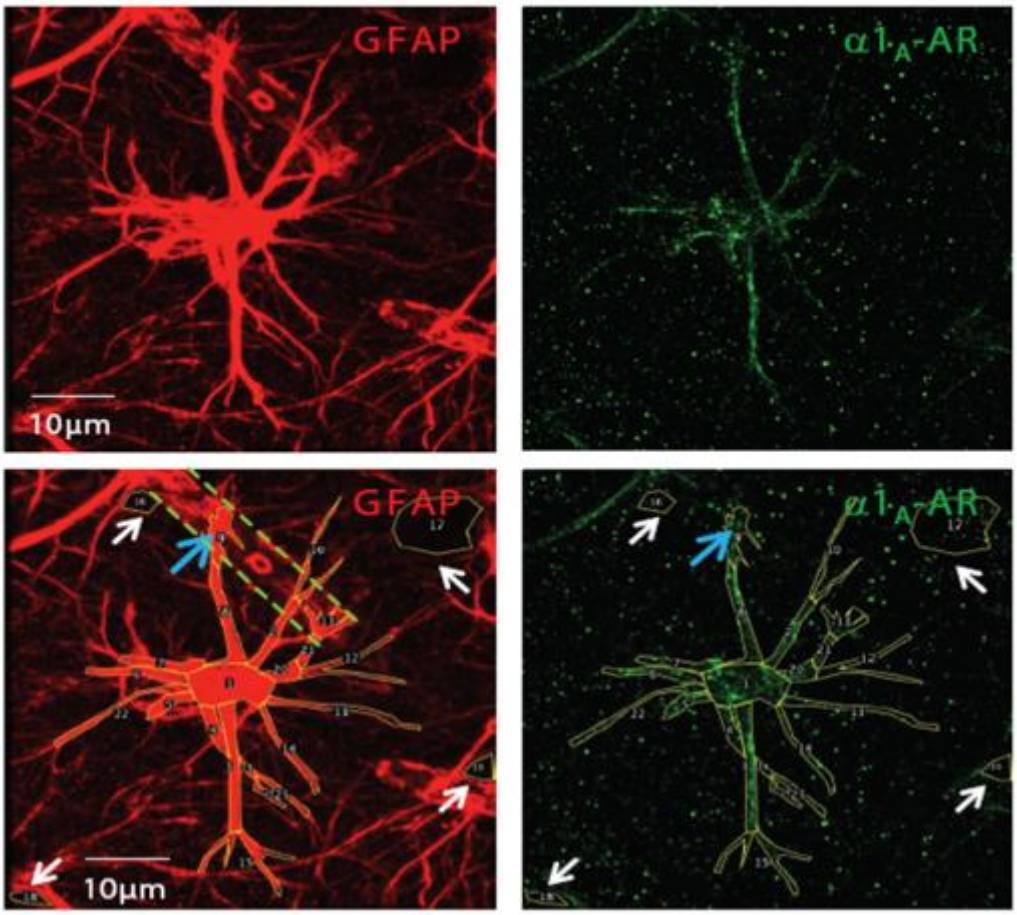

Figure 4.1: Quantification of signal intensity and receptor density within each astrocyte compartment.
Top: raw images. Bottom: segmentation of different areas (yellow lines defined on GFAP image and copied to AR image). Each astrocyte was divided into four morphological compartments (using the red GFAP signal as a guide): the soma (i.e. the region surrounding the cell nucleus), proximal processes (i.e. processes before the first branching point), distal processes (i.e. processes after the first branching point), and endfeet (the area associated with a blood vessel, blue arrows: endfeet, green dashed line: blood vessel). The boundaries of each compartment were marked manually in ImageJ. The total (spatially integrated) signal for the adrenoceptors (the green channel) was measured for each compartment. Signal intensity for adrenoceptors within the non-astrocyte regions (marked with white arrows) was also calculated. For the analysis of receptor density within each astrocytic compartment, the average intensity of AR labelling per μm^2 of surface area was measured. Inferences regarding the surface area were made by assuming that the soma corresponded to a sphere, while astrocyte processes were akin to cylinders. Thus, the radius of the soma, the radius of each astrocytic process and the length of each astrocytic process were measured manually. Analysis of receptor density was done for all the compartments except for the endfeet which had more complex surface areas.

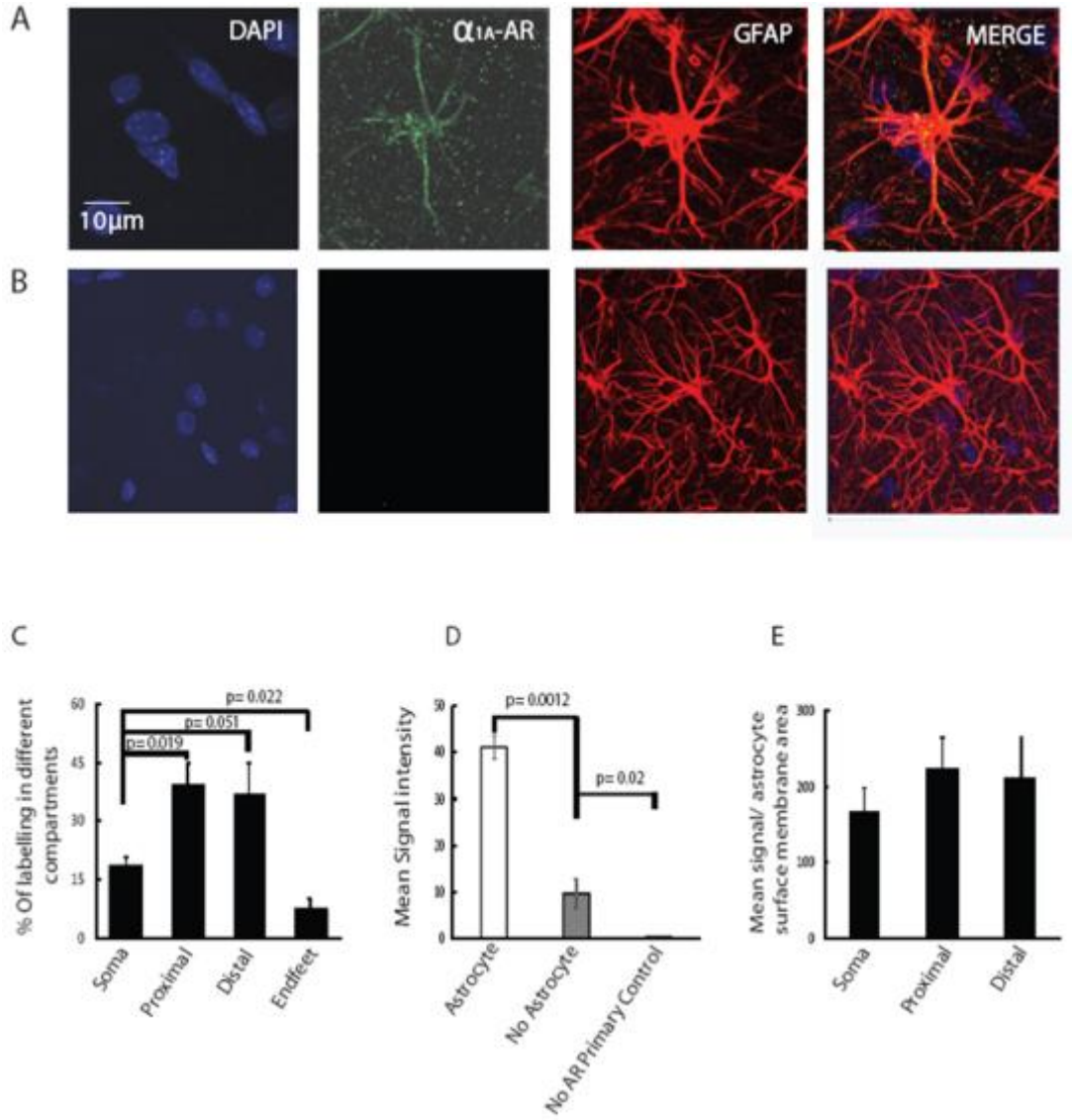

Figure 4.2: Expression of α_{1A}-ARs in hippocampal astrocytes.
A. Double immunofluorescence staining for α_{1A}-AR (green) and the astroglial marker GFAP (red) in hippocampal astrocytes, along with the nuclear marker DAPI (blue). **B.** Control experiments were carried out in the presence of the primary antibody against GFAP (red) while the adrenoceptor antibody was absent. **C.** Expression pattern of α_{1A}-AR across different compartments of astrocytes, with most receptors being in the processes. **D.** α_{1A}-AR staining showed reasonable specificity for astrocytes (white bar) compared to the "non-astrocyte" regions (grey bar) which may have neuronal labelling in them. In addition, α_{1A}-AR expression in the non-astrocytic regions was stronger than in the negative control sample (i.e. with no primary antibody against α_{1B}-AR present, 'No AR primary control', black bar) **E.** Average α_{1A}-AR density per μm^2 surface area in different spatial compartments (excluding endfeet) revealed a homogenous density of expression. P-values were corrected for multiple testing within panels C & D.

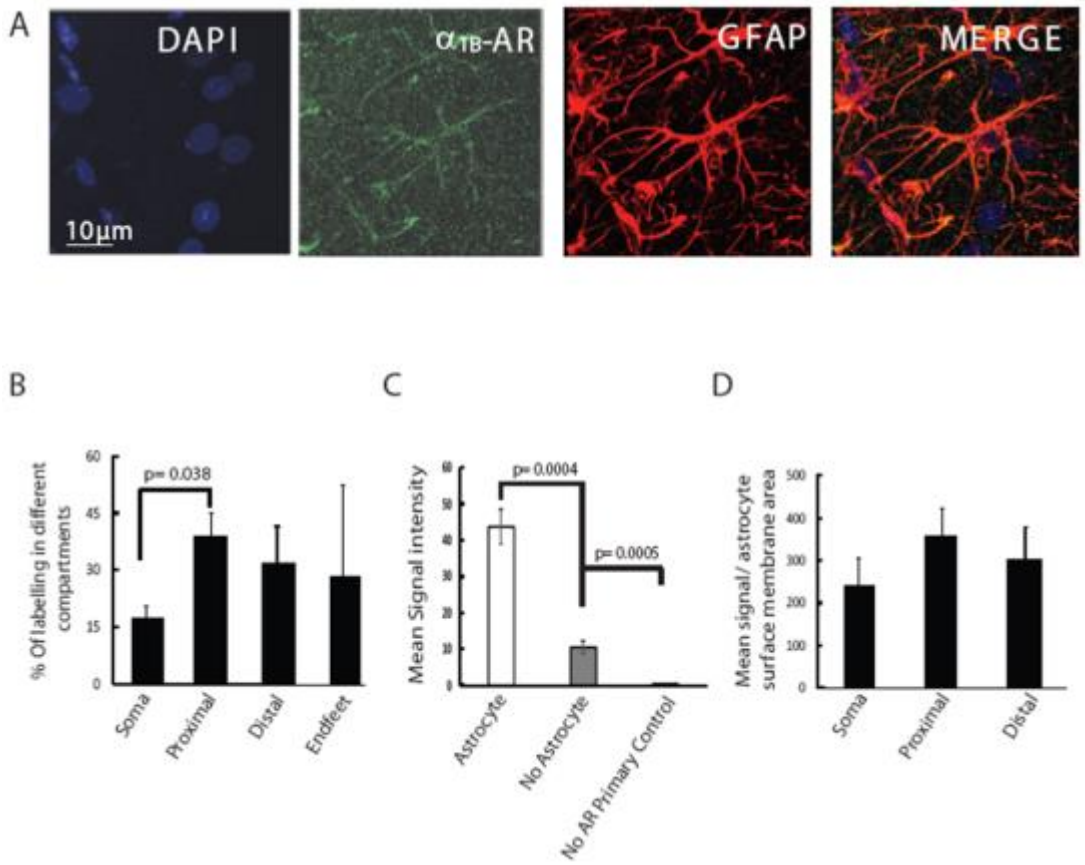

Figure 4.3: Expression of α_{1B}-ARs in hippocampal astrocytes.

A. Double immunofluorescence staining for α_{1B}-AR (green) and the astroglial marker GFAP (red) in hippocampal astrocytes, along with the nuclear marker DAPI (blue). **B.** α_{1B}-AR staining revealed a variation across different compartments of astrocytes, with the highest expression per compartment in the processes. **C.** α_{1B}-AR staining showed specificity for astrocytes (white bar) compared to the non-astrocyte regions (grey bar), and α_{1B}-AR expression in the non-astrocytic regions was stronger than in the negative control sample (i.e. with no primary antibody against α_{1B}-AR present, 'No AR primary control', black bar). **D.** Average α_{1B}-AR density per μm^2 surface area of different spatial compartments (excluding endfeet) revealed a fairly homogenous pattern of expression. p-values were corrected for multiple testing within panel B & C.

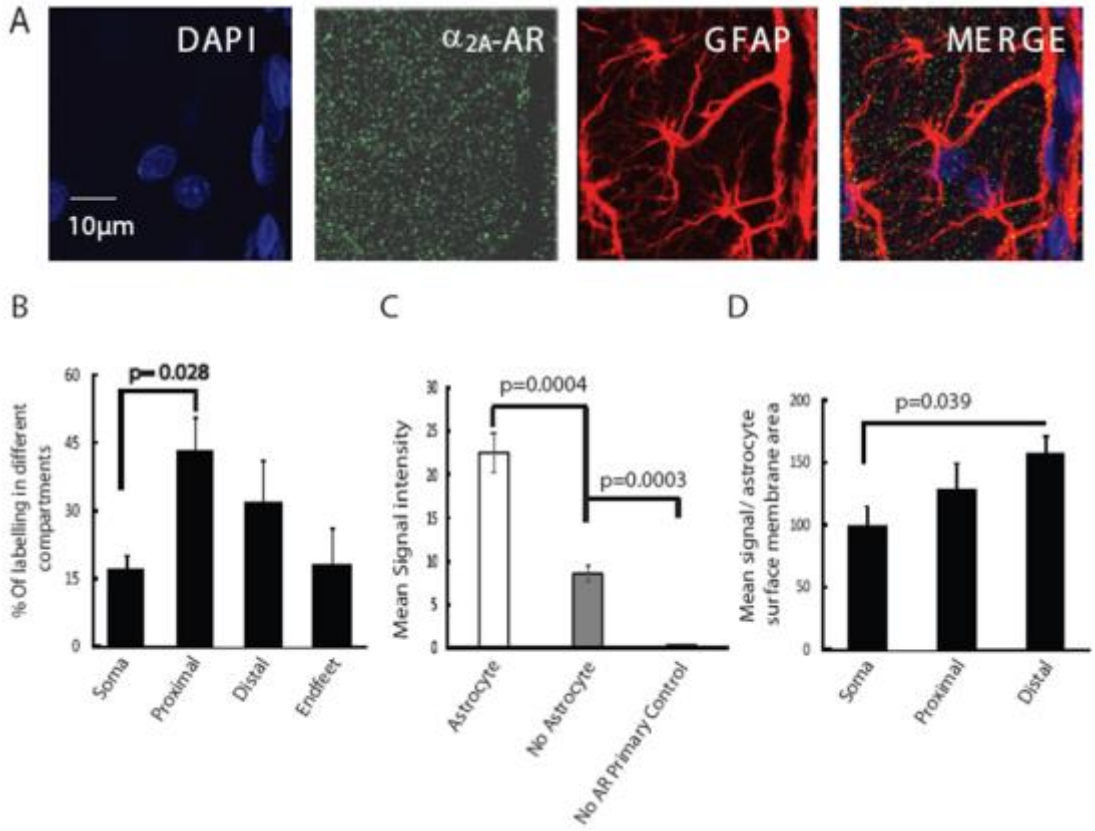

Figure 4.4: Expression of α_{2A}-ARs in hippocampal astrocytes.
A. Double immunofluorescence staining for α_{2A}-AR (green) and the astroglial marker GFAP (red) in hippocampal astrocytes, along with the nuclear marker DAPI (blue). **B.** α_{2A}-ARs staining revealed a variation across different compartments of astrocytes, with the highest expression in the proximal processes. **C.** α_{2A}-AR staining showed specificity for astrocytes (white bar) compared to the non-astrocyte regions (grey bar), and α_{2A}-AR expression in the non-astrocytic regions was stronger than in the negative control sample (i.e. no primary antibody against α_{2A}-AR was present, 'No AR primary control', black bar). **D.** Average α_{2A}-AR density per μm^2 surface area of different spatial compartments (excluding endfeet) revealed a higher density of α_{2A}-ARs in the distal processes compared to the soma, while there was no difference seen between the somata and the proximal processes. P-values were corrected for multiple testing within panels B-D.

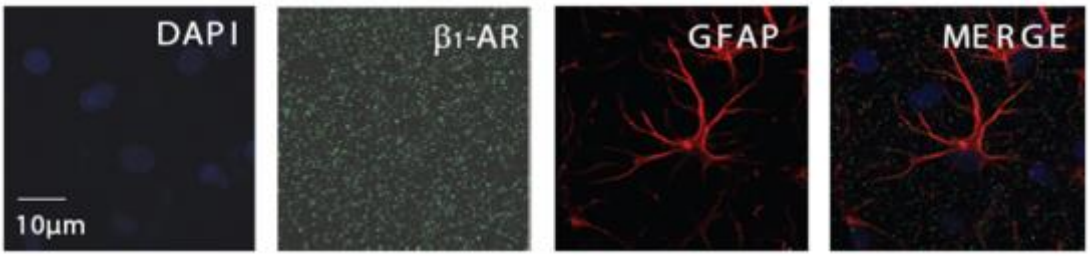

Figure 4.5: Expression of β_1-ARs in hippocampal astrocytes.

A. Double immunofluorescence staining for β_1-AR (green) and the astroglial marker GFAP (red) in hippocampal astrocytes, along with the nuclear marker DAPI (blue).

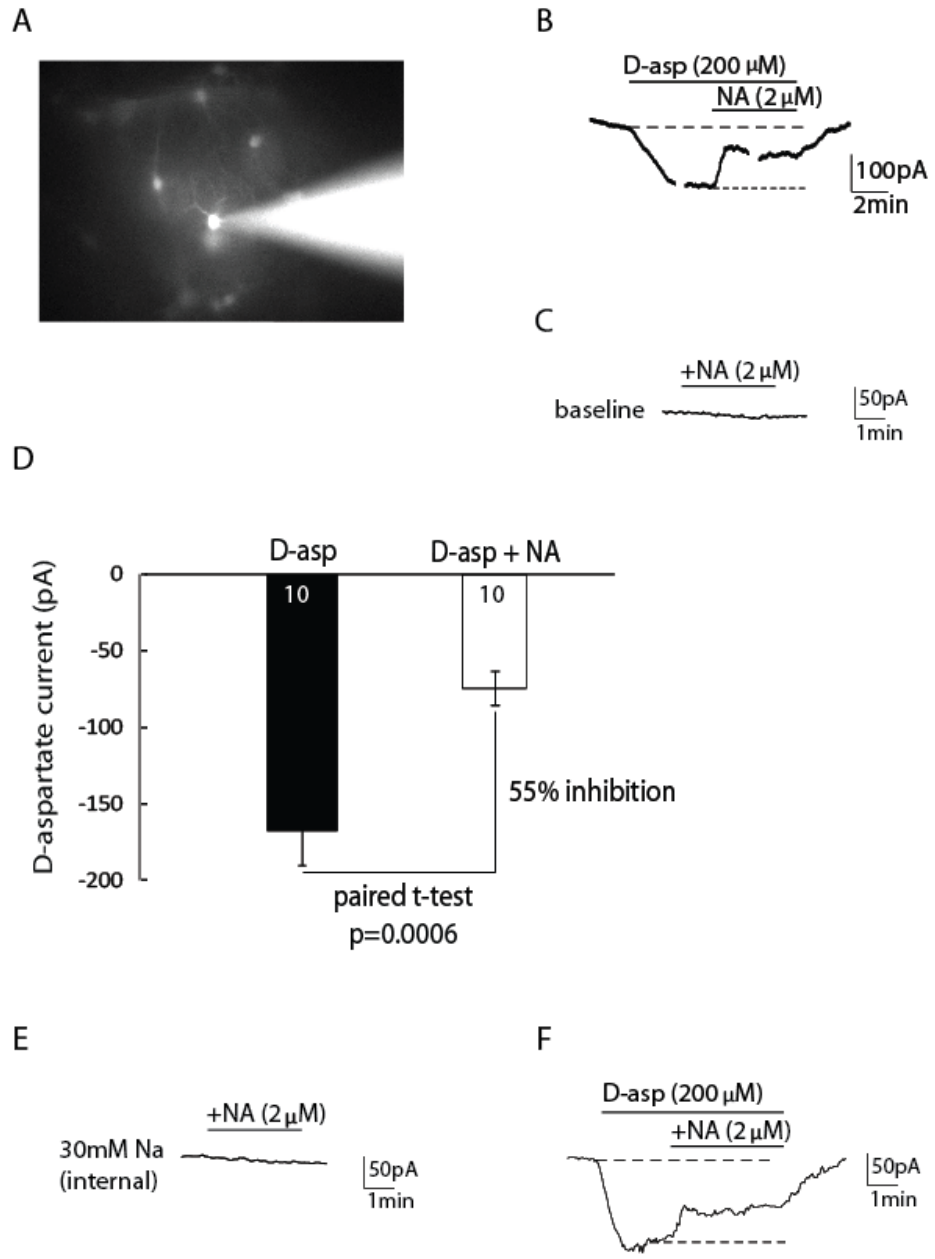

4.6 Noradrenaline inhibits glutamate uptake in astrocytes

A. A sample image of a whole-cell patch clamped astrocyte in the stratum radiatum region of the hippocampus and its gap junctionally coupled neighbouring astrocytes, revealed by dialysis with the membrane impermeable dye Alexa 488. **B.** A sample trace showing the current evoked by D-aspartate (200 µM) alone and in the presence of noradrenaline (2 µM). **C.** A sample trace showing the failure of noradrenaline (2 µM) to evoke a current in the absence of D-aspartate. **D.** Quantification of the glutamate uptake current (proportional to the rate of D-aspartate uptake) in astrocytes revealed a significant reduction when noradrenaline (NA) was present. **E.** A sample trace showing the failure of noradrenaline (2 µM) to evoke a current in the absence of D-aspartate, when 30 mM sodium was added to the internal solution via the patch pipette. **F.** A sample trace showing the inhibition of the D-aspartate evoked current by noradrenaline with high $[Na^+]_i$ in the internal solution.

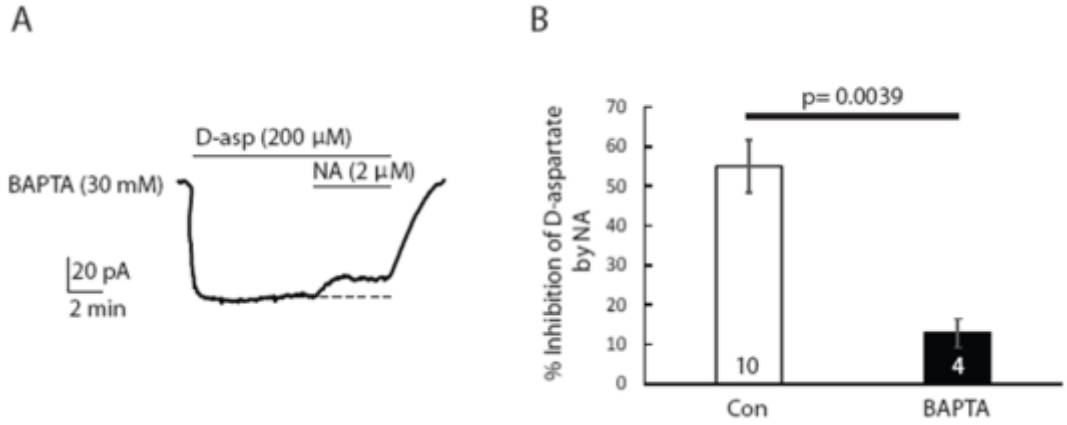

4.7 Calcium mediates the noradrenaline evoked-inhibition of glutamate uptake

A. A sample trace showing the current evoked by D-aspartate (200 µM) alone and in the presence of noradrenaline (NA, 2 µM) when a high concentration of calcium chelator BAPTA (30 mM) was added to the internal solution through the patch pipette. **B.** Quantification of the percentage inhibition of the glutamate uptake current by noradrenaline, with 10 mM EGTA in the internal solution (white bar, 'Con', from Fig. 4.6) or when BAPTA replaced EGTA (black bar, 'BAPTA').

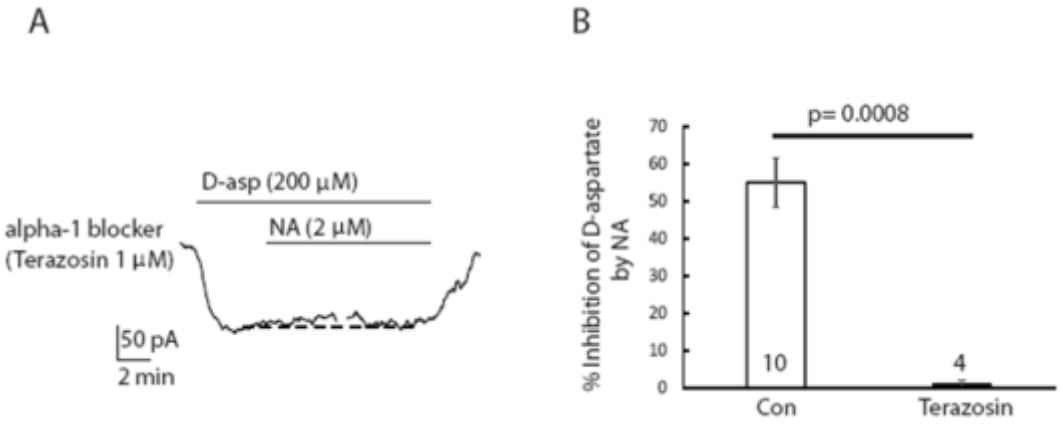

4.8 α_1-evoked calcium elevations mediate the effect of noradrenaline on glutamate uptake

A. A sample trace showing the current evoked by D-aspartate (200 µM) alone and in the presence of noradrenaline (NA, 2 µM) in the presence of an α_1-AR blocker terazosin (1 µM, added to the aCSF and present throughout the experiment). **B.** Quantification of the percentage inhibition of the glutamate uptake current by noradrenaline alone (white bar, 'Con', from Fig. 4.6) or when terazosin was present (black bar, 'terazosin').

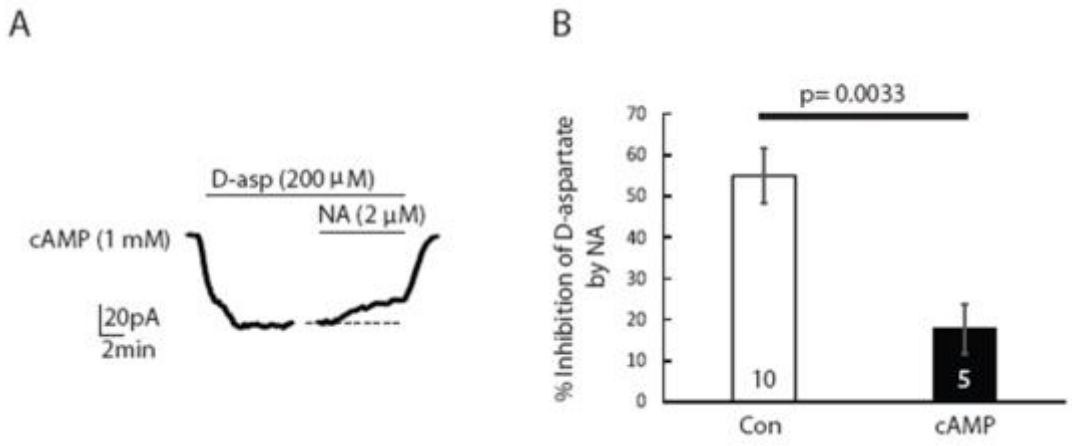

4.9 cAMP abolishes the noradrenaline evoked-inhibition of the glutamate uptake current

A. A sample trace showing the current evoked by D-aspartate (200 µM) alone and in the presence of noradrenaline (NA, 2 µM) when a high concentration of cAMP (1 mM) was added to the internal solution through the patch pipette. **B.** Quantification of the percentage inhibition of the glutamate uptake current by noradrenaline alone (white bar, 'Con', from Fig. 4.6) or when cAMP was present (black bar, 'cAMP').

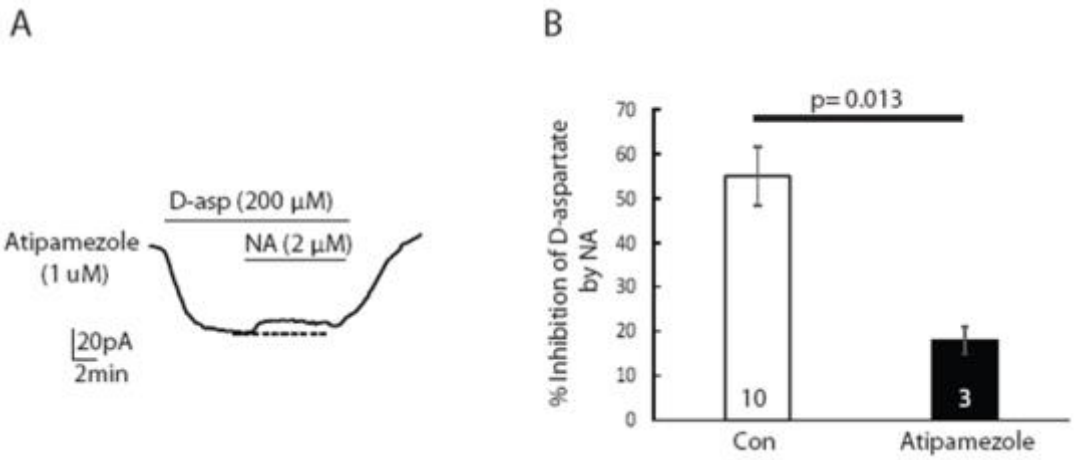

4.10 α_2-evoked decrease in cAMP levels contributes to the inhibitory effects of noradrenaline on glutamate uptake

A. A sample trace showing the current evoked by D-aspartate (200 µM) alone or in the presence of noradrenaline (NA, 2 µM) in the presence of an α_{2A}-AR blocker atipamezole (1 µM, added to the aCSF and present throughout the experiment). **B.** Quantification of the percentage inhibition of the glutamate uptake current by noradrenaline alone (white bar, 'Con', from Fig. 4.6) or when atipamezole was present (black bar, 'atipamezole').

Chapter 5:

Regulation of the glutamate transporter GLT-1 by the intracellular protein nischarin

5.1 Summary of this chapter

GLT-1 is the most highly expressed glutamate transporter in the forebrain, especially in the hippocampus. Factors that regulate the internalization of this transporter can affect the GLT-1 surface expression level and hence the extracellular concentration of glutamate. Unpublished biochemical data from the Attwell and Kittler Labs have shown that nischarin, a mouse homologue of the human imidazoline type 1 receptor, binds directly to GLT-1 and helps to internalize this transporter, which leads to a reduction in GLT-1 surface levels. I will provide functional evidence from whole-cell patch-clamp recordings in astrocytes from embryonic hippocampal tissue cultures showing that the expression of nischarin reduces glutamate uptake.

5.2 Introduction

The removal of glutamate from the extracellular space, especially the synaptic cleft, by glutamate transporters ensures precision in glutamatergic transmission, and maintains a low extracellular glutamate level to avoid excitotoxicity (see section 1.2.7 for more details). In the forebrain, the task of glutamate uptake is mainly carried out by GLT-1 glutamate transporters, which constitute about 80% of the transporters present (Danbolt *et al*., 1994; Lehre *et al*., 1995; Chaudhry *et al.*, 1995; Haugeto *et al*., 1996). The mechanisms by which glutamate transport by GLT-1 is regulated inside the cell, are however, poorly understood.

Intracellular proteins can interact with, and modulate the activity, and surface levels of, glutamate transporters, as described in section 1.2.7.7. A protein that has been shown to directly interact with GLT-1 is nischarin (unpublished data from the Attwell and Kittler Labs), a mouse homologue of the human imidazoline receptor (Piletz *et al.*, 2003; Zhang & Abdel-Rahman, 2006, see section 1.2.7.7 for more details) that may act as a membrane-associated mediator of receptor signaling. Nischarin, which belongs to the super family of Rab and Rac GTPases, contains an N-terminal PHOX domain that binds to the intracellular N-terminus of the GLT-1 transporter (Fig. 5.1, unpublished data from the Kittler Lab). This interaction promotes the internalization and endosomal targeting of GLT-1 (Fig. 5.1). In fact, unpublished results from the same group have shown that global deletion of the nischarin gene significantly increases the total expression of GLT-1 transporters in astrocytes (Fig. 5.2), as measured by the antibody signal intensity within the intracellular and plasma membrane compartments of astrocytes. The overall increase in GLT-1 expression (as seen in Fig. 5.2) when nischarin is absent, in conjunction with unpublished data showing an increase in internalization and endosomal targeting of GLT-1 when nischarin is deleted (data not shown), suggest that the expression of nischarin not only evokes the internalization of GLT-1 from the plasma membrane but also may trigger its degradation following its transport to the endosome (Fig. 5.2 A & B, unpublished data from the Kittler Lab).

On the basis of this previous knowledge, I examined the functional consequences of nischarin gene deletion for glutamate uptake in astrocytes, in embryonic hippocampal tissue cultures prepared from mice that either express nischarin (i.e. the wildtype, WT) or lack nischarin (i.e. the knockout, KO). I will

provide evidence from whole-cell patch clamp recordings from astrocytes for an increase in glutamate uptake when nischarin expression is abolished.

5.3 Methods

5.3.1 Cultures

Embryonic hippocampal cultures were obtained (from the Kittler lab) on their tenth day *in vitro*. Cultures were prepared from nischarin WT or KO mice embryos at 16 days post-fertilization. The *Nisch* KO mouse line was generated by the Wellcome Trust Sanger Institute by inserting a L1L2_Bact_P cassette encoding an engrailed1 splice acceptor sequence, a LacZ reporter and a neomycin resistance gene between exons 4 and 5, thus disrupting *Nisch* transcription. Homozygous mice ($Nisch^{-/-}$) and their control wild-type ($Nisch^{+/+}$) littermates were obtained by crossing the heterozygous mice ($Nisch^{+/-}$).

5.3.2 Electrophysiology

Electrophysiology was carried with a HEPES-based external solution and a potassium gluconate based internal solution, as described in chapter 2 (sections 2.3.1 and 2.3.2). Astrocytes were recognised visually by their low contrast soma, with an angular morphology, stellate processes revealed by dye-coupling and usually gap junctional coupling allowing dye spread to other nearby astrocytes (Fig. 5.3A).

5.3.3 Statistical analysis

Statistical significance was determined with Origin Pro or Excel. All the values in the text and figures are means ± s.e.m. Further details of the statistical analysis are given in section 2.10.

5.4 Results

In order to assess whether the increase in total GLT-1 present when nischarin is deleted (as shown in Fig. 5.2) produces an increase in surface membrane glutamate transport, I compared the magnitude of the glutamate transporter current evoked by D-aspartate (i.e. reflecting glutamate uptake, see section 1.2.7.5) in WT and KO hippocampal astrocytes in hippocampal tissue cultures. To do this, astrocytes were whole-cell voltage clamped (near their resting potential, see Fig. 5.3A for examples of patch-clamped astrocytes) and responses to D-aspartate (200 μM) were recorded in the presence and absence of the glutamate transporter blocker, TFB-TBOA (see section 1.2.7.4 in chapter 1 for more information).

Interestingly, and as might be expected from the increase of the surface GLT-1 level when nischarin was deleted (See Fig. 5.2B), the size of the glutamate uptake current was significantly larger when nischarin was deleted in astrocytes compared to WT astrocytes (Fig. 5.3B-C, mean current=-103±17 pA for the WT, n=10; and -225±54 pA for the KO, n=8, unpaired t-test p=0.029). The glial glutamate transporter blocker, TFB-TBOA, which blocks both GLT-1 and GLAST transporters (Shimamoto *et al*., 1998), blocked the D-aspartate evoked current in both the WT and the KO, confirming that the current is generated by glutamate transporters (Fig. 5.3D, mean percentage block=99.0±1.4% for the WT, and 99.6±0.3% for the KO, not significantly different, unpaired t-test p=0.67).

The expression of nischarin did not affect the membrane resistance (Fig. 5.4A, mean resistance=18±4 MΩ for the WT, n=10; and 23±5 MΩ for the KO, n=8, unpaired t-test p=0.4), or the cell capacitance (Fig. 5.4B, mean capacitance=66±9 pF for the WT, n=10; and 55±16 pF for the KO, n=8, unpaired t-test p=0.9) of astrocytes.

Importantly, the glutamate uptake current was still significantly larger in the nischarin KO astrocytes compared to the WT astrocytes when the size of the D-aspartate evoked current was normalised to the astrocyte capacitance in each cell (Fig. 5.4C, normalised uptake current=1.9±0.4 pA/pF for the WT, n=10; and 3.6±0.7 pA/pF for the KO, n=8, unpaired t-test p=0.04).

These results suggest that the expression of nischarin reduces glutamate uptake into astrocytes, presumably by promoting the net removal of GLT-1 transporters from the surface membrane, resulting in them being targeted to the endosome where they are degraded.

5.5 Discussion

Nischarin has been proposed as a mouse homologue of the human imidazoline receptor (Piletz *et al*., 2003; Zhang & Abdel-Rahman, 2006, see section 1.2.7.7 for more details). Recent unpublished data from the Attwell and Kittler labs suggest that nischarin directly binds to GLT-1 (Fig. 5.1). Furthermore, this interaction decreases the total number of GLT-1 glutamate transrporters in astrocytes in culture by promoting GLT-1 internalization and thus its degradation (see Fig. 5.2; unpublished data from the Kittler lab).

In agreement with an inhibitory effect of nischarin on GLT-1 expression (as shown in Fig. 5.2), I demonstrated an increase in glutamate uptake current in astrocytes when nischarin was deleted, compared to WT astrocytes (Fig. 5.3B & C). In addition, I confirmed that the inward current that was evoked by D-aspartate was indeed generated by glutamate transporters since it was fully abolished by the glial glutamate transporter blocker TFB-TBOA (Fig. 5.3D). Thus, the increase in total expression of GLT-1 in the nischarin KO also leads to more GLT-1 being present in the astrocyte's surface membrane.

Furthermore, I showed that the increase in glutamate uptake current in cultured astrocytes in nischarin KO tissue was not due to an increase of cell area, since the cells had a similar capacitance (Fig. 5.4B) in the WT and KO. Indeed, glutamate uptake was significantly larger in the KO compared to the WT even when the glutamate uptake was normalised to the astrocyte cells' capacitance in each cell.

Results from this chapter suggest a key role for nischarin in regulating glutamate uptake in astrocytes. There are, however, important questions that need further examination.

Although, the unpublished data from the Attwell and Kittler labs have suggested a direct interaction between nischarin and GLT-1, but not GLAST, it is not known whether nischarin-mediated internalization of GLT-1 may indirectly affect the total level of GLAST in the astrocyte plasma membrane (which could occur if GLT-1 and GLAST can form heterotrimers, as seen for WT and mutated EAAC1: Yernool *et al.*, 2004; Grewer *et al.*, 2005). Furthermore, it is not clear what proportion of the D-aspartate evoked-current that was recorded in Fig. 5.3 is generated by GLT-1 as opposed to GLAST. Demonstrating a selective inhibition of GLT-1 transporters by dihydrokainate (DHK, Arriza et al., 1994), which there was not time to do for my thesis, would determine whether the larger D-aspartate evoked current in the KO is generated by GLT-1 or GLAST.

GLT-1 expression levels increase during development (Kugler & Schleyer, 2004), thus, the inhibition of total GLT-1 protein level by nischarin (Fig. 5.2) raises the question as to whether nischarin expression itself decreases during development.

While GLT-1 is highly expressed in astrocytes, neurons and oligodendrocyte precursor cells also express GLT-1 but at a lower level (Furness *et al.*, 2008; Zhang *et al.*, 2014). It has been estimated that, in hippocampus, 10% of the total GLT-1 is present in the CA3 hippocampal axonal terminals (Furness *et al.*, 2008). Nischarin, on the other hand, is expressed in most cell types (Zhang *et al.*, 2014). Therefore, it would be useful to examine whether nischarin reduces glutamate uptake in other cell types like it does in astrocytes. In addition, a confirmation of the effect of nischarin on glutamate uptake in brain slices would further strengthen this finding.

In addition, nischarin, as a mouse homologue of the human imidazoline receptor type 1 (Piletz *et al.*, 2003; Zhang, J. & Abdel-Rahman, 2006), has been suggested to code for a functional imidazoline receptor in pheochromocytoma cells

(Sun *et al*., 2007). However, it not clear if nischarin acts as a functional receptor with an extracellular domain for the binding of imidazolines, the activation of which may perhaps lead to the internalisation of GLT-1 transporters. Thus, further experiments assessing the effect of imidazoline signalling on glutamate uptake in the WT and nischarin KO would be informative.

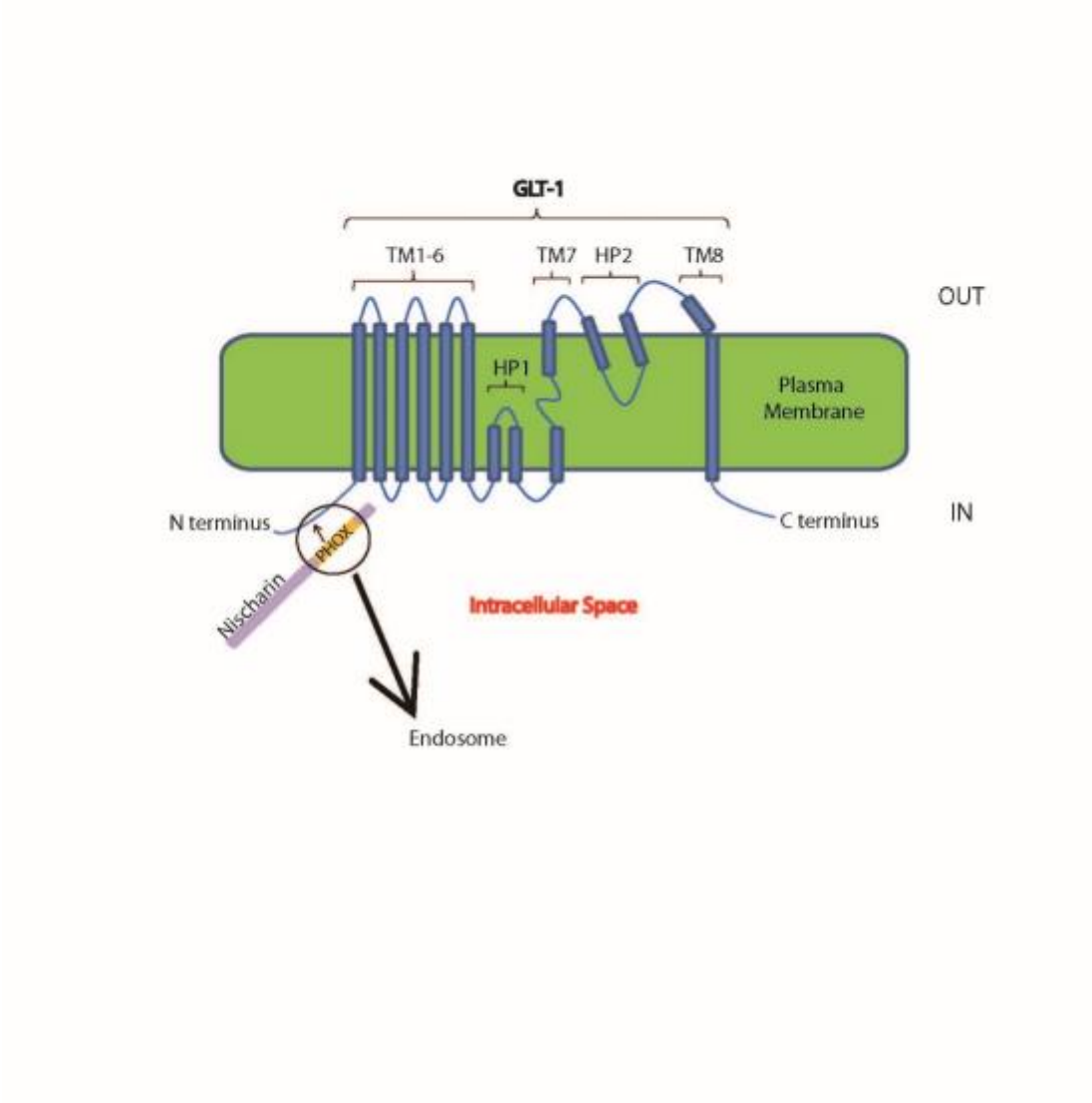

Figure 5.1: Nischarin binds to GLT-1 glutamate transporters.

A schematic of GLT-1 structure is shown which contains 8 transmembrane domains (TM1-8) and two hairpins (HP1 & 2) based on the crystal structure of a bacterial homologue (see Yernool *et al*., 2004 for more details). Early data from the Attwell lab by Hélène Marie showed that nischarin directly binds to GLT-1. More recently, the Kittler lab has shown that nischarin binds to the N-terminus of GLT-1 via its N-terminal PHOX domain. This interaction triggers internalisation of GLT-1, and its targeting to the endosome.

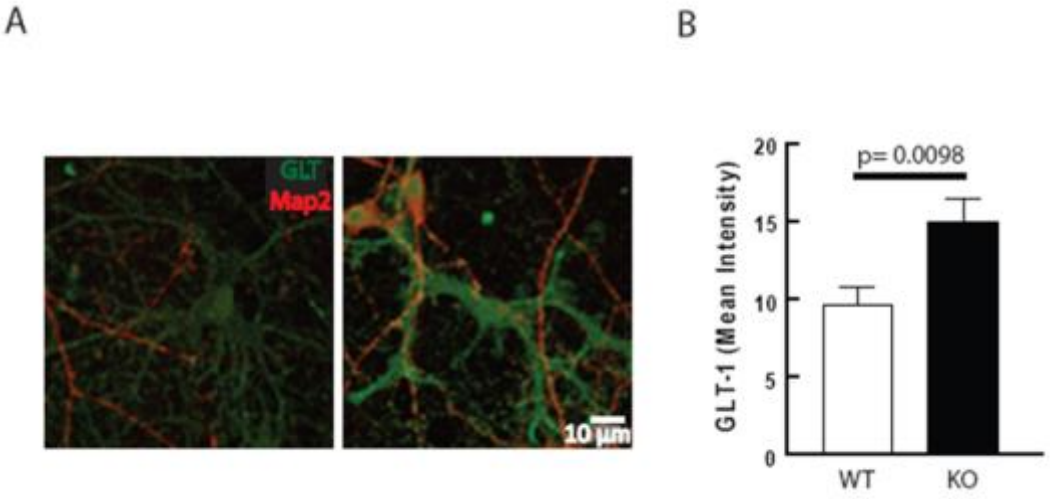

Figure 5.2: Nischarin regulates the expression of GLT-1 in cultured astrocytes.

A. A sample image of double immunolabelling for neurons (Map2 positive, shown in red), and astrocytes (GLT-1 positive and Map2 negative, shown in green) are presented for WT and nischarin KO astrocytes in hippocampal tissue culture. **B.** Quantification of the GLT-1 signal intensity in the WT and nischarin KO shows a significant elevation of GLT-1 expression in the KO. Data shown are the mean ± s.e.m.

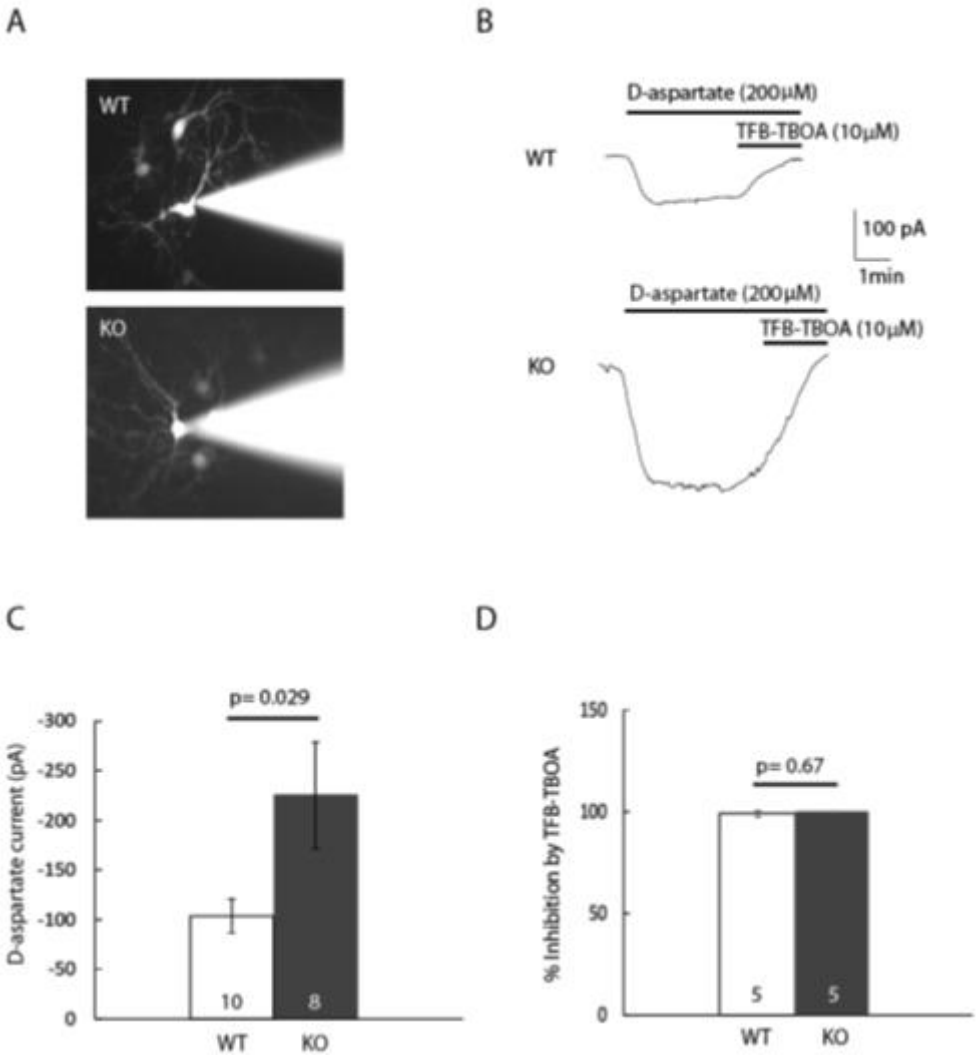

Figure 5.3: Nischarin expression reduces glutamate uptake in astrocytes.

A. Examples Alexa 488 filled astrocytes in the WT and nischarin KO hippocampal tissue culture cultures (at day *in vitro* 10). **B.** A sample trace showing the D-aspartate evoked (200 μM) current and its inhibition by a GLT-1 and GLAST transporter blocker, TFB-TBOA (10 μM), in WT and nischarin KO astrocytes. **C.** Genetic deletion of nischarin results in a significant increase in the size of the D-aspartate evoked current recorded in the KO astrocytes compared to the WT. **D.** D-aspartate evoked current is completely blocked by TFB-TBOA. Data shown are the mean ± s.e.m.

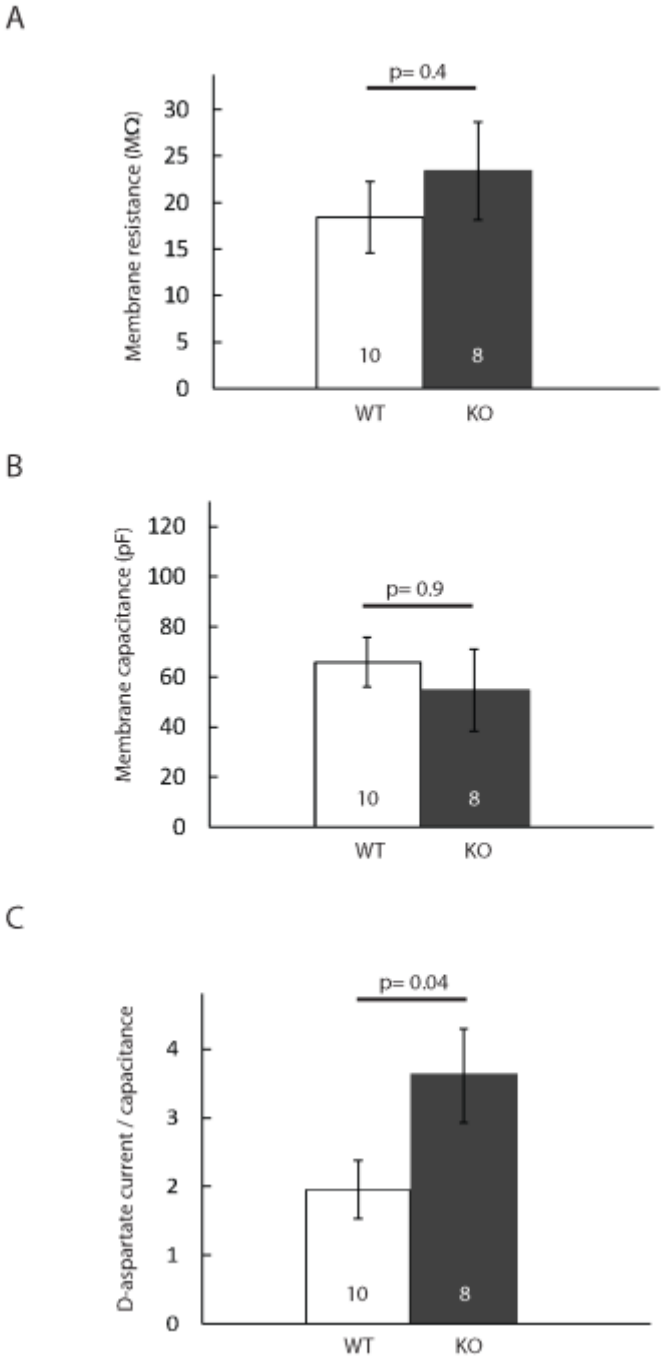

Figure 5.4: Nischarin expression does not affect the basic electrophysiological properties of astrocytes.
A & B. Astrocytes from WT and nischarin KO hippocampal tissue culture showed a similar membrane resistance (**A**), and cell capacitance (**B**). **C.** The D-aspartate evoked current was significantly larger in the nischarin KO astrocytes compared to the WT astrocytes when normalised to the astrocyte capacitance. Data shown are the mean ± s.e.m.

Chapter 6:

The role of astrocyte calcium in basal and noradrenaline-modulated synaptic transmission

6.1 Summary of this chapter

I assessed the role of astrocyte calcium signalling in spontaneous excitatory and inhibitory synaptic transmission, in CA1 pyramidal neurons, in the absence or presence of noradrenaline. The results showed that: (i) the majority of spontaneous excitatory transmission recorded in CA1 pyramidal neurons results from action potential-independent release of vesicles from synaptic terminals, while the majority of spontaneous inhibitory transmission reflects action potential-dependent release of vesicles from neighbouring interneurons; (ii) changes in astrocyte calcium concentration do not affect the presynaptic release probability (i.e. rate) or the postsynaptic magnitude (i.e. amplitude) of the spontaneous excitatory postsynaptic currents (EPSCs); (iii) changes in astrocyte $[Ca^{2+}]_i$ regulate the rate of spontaneous inhibitory postsynaptic currents (IPSCs); and (iv) noradrenaline (NA) enhances the rate and amplitude of action potential-dependent inhibitory transmission in this region, but these effects are largely independent of astrocyte Ca^{2+} signalling.

6.2 Introduction

Neuron-to-astrocyte signalling, by means of neurotransmitters like glutamate, GABA and ATP, can lead to widespread or focal elevations of calcium concentration, $[Ca^{2+}]_i$, in the astrocyte somata or fine processes (reviewed by Bazargani & Attwell, 2016). These Ca^{2+} signals, in turn, have been suggested to evoke the release of

gliotransmitters from astrocytes, which can alter the function of nearby neurons (as reviewed extensively in chapter 1, section 1.2.6). The mechanisms underlying neurotransmitter-evoked elevations in $[Ca^{2+}]_i$ in astrocytes, and the subsequent Ca^{2+}-evoked release of gliotransmitters, are highly controversial (Bazargani & Attwell, 2016). Originally, it was proposed that neurotransmitters bind to G-protein coupled receptors to raise $[Ca^{2+}]_i$ through an IP_3-dependent pathway that liberates Ca^{2+} from the endoplasmic reticulum (Porter & McCarthy (1996); Zonta et al. (2003); Newman, 2001). However, more recently, it has become clear that Ca^{2+} can also enter astrocytes via Ca^{2+}-permeable ion channels (Shigetomi et al., 2012; Hamilton et al. 2008; Palygin et al. 2010; Newman, 2005). Furthermore, astrocyte Ca^{2+} transients display different kinetics in the somata and in the fine astrocytic processes that envelope synapses, which may be partly due to differences in the mechanisms by which they arise (see Bazargani & Attwell (2016) and Shigetomi, Patel & Khakh (2016) for recent reviews). The faster, more local, Ca^{2+} transients in the fine processes appear to evoke the release of gliotransmitters near synapses (Di Castro et al., 2012), thus regulating neuronal information processing (Yang et al., 2003; Mothet et al., 2005; Henneberger et al., 2010), sleep (Halassa et al. (2009), energy supply to the brain (Gordon et al., 2008; Attwell et al. 2010), and respiration (Angelova et al., 2015).

Various tools have been used to study the effects of astrocyte $[Ca^{2+}]_i$ changes on their neighbouring neurons (see section 1.2.6 for more details). These tools include: (i) stimulation-evoked release of neurotransmitters from synapses (Di Castro et al., 2011; Panatier et al., 2011), (ii) calcium uncaging in, or glutamate uncaging near, astrocytes to regulate postsynaptic excitatory (Wang et al., 2013) and inhibitory transmission (Lalo et al., 2014), (iii) disrupting the vesicular-release machinery in astrocytes to modulate excitatory and inhibitory neurotransmission (Deng et al., 2011;

Lalo et al., 2014), (iv) raising astrocyte $[Ca^{2+}]_i$, by expressing in astrocytes a nonmammalian G_q-coupled receptor that could be activated by an exogenous molecule (a designer receptor exclusively activated by a designer drug, or DREADD) (Bonder & McCarthy, 2015; Fiacco et al., 2007), and (v) *in vivo* optogenetic stimulation of astrocytes to evoke Ca^{2+}-dependent release of gliotransmitters - glutamate to regulate visual information processing (Perea & Sur, 2014) and ATP to control breathing (Gourine et al., 2010).

These experiments have yielded interesting but somewhat variable findings. While some dispute the identity of the signalling molecules that raise $[Ca^{2+}]$ in the fine processes of the astrocytes, and also the identity of the gliotransmitters released from astrocytes that regulate presynaptic release probability (Di Castro et al., 2011; Panatier et al., 2011; Lalo et al., 2014; Shigetomi et al., 2012), others even question the functional importance of astrocyte $[Ca^{2+}]_i$ for modulating neuronal function (Bonder & McCarthy, 2015; Fiacco et al., 2007, see detailed discussion in section 1.2.6). Reinforcing skepticism over the physiological relevance of astrocyte Ca^{2+} in regulating neurotransmission, some researchers show either an increase or a decrease in the spontaneous activity of the same class of neurons following astrocytic Ca^{2+} rises (Perea et al. 2014). Thus, despite all the advances made to expand our understanding of neuron-astrocyte interactions, the mechanisms of these astrocyte Ca^{2+} events and their downstream effects on neuronal function are still not fully understood.

A particular lack of understanding surrounds the effects of neuromodulatory transmitters, including noradrenaline, which regulates the presynaptic release and postsynaptic effects of the fast neurotransmitters glutamate and GABA (see Salgado, Trevino & Atzori, 2016 for a recent review). Noradrenaline also raises $[Ca^{2+}]_i$ in astrocytes (Duffy & MacVicar, 1995), and recent evidence from awake animals

suggests that these $[Ca^{2+}]_i$ rises regulate the astrocytes' responsiveness to other neurotransmitters (Paukert et al., 2014). This raises the question of whether noradrenaline-evoked astrocyte $[Ca^{2+}]_i$ changes may also contribute to the effects of noradrenaline on synaptic transmission.

In this chapter I will first assess the effects of changes in $[Ca^{2+}]_i$ in hippocampal astrocytes within the stratum radiatum on spontaneous excitatory and inhibitory synaptic transmission to CA1 pyramidal neurons. Secondly, I will examine the influence of astrocyte Ca^{2+} signalling on noradrenaline-evoked changes in synaptic transmission in the same region.

6.3 Methods

6.3.1 Hippocampal slice preparation

Sprague-Dawley rats at postnatal day 12 were used for the preparation of hippocampal slices.

6.3.2 Extracellular solutions

Brain slices were perfused with a bicarbonate-based buffer solution mimicking cerebrospinal fluid (artificial cerebrospinal fluid, aCSF) as described in section 2.3.1. Kynurenic acid present in the slicing solution to prevent glutamate receptor activation (Min et al., 1999) was washed out for at least 10 mins before starting recording. With the exception of experiments studying the effects of noradrenaline on IPSC events, which were at RT, all other recordings were made at a physiological temperature by passing the extracellular solution through a heating block where its temperature was adjusted to 32-35°C (as described in section 2.2). NA (5-20 μM) was added to the aCSF at the time of recording and diluted 10,000-fold from a stock that was made on the same day and was kept on ice in order to minimize its oxidation (ascorbic acid, a commonly employed antioxidant, was not used for the experiments in this chapter as it may block calcium channels: Parsey & Matteson, 1993; Todorovic & Jevtovic-Todorovic, 2011). TTX (100-500 nM; to block action potentials), was also present in some experiments as indicated in the relevant figure captions. The agonist for the protease-activated receptor PAR1, TFLLR (30 μM), was also used in some experiments as indicated in the relevant figure captions. For calcium imaging experiments, puff applications of NA (20 μM) were delivered every 3 secs (at 1psi). NA was added to a HEPES-based aCSF (pH with NaOH) inside a glass electrode pipette.

6.3.3 Intracellular solution

Dual whole-cell patch-clamping experiments were performed using a caesium gluconate based solution for recording from neurons which included Alexa Fluor 488 (20 μM) to dye-label the cells (replacing K^+ with Cs^+ in the cell increases the input resistance and improves voltage-clamp quality), and a potassium gluconate based solution for recording from astrocytes which included Alexa Fluor 594 (20 μM) to dye-label the cells (as described in section 2.3.2). Images and membrane current data from specimen cells are shown in Fig. 6.2A. To examine the effect of astrocyte $[Ca^{2+}]_i$ changes on spontaneous excitatory and inhibitory postsynaptic currents (EPSCs and IPSCs) in adjacent pyramidal neurons, the faster calcium chelating agent BAPTA (30 mM) was employed in the internal solution in some experiments (as indicated in the relevant figure legends) instead of 10 mM EGTA (as described in section 2.3.2). The amount of $CaCl_2$ added was adjusted to maintain the free calcium concentration at ~20 nM for both the EGTA-containing and the BAPTA-containing internal solutions.

To examine the effect of astrocyte cyclic nucleotide signalling on spontaneous EPSC and IPSC events in adjacent pyramidal neurons, cyclic adenosine monophosphate (cAMP, 5 mM) was added to the internal solution (described in section 2.3.2) on the day of the experiment, with the aim of saturating any mechanisms dependent on cAMP and preventing any significant change in the cAMP concentation when receptors were activated. The pH of the solution was not altered by this addition.

For calcium imaging experiments, 50 μM Fluo-4 was added to the internal solution and the fluorescent signal was measured on a Zeiss LSM700 confocal microscope, using excitation at 488 nm and collecting emitted light of > 515 nm wavelength.

6.3.4 Experimental protocol

Neurons in the pyramidal layer of area CA1 and astrocytes in the hippocampal stratum radiatum were patch-clamped as describe in sections 2.4 and 2.5. Pyramidal neurons were held in voltage clamp mode at -50 mV so that inward EPSCs (reversal potential ~0 mV) and outward IPSCs (reversal potential ~-64 mV) could be simultaneously detected. Astrocytes were held in voltage clamp mode at a potential close to their resting potential (which typically had a value around -90 mV).

Spontaneous excitatory and inhibitory currents were detected using Clampfit10.2 software (Molecular Devices). To do this, any slow drift in the baseline was removed using a high-pass filter (0.1 Hz), and the standard deviation of the baseline noise was estimated within an apparently "event-free" region of the trace (of typical duration 0.5 sec) for each cell. Subsequently, inward excitatory currents or outward inhibitory currents that were larger than three times the standard deviation of the baseline noise were detected automatically using Clampfit event detection software, using minimum duration criteria (i.e.a cut-off of 3ms above the threshold for EPSCs, or 5ms above the threshold for IPSCs, was chosen). Events with a rising phase slower than the decay phase (defined by time constant of the rise and fall) were also removed as they were not likely to represent true synaptic currents.

6.3.5 Statistical Analysis

Synaptic current frequency and amplitude data (acquired using pClamp 10) were normalised by dividing the value at each time point by the value averaged over at least the initial 5 minutes (see each figure for more information) of the baseline condition. Two-tailed paired or unpaired t-tests (as appropriate) were performed to assess the difference between the different conditions.

6.4 Results

6.4.1 Excitatory and inhibitory spontaneous postsynaptic currents reflect action potential independent and action potential dependent transmitter release, respectively

I examined spontaneously occurring EPSCs and IPSCs in CA1 pyramidal neurons to determine their transmitter release mechanisms. Synaptic currents can arise from spontaneous vesicle release independent of action potentials, generating so-called 'miniature synaptic currents' (Fatt & Katz, 1952), or via vesicle release driven by calcium entry evoked by action potentials. As shown in Fig. 6.1A, inward EPSCs had an amplitude of ~ -33±1.6 pA at a potential of -50 mV, with a fast rising phase (time to peak < 5.0±0.4 msec) and a slower falling phase (with a decay time constant of 10.1±0.7 msec). Although the mean rate of EPSC events was nearly halved following TTX (500 nM) application (Fig. 6.1B), this reduction was not significant (the EPSC rate was reduced by 46±6%, two-tailed paired t-test p=0.07, n=3, comparing EPSC rate for 6 minutes of TTX perfusion with 6 minutes of the baseline data). Data in this and subsequent figures are normalised to the control period as described in section 6.3.5 (the mean frequency of EPSCs at baseline was 0.23±0.07 Hz). Larger error bars prior to TTX application may imply the occurrence of infrequent action potential evoked events. The postsynaptic amplitude of EPSCs did not show a significant change in TTX (Fig. 6.1D, reduced by 13±2%, two-tailed paired t-test p=0.43, n=3).

Outward IPSCs had an amplitude of 25.4±0.4 pA at a potential of -50 mV, with a fast rising phase (Time to peak < 4.2±0.6 msec) and slower falling phase (decay time constant 13.3±0.9 msec) as shown in Fig. 6.1A. In contrast to EPSCs, the occurrence of IPSC events was nearly abolished in the presence of TTX (Fig. 6.1C, reduced by

85±3%, two-tailed paired t-test $p=2.3x10^{-6}$, n=3: mean frequency of IPSCs at baseline was 2.2±0.3 Hz). In contrast to EPSCs, the few miniature IPSCs remaining in TTX had a slightly smaller amplitude compared to action potential evoked IPSCs (Fig. 6.1E, reduced by 12%, two-tailed paired t-test p=0.03, n=3).

These data indicate that most spontaneous EPSCs are miniature events, while most spontaneous IPSCs are evoked by action potentials in interneurons. Thus, in order to simultaneously assess the effect of astrocyte Ca^{2+} signalling on excitatory and inhibitory synaptic transmission, all subsequent recordings were made in the absence of TTX, to allow both EPSCs and IPSCs to occur. In contrast, Shigetomi et al. (2012) only examined the effect of astrocyte $[Ca^{2+}]_i$ on miniature IPSCs.

6.4.2 The effect of astrocyte calcium concentration on spontaneous postsynaptic currents

Having carried out this basic characterization of the EPSC and IPSC properties, I investigated whether astrocyte $[Ca^{2+}]_i$ regulated these synaptic currents.

6.4.2.1 Astrocyte $[Ca^{2+}]_i$ does not affect spontaneous excitatory transmission

Chelating calcium inside astrocytes has been reported to reduce stimulation-evoked EPSCs (Panatier et al., 2011, Di Castro et al., 2011). Thus, in order to investigate whether astrocyte $[Ca^{2+}]_i$ affects spontaneous EPSCs, dual-whole cell patch-clamp recordings were made from a hippocampal CA1 neuron and an astrocyte in the vicinity of the neuron's apical dendrites, and astrocyte $[Ca^{2+}]_i$ was manipulated. After recording baseline EPSCs in the neuron (for ~5 minutes), whole-cell patch-clamp recording mode was achieved in the astrocyte. The astrocyte pipette solution, which dialyses the cell, included either a low concentration of a slow calcium buffer

(EGTA, 1 mM), or a high concentration of a faster calcium buffer (BAPTA, 30 mM) to reduce any rise in $[Ca^{2+}]_i$ (see Fig. 6.2A for an example of a dye-filled astrocyte and a nearby CA1 pyramidal neuron). A time dependent effect of intracellular BAPTA was reported previously for inhibitory transmission, for which the effect of BAPTA was apparent only when dialysed for over 15 minutes (Shigetomi et al., 2012). Therefore, in this experiment I used a dialysis period of >15 mins to assess the effect on EPSCs of chelating astrocyte $[Ca^{2+}]_i$ with BAPTA.

Dialyzing the astrocyte network for >15 minutes with either EGTA or BAPTA did not have a significant effect on the rate of EPSCs, compared to baseline (Fig. 6.2B & C, decreased by 13±2% two-tailed paired t-test p=0.58 for EGTA, n=6, and increased by 10±3% p=0.72 for BAPTA, n=5, comparing the period from 15 to 19 minutes after the start of EGTA/BAPTA dialysis with baseline). The rate of EPSCs after dialysis for 15 min was also not significantly different with EGTA versus BAPTA in the pipette (p=0.52).

The postsynaptic EPSC amplitude was also not affected following dialysis of astrocytes with EGTA or BAPTA, when compared with the pre-dialysis baseline (Fig. 6.2D, decreased by 2±1% p=0.83 for EGTA; decreased by 10±1% p=0.23 for BAPTA). Similarly, after dialysis for 15 min the EPSC amplitude also did not differ significantly between EGTA and BAPTA (p=0.96).

These results strongly suggest that, in contrast to action potential-evoked EPSCs (Panatier et al., 2011; Di Castro et al., 2011), spontaneously occurring EPSCs at the CA3-CA1 synapse, which are mainly composed of miniature events (see section 6.4.1), are not regulated by $[Ca^{2+}]$-driven gliotransmission from astrocytes.

6.4.2.2 Astrocyte $[Ca^{2+}]_i$ regulates spontaneous inhibitory transmission

Astrocyte $[Ca^{2+}]_i$ has been reported to regulate the postsynaptic amplitude of miniature IPSCs in hippocampal interneurons (Shigetomi et al., 2012). In order to investigate whether astrocyte $[Ca^{2+}]_i$ can affect spontaneous IPSCs, dual-whole cell patch-clamp recordings were made from a hippocampal CA1 pyramidal neuron and a nearby astrocyte in the vicinity of the neuron's apical dendrites, using a protocol similar to that described above for EPSCs (section 6.4.2.1). A 5 minute period of baseline IPSCs was recorded from pyramidal neurons prior to whole-cell patch-clamping of the astrocyte with internal solution containing either EGTA (1 mM) or BAPTA (30 mM).

The majority of IPSCs consisted of distinguishable "singular" events. However, less frequently, multipeak large amplitude events were also observed (but not in all recordings, see Fig. 6.3A & C legends).

Dialyzing the astrocyte network for >15 minutes with either EGTA or BAPTA did not have a significant effect on the IPSC frequency in the first 8 minutes of dialysis (Fig. 6.3A & B, decreased by 7±1% two-tailed paired t-test for EGTA p=0.32, n=13; and increased by 13±1% for BAPTA p=0.34, n=16, when comparing 3-8 minutes after the start of dialysis with baseline), nor on the amplitude of IPSCs compared to baseline period (Fig. 6.C, increased by 4±2% for EGTA p=0.24, n=13; and increased by 2±1% for BAPTA p=0.45, n=16).

However, with further dialysis of BAPTA, there was a significant reduction in the rate of inhibitory transmission (Fig. 6.3A & B, decreased by 44±5% two-tailed paired t-test p=0.0007, n=5, when comparing 15-19 minutes after the start of dialysis with baseline). In contrast, there was no change in the IPSC rate when the astrocyte was dialysed with EGTA (Fig. 6.3B, decreased by 11±2%, p=0.27, n=6). Consistent

with these data, the rate of IPSCs following >15 mins dialysis with BAPTA was also significantly lower than with an equivalent period of EGTA dialysis (p=0.016).

Such extended dialysis of BAPTA did not, however, significantly affect the amplitude of inhibitory synaptic currents (Fig. 3.6C, decreased by 10±1% for EGTA p=0.18; and increased by 12±1% for BAPTA p=0.07, when comparing 15-19 minutes after the start of dialysis with baseline), although there was a late increase in the amplitude of IPSCs when dialysing with BAPTA compared to EGTA, p=0.03). This increase in mean IPSC amplitude may be the result of a reduction in the rate of smaller magnitude and more frequent spontaneous IPSCs following dialysis with BAPTA, while large amplitude multipeak events persisted following BAPTA. However, due to the infrequent nature of these multipeak events in slices, it was not feasible to quantify the effect of BAPTA on these multipeak IPSCs.

Overall, these results from dialyzing the astrocyte network with the calcium chelator BAPTA suggest that astrocyte calcium signalling regulates the rate of inhibitory transmission.

6.4.2.3 A receptor-mediated astrocyte $[Ca^{2+}]_i$ rise does not regulate IPSCs

In order to better understand the effect of astrocyte calcium on inhibitory synaptic transmission, $[Ca^{2+}]_i$ transients were evoked pharmacologically by activating the protease-activated receptor 1 (PAR1), which is known to raise astrocyte $[Ca^{2+}]_i$ (Fujita et al., 2009; Lalo et al., 2014; Park et al., 2013; Oh et al., 2012), while recording inhibitory currents in CA1 pyramidal neurons. PAR1, a G protein coupled receptor that is activated when cleaved by serine proteases like thrombin, is mostly expressed in astrocytes (Junge et al., 2004; Zhang et al., 2016). It can interact with G_q proteins that trigger the release of Ca^{2+} from internal stores (McCoy et al., 2012). To activate

PAR1, a synthetic 5 amino acid peptide, TFLLR-NH2, that has an amino acid sequence similar to that of the endogenous ligand for PAR1, was applied (Androutsou et al., 2010).

Activation of PAR1 receptors with TFLLR did not affect the rate or amplitude of spontaneous IPSCs recorded in CA1 pyramidal neurons when comparing the final 5 minutes of baseline (starting at t=5 min) with an equivalent period following the bath perfusion of TFLLR-NH2 (starting at t=13 min; Fig. 6.4A & B, two-tailed t-test p=0.85 for normalized frequency, p=0.86 for normalized amplitude, n=5). Thus, although the TFLLR was only applied for 8 mins (while BAPTA dialysis required 15 mins to produce its full effect: Fig. 6.3) it appears that while reducing $[Ca^{2+}]_i$ elevations with BAPTA inside astrocytes significantly reduces spontaneous IPSC rate in nearby pyramidal neurons, increasing the $[Ca^{2+}]$ inside astrocytes does not seem to enhance this inhibitory transmission. I will examine the implications of this result in the discussion section.

6.4.3 The role of astrocyte calcium signaling in the effect of noradrenaline on postsynaptic currents

Noradrenaline is known to regulate the strength of excitatory and inhibitory synaptic transmission in the hippocampus. For example, NA reduces the firing rate of CA3 cells (via α_1-adrenoceptors; Curet & de Montigny, 1998), while it increases the release of glutamate at the CA3-CA1 synapse (via β-adrenoceptors: Gereau & Conn, 1994). Similarly, NA increases the rate and amplitude of IPSCs in CA1 pyramidal neurons by depolarising interneurons (Bergles et al., 1996). However, low concentrations of NA (1-2 μM) also induce $[Ca^{2+}]_i$ elevations in astrocytes (Duffy & MacVicar, 1995), independent of neuronal action potential activity (Espallergues et

al., 2007). In line with this, my unpublished data (obtained with Fergus O'Farrell, Fig. 6.5) show that NA reliably induces a calcium concentration rise in astrocytes in the presence of TTX.

I therefore investigated whether this NA-evoked $[Ca^{2+}]_i$ rise in the network of astrocytes contributes to the effects of NA seen on IPSCs and EPSCs in CA1 pyramidal neurons.

6.4.3.1 Noradrenaline potentiates inhibitory transmission

In line with the results of Bergles et al. (1996), bath application of NA (20 μM) significantly enhanced the spontaneous IPSC rate (Fig. 6.6A & C, increased by 64±5% two-tailed unpaired t-test p=0.005 comparing the final 4 minutes of normalized frequency (starting at t=10 min, n=6) with an equivalent period in cells with control solution lacking noradrenaline (n=5). Noradrenaline also increased the mean IPSC amplitude (Fig. 6.6A & C, increased by 31±1%, p=0.03). This strong potentiation of inhibitory transmission only washed out after 20-25 min (data not shown), possibly because of the high NA concentration (20 μM) used.

The NA-evoked potentiation of inhibitory transmission was dependent on interneurons firing action potentials, as this effect was abolished by TTX (100 nM, Fig. 6.6B, D & F). Thus, IPSC properties in the presence of NA and TTX were indistinguishable from those recorded in control solution (two-tailed unpaired t-tests, p=0.81 for frequency and p=0.68 for amplitude). This result suggests that the data in Fig. 6.6 A and C reflect an increase in the rate of action potential driven IPSCs, which have a larger amplitude than miniature IPSCs.

These results confirm the notion (Bergles et al., 1996) that NA is a robust regulator of inhibitory transmission. As inhibitory transmission is also regulated by

astrocyte Ca^{2+} signalling (see Fig. 6.3), I investigated the possibility that NA may exert its potentiating effect on inhibitory transmission partly through astrocyte [Ca^{2+}]-dependent gliotransmission onto interneurons.

6.4.3.2 The role of astrocyte $[Ca^{2+}]_i$ in the effect of NA on IPSCs

In order to assess the role of astrocyte Ca^{2+} signaling in NA-evoked postsynaptic current changes, dual whole-cell patch-clamp recordings were made from CA1 pyramidal neurons and nearby astrocytes in the stratum radiatum (Gereau & Conn, 1994). In each paired recording experiment, a baseline current recording containing both EPSCs and IPSCs was obtained prior to dialysing the astrocytes with an internal solution containing either EGTA, or the more rapid calcium chelator BAPTA, for >15 minutes. This method allowed me to investigate the contribution of astrocyte Ca^{2+} signalling to both the basal synaptic current rate (as described in Fig. 6.3) and the noradrenergic effect on neurons. Subsequently, NA (5 μM) was bath applied. This concentration was used (rather than the 20 μM used in Fig. 6.6 and by Bergles et al. (1996)) in order to generate a detectable effect, while ensuring a washout of the NA effect within a reasonable time. Interestingly, lower concentrations of noradrenaline (1-2 μM) raise astrocyte $[Ca^{2+}]_i$ (Duffy & MacVicar (1995) and Fig. 6.5 above) and also affect the vasculature (Hall et al., 2014), however applying 2 μM NA did not evoke a strong and convincing effect on the postsynaptic currents recorded in the CA1 pyramidal neurons at -50mV (data not shown).

I found that the strong potentiation of the rate of IPSCs by 5 μM NA did not depend on astrocyte $[Ca^{2+}]_i$ changes (Fig. 6.7A & B, two-tailed unpaired t-test p=0.64, comparing the final 5 minutes of normalised frequency data in NA (starting at t=26) when the astrocyte is dialysed with BAPTA (n=5) with an equivalent period in EGTA

(n=6)). It is, however, noteworthy that the percentage change in the rate of IPSCs evoked by NA with BAPTA in the astrocyte is numerically larger with EGTA, as the IPSC rate just prior to NA application was significantly lower with BAPTA compared to EGTA (see Figs. 6.3B and 6.7B). However, this difference in the percentage change of IPSC rate was not significant even if the IPSC rate in NA was normalized to that occurring just before NA separately for EGTA and BAPTA (data not shown, p=0.47).

In contrast to the increase in IPSC amplitude seen when using 20 μM NA in Fig. 6.6E, in these experiments using 5 μM NA no significant NA-evoked change was seen in the amplitude of spontaneous IPSCs. This was independent of whether the astrocyte was filled with EGTA or with BAPTA (Fig. 6.7C, p=0.77 comparing EGTA with BAPTA).

These results suggest that the potentiation of IPSC rate by NA in hippocampal CA1 pyramidal neurons is independent of astrocyte calcium signalling and the Ca^{2+}-dependent release of gliotransmitters.

6.4.3.3 NA-evoked effects on excitatory transmission and the role of astrocyte calcium signalling

In contrast to the results of Curet & de Montigny (1988) who released noradrenaline using locus coeuruleus stimulation, no significant change was seen in the rate of spontaneous EPSCs after NA application, independent of whether the patch-clamped astrocyte was filled with either EGTA or BAPTA for 19 minutes (Fig. 6.8A & B, two-tailed paired t-test, p=0.52 for EGTA, n=6, and p=0.88 for BAPTA, n=5, when comparing 5 minutes of normalised frequency data in NA starting at t=26 min with 5 minutes of data before NA application starting at t=18 min). Similarly, there

was no change in the amplitude of the spontaneous EPSCs (Fig. 6.8A & C, p=0.98 for EGTA and p=0.88 for BAPTA).

These results show that 5 µM noradrenaline does not affect spontaneous EPSCs in hippocampal CA1 pyramidal neurons, independent of whether astrocyte calcium is strongly buffered or not.

6.4.4 Assessment of astrocyte cAMP signalling as a regulator of EPSCs and IPSCs

Many astrocyte neurotransmitter receptors signal through G proteins that alter cyclic AMP concentration, [cAMP], rather than releasing Ca^{2+} from internal stores. I therefore investigated whether raising the [cAMP] in astrocytes affected the spontaneous EPSC and IPSC events recorded in nearby pyramidal neurons. The results show that the addition of cAMP (5 mM) to the internal solution of astrocytes increased the frequency of EPSCs (Fig. 6.9A & B). The frequency increased by 49±9% with time after starting dialysis with internal cAMP (p=0.046 from a two-tailed unpaired t-test), and decreased with time by 16±7% without added cAMP (p=0.23; in both cases I compared the final 5 mins starting at t=13 with 5 mins of baseline). Consistent with internal cAMP increasing the spontaneous EPSC rate, the EPSC frequency following dialysis with cAMP (normalised to the initial value before astrocyte dialysis) was also higher than with an equivalent period of control internal solution (p=0.012, when comparing the final 6 mins starting at t=12).

There was no effect on the amplitude of spontaneous EPSCs (Fig. 6.9C, p=0.51), nor on the rate and amplitude of spontaneous IPSCs (Fig. 6.9D & E, p=0.78 for frequency and p=0.58 for amplitude), when cAMP was dialysed into the astrocyte.

These results show that signalling through astrocyte G protein coupled receptors that target adenylate cyclase, and thus increase or decrease the intracellular

concentration of cAMP, may also be a route by which astrocytes regulate excitatory transmission.

6.5 Discussion

In this chapter I assessed whether intracellular signalling mechanisms in astrocytes regulate synaptic transmission to CA1 pyramidal cells in the presence or absence of noradrenaline (NA). This was done by measuring spontaneous excitatory and inhibitory currents in CA1 pyramidal neurons adjacent to astrocytes that were filled with internal solutions containing 1 mM EGTA (a weak and slow Ca^{2+} buffer), or 30 mM BAPTA (a strong fast Ca^{2+} buffer).

6.5.1 The effect of astrocyte Ca^{2+}signalling on spontaneous EPSCs

I first studied the pattern of spontaneous activity recorded in CA1 pyramidal neurons in hippocampal slices. The results showed that the rate of spontaneous excitatory activity (0.23±0.07 Hz) is much lower than that of inhibitory activity (2.2±0.3 Hz), recorded in the same cells. The rate of spontaneous EPSCs that I observed at P12 is lower than the 0.9 Hz in P8 rats reported by Groc et al. (2002) but are similar to the frequency of spontaneous mEPSCs reported at P14 by De Simoni et al. (2003).

EPSCs were largely unaffected when action potential firing was inhibited (by adding TTX). This suggests that the majority of EPSCs arise from spontaneous release of glutamate-containing vesicles, in the absence of action potentials. Thus, the glutamatergic projections from CA3 pyramidal neurons, which are the major excitatory input at the CA3-CA1 synapse, do not exhibit a high rate of firing in brain slices.

Dialysing into astrocytes an internal solution containing BAPTA, which strongly buffers $[Ca^{2+}]_i$ transients, did not reveal a convincing role for astrocyte Ca^{2+} signalling, and downstream gliotransmission, in regulating the frequency of miniature

EPSCs (see Fig. 6.2). In line with this finding, a recent study by Wang et al. (2013) in which astrocytes selectively expressed the MrgA1 G_q-linked receptor showed that, agonist-induced $[Ca^{2+}]_i$ rises failed to potentiate miniature excitatory synaptic currents in nearby CA1 pyramidal neurons. Surprisingly, however, in that study photolysis of caged calcium in astrocytes, unlike a receptor-mediated $[Ca^{2+}]_i$ rise, did increase the rate of miniature EPSCs, which raises the question as to the physiological relevance of astrocyte Ca^{2+} signalling for excitatory transmission. In addition, a recent study has shown that optogenetic stimulation of astrocyte Ca^{2+} signalling in the visual cortex *in vivo* has variable effects on excitatory transmission (either increasing or decreasing it: Perea et al., 2013). These findings, in conjunction with the results from this chapter, appear at odds with the conclusive results of Di Castro el al. (2012) and Panatier et al. (2012), who found that astrocyte Ca^{2+} signaling in astrocytic fine processes near synapses were necessary to maintain minimal stimulation-evoked excitatory synaptic currents in hippocampus.

This contradiction may be partly explained by the fact that Wang et al. (2013) measured a spatially-widespread calcium concentration rise in the somata, not local calcium transients in the processes near the synapses as imaged by Di Castro el al. (2012) and Panatier et al. (2012). In addition, the effect of astrocyte Ca^{2+} signaling on EPSCs could be region specific, as the *in vivo* experiments of Perea et al. (2013) were done in visual cortex unlike the hippocampus used by Di Castro el al. (2012) and Panatier et al. (2012). Furthermore, for the experiments in this chapter, the rate of spontaneous EPSCs was quite low across all the recordings (0.24±0.04 Hz for those with a nearby astrocyte filled with EGTA, and 0.39±0.08 Hz for those with a nearby astrocyte filled with BAPTA) when compared with the IPSC events (1.80±0.35 Hz for those with a nearby astrocyte filled with EGTA, and 2.03±0.52 Hz for those with a

nearby astrocyte filled with BAPTA). This implies a lower sensitivity for detecting effects of astrocyte calcium chelation on EPSCs: such an effect might have gone undetected due to the low EPSC rate and the correspondingly large variability within the small sample size.

6.5.2 The effect of astrocyte Ca^{2+}signalling on spontaneous IPSCs

In contrast to EPSCs, I found that the majority of IPSCs are action potential dependent (see Fig. 6.1C), implying that they arise from the firing of GABAergic interneurons within the vicinity of the CA1 neurons (consistent with Liu et al., 2004).

Astrocyte $[Ca^{2+}]_i$ has been reported to regulate the amplitude of the miniature IPSCs recorded in hippocampal inhibitory interneurons. "Spotty" calcium microdomains, which arise from Ca^{2+} influx through TRPA1 channels, are suggested to control the astrocytic surface expression of the GABA transporter, GAT-3 (Shigetomi et al., 2012). The authors claim that an increase in $[Ca^{2+}]$ promotes insertion of GAT-3 into the astrocyte membrane. This takes up extracellular GABA and increases the amplitude of miniature IPSCs in nearby interneurons (Shigetomi et al., 2012), presumably through the removal of postsynaptic $GABA_A$ desensitisation (Overstreet et al., 2000). In contrast to the effects they observed in interneurons, Shigetomi et al. (2012) failed to detect any effect of dialyzing astrocytes with BAPTA on either the miniature EPSCs or IPSCs in pyramidal neurons.

I dialysed astrocytes with a BAPTA-based internal solution to investigate the effect of astrocyte $[Ca^{2+}]$ on action potential evoked IPSCs. Although a short duration of dialysis with either EGTA or BAPTA (~10 min) did not have an effect on spontaneous IPSCs (unlike the rapid effect of BAPTA dialysis on evoked EPSCs reported by Di Castro el al. (2012) and Panatier et al. (2012), longer dialysis (>15 min)

significantly reduced the IPSC rate (see Figs. 6.3B and 6.7B). Thus it appears that astrocyte Ca^{2+} signalling can regulate the firing likelihood of inhibitory interneurons.

This strong effect of astrocyte Ca^{2+} on the rate of spontaneous IPSCs in pyramidal cells differs, in two respects, from the report of Shigetomi el al. (2012). Firstly, they reported an effect of astrocyte calcium signalling only on interneurons: dialysis of astrocytes with BAPTA affected the miniature IPSCs in interneurons without affecting miniature IPSCs in pyramidal neurons. Secondly, I observed an effect of astrocyte calcium signalling on IPSC frequency, whereas they observed an effect on amplitude. To add to the complexity, Liu et al. (2004) reported a finding opposite to Shigetomi et al. (2012), whereby increasing astrocyte calcium concentration through uncaging (as opposed to buffering it) decreased the frequency of miniature IPSCs in a nearby hippocampal interneuron.

The most likely explanation for why Shigetomi et al. (2012) failed to observe an effect on pyramidal neurons is that they focused on miniature inhibitory events, which comprise a small fraction of the total inhibitory events (Fig. 6.1C).

Regulation of action potential-evoked GABA release by astrocyte Ca^{2+} signaling, as shown by the decrease in IPSC rate seen when BAPTA is inside astrocytes (Fig. 6.3B), suggests that $[Ca^{2+}]$-dependent gliotransmission is necessary for interneuron depolarization and action potential firing. Support for this comes from various sources: (1) *in vivo* stimulation of astrocyte Ca^{2+} signalling using channelrhodopsin-2 enhances the rate of spontaneous IPSCs in layer 2/3 of the visual cortex, without affecting the amplitude (Perea et al., 2013); (2) uncaging Ca^{2+} in astrocytes evokes an action potential-dependent increase in the rate of IPSCs recorded in nearby interneurons, without affecting the amplitude (Liu et al., 2004).

The IPSCs in CA1 pyramidal cells are produced by different types of interneuron (which have varying firing frequencies: Klausberger et al., 2003). Astrocyte Ca^{2+} signalling may not affect all these classes equally: a rise of $[Ca^{2+}]_i$ may stimulate astrocyte-to-interneuron transmission to depolarize particular classes of interneuron. To further test this hypothesis, simultaneous cell-attached recordings from rhythmically active interneurons could be made while manipulating Ca^{2+} levels in nearby astrocytes.

6.5.3 Effects of raising $[Ca^{2+}]_i$ in astrocytes

Another approach to assessing the effect of astrocyte Ca^{2+} signalling on spontaneous IPSCs is to artificially raise $[Ca^{2+}]$ (instead of buffering $[Ca^{2+}]_i$ with BAPTA). I did this by applying TFLLR-NH2 to activate the protease-activated receptor 1 (PAR1), which is known to raise $[Ca^{2+}]_i$ in astrocytes (Fujita et al., 2009; Lalo et al., 2014; Park et al., 2013; Oh et al., 2012).

TFLLR did not affect the rate or the amplitude of spontaneous IPSCs recorded in CA1 pyramidal neurons. This is consistent with the report of Shigetomi et al. (2012) who failed to observe any effect on inhibitory transmission of raising the intracellular free calcium concentration (up to 310 and 500 nM). This is hard to explain, given the inhibitory effect of BAPTA in Fig. 6.3, but may suggest one of the following possibilities. (1) A reduction in the occurance of ongoing Ca^{2+} transients may have a bigger impact on the activity of nearby interneurons than does generating Ca^{2+} concentration rise with TFLLR. This is unlikely, however, as others have suggested enhancement of inhibitory transmission following a $[Ca^{2+}]_i$ increase in astrocytes both *in vivo* and *in vitro* (Perea et al., 2013; Liu et al., 2004, respectively). (2) Ca^{2+} entry from the extracellular space at a particular location, and not a G protein coupled

receptor-mediated $[Ca^{2+}]_i$ rise, is needed to regulate the detected rate of IPSCs, perhaps by altering insertion of the GABA transporter GAT-3 into the membrane or by releasing excitatory gliotransmitters. However, more in-depth examination will be required to strengthen this hypothesis (see section 7.4 for further discussion).

6.5.4 Noradrenaline and astrocyte Ca^{2+} signalling

Astrocytes express many G_q-coupled receptors that can release Ca^{2+} from intracellular stores upon the binding of their substrates, such as noradrenaline (NA) via α_1-adrenoceptors (Duffy & MacVicar, 1995; Paukert et al., 2014). NA is released from locus coeruleus (LC) neurons and modulates functions such as neuronal activity, energy metabolism, neuroplasticity and inflammation (see O'Donnell, 2012, for a review). Thus understanding the effects of NA on astrocytes is potentially of great importance. It is already known that NA (via α_1) evokes a $[Ca^{2+}]$ rise in astrocytes (Ding et al., 2013) and also regulates the responsiveness of astrocyte Ca^{2+} signalling to incoming stimuli mediated by other neurotransmitters in awake behaving animals (Paukert et al., 2014). Low concentrations of NA (1-2 μM) induce Ca^{2+} responses in astrocytes in slices (Duffy & MacVicar, 1995), independent of neuronal action potential activity (Espallergues et al., 2007). Nevertheless, a broader understanding of how astrocytes may contribute to the synaptic effects of NA is lacking. Therefore, I examined the potential contribution of astrocyte Ca^{2+} signalling to NA-evoked neuromodulation in CA1 pyramidal neurons.

The effect of NA on hippocampal excitatory transmission appears to be dependent on the adrenoceptor subtype it acts on, as both excitatory (via β-adrenoceptors: Gereau & Conn, 1994) and inhibitory effects (via α_1-adrenoceptors; Curet & de Montigny, 1998) have been noted. In contrast, I found no evidence for an

effect of 5 μM NA on EPSC rate or amplitude in slices, irrespective of whether the patch-clamped astrocyte was filled with EGTA or BAPTA (Fig. 6.8). This is at least in part due to the low and variable rate of spontaneous EPSCs in hippocampal CA1 pyramidal neurons. Hence no definite conclusion can be made about the contribution of astrocyte calcium signalling to NA-evoked EPSC modulation. Specific targeting of α- and β-adrenoceptors (as previously done by Curet & de Montigny, 1998; and Gereau & Conn, 1994), would be a better approach to isolate the effects astrocyte Ca^{2+} signalling on adrenergic-evoked changes in hippocampus. It might be surprising that the NA-evoked inhibition of glutamate uptake that I reported in chapter 4 had no effect on EPSCs. However, it has been shown previously that reduction of glutamate uptake has a larger effect on action potential evoked EPSCs, when many axons release glutamate, than on EPSCs generated by release at a single synapse, as occurs for the miniature EPSCs studied here (Marcaggi *et al*., 2003).

In contrast to the effect of NA on excitatory transmission in hippocampus, its effect on inhibitory transmission is robust. In agreement with previous work by Bergles et al. (1996), I showed that NA robustly enhances inhibitory transmission in a manner dependent on the action potential firing of interneurons (see section *6.4.3.1*). This potentiation of inhibitory transmission by NA is most dramatic for the rate of inhibitory transmission, as even a low NA concentration (5 μM) induces a robust increase in IPSC rate but a much less convincing effect on IPSC amplitude (compare Fig. 6.6A & C with Fig. 6.7B & C).

This strong potentiation of the IPSC rate does not, however, depend on astrocyte $[Ca^{2+}]_i$ changes. This was shown by demonstrating, with dual whole-cell patch-clamp recordings, that the effects of NA on the IPSC rate or amplitude were

independent of whether astrocytes were dialysed with 30 mM BAPTA or with 1 mM EGTA as the calcium buffer (Fig. 6.7).

These results suggest that, although astrocyte Ca^{2+} signalling regulates the rate of inhibitory transmission in hippocampus in the absence of added NA, the NA-evoked potentiation of inhibitory transmission must be via a direct depolarizing action of NA on interneurons, as suggested by Bergles et al. (1996).

6.5.5 Astrocyte regulation of synaptic transmission through cyclic nucleotides

Apart from Ca^{2+} signaling, many astrocyte neurotransmitter receptors evoke changes of cAMP concentration rather than of $[Ca^{2+}]_i$. Thus, it is conceivable that cAMP-mediated signalling in astrocytes could also influence synaptic transmission. Therefore, I investigated whether increasing the concentration of cyclic AMP in astrocytes (through the addition of 5 mM cAMP to the internal solution) could regulate the spontaneous EPSCs and IPSCs recorded in nearby CA1 neurons. These experiments were promising as they suggested that elevating the levels of cAMP might potentiate the rate of excitatory transmission. This finding is of interest for two reasons: Firstly, it has been reported that, in CA1 pyramidal neurons, β-adrenergic signalling potentiates EPSCs though a mechanism dependent on an increase in cAMP levels (Gereau & Conn, 1994). Secondly, NA regulates the responsiveness of astrocyte Ca^{2+} signalling to incoming stimuli (Paukert et al., 2014). Therefore, it would be of great interest to explore how cAMP signalling and Ca^{2+} signalling interact within astrocytes, following the release of NA in behaving animals, and how this interaction may affect the neuronal activity

6.6 Conclusion

The results from this chapter argue that, while the majority of spontaneous excitatory events recorded at CA1 neurons in brain slices are driven by action potential-independent release of glutamatergic vesicles, spontaneous inhibitory events depend largely on the action potential firing of interneurons. Importantly, I showed that, in the absence of noradrenaline, the maintenance of this inhibitory transmission depends on astrocyte Ca^{2+} signalling. Lastly, I characterized the effects of low levels of noradrenaline on neurotransmission at these inhibitory synapses, and concluded that the strong potentiation of inhibitory transmission by NA observed does not reflect NA-evoked astrocyte Ca^{2+} signalling and so is presumably due to a direct effect of NA on interneurons.

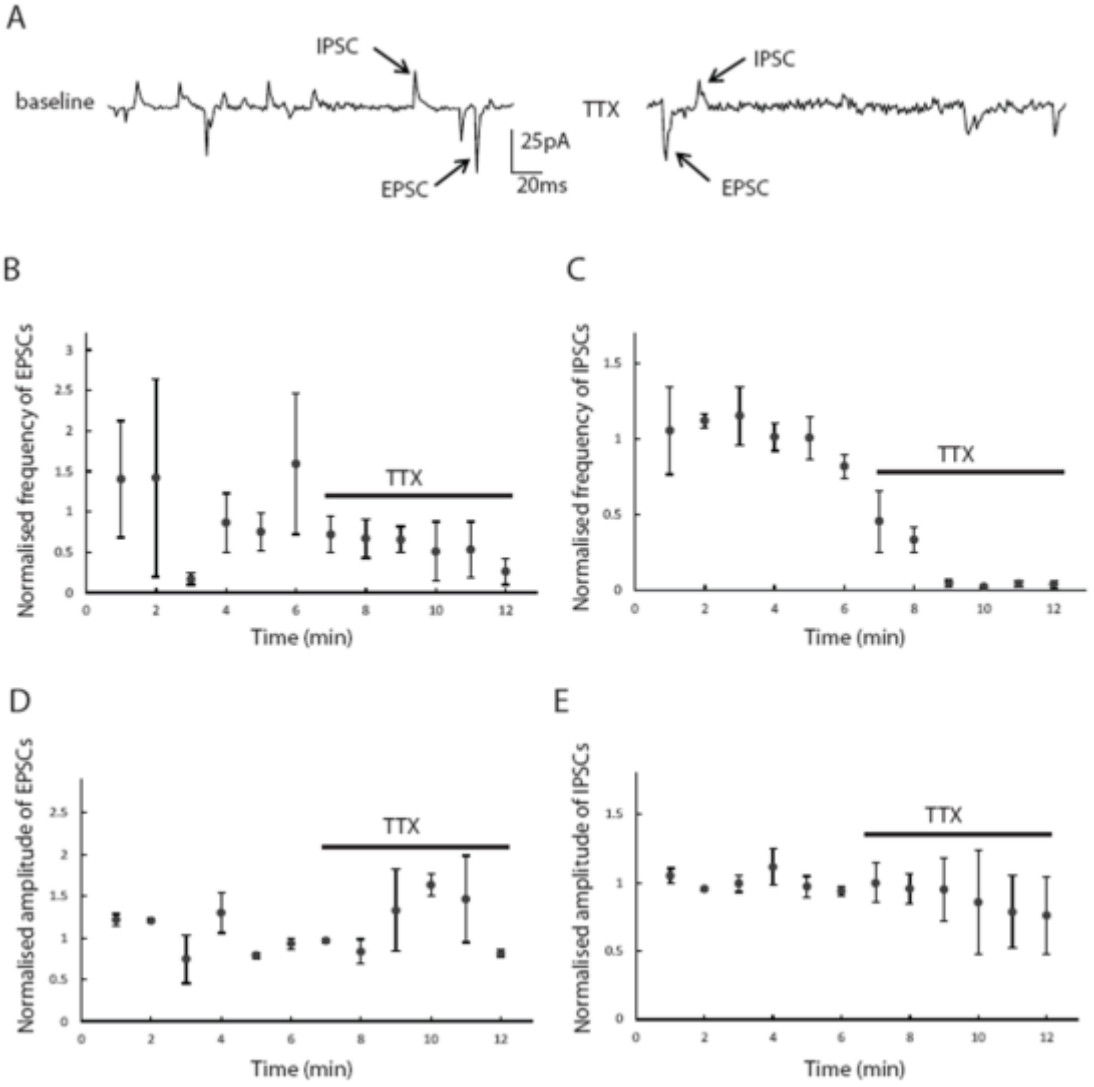

Figure 6.1: Excitatory and inhibitory spontaneous postsynaptic currents in hippocampal brain slices

Spontaneous EPSCs and IPSCs reflect action potential independent and action potential dependent transmitter release, respectively. (**A**) Samples traces recorded at -50mV in hippocampal brain slices in the control solution (left panel, baseline) and in the presence of TTX (500nM, right panel) displaying inward EPSCs and outward IPSCs (marked by arrows). (**B**) Normalised frequency and (**D**) amplitude of EPSCs did not show a significant change in TTX, suggesting they are action potential independent in slices. In contrast, (**C**) the frequency of IPSCs, but not the amplitude (**E**), was significantly reduced in the presence of TTX. This suggests that the majority of IPSCs are action potential evoked.

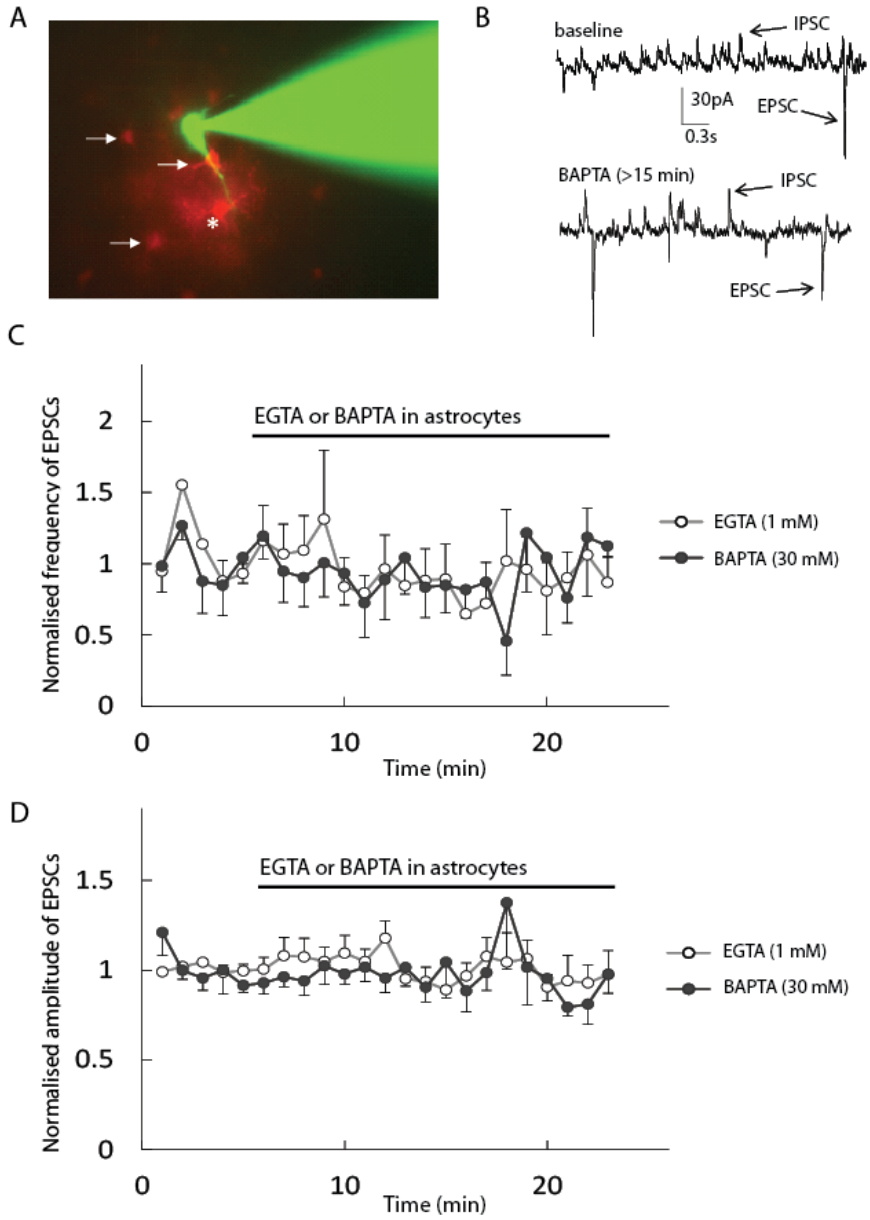

Figure 6.2: Buffering astrocyte $[Ca^{2+}]_i$ does not affect spontaneous excitatory transmission

(**A**) a representative Alexa-dye filled image of a CA1 pyramidal neuron filled with Alexa 488 (green) and a nearby astrocyte filled with Alexa 594 (red, patch-clamped astrocyted marked with a star) in the stratum radiatum. Gap junction coupling is evident from Alexa 594 dye spread from the patch clamped astrocyte to the surrounding astrocyte network (white arrows). (**B**) Samples traces (at -50mV) displaying simultanously occuring inward EPSCs and outward IPSCs (marked by arrows) during the baseline period (top panel), and after 15 mins of dialysis of the astrocyte with BAPTA. (**C-D**) Normalised frequency and amplitude of EPSCs did not show a significant change whether the astrocyte was dialysed with 1 mM EGTA (white) or 30 mM BAPTA (black). Note that only a subset of cells were dialysed for a period longer than 10 min. The graphs show the combined data (i.e. following >9 min dialysis of astrocytes, starting at t=15 min, the graph shows data from fewer cells compared to the initial period of dialysis, (i.e. 6 cells out of the total of 13 cells for EGTA, and 5 cells out of the total of 16 cells for BAPTA)).

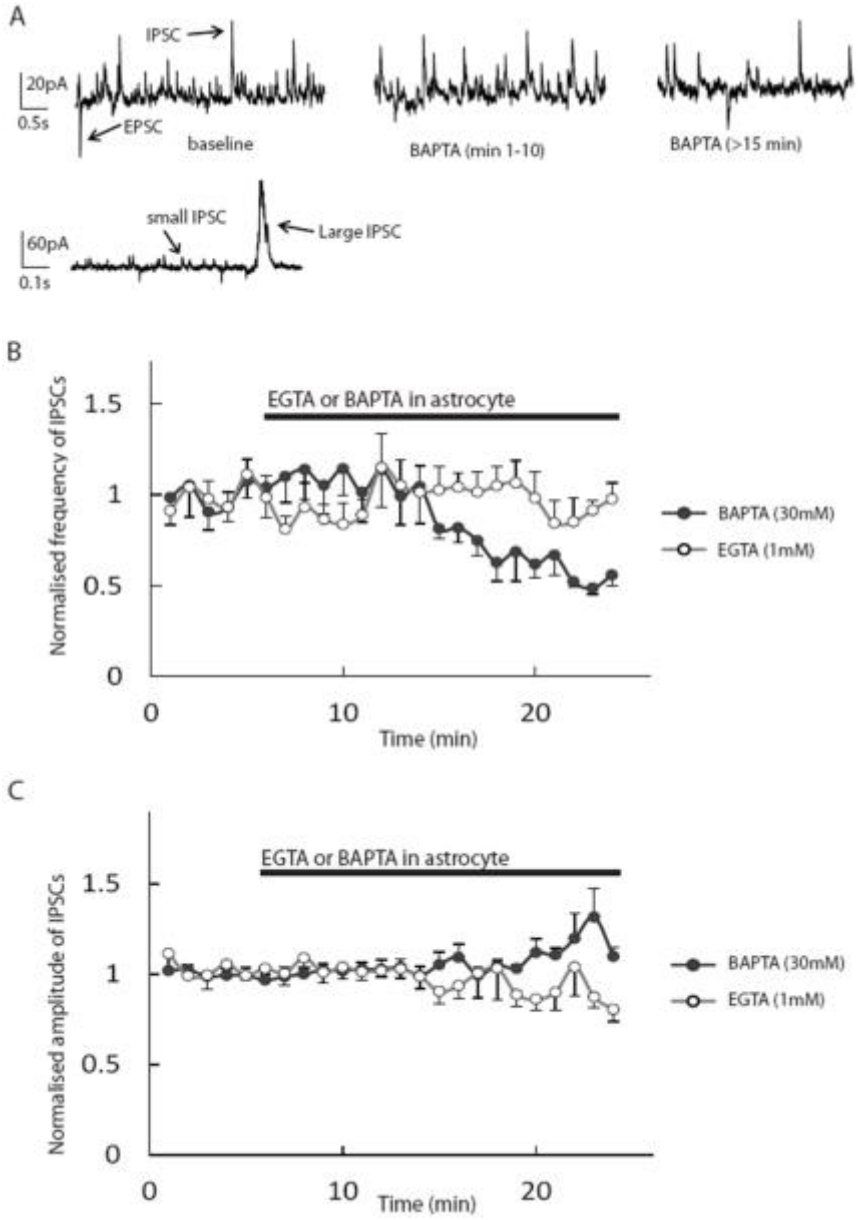

Figure 6.3: Astrocyte $[Ca^{2+}]_i$ regulates the rate of spontaneous inhibitory transmission

(**A**) Samples traces (at -50mV) for the common "singular" (top panels) and infrequent "multipeak" large amplitude events (bottom panel). Simultaneously occurring inward EPSCs and outward IPSCs (marked by arrows) are shown during the baseline period (left), after less than 10 mins astrocyte dialysis with BAPTA (middle), and after >15 mins of dialysis with BAPTA (right). (**B**) The normalised frequency of IPSCs showed a significant reduction following prolonged dialysis of astrocytes with 30 mM BAPTA (black) compared to 1 mM EGTA (white). Note that only a subset of cells were dialysed for a period longer than 10 min. The graphs show the combined data (i.e. following >9 min dialysis of astrocytes, starting at t=15 min, the graph shows data from fewer cells compared to the initial period of dialysis, (i.e. 6 cells out of the total 13 of cells for EGTA, and 5 cells out of the total of 16 cells for BAPTA)) (**C**) Unlike IPSC rate, the amplitude of IPSCs did not show a convincing change with EGTA (white) or BAPTA (black). The delayed apparent increase in BAPTA amplitude is largely due to the occurrence of multipeak IPSCs events, and at the same time a significant decrease in the occurrence of singular smaller amplitude events.

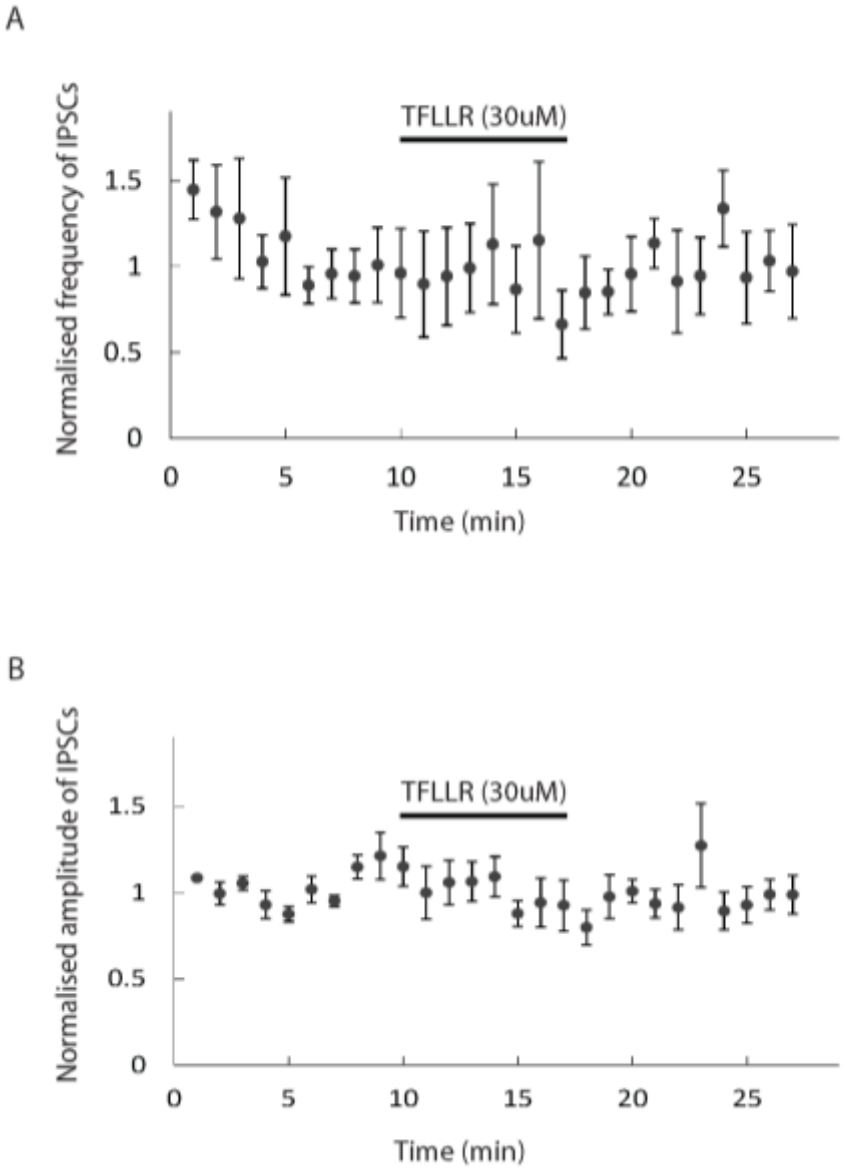

Figure 6.4: PAR-1 mediated signalling does not regulate IPSCs

Bath application of 30μM TFLLR-NH2 for 8 mins, which stimulates a PAR1-mediated increase in [Ca^{2+}] in astrocytes, failed to change the (**A**) frequency or (**B**) amplitude of spontaneous IPSCs recorded in CA1 pyramidal neurons at 0mV.

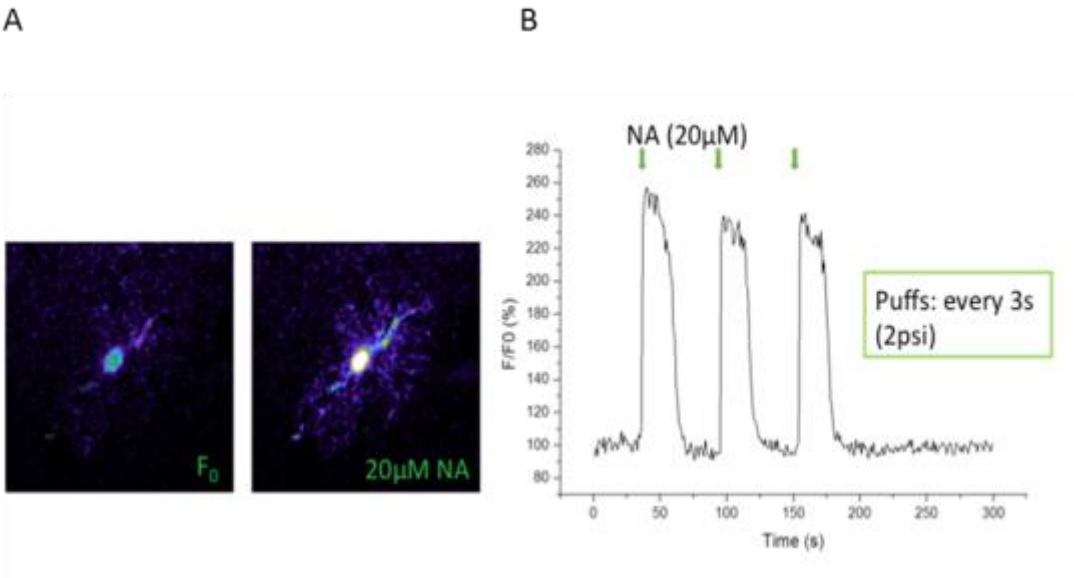

Figure 6.5: Noradrenaline evokes a rise in astrocyte intracellular calcium concentration

(**A**) A sample image of an astrocyte filled with Fluo-4 before (left) and after (right) puff applications of NA (20 µM). (**B**) NA (applied every 3 secs at 2 psi) reliably evoked a calcium concentration rise in astrocytes in the presence of TTX (500nM) (data obtained in collaboration with Fergus O'Farrell).

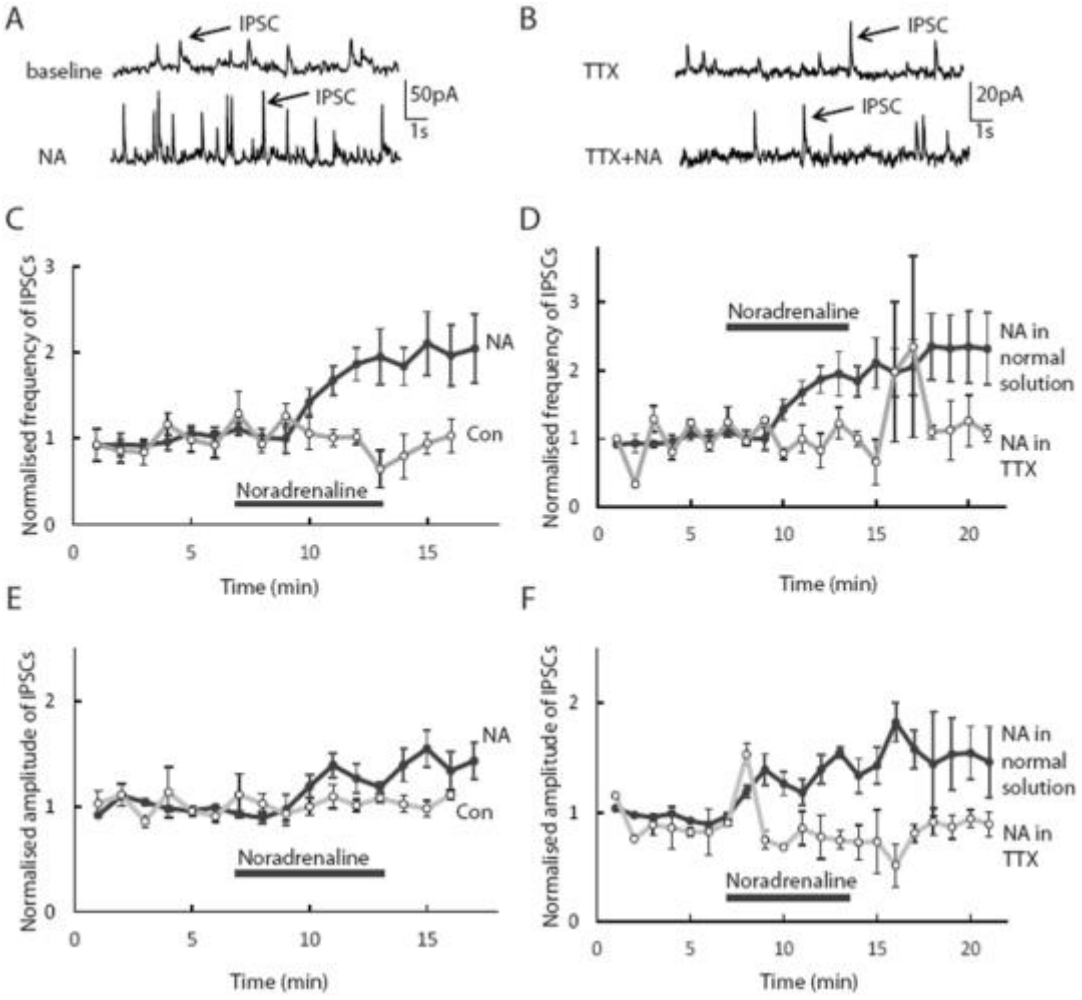

Figure 6.6: Noradrenaline potentiates inhibitory transmission

(**A**) Samples traces (at 0 mV) displaying outward IPSCs during baseline (top panel) and following bath application of NA (20 μM). (**B**) Samples traces for IPSCs durring TTX (500 nM, top panel), and following NA addition to TTX solution (bottom panel, 20 μM). (**C**) IPSC frequency showed a significant increase following bath application of NA (black) compared to control (white). (**D**) NA-evoked increase in IPSC frequency (black) was abolished when TTX is present (white), comparing data following NA perfusion in the presence and absence of TTX. The NA alone data in this panel are the same as in panel C but extend to a longer time (data for this longer time were not recorded for the control in C). (**E**) IPSC amplitude also showed an increase following bath application of NA (black) compared to control (white), and (**F**) this increase (black) was similarly abolished when TTX is present (white), comparing data following NA perfusion in the presence and absence of TTX.

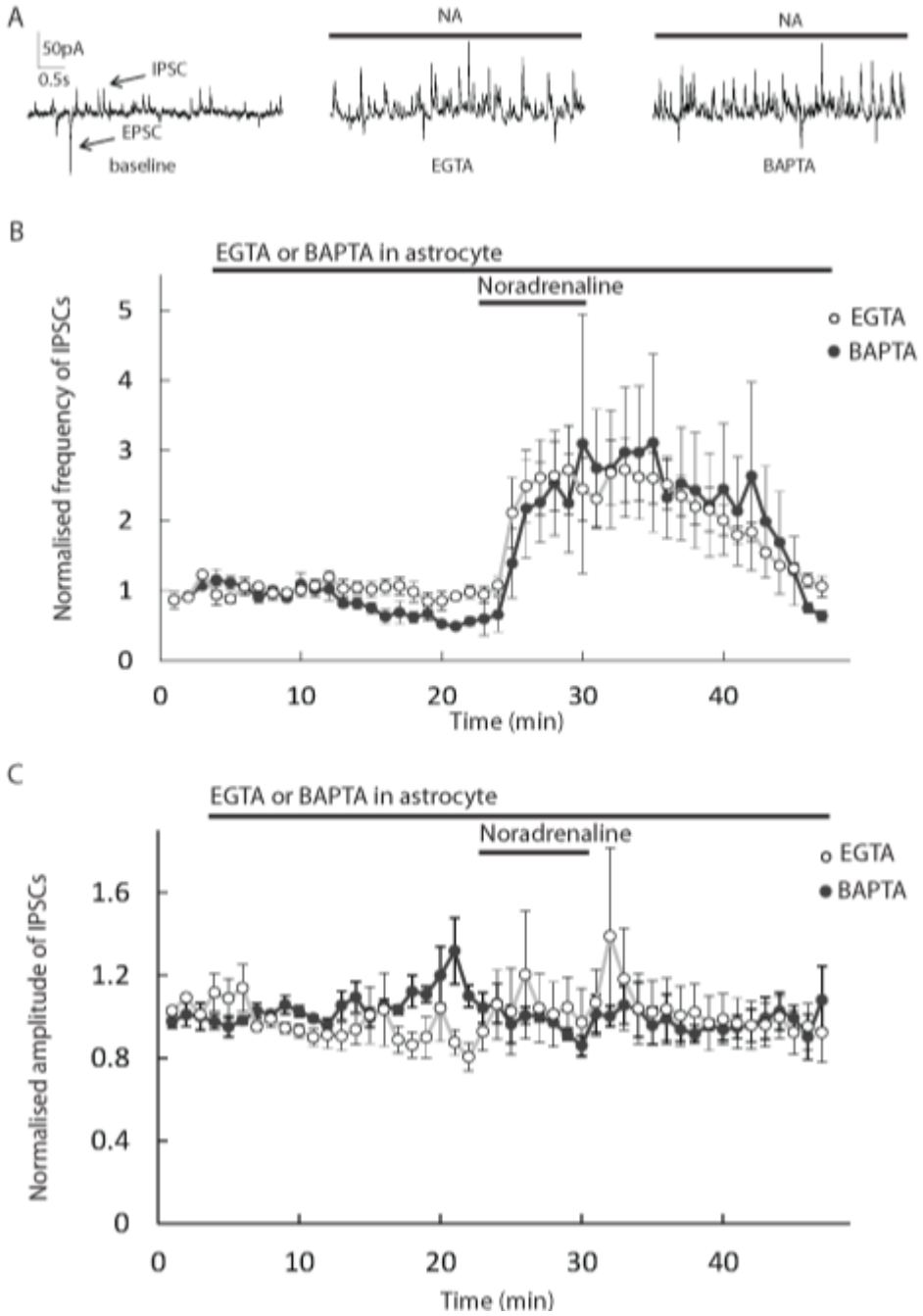

Figure 6.7: NA-evoked potentiation of inhibitory postsynaptic transmission in hippocampal CA1 neurons does not depend on astrocyte calcium signalling
(**A**) Sample traces (at -50 mV) display outward IPSCs (marked by arrows) during baseline period (left), and >15 mins of astrocyte dialysis with EGTA (middle) or BAPTA (right). (**B**) As described in Fig. 6.3, IPSC frequency showed a significant reduction following prolonged dialysis of astrocytes with 30 mM BAPTA (black, n=5) compared to 1 mM EGTA (white, n=6). However, the NA (5 μM)-evoked potentiation of IPSC rate following prolonged dialysis of astrocytes was not affected by buffering astrocyte $[Ca^{2+}]_i$ changes. (**C**) The amplitude of IPSCs did not show a convincing change when 5 μM NA was applied following prolonged dialysis with EGTA (white) or BAPTA (black) in the presence or absence of NA (5 μM).

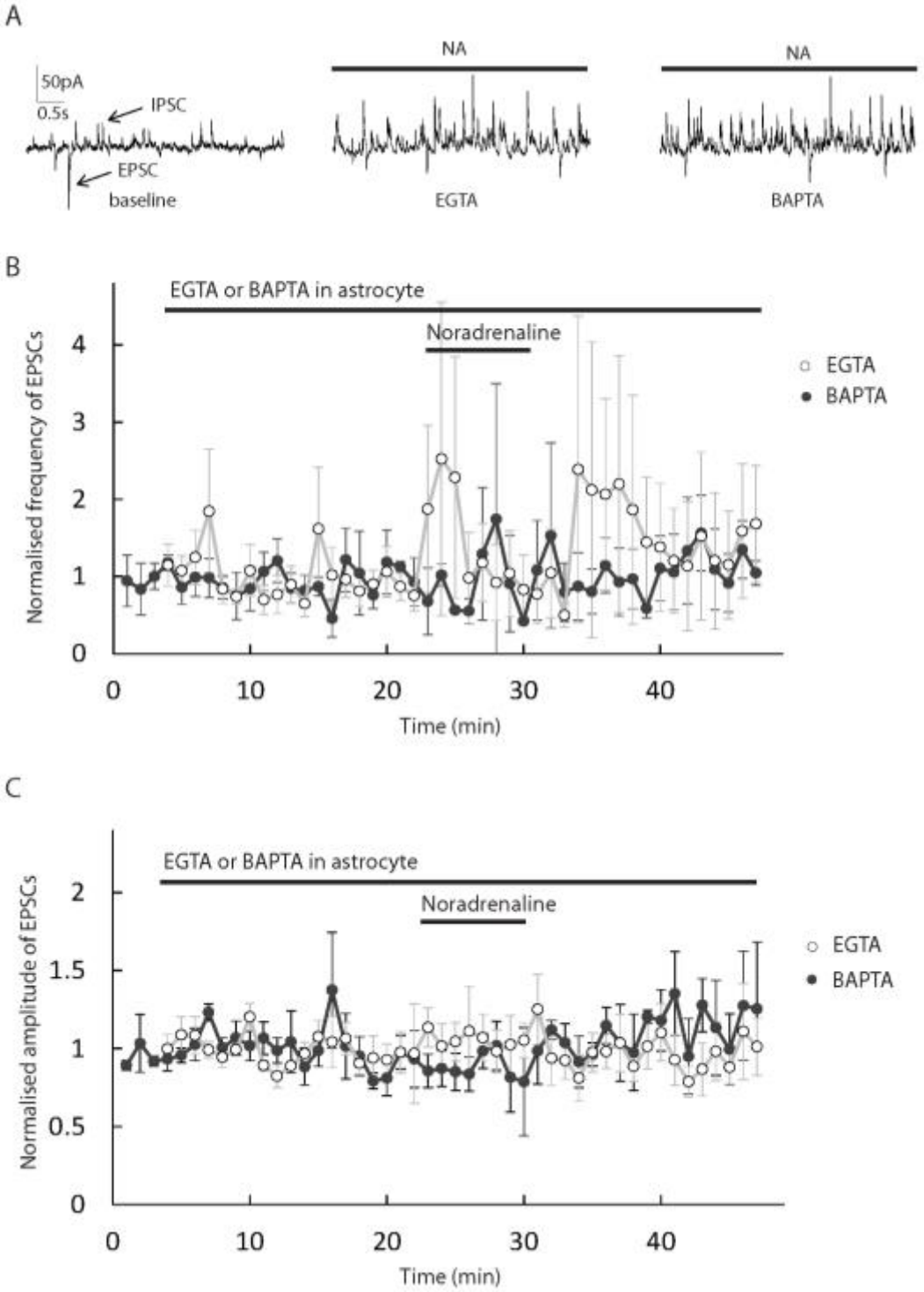

Figure 6.8: The failure of NA to evoke changes in EPSC does not depend on astrocyte $[Ca^{2+}]_i$

(**A**) Sample traces (at -50 mV) display inward EPSCs (marked by arrows) during the baseline period (left), and after >15 mins of astrocyte dialysis with EGTA (middle) or BAPTA (right). (**B**) The frequency and (**C**) the amplitude of spontaneous EPSCs did not show a convincing change on application of 5 μM NA following prolonged dialysis with EGTA (white, n=6) or BAPTA (black, n=5).

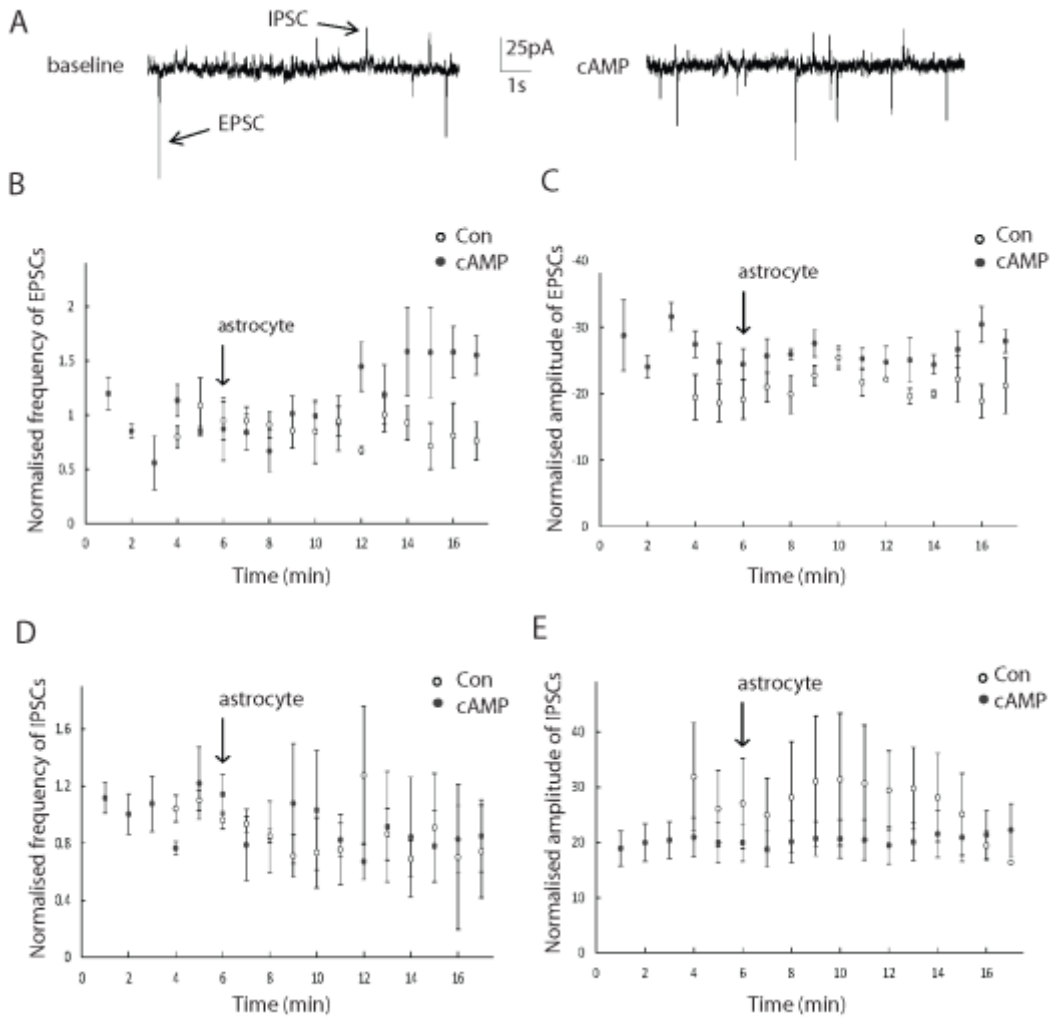

Figure 6.9: Raising astrocyte $[cAMP]_i$ increases the rate of spontaneous EPSCs. (**A**) Sample traces (recorded at -50 mV in CA1 neurons) display simultanously occuring inward EPSCs and outward IPSCs (marked by arrows) before (left panel) and after (right panel) dialysis of a nearby astrocyte with cAMP (5 mM). (**B**) The frequency increased with time after starting dialysis with internal cAMP (black). (**C**) The amplitude of EPSCs, and (**D & E**) the frequency and amplitude of IPSCs, showed no change when cAMP was dialysed into the astrocyte.

Chapter 7:

Discussion

Throughout this thesis, I have investigated ways by which glutamate transport is regulated in hippocampal astrocytes, and how astrocytes can interact with, and modulate the activity of, neurons. In this chapter, I will briefly summarise the findings from each of the results chapters and discuss the future experiments required to better understand the findings. A more detailed discussion of the results is given in the relevant discussion section in each chapter.

7.1 Neuroprotective role of a glial specific GPCR

Results from chapter 3, in collaboration with the Richardson Lab, showed that GPCR37L1 is expressed in a subset of astrocytes and OPCs (Fig. 3.1). Despite a lack of expression at birth, GPCR37L1 expression was high at P8 and was maintained through to adulthood (measured at 4 months, Fig. 3.1).

My results from whole-cell patch-clamp recording from hippocampal astrocytes showed that the expression or deletion of GPCR37L1 did not affect the astrocyte membrane properties (i.e. membrane resistance and resting potential, Fig. 3.2), nor their gap junctional coupling (Fig. 3.3).

Nevertheless, I suggest a neuroprotective role for this GPCR37L1 during ischaemia, as the expression of this receptor alone, or the addition of its ligand analogue prosaptide, reduced cell death in the pyramidal layer of the WT compared to the KO (Fig. 3.4) in brain slices. Prosaptide also decreased cell death in the pyramidal layer of the KO slices but to a lesser extent (Fig. 3.4C). This suggests that the

activation of other receptors that are activated by prosaptide, such as GPR37 (which shares more than 40% amino acid sequence similarity with GPCR37L1 Meyer et al. 2013) which is expressed in mature oligodendrocytes and a subpopulation of neurons but not in astrocytes (unpublished data from the Richardson Lab), also plays a neuroprotective role in ischaemia.

These results, for the first time, link the previous knowledge of a neuroprotective role for prosaposin during ischaemia (see section 3.2) with the activity of the newly characterized receptor GPCR37L1.

I next assessed the mechanism(s) by which this protection of neurons by GPCR37L1 expressed in astrocytes occurs. Glutamate receptor mediated depolarisation and calcium entry (in particular through NMDARs) is the major cause of neuronal damage in ischaemia (Goldberg *et al*., 1987; Vornov & Coyle, 1991; Rossi, Oshima & Attwell, 2000; Brassai *et al.* 2015; Robinson & Jackson, 2016). Thus, a decrease in survival of CA1 pyramidal neurons during ischaemia in the GPCR37L1 KO may reflect an increase in the extracellular level of glutamate around CA1 pyramidal cells (see section. 3.4.4). My electrophysiological analysis of the excitability of CA3 neurons (i.e. their firing likelihood and latency to the first action potential, Fig. 3.5), and their stimulation threshold for glutamate release (Fig. 3.6), however, revealed no difference between the WT and KO.

Furthermore, I showed that a decrease in cell survival in the KO during ischaemia (Fig. 3.4) was not due to a change in the number or conductance of the glutamate receptors in CA1 pyramidal neurons, by comparing the magnitude of the kainate-evoked, and NMDA-evoked currents in WT and GPCR37L1 KO cells (Fig. 3.7).

Despite the lack of an apparent change in the currents mediated by AMPARs and NMDARs, I observed a slow increase in the conductance of the NMDA receptors upon repeated application of NMDA which turned out to be the key to understanding how GPCR37L1 is neuroprotective. In both the WT and the KO, the response to the second application of NMDA was always bigger (Fig. 3.8A & B), leading to a ratio > 1 when comparing the second to the initial response. This increase in the NMDA receptor-mediated current may also be expected to occur during the prolonged glutamate release that occurs in ischaemia.

Surprisingly, I found that the presence of prosaptide during the second application of NMDA inhibited the potentiation of the NMDA current that would normally occur in the WT (Fig. 3.8C), without affecting the potentiation that occurred in the KO (Fig. 3.8C). Thus, activation of GPCR37L1-mediated signalling in astrocytes somehow blocks the increase of the neuronal NMDA response. Consequently, an increase in endogenous prosaposin release (or the addition of prosaptide) during ischaemia may activate GPCR37L1-mediated signalling (presumably within astrocytes), which in turn would reduce NMDAR-mediated calcium entry and cell death.

What is the mechanism of this effect? Since GPCR37L1 is on astrocytes and the NMDA receptors are neuronal, an astrocyte to neuron messenger must be involved. Modulation by GPCR37L1 of D-serine release from astrocytes is one possibility. Activation of NMDA receptors (NMDARs) requires the binding of glutamate to the NR2 subunit, and the binding of a co-agonist, glycine or D-serine, to the glycine-binding site on the NR1 subunit (Johnson & Ascher, 1987; Papouin *et al.*, 2012; Zhang *et al.*, 2014; Li *et al.*, 2014). Both glycine and D-serine are known to potentiate NMDA responses in culture (Johnson & Ascher, 1987; Fadda *et al.*, 1988; Salt, 1989) and in

brain slices (Rosenberg et al, 2013; Kang et al., 2013; Henneberger et al., 2010). Like glycine, D-serine is present in abundance in the extracellular space (Hashimoto et al., 1993). However, the glycine/D-serine binding site is not saturated in cortical brain slices (Fossat et al., 2012), implying that an increase of the NMDA response will occur upon further release of D-serine (or glycine), if such a release occurs during prolonged application of NMDA and ischaemia. Moreover, astrocyte-derived D-serine (Kang et al., 2013; Shigetomi et al., 2013; Henneberger et al., 2010) has been shown to co-activate postsynaptic NMDARs.

Given that GPCR37L1 is located on astrocytes, which are able to regulate neuronal NMDA responses by releasing D-serine, it is plausible that the GPCR37L1-mediated inhibition of NMDA responses (Fig. 3.8C) involves a reduction in D-serine release from astrocytes, and that prosaposin release in ischaemia thus decreases activation of neuronal NMDA receptors. To investigate this hypothesis, I intend to confirm that D-serine can potentiate the NMDA response of CA1 neurons, and investigate whether the presence of exogenous D-serine throughout the experiment can prevent the potentiation of the NMDA current, by saturating of the co-agonist binding site on the NMDARs, thus rendering superfluous any increase in the release of D-serine from astrocytes that may occur during ischaemia.

As an alternative to D-serine, I will investigate the possibility that the GPCR37L1-mediated inhibition of NMDA responses (Fig. 3.8C) may involve a reduction in the release of tumor necrosis factor alpha (TNF-α) from astrocytes. This is because TNF-α has also been shown to enhance the neuronal NMDA response (Glazner *et al*., 2000; Marchetti *et al*., 2004; Jara *et al*., 2007) presumably by upregulating NMDA receptor insertion into the postsynaptic membrane (Wheeler *et al*., 2009). Furthermore, astrocytes are known to be the source of the TNF-α which

potentiates the neuronal NMDA response (Stellwagen & Malenka, 2006). This idea could be checked by determining whether the presence of exgenous TNF-α occludes the increase of NMDA receptor response on repeated NMDA application.

Altered transport of glutamate by glial or neuronal transporters could elevate extracellular levels of glutamate and contribute to cell death in ischaemia (Robinson & Jackson, 2016) via NMDA receptors (Vornov & Coyle, 1991; Brassai *et al.* 2015). Although my recordings of the glutamate uptake current (measured as the current evoked by the glutamate analogue, D-aspartate) in WT and GPCR37L1 KO hippocampal astrocytes revealed no change in the absence of prosaptide (Fig. 3.10B), the addition of prosaptide significantly reduced the uptake current in the WT without affecting the current in the KO (Fig. 3.11B & C).

Thus if glial glutamate transporters do reverse in severe ischaemia and contribute significantly to the release of glutamate (which has been questioned early in ischaemia by the work of Hamann *et al.*, 2002), then inhibition of the rate of reversed glial glutamate transport may be another mechanism (in addition to reduced D-serine or TNF-α release) by which prosaptide-evoked GPCR37L1 signalling exerts its neuroprotective effect during ischaemia.

Overall, these results are encouraging in proposing a neuroprotective role for the glial-specific GPCR37L1 during excitotoxic conditions. There are, however, other questions that still remain unanswered.

Results from this chapter suggest that GPCR37L1 is not constitutively active, contradicting the recent report by Coleman et al. (2016), and also suggest that the baseline level of endogenous prosaposin in physiological conditions (i.e. with no ischaemia) is minimal in brain slices. I saw no difference between the WT and the GPCR37L1 KO in the size of NMDA-evoked responses in CA1 neurons, or in the

glutamate uptake current in astrocytes, in the absence of prosaptide. In contrast, when prosaptide was added, the NMDA-evoked current and the glutamate uptake current were reduced in the WT while remaining unchanged in the KO.

Morishita *et al.* (2014) reported that prosaposin is expressed in hippocampus. The lack of extracellular prosaposin to activate GPCR37L1 that is implied by my experiments may reflect either a lack of activation of a release mechanism in baseline conditions, or the fact that prosaposin immunoreactivity in the dentate gyrus declines after postnatal day 14 (Morishita *et al.*, 2014), while my experiments were from mice at postnatal days 14-16. Furthermore, they performed immunolabelling against prosaposin on perfusion fixed brain tissue (Morishita *et al.*, 2014), which might have preserved endogenous levels of prosaposin more faithfully. In contrast, I cannot rule out a potential dilution of the extracellular levels of prosaposin following tissue slicing, and a minimum 1 hour recovery period prior to electrophysiological recordings.

More information on the subcellular localisation of GPCR37L1 in astrocytes may provide critical information about how the receptors interact with glutamatergic synapses in the hippocampus. Are the GPCR37L1 expressed near synapses, on the fine processes of the astrocytes, or are they more clustered near the astrocyte somata? Previous work on the effect of astrocyte signalling to neurons, measuring changes in their intracellular levels of calcium, suggests that GPCRs and ion channels on the fine processes of the astrocytes are likely to exert the most influence on the synaptic behaviour of neurons (see Bazargani & Attwell, 2016 for a recent review).

Meyer et al. (2013) claim that GPCR37L1 signalling leads to the activation of a G_i-coupled protein that would lower intracellular levels of cAMP (but see Coleman *et al.*, 2016, who claim GPCR37L1 is G_s-coupled). Thus, increasing the intracellular

level of cAMP (e.g. via the patch pipette) would be one way to assess whether the effects of GPCR37L1 activation on NMDARs and glutamate transporters (as reported in this chapter) are mediated by a decrease in the intracellular level of cAMP or not. Moreover, it would be interesting to assess whether the activation of GPCR37L1 (with prosaptide) can evoke changes in the intracellular level of calcium, since even G_i-coupled receptors are reported to raise $[Ca^{2+}]_i$ in astrocytes (Haustein *et al.*, 2014) and previous work has suggested that astrocyte $[Ca^{2+}]_i$ regulates D-serine release (Henneberger *et al.*, 2010; Shigetomi *et al.*, 2013). Dialysing BAPTA into the astrocytes would then be worth testing for an effect on response potentiation with repeated application of NMDA.

Meyer et al., (2013) also reported that activation of GPCR37L1 and GPCR37 by prosaptide is glioprotective in conditions of oxidative stress, via activation of the Erk kinase signalling pathway. Interestingly, others have also shown that prosaposin prevents cell death by activating the same Erk pathway (Misasi, 2004). Therefore, it would be useful to know if GPCR37L1-mediated regulation of neuronal NMDAR activity and its inhibition of glutamate uptake in astrocytes, involve the same pathway.

7.2 Regulation of glial glutamate uptake by noradrenaline

In chapter 4, I assessed the cellular distribution of adrenoceptor subtypes and their role in regulating glutamate uptake, in hippocampal astrocytes within the stratum radiatum region.

Analysis of antibody signal intensities provided evidence for selective staining of α_1- and α_2-ARs in hippocampal astrocytes. In particular, the results showed that the G_q-coupled α_{1A}- and α_{1B}-ARs were highly expressed in the proximal processes compared to the soma when quantified as total number of receptors (Figs. 4.2C &

4.3B), while analysis of the receptor density per membrane area showed that these receptors were distributed fairly uniformly per membrane area in different astrocyte compartments (Fig. 4.2E). Thus, the larger total signal in the proximal processes reflects this compartment having a larger membrane area compared to the soma, in the astrocytes that were assessed.

Analysis of the expression of α_{2A}-ARs (which are G_i-coupled) revealed a higher total expression of α_{2A}-AR in the proximal processes (based on the receptor's integrated signal intensity, Fig. 4.4B), while the analysis of receptor density showed that α_{2A}-ARs are more dense per membrane area in the distal processes (which wrap synapses) compared to the other astrocyte compartments (Fig. 4.4D).

The antibody to β_1-AR did not produce convincing staining (Fig. 4.5A & B), despite evidence for expression of this receptor in astrocytes (Aoki, 1992; Junker *et al*., 2002; Zhang *et al*., 2014, and 2016). Therefore, further quantification of the β_1-AR distribution with a more specific receptor staining method is needed.

I next showed that noradrenaline regulates glutamate uptake in astrocytes in brain slices. Despite earlier claims, made in studies using cultured astrocytes, that noradrenaline evokes an increase in glutamate uptake (Fahrig, 1993; Hansson & Rönnbäck, 1991), bath application of noradrenaline significantly inhibited the current evoked by D-aspartate in my recordings from patch-clamped astrocytes in the stratum radiatum region of the hippocampus (Fig. 4.6).

Furthermore, I showed that the NA-evoked inhibition of glutamate transporters depends on changes in the intracellular calcium concentration in astrocytes. This is because abolishing calcium concentration elevations inside astrocytes using the chelating agent BAPTA (dialysed via the patch pipette), largely inhibited the reduction of glutamate uptake evoked by noradrenaline (Fig. 4.7). In addition, inhibiting α_1-AR

activation with the potent selective blocker terazosin (Fig. 4.8) strongly abolished the reduction of glutamate uptake by noradrenaline. Thus, it appears that a rise in astrocyte $[Ca^{2+}]_i$, presumably via α_1-AR activation, is essential for the inhibitory effects of noradrenaline on the glutamate transporter current.

However the signalling regulating glutamate uptake involves more than Ca^{2+}. I showed that dialysis of a high concentration of cAMP (1 mM) into the astrocytes (via the patch pipette), also largely abolished the inhibition of the D-aspartate-evoked transporter current that was produced by noradrenaline (Fig. 4.9), presumably by preventing a reduction of $[cAMP]_i$. In support of this, blocking the activity of α_2-ARs with a potent selective α_2-AR blocker atipamezole also inhibited the inhibition of the D-aspartate evoked current by noradrenaline (Fig. 4.10).

The results from these experiments imply that both a reduction in the intracellular concentration of cAMP (via α_2-ARs), and an increase in the concentration of calcium (via α_1-ARs), are needed to mediate the inhibition of glutamate transporters by noradrenaline in hippocampal astrocytes.

The functional consequences of the noradrenaline-evoked inhibition of glutamate uptake are, however, not clear. Inhibition of glutamate transporters by noradrenaline (Fig. 4.6) will result in a rise in the baseline extracellular concentration of glutamate and slower removal of synaptically released glutamate. This might either enhance excitatory transmission (as previously reported for activation of α_1-AR, Williams *et al*., 2014) or could dampen excitatory transmission by desensitizing postsynaptic glutamate receptors (as previously reported for activation of via α_1-ARs, Salgado *et al*. (2012), and α_2-ARs, Yuen *et al*. (2014)). My results from chapter 6 (which will be discussed below) showed a strong potentiation of inhibitory transmission by noradrenaline in hippocampus, an effect that is known to be mediated

by the α_1-ARs on interneurons (Bergles *et al*., 1996). It is plausible that the inhibition of glutamate uptake in astrocytes by noradrenaline, and the subsequent rise of extracellular glutamate, may facilitate the noradrenaline-evoked potentiation of inhibitory transmission (see below for discussion). Further examination of the effect of calcium and cAMP signalling in astrocytes on excitatory and inhibitory transmission in hippocampus may help us to understand the functional consequences of the noradrenaline-evoked inhibition of glutamate uptake in astrocytes (see below for more details).

7.3 Regulation of the glutamate transporter GLT-1 by the intracellular protein nischarin

In chapter 5, I presented unpublished data from the Attwell and Kittler labs which suggest that the intracellular protein nischarin, a mouse homologue of the human imidazoline receptor (Piletz *et al*., 2003; Zhang & Abdel-Rahman, 2006, see section 1.2.7.7 for more details), directly binds to GLT-1 (Fig. 5.1). Furthermore, this interaction decreases the total number of GLT-1 glutamate transporters in astrocytes in culture by promoting GLT-1 internalization and thus its degradation (see Fig. 5.2; unpublished data from the Kittler lab).

My electrophysiological recordings from astrocytes in cultures confirmed an inhibitory effect of nischarin on GLT-1 expression in the astrocyte surface membrane by showing an increase in glutamate uptake current in astrocytes when nischarin was deleted, compared to WT astrocytes (Fig. 5.3B). The larger glutamate uptake current in nischarin KO astrocytes was not due to an increase of cell area, since the cells had a similar capacitance (Fig. 5.4B) in the WT and KO. Indeed, glutamate uptake was

significantly larger in the KO compared to the WT even when the glutamate uptake current was normalised to the capacitance of each cell.

Thus, nischarin can play a key role in regulating glutamate uptake in astrocytes. However, it is not known whether nischarin-mediated internalization of GLT-1 may also indirectly affect the total levels of GLAST in the astrocyte plasma membrane, e.g. if GLAST and GLT-1 form heterotrimers (Koch & Larsson, 2005). Furthermore, it is not clear what proportion of the D-aspartate evoked-current that was recorded in Fig. 5.3 is generated via GLT-1 as oppose to GLAST. Demonstrating a large fractional inhibition of the uptake current by the selective blocker of GLT-1 transporters dihydrokainate (DHK, Arriza et al., 1994), would confirm that the D-aspartate evoked current is generated largely by GLT-1.

It is also not known whether nischarin reduces glutamate uptake in other cell types that express GLT-1 (e.g. neurons and OPCs, Zhang *et al.*, 2014) as it does in astrocytes, and this should be investigated.

Lastly, nischarin has been proposed as a mouse homologue of the human imidazoline receptor type 1 (Piletz *et al.*, 2003; Zhang, J. & Abdel-Rahman, 2006), however, it is not clear whether nischarin acts as a functional receptor with an extracellular domain for the binding of imidazolines, the activation of which may then perhaps lead to the internalisation of GLT-1 transporters. Thus, further experiments assessing the effect of imidazoline signalling on glutamate uptake in the WT and nischarin KO would be informative.

7.4 The role of astrocyte calcium in basal and noradrenaline-modulated synaptic transmission

In this chapter I assessed whether intracellular signalling mechanisms in astrocytes regulate synaptic transmission to CA1 pyramidal cells in the presence or absence of noradrenaline (NA).

I initially demonstrated that the pattern of spontaneous synaptic currents was different for excitatory and inhibitory transmission, in patch-clamp recordings from CA1 pyramidal neurons in hippocampal slices. The rate of spontaneous excitatory activity, which was largely independent of action potential firing, was much lower than that of spontaneous inhibitory activity, recorded in the same cells, which was strongly dependent on action potentials (Fig. 6.1).Thus, the glutamatergic projections from CA3 pyramidal neurons, which are the major excitatory input at the CA3-CA1 synapse, do not exhibit high frequency firing in brain slices, while interneurons exhibit a high spontaneous action potential firing pattern.

I next examined whether calcium signalling in astrocytes regulates spontaneous activity in neighbouring neurons by dialysing into astrocytes an internal solution containing BAPTA (replacing EGTA), that strongly buffers $[Ca^{2+}]_i$ transients. However, these experiments did not reveal a convincing role for astrocyte Ca^{2+} signalling, and downstream gliotransmission, in regulating the frequency of the excitatory postsynaptic current (EPSCs, Fig.6.2).

In contrast to EPSCs, I found that dialysis of BAPTA (for >15 min) significantly reduced the rate of the inhibitory current (IPSCs, Fig. 6.3). Thus it appears that astrocyte Ca^{2+} signalling can regulate the firing likelihood of inhibitory interneurons. Conversely, evoking an artificial rise in $[Ca^{2+}]_i$ in astrocytes (instead of buffering $[Ca^{2+}]_i$ with BAPTA), by applying TFLLR-NH2 (which activates PAR1

receptors and raises $[Ca^{2+}]_i$, Lalo et al., 2014; Park et al., 2013; Oh et al., 2012) did not affect the rate or the amplitude of spontaneous IPSCs recorded in CA1 pyramidal neurons (Fig. 6.4). This is consistent with the report of Shigetomi et al. (2012), who failed to observe any effect of raising the intracellular free calcium concentration (up to 500 nM) on inhibitory transmission. This suggests that either a reduction in calcium concentration in astrocytes has a bigger impact on the action potential activity of nearby interneurons than does a calcium concentration rise, or that Ca^{2+} entry into the astrocyte from the extracellular space, and not a G protein coupled receptor-mediated $[Ca^{2+}]_i$ rise, is needed to regulate the detected rate of IPSCs (presumably by altering insertion of the GABA transporter GAT-3 into the membrane or by releasing excitatory gliotransmitters to alter action potential occurrence in interneurons). Direct recordings of interneuron firing should be carried out to investigate whether manipulating astrocyte $[Ca^{2+}]_i$ does alter action potential rate.

I next examined the effects of noradrenaline on spontaneous synaptic currents in hippocampal CA1 neurons, and whether these effects are at least partly mediated by an effect of noradrenaline on astrocyte calcium signalling. This is possible because even low concentrations of NA (1-2 μM) have been shown to induce Ca^{2+} responses in astrocytes in slices (Duffy & MacVicar, 1995, also see Fig. 6.5), independent of neuronal action potential activity (Espallergues et al., 2007).

In agreement with previous work by Bergles et al. (1996), I showed that noradrenaline robustly enhances inhibitory transmission in a manner dependent on the action potential firing of interneurons (Fig. 6.6). This strong potentiation of the IPSC rate does not, however, depend on astrocyte $[Ca^{2+}]_i$ changes. This was shown by demonstrating, with dual whole-cell patch-clamp recordings, that the effects of noradrenaline (5 μM) on the IPSC rate or amplitude were independent of whether

astrocytes were dialysed with 30 mM BAPTA or with 1 mM EGTA as the calcium buffer (Fig. 6.7). Furthermore, I found no evidence for an effect of noradrenaline on EPSC rate or amplitude in slices, irrespective of whether the patch-clamped astrocyte was filled with EGTA or BAPTA (Fig. 6.8).

Thus, although astrocyte Ca^{2+} signalling regulates the rate of inhibitory transmission in hippocampus in the absence of added NA (Fig. 6.3), the NA-evoked potentiation of inhibitory transmission must be via a direct depolarizing action of NA on interneurons, as suggested by Bergles et al. (1996). This also suggests that the $[Ca^{2+}]$-dependent inhibition of glutamate uptake produced by noradrenaline (Figs. 4.7) following the activation of α_1-adrenoceptors (Fig. 4.8), and the resulting rise in the baseline extracellular level of glutamate, do not significantly affect spontaneous inhibitory transmission in hippocampus.

Apart from investigating the effect of calcium signalling in astrocytes on synaptic activity, I also examined whether increasing the concentration of cyclic AMP in astrocytes (through the addition of 5mM cAMP to the internal solution) could regulate the spontaneous EPSCs and IPSCs recorded in nearby CA1 neurons. Preliminary results suggest that elevating the levels of cAMP might potentiate the rate of excitatory transmission (Fig. 6.9). This finding is of interest as I previously showed that a reduction in $[cAMP]_i$ inside astrocytes mediated a noradrenaline-evoked inhibition of glutamate uptake in patch-clamp recordings from hippocampal astrocytes (Fig. 4.10). Thus, an increase in the neuronal EPSC rate when $[cAMP]_i$ is high inside astrocytes (as seen in Fig. 6.9), when glutamate uptake is presumably increased, suggest that the noradrenaline-evoked inhibition of glutamate uptake in hippocampus (see Fig. 4.6) may dampen excitatory transmission in hippocampus presumably by

raising the extracellular glutamate concentration and desensitizing AMPA receptors, making EPSCs smaller and harder to detect.

It would be curious to know whether these effects of noradrenaline on glutamate uptake, and the resulting changes in excitatory transmission in the hippocampus, are involved in hippocampal dependent behaviours such as the promotion of memory formation and attention.

Bibliography

Abbott, N. J. Astrocyte-endothelial interactions and blood-brain barrier permeability. *J. Anat.* **200,** 629–638 (2002).

Acin-Perez, R. *et al.* Cyclic AMP Produced inside Mitochondria Regulates Oxidative Phosphorylation. *Cell Metabolism* **9,** 265–276 (2009).

Adelman WJ Jr, Fitzhugh R. Solutions of the Hodgkin-Huxley equations modified for potassium accumulation in a periaxonal space. *Fed Proc.* **34**:1322–1329 (1975).

Agulhon, C., Fiacco, T.A. & McCarthy, K.D. Hippocampal short- and long-term plasticity are not modulated by astrocyte Ca2+ signaling. Science 327, 1250–1254 (2010).

Alahari, S. K., Lee, J. W. & Juliano, R. L. Nischarin, a novel protein that interacts with the integrin alpha5 subunit and inhibits cell migration. *J. Cell Biol.* **151,** 1141–1154 (2000).

Alexander, G. M., Grothusen, J. R., Gordon, S. W. & Schwartzman, R. J. Intracerebral microdialysis study of glutamate reuptake in awake, behaving rats. *Brain Res.* **766,** 1–10 (1997).

Amédée, T., Robert, A. & Coles, J. A. Potassium homeostasis and glial energy metabolism. *Glia* **21,** 46–55 (1997).

Anders, S. *et al.* Spatial properties of astrocyte gap junction coupling in the rat hippocampus. *Phil. Trans. R. Soc. B* **369,** 20130600 (2014).

Anderson, Christopher M. *et al.* Differing effects of substrate and non-substrate transport inhibitors on glutamate uptake reversal. *Journal of Neurochemistry* **79,** 1207–1216 (2001).

Androutsou, M.E., Saifeddine, M., Hollenberg, M.D., Matsoukas, J., Agelis, G. Design, synthesis and biological evaluation of non-peptide PAR1 thrombin receptor antagonists based on small bifunctional templates: arginine and phenylalanine side chain groups are keys for receptor activity. *Amino Acids.* **38**(4):985-90 (2010)

Angelova, P.R., Kasymov, V., Christie, I., Sheikhbahaei, S., Turovsky, E., Marina, N., Korsak, A., Zwicker, J., Teschemacher, A.G., Ackland, G.L., Funk, G.D., Kasparov, S., Abramov, A.Y., Gourine, A.V. Functional Oxygen Sensitivity of Astrocytes. *J Neurosci*. **35**(29):10460 –10473 (2015).

Angulo, M.C., Kozlov, A.S., Charpak, S. & Audinat, E. Glutamate released from glial cells synchronizes neuronal activity in the hippocampus. J. Neurosci. **24**, 6920–6927 (2004).

Aoki, C. Beta-adrenergic receptors: astrocytic localization in the adult visual cortex and their relation to catecholamine axon terminals as revealed by electron microscopic immunocytochemistry. *J. Neurosci.* **12,** 781–792 (1992).

Araque, A., Li, N., Doyle, R.T. & Haydon, P.G. SNARE protein-dependent glutamate release from astrocytes. J. Neurosci. **20**, 666–673 (2000).

Araque, A., Sanzgiri, R.P., Parpura, V. & Haydon, P.G. Calcium elevation in astrocytes causes an NMDA receptor-dependent increase in the frequency of miniature synaptic currents in cultured hippocampal neurons. J. Neurosci. **18**, 6822–6829 (1998).

Arriza, J. L. *et al.* Cloning and expression of a human neutral amino acid transporter with structural similarity to the glutamate transporter gene family. *J. Biol. Chem.* **268,** 15329–15332 (1993).

Arriza, J. L., Eliasof, S., Kavanaugh, M. P. & Amara, S. G. Excitatory amino acid transporter 5, a retinal glutamate transporter coupled to a chloride conductance. *Proc. Natl. Acad. Sci. U.S.A.* **94,** 4155–4160 (1997).

Attwell, D. et al. Glial and neuronal control of brain blood flow. Nature 468, 232–243 (2010).

Auger, C. & Attwell, D. Fast removal of synaptic glutamate by postsynaptic transporters. *Neuron* **28,** 547–558 (2000).

Barbour, B., Brew, H. & Attwell, D. Electrogenic glutamate uptake in glial cells is activated by intracellular potassium. *Nature* **335,** 433–435 (1988).

Barbour, B., Brew, H. & Attwell, D. Electrogenic uptake of glutamate and aspartate into glial cells isolated from the salamander (Ambystoma) retina. *J. Physiol. (Lond.)* **436,** 169–193 (1991).

Barrett, S., Honbo, N. & Karliner, J. S. Alpha 1-adrenoceptor-mediated inhibition of cellular cAMP accumulation in neonatal rat ventricular myocytes. *Naunyn Schmiedebergs Arch. Pharmacol.* **347,** 384–393 (1993).

Barros, L. F. Metabolic signaling by lactate in the brain. *Trends Neurosci.* **36,** 396–404 (2013).

Bayraktar, O. A., Fuentealba, L. C., Alvarez-Buylla, A. & Rowitch, D. H. Astrocyte development and heterogeneity. *Cold Spring Harb Perspect Biol* **7,** a020362 (2015).

Bazargani, N. & Attwell, D. Astrocyte calcium signaling: the third wave. *Nat Neurosci* **19,** 182–189 (2016).

Bender, A. S., Woodbury, D. M. & White, H. S. The rapid L- and D-aspartate uptake in cultured astrocytes. *Neurochem. Res.* **22,** 721–726 (1997).

Benveniste, H. *et al.* Ischemic damage in hippocampal CA1 is dependent on glutamate release and intact innervation from CA3. *J. Cereb. Blood Flow Metab.* **9,** 629–639 (1989).

Beppu, K. et al. Optogenetic countering of glial acidosis suppresses glial glutamate release and ischemic brain damage. Neuron 81, 314–320 (2014).

Bergles, D.E., Doze, V.A., Madison, D.V., Smith, S.J. Excitatory Actions of Norepinephrine on Multiple Classes of Hippocampal CA1 Interneurons. *J Neurosci.* **16**(2): 572-75 (1996)

Bergles, D. E., Roberts, J. D., Somogyi, P. & Jahr, C. E. Glutamatergic synapses on oligodendrocyte precursor cells in the hippocampus. *Nature* **405,** 187–191 (2000).

Berridge, C. W. & Waterhouse, B. D. The locus coeruleus-noradrenergic system: modulation of behavioral state and state-dependent cognitive processes. *Brain Res. Brain Res. Rev.* **42,** 33–84 (2003).

Berridge, C. W., Page, M. E., Valentino, R. J. & Foote, S. L. Effects of locus coeruleus inactivation on electroencephalographic activity in neocortex and hippocampus. *Neuroscience* **55,** 381–393 (1993).

Bezzi, P. et al. Prostaglandins stimulate calcium-dependent glutamate release in astrocytes. Nature **391**, 281–285 (1998).

Billups, B., Rossi, D. & Attwell, D. Anion conductance behavior of the glutamate uptake carrier in salamander retinal glial cells. *J. Neurosci.* **16,** 6722–6731 (1996).

Billups, D., Marx, M.-C., Mela, I. & Billups, B. Inducible presynaptic glutamine transport supports glutamatergic transmission at the calyx of Held synapse. *J. Neurosci.* **33,** 17429–17434 (2013).

Bischofberger, J., Engel, D., Li, L., Geiger, J. R. & Jonas, P. Patch-clamp recording from mossy fiber terminals in hippocampal slices. *Nat. Protocols* **1,** 2075–2081 (2006).

Bonder, D.E. & McCarthy, K.D. Astrocytic Gq-GPCR-linked IP3R-dependent Ca2+ signaling does not mediate neurovascular coupling in mouse visual cortex in vivo. J. Neurosci. **34**, 13139–13150 (2014).

Bowser, D.N. & Khakh, B.S. Vesicular ATP is the predominant cause of intercellular calcium waves in astrocytes. J. Gen. Physiol. **129**, 485–491 (2007).

Bradford HF, Ward HK, Thomas AJ. Glutamine—a major substrate for nerve endings. *J Neurochem.* **30**:1453–1459 (1978).

Bradley, S. J. & Challiss, R. A. J. G protein-coupled receptor signalling in astrocytes in health and disease: a focus on metabotropic glutamate receptors. *Biochem. Pharmacol.* **84,** 249–259 (2012).

Brassai, A., Suvanjeiev, R.-G., Bán, E.-G. & Lakatos, M. Role of synaptic and nonsynaptic glutamate receptors in ischaemia induced neurotoxicity. *Brain Res. Bull.* **112,** 1–6 (2015).

Brew, H. & Attwell, D. Electrogenic glutamate uptake is a major current carrier in the membrane of axolotl retinal glial cells. *Nature* **327,** 707–709 (1987).

Bridges, R. J., Kavanaugh, M. P. & Chamberlin, A. R. A pharmacological review of competitive inhibitors and substrates of high-affinity, sodium-dependent glutamate transport in the central nervous system. *Curr. Pharm. Des.* **5,** 363–379 (1999).

Burger, P. M. *et al.* Synaptic vesicles immunoisolated from rat cerebral cortex contain high levels of glutamate. *Neuron* **3,** 715–720 (1989).

Cahoy JD, Emery B, Kaushal A, Foo LC, Zamanian JL, Christopherson KS, Xing Y, Lubischer JL, Krieg PA, Krupenko SA and others. A transcriptome database for astrocytes, neurons, and oligodendrocytes: a new resource for understanding brain development and function. J Neurosci **28**:264-78 (2008).

Carriba, P. *et al.* ATP and noradrenaline activate CREB in astrocytes via noncanonical Ca(2+) and cyclic AMP independent pathways. *Glia* **60,** 1330–1344 (2012).

Cavelier, P. & Attwell, D. Tonic release of glutamate by a DIDS-sensitive mechanism in rat hippocampal slices. *J. Physiol. (Lond.)* **564,** 397–410 (2005).

Chabre, O., Conklin, B. R., Brandon, S., Bourne, H. R. & Limbird, L. E. Coupling of the alpha 2A-adrenergic receptor to multiple G-proteins. A simple approach for estimating receptor-G-protein coupling efficiency in a transient expression system. *J. Biol. Chem.* **269,** 5730–5734 (1994).

Chaudhry, F. A. *et al.* Glutamate transporters in glial plasma membranes: Highly differentiated localizations revealed by quantitative ultrastructural immunocytochemistry. *Neuron* **15,** 711–720 (1995).

Chen, N. et al. Nucleus basalis-enabled stimulus-specific plasticity in the visual cortex is mediated by astrocytes. Proc. Natl. Acad. Sci. USA 109, E2832–E2841 (2012).

Chittajallu, R., Braithwaite, S.P., Clarke, V.R., Henley, J.M. Kainate receptors: subunits, synaptic localization and function.*Trends Pharmacol Sci.* 20(1):26-35 (1999).

Clarke, L. E. & Barres, B. A. Emerging roles of astrocytes in neural circuit development. *Nat Rev Neurosci* **14,** 311–321 (2013).

Clarke, L. E. & Barres, B. A. Glia keep synapse distribution under wraps. *Cell* **154,** 267–268 (2013).

Coleman JL, Ngo T, Schmidt J, Mrad N, Liew CK, Jones NM, Graham RM, Smith NJ. Metalloprotease cleavage of the N terminus of the orphan G protein-coupled receptor GPR37L1 reduces its constitutive activity. Sci Signal 9:ra36 (2016).

Connors BW, Ransom BR, Kunis DM, et al. Activity-dependent K+ accumulation in the developing rat optic nerve. *Science*. **216**:1341–1343 (1982).

Conti, F., DeBiasi, S., Minelli, A., Rothstein, J. D. & Melone, M. EAAC1, a high-affinity glutamate tranporter, is localized to astrocytes and gabaergic neurons besides pyramidal cells in the rat cerebral cortex. *Cereb. Cortex* **8,** 108–116 (1998).

Cornell-Bell, A.H., Finkbeiner, S.M., Cooper, M.S. & Smith, S.J. Glutamate induces calcium waves in cultured astrocytes: long-range glial signaling. Science **247**, 470–473 (1990).

Costain WJ, Haqqani AS, Rasquinha I, Giguere MS, Slinn J, Zurakowski B, Stanimirovic DB. Proteomic analysis of synaptosomal protein expression reveals that cerebral ischaemia alters lysosomal Psap processing. Proteomics 10:3272-91 (2010).

Curet, O., de Montigny, C. Electrophysiological characterization of adrenoceptors in the rat dorsal hippocampus. II. Receptors mediating the effect of synaptically released norepinephrine. *Brain Res*. **475**(1):47-5(1998)

Curran AK, Rodman JR, Eastwood PR, Henderson KS, Dempsey JA, Smith CA. Ventilatory responses to specific CNS hypoxia in sleeping dogs. J Appl Physiol (1985) **88**:1840 –1852 (2000).

D'Ascenzo, M. et al. mGluR5 stimulates gliotransmission in the nucleus accumbens. Proc. Natl. Acad. Sci. USA 104, 1995–2000 (2007).

Danbolt, N. C. Glutamate uptake. *Progress in Neurobiology* **65,** 1–105 (2001).

Danbolt, N. C. The high affinity uptake system for excitatory amino acids in the brain. *Prog. Neurobiol.* **44,** 377–396 (1994).

Danbolt, N. C., Storm-Mathisen, J. & Kanner, B. I. An [Na+ + K+]coupled L-glutamate transporter purified from rat brain is located in glial cell processes. *Neuroscience* **51,** 295–310 (1992).

Dani, J.W., Chernjavsky, A. & Smith, S.J. Neuronal activity triggers calcium waves in hippocampal astrocyte networks. Neuron **8**, 429–440 (1992).

Davenport HW, Brewer G, Chambers AH, Goldschmidt S. The respiratory responses to anoxemia of unanesthetized dogs with chronically denervated aortic and carotid chemoreceptors and their causes. Am J Physiol. **148**:406–416 (1947).

Davis, K. E. *et al.* Multiple signaling pathways regulate cell surface expression and activity of the excitatory amino acid carrier 1 subtype of Glu transporter in C6 glioma. *J. Neurosci.* **18,** 2475–2485 (1998).

Dawson, L. A., Djali, S., Gonzales, C., Vinegra, M. A. & Zaleska, M. M. Characterization of transient focal ischaemia-induced increases in extracellular glutamate and aspartate in spontaneously hypertensive rats. *Brain Res. Bull.* **53,** 767–776 (2000).

Day, J. S. *et al.* Noradrenaline acting on astrocytic β_2-adrenoceptors induces neurite outgrowth in primary cortical neurons. *Neuropharmacology* **77,** 234–248 (2014).

Deng, Q., Terunuma, M., Fellin, T., Moss, S.J., Haydon, P.G., Astrocytic activation of A1 receptors regulates the surface expression of NMDA receptors through a Src kinase dependent pathway. *Glia*. **59**(7): 1084-93 (2011).

Derouiche A, Frotscher M. Astroglial processes around identified glutamatergic synapses contain glutamine synthetase: evidence for transmitter degradation. *Brain Res.* **552**:346–350 (1991).

Derouiche, A. & Rauen, T. Coincidence of L-glutamate/L-aspartate transporter (GLAST) and glutamine synthetase (GS) immunoreactions in retinal glia: evidence for coupling of GLAST and GS in transmitter clearance. *J. Neurosci. Res.* **42,** 131–143 (1995).

Descarries, L. & Saucier, G. Disappearance of the locus coeruleus in the rat after intraventricular 6-hydroxdopamine. *Brain Res.* **37,** 310–316 (1972).

Devaraju, P., Sun, M.Y., Myers, T.L., Lauderdale, K. & Fiacco, T.A. Astrocytic group I mGluR-dependent potentiation of astrocytic glutamate and potassium uptake. J. Neurophysiol. **109**, 2404–2414 (2013).

Di Castro, M.A. *et al*. Local Ca^{2+} detection and modulation of synaptic release by astrocytes. *Nat. Neurosci.* **14**, 1276–1284 (2011)

Dienel, G. A. & Cruz, N. F. Aerobic glycolysis during brain activation: adrenergic regulation and influence of norepinephrine on astrocytic metabolism. *J. Neurochem.* **138,** 14–52 (2016).

Ding, F. α1-Adrenergic receptors mediate coordinated Ca2+ signaling of cortical astrocytes in awake, behaving mice. Cell Calcium **54**, 387–394 (2013).

Doengi, M. et al. GABA uptake-dependent Ca2+ signaling in developing olfactory bulb astrocytes. Proc. Natl. Acad. Sci. USA **106**, 17570–17575 (2009).

Doyle JP, Dougherty JD, Heiman M, Schmidt EF, Stevens TR, Ma G, Bupp S, Shrestha P, Shah RD, Doughty ML and others. Application of a translational profiling approach for the comparative analysis of CNS cell types. Cell **135**:749-62 (2008).

Duffy, S. & MacVicar, B.A. Adrenergic calcium signaling in astrocyte networks within the hippocampal slice. J. Neurosci. 15, 5535–5550 (1995).

Dunlop, J. Substrate exchange properties of the high-affinity glutamate transporter EAAT2. *J. Neurosci. Res.* **66,** 482–486 (2001).

Edwards, F. A., Konnerth, A., Sakmann, B. & Takahashi, T. A thin slice preparation for patch clamp recordings from neurones of the mammalian central nervous system. *Pflugers Arch.* **414,** 600–612 (1989).

Erecińska, M., Troeger, M. B., Wilson, D. F. & Silver, I. A. The role of glial cells in regulation of neurotransmitter amino acids in the external environment. II. Mechanism of aspartate transport. *Brain Res.* **369,** 203–214 (1986).

Espallergues, J., Solovieva, O., Técher, V., Bauer, K., Alonso, G., Vincent, A., Hussy, N. Synergistic activation of astrocytes by ATP and norepinephrine in the rat supraoptic nucleus. *Mol Neurosci.* **148**(3): 712–723 (2007)

Fadda, E., Danysz, W., Wroblewski, J. T. & Costa, E. Glycine and D-serine increase the affinity of N-methyl-D-aspartate sensitive glutamate binding sites in rat brain synaptic membranes. *Neuropharmacology* **27**, 1183–1185 (1988).

Fahrig, T. Receptor subtype involved and mechanism of norepinephrine-induced stimulation of glutamate uptake into primary cultures of rat brain astrocytes. *Glia* **7**, 212–218 (1993).

Fairman, W. A., Vandenberg, R. J., Arriza, J. L., Kavanaugh, M. P. & Amara, S. G. An excitatory amino-acid transporter with properties of a ligand-gated chloride channel. *Nature* **375,** 599–603 (1995).

Feldmann, A. et al. Transport of the major myelin proteolipid protein is directed by VAMP3 and VAMP7. J. Neurosci. **31**, 5659–5672 (2011).

Fellin, T. et al. Neuronal synchrony mediated by astrocytic glutamate through activation of extrasynaptic NMDA receptors. Neuron **43**, 729–743 (2004).

Fiacco, T.A. & McCarthy, K.D. Intracellular astrocyte calcium waves in situ increase the frequency of spontaneous AMPA receptor currents in CA1 pyramidal neurons. J. Neurosci. **24**, 722–732 (2004).

Fiacco, T.A., Agulhon, C., Taves, S.R., Petravicz, J., Casper, K.B., Dong, X., Chen, J., McCarthy, K.D. Selective Stimulation of Astrocyte Calcium In Situ Does Not Affect Neuronal Excitatory Synaptic Activity. Neuron. **54**(4): 611–626 (2007).

Figiel, M., Maucher, T., Rozyczka, J., Bayatti, N. & Engele, J. Regulation of glial glutamate transporter expression by growth factors. *Experimental Neurology* **183,** 124–135 (2003).

Florey, E. An inhibitory and an excitatory factor of mammalian central nervous system, and their action of a single sensory neuron. *Arch Int Physiol* **62,** 33–53 (1954).
Fossat, P. *et al.* Glial D-serine gates NMDA receptors at excitatory synapses in prefrontal cortex. *Cereb. Cortex* **22,** 595–606 (2012).

Franciolini, F. Patch clamp technique and biophysical study of membrane channels. *Experientia* **42,** 589–594 (1986).

Freeman MR. Specification and morphogenesis of astrocytes. Science **330**:774-8 (2010).

Fujita, T. et al. Neuronal transgene expression in dominant-negative SNARE mice. J. Neurosci. **34**, 16594–16604 (2014).

Fujita, T., Liu, T., Nakatsuka, T., Kumamoto, E. Proteinase-activated receptor-1 activation presynaptically enhances spontaneous glutamatergic excitatory transmission in adult rat substantia gelatinosa neurons. *J Neurophysiol*. **102**(1):312-9 (2009)

Furness, D. N., Dehnes, Y., Akhtar, A.Q., Rossi, D.J., Hamann, M. *et al.* A quantitative assessment of glutamate uptake into hippocampal synaptic terminals and astrocytes: new insights into a neuronal role for excitatory amino acid transporter 2 (EAAT2). *Neuroscience* **157,** 80–94 (2008).

Gebhardt, C., Körner, R. & Heinemann, U. Delayed anoxic depolarizations in hippocampal neurons of mice lacking the excitatory amino acid carrier 1. *J. Cereb. Blood Flow Metab.* **22,** 569–575 (2002).

Gereau, R.W., Conn, P.J. Presynaptic enhancement of excitatory synaptic transmission by beta-adrenergic receptor activation. *J Neurophysiol*. **72**(3):1438-42 (1994)

Glancy, B., Willis, W. T., Chess, D. J. & Balaban, R. S. Effect of calcium on the oxidative phosphorylation cascade in skeletal muscle mitochondria. *Biochemistry* **52,** 2793–2809 (2013).

Glavin, G. B. Stress and brain noradrenaline: a review. *Neurosci Biobehav Rev* **9,** 233–243 (1985).

Glazner, G. W. & Mattson, M. P. Differential effects of BDNF, ADNF9, and TNFalpha on levels of NMDA receptor subunits, calcium homeostasis, and neuronal vulnerability to excitotoxicity. *Exp. Neurol.* **161,** 442–452 (2000).

Glitsch, H. G., Krahn, T. & Pusch, H. The dependence of sodium pump current on internal Na concentration and membrane potential in cardioballs from sheep Purkinje fibres. *Pflugers Arch.* **414,** 52–58 (1989).

Gochenauer, G. E. & Robinson, M. B. Dibutyryl-cAMP (dbcAMP) up-regulates astrocytic chloride-dependent L-[3H]glutamate transport and expression of both system xc(-) subunits. *J. Neurochem.* **78,** 276–286 (2001).

Goldberg, M. P., Weiss, J. H., Pham, P. C. & Choi, D. W. N-methyl-D-aspartate receptors mediate hypoxic neuronal injury in cortical culture. *J. Pharmacol. Exp. Ther.* **243,** 784–791 (1987).

Gordon, G.R., Choi, H.B., Rungta, R.L., Ellis-Davies, G.C. & MacVicar, B.A. Brain metabolism dictates the polarity of astrocyte control over arterioles. Nature **456**, 745–749 (2008).

Gordon, G.R., Choi, H.B., Rungta, R.L., Ellis-Davies, G.C. & MacVicar, B.A. Brain metabolism dictates the polarity of astrocyte control over arterioles. *Nature* **456**, 745–749(2008)

Gourine AV, Kasymov V, Marina N et al. Astrocytes control breathing through pH-dependent release of ATP. Science. **329**:571–575 (2010).

Gourine AV, Llaudet E, Dale N, Spyer KM. ATP is a mediator of chemosensory transduction in the central nervous system. *Nature*. **436**:108–111 (2005).

Gundersen, V., Shupliakov, O., Brodin, L., Ottersen, O. P. & Storm-Mathisen, J. Quantification of excitatory amino acid uptake at intact glutamatergic synapses by immunocytochemistry of exogenous D-aspartate. *J. Neurosci.* **15,** 4417–4428 (1995).

Halassa, M.M. *et al*. Astrocytic modulation of sleep homeostasis and cognitive consequences of sleep loss. *Neuron* **61**, 213–219 (2009)

Hall, C.N., Reynell, C., Gesslein, B., Hamilton, N.B., Mishra, A., Sutherland, B.A., O'Farrell, F.M., Buchan, A.M., Lauritzen, M., Attwell, D. Capillary pericytes regulate cerebral blood flow in health and disease. Nature. **508**(7494):55-60 (2014)

Hamada, K. *et al.* Properties of the Na+/K+ pump current in small neurons from adult rat dorsal root ganglia. *British Journal of Pharmacology* **138,** 1517–1527 (2003).

Hamann, M., Rossi, D. J., Marie, H. & Attwell, D. Knocking out the glial glutamate transporter GLT-1 reduces glutamate uptake but does not affect hippocampal glutamate dynamics in early simulated ischaemia. *Eur. J. Neurosci.* **15,** 308–314 (2002).

Hamberger AC, Chiang GH, Nylen ES, et al. Glutamate as a CNS transmitter. I. Evaluation of glucose and glutamine as precursors for the synthesis of preferentially released glutamate.*Brain Res.* **168**:513–530 (1979).

Hamberger, A., Berthold, C.-H., Karlsson, B., Lehmann, A., Nystrom, B. Extracellular GABA, glutamate and glutamine in vivo perfusion-dialysis of rabbit hippocampus. Neurol. Neurobiol. 7, 473–492 (1983).

Hamill, O. P., Marty, A., Neher, E., Sakmann, B. & Sigworth, F. J. Improved patch-clamp techniques for high-resolution current recording from cells and cell-free membrane patches. *Pflugers Arch.* **391,** 85–100 (1981).

Hamilton, N. *et al.* Mechanisms of ATP- and glutamate-mediated calcium signaling in white matter astrocytes. *Glia* **56**, 734–749 (2008)

Hamilton, N.B. & Attwell, D. Do astrocytes really exocytose neurotransmitters? Nat. Rev. Neurosci. **11**, 227–238 (2010).

Han, X. et al. Forebrain engraftment by human glial progenitor cells enhances synaptic plasticity and learning in adult mice. Cell Stem Cell 12, 342–353 (2013).

Hansen AJ. Effect of anoxia on ion distribution in the brain. *Physiol Rev.* **65**:101–148 (1985).

Hansson, E. & Rönnbäck, L. Receptor regulation of the glutamate, GABA and taurine high-affinity uptake into astrocytes in primary culture. *Brain Research* **548,** 215–221 (1991).

Harada, T. *et al.* Functions of the two glutamate transporters GLAST and GLT-1 in the retina. *Proc. Natl. Acad. Sci. U.S.A.* **95,** 4663–4666 (1998).

Hashimoto, A., Nishikawa, T., Oka, T. & Takahashi, K. Endogenous D-serine in rat brain: N-methyl-D-aspartate receptor-related distribution and aging. *J. Neurochem.* **60,** 783–786 (1993).

Hassel B, Brathe A. Neuronal pyruvate carboxylation supports formation of transmitter glutamate. *J Neurosci.* **20**:1342–1347 (2000).

Haugeto, O. *et al.* Brain glutamate transporter proteins form homomultimers. *J. Biol. Chem.* **271,** 27715–27722 (1996).

Haustein, M.D. et al. Conditions and constraints for astrocyte calcium signaling in the hippocampal mossy fiber pathway. Neuron 82, 413–429 (2014).

Head, G. A. & Mayorov, D. N. Imidazoline receptors, novel agents and therapeutic potential. *Cardiovasc Hematol Agents Med Chem* **4,** 17–32 (2006).

Headley, P. M. & Grillner, S. Excitatory amino acids and synaptic transmission: the evidence for a physiological function. *Trends Pharmacol. Sci.* **11,** 205–211 (1990).

Heeringa J, Berkenbosch A, de GJ, Olievier CN. Relative contribution of central and peripheral chemoreceptors to the ventilatory response to CO2 during hyperoxia. Respir Physiol. **37**:365–379 (1979).

Heinemann U, Lux HD. Ceiling of stimulus induced rises in extracellular potassium concentration in the cerebral cortex of cat. *Brain Res*. **120**:231–249 (1977).

Henneberger, C., Papouin, T., Oliet, S.H. & Rusakov, D.A. Long-term potentiation depends on release of D-serine from astrocytes. Nature **463**, 232–236 (2010).

Hertz, L., Lovatt, D., Goldman, S. A. & Nedergaard, M. Adrenoceptors in brain: cellular gene expression and effects on astrocytic metabolism and [Ca(2+)]i. *Neurochem. Int.* **57,** 411–420 (2010).

Hinojosa, A. E., Caso, J. R., García-Bueno, B., Leza, J. C. & Madrigal, J. L. M. Dual effects of noradrenaline on astroglial production of chemokines and pro-inflammatory mediators. *J Neuroinflammation* **10,** 81 (2013).

Hiraiwa M, Liu J, Lu AG, Wang CY, Misasi R, Yamauchi T, Hozumi I, Inuzuka T, O'Brien JS. Regulation of gene expression in response to brain injury: enhanced expression and alternative splicing of rat prosaposin (SGP-1) mRNA in injured brain. J Neurotrauma **20**:755-65 (2003).

Hirase, H., Qian, L., Barthó, P. & Buzsáki, G. Calcium dynamics of cortical astrocytic networks in vivo. PLoS Biol. 2, E96 (2004).

Holleran J, Babbie M, Erlichman JS. Ventilatory effects of impaired glial function in a brain stem chemoreceptor region in the conscious rat. *J Appl Physiol*. **90**:1539–1547 (2001).

Huang, R. & Hertz, L. Noradrenaline-induced stimulation of glutamine metabolism in primary cultures of astrocytes. *J. Neurosci. Res.* **41,** 677–683 (1995).

Hubbard, K. B. & Hepler, J. R. Cell signalling diversity of the Gqalpha family of heterotrimeric G proteins. *Cell. Signal.* **18,** 135–150 (2006).

Hugh, D., Grennan, A., Abugila, M. A. & Weinkove, C. Ascorbic acid as an antioxidant in measurements of catecholamines in plasma. *Clin. Chem.* **33,** 569–571 (1987).

Hughes, E. G., Maguire, J. L., McMinn, M. T., Scholz, R. E. & Sutherland, M. L. Loss of glial fibrillary acidic protein results in decreased glutamate transport and inhibition of PKA-induced EAAT2 cell surface trafficking. *Brain Res. Mol. Brain Res.* **124,** 114–123 (2004).

Hunsberger, H. C., Rudy, C. C., Batten, S. R., Gerhardt, G. A. & Reed, M. N. P301L tau expression affects glutamate release and clearance in the hippocampal trisynaptic pathway. *J. Neurochem.* **132,** 169–182 (2015).

Hutchinson, D. S., Catus, S. L., Merlin, J., Summers, R. J. & Gibbs, M. E. α_2-Adrenoceptors activate noradrenaline-mediated glycogen turnover in chick astrocytes. *J. Neurochem.* **117,** 915–926 (2011).

Ibáñez, I., Díez-Guerra, F. J., Giménez, C. & Zafra, F. Activity dependent internalization of the glutamate transporter GLT-1 mediated by β-arrestin 1 and ubiquitination. *Neuropharmacology* **107,** 376–386 (2016).

Imai Y, Soda M, Inoue H, Hattori N, Mizuno Y, Takahashi R. An unfolded putative transmembrane polypeptide, which can lead to endoplasmic reticulum stress, is a substrate of Parkin. Cell **105**:891-902 (2001).

Ishiwata, S., Umino, A., Balu, D. T., Coyle, J. T. & Nishikawa, T. Neuronal serine racemase regulates extracellular D-serine levels in the adult mouse hippocampus. *J Neural Transm (Vienna)* **122,** 1099–1103 (2015).

Ito J, Ito M, Nambu H, Fujikawa T, Tanaka K, Iwaasa H, Tokita S. Anatomical and histological profiling of orphan G-protein-coupled receptor expression in gastrointestinal tract of C57BL/6J mice. Cell Tissue Res 338:257-69 (2009).

Jabaudon, D. *et al.* Inhibition of uptake unmasks rapid extracellular turnover of glutamate of nonvesicular origin. *Proc Natl Acad Sci U S A* **96,** 8733–8738 (1999).

Jackson, M. *et al.* Modulation of the neuronal glutamate transporter EAAT4 by two interacting proteins. *Nature* **410,** 89–93 (2001).

Jara, J. H., Singh, B. B., Floden, A. M. & Combs, C. K. Tumor necrosis factor alpha stimulates NMDA receptor activity in mouse cortical neurons resulting in ERK-dependent death. *J. Neurochem.* **100,** 1407–1420 (2007).

Johnson, J. W. & Ascher, P. Glycine potentiates the NMDA response in cultured mouse brain neurons. *Nature* **325,** 529–531 (1987).

Jourdain, P. et al. Glutamate exocytosis from astrocytes controls synaptic strength. Nat. Neurosci. **10**, 331–339 (2007).

Junge, C.E., Sugawara, T., Mannaioni, G., Alagarsamy, S., Conn, P., Brat, D.J., Chan, P.H., Traynelis, S.F. The contribution of protease-activated receptor 1 to neuronal damage caused by transient focal cerebral ischemia. *Proc Natl Acad Sci U S A.* **100**(22): 13019–13024

Junker, V. *et al.* Stimulation of beta-adrenoceptors activates astrocytes and provides neuroprotection. *Eur. J. Pharmacol.* **446,** 25–36 (2002).

Jurado, S. et al. LTP requires a unique postsynaptic SNARE fusion machinery. Neuron 77, 542–558 (2013).

Kajikawa, Y., Saitoh, N. & Takahashi, T. GTP-binding protein βγ subunits mediate presynaptic calcium current inhibition by GABAB receptor. *Proc Natl Acad Sci U S A* **98,** 8054–8058 (2001).

Kalandadze, A., Wu, Y. & Robinson, M.B. Protein kinase C activation decreases cell surface expression of the GLT-1 subtype of glutamate transporter. Requirement of a carboxyl-terminal domain and partial dependence on serine 486. J. Biol. Chem. **277**, 45741–45750 (2002)

Kang, J., Jiang, L., Goldman, S.A. & Nedergaard, M. Astrocyte-mediated potentiation of inhibitory synaptic transmission. Nat. Neurosci. **1**, 683–692 (1998).

Kang, N. *et al.* Astrocytes release D-serine by a large vesicle. *Neuroscience* **240,** 243–257 (2013).

Kettenmann, H. & Ransom, B. R. *Neuroglia*. (OUP USA, 2013).

Kimelberg, H. K. The problem of astrocyte identity. *Neurochem. Int.* **45,** 191–202 (2004).

Klausberger, T., Magill, P.J., Márton, L.F., Roberts, J.D., Cobden, P.M., Buzsáki, G., Somogyi, P. Brain-state- and cell-type-specific firing of hippocampal interneurons in vivo. Nature. **421**(6925):844-8 (2003)

Klöckner, U., Storck, T., Conradt, M. & Stoffel, W. Functional properties and substrate specificity of the cloned L-glutamate/L-aspartate transporter GLAST-1 from rat brain expressed in Xenopus oocytes. *J. Neurosci.* **14,** 5759–5765 (1994).

Koch, H. P. & Larsson, H. P. Small-Scale Molecular Motions Accomplish Glutamate Uptake in Human Glutamate Transporters. *J. Neurosci.* **25,** 1730–1736 (2005).

Koch, H. P., Chamberlin, A. R. & Bridges, R. J. Nontransportable inhibitors attenuate reversal of glutamate uptake in synaptosomes following a metabolic insult. *Mol. Pharmacol.* **55,** 1044–1048 (1999).

Kozlov, A.S., Angulo, M.C., Audinat, E. & Charpak, S. Target cell-specific modulation of neuronal activity by astrocytes. Proc. Natl. Acad. Sci. USA 103, 10058–10063 (2006).

Krzyżanowska, W., Pomierny, B., Filip, M. & Pera, J. Glutamate transporters in brain ischaemia: to modulate or not? *Acta Pharmacol Sin* **35,** 444–462 (2014).

Kugler, P., Schleyer, V. Developmental expression of glutamate transporters and glutamate dehydrogenase in astrocytes of the postnatal rat hippocampus. *Hippocampus.* 14(8):975-85 (2004).

Kuijl, C. *et al.* Rac and Rab GTPases dual effector Nischarin regulates vesicle maturation to facilitate survival of intracellular bacteria. *EMBO J.* **32,** 713–727 (2013).
Lalo, U. *et al*. Exocytosis of ATP from astrocytes modulates phasic and tonic inhibition in the neocortex. *PLoS Biol.* **12**, e1001747 (2014)

Lalo, U., Pankratov, Y., Kirchhoff, F., North, R. A. & Verkhratsky, A. NMDA receptors mediate neuron-to-glia signaling in mouse cortical astrocytes. *J. Neurosci.* **26,** 2673–2683 (2006).

Lalo, U., Pankratov, Y., Parpura, V. & Verkhratsky, A. Ionotropic receptors in neuronal-astroglial signalling: what is the role of 'excitable' molecules in non-excitable cells. *Biochim. Biophys. Acta* **1813,** 992–1002 (2011).

Lee, S. et al. Channel-mediated tonic GABA release from glia. Science 330, 790–796 (2010).

Lee, S. L. & Phillis, J. W. Stimulation of cerebral cortical synaptosomal Na-K-ATPase by biogenic amines. *Can. J. Physiol. Pharmacol.* **55,** 961–964 (1977).

Lehre, K. P. & Danbolt, N. C. The number of glutamate transporter subtype molecules at glutamatergic synapses: chemical and stereological quantification in young adult rat brain. *J. Neurosci.* **18,** 8751–8757 (1998).

Lehre, K. P., Levy, L. M., Ottersen, O. P., Storm-Mathisen, J. & Danbolt, N. C. Differential expression of two glial glutamate transporters in the rat brain: quantitative and immunocytochemical observations. *J. Neurosci.* **15,** 1835–1853 (1995).

Leng N, Gu G, Simerly RB, Spindel ER. Molecular cloning and characterization of two putative G protein-coupled receptors which are highly expressed in the central nervous system. Brain Res Mol Brain Res 69:73-83 (1999).

Levitt, P. & Moore, R. Y. Noradrenaline neuron innervation of the neocortex in the rat. *Brain Res.* **139,** 219–231 (1978).

Levy, L. M., Lehre, K. P., Rolstad, B. & Danbolt, N. C. A monoclonal antibody raised against an [Na(+)+K+]coupled L-glutamate transporter purified from rat brain confirms glial cell localization. *FEBS Lett.* **317,** 79–84 (1993).

Levy, L. M., Lehre, K. P., Walaas, S. I., Storm-Mathisen, J. & Danbolt, N. C. Down-regulation of glial glutamate transporters after glutamatergic denervation in the rat brain. *Eur. J. Neurosci.* **7,** 2036–2041 (1995).

Levy, L. M., Warr, O. & Attwell, D. Stoichiometry of the glial glutamate transporter GLT-1 expressed inducibly in a Chinese hamster ovary cell line selected for low endogenous Na+-dependent glutamate uptake. *J. Neurosci.* **18,** 9620–9628 (1998).

Li, X. *et al.* D-serine-induced inactivation of NMDA receptors in cultured rat hippocampal neurons expressing NR2A subunits is Ca2+-dependent. *CNS Neurosci Ther* **20,** 951–960 (2014).
Li, D. et al. Lack of evidence for vesicular glutamate transporter expression in mouse astrocytes. J. Neurosci. **33**, 4434–4455 (2013).

Li, S., Mallory, M., Alford, M., Tanaka, S. & Masliah, E. Glutamate transporter alterations in Alzheimer disease are possibly associated with abnormal APP expression. *J. Neuropathol. Exp. Neurol.* **56,** 901–911 (1997).

Liaw, S. H., Kuo, I. & Eisenberg, D. Discovery of the ammonium substrate site on glutamine synthetase, a third cation binding site. *Protein Sci* **4,** 2358–2365 (1995).

Lin, C. I. *et al.* Modulation of the neuronal glutamate transporter EAAC1 by the interacting protein GTRAP3-18. *Nature* **410,** 84–88 (2001).

Liu, Q., Xu, Q., Arcuino, G., Kang, J. & Nedergaard, M. Astrocyte-mediated activation of neuronal kainate receptors. *Proc. Natl. Acad. Sci. U.S.A.* **101**, 3172–3177 (2004).

Liu, Q.Y., Schaffner, A.E., Chang, Y.H., Maric, D. & Barker, J.L. Persistent activation of GABAA receptor/Cl− channels by astrocyte-derived GABA in cultured embryonic rat hippocampal neurons. J. Neurophysiol. 84, 1392–1403 (2000).

Loaiza, A., Porras, O.H. & Barros, L.F. Glutamate triggers rapid glucose transport stimulation in astrocytes as evidenced by real-time confocal microscopy. J. Neurosci. 23, 7337–7342 (2003).

Lu, A. G., Otero, D. A., Hiraiwa, M. & O'Brien, J. S. Neuroprotective effect of retro-inverso Prosaptide D5 on focal cerebral ischaemia in rat. *Neuroreport* **11,** 1791–1794 (2000).

Mack, A. F. & Wolburg, H. A novel look at astrocytes: aquaporins, ionic homeostasis, and the role of the microenvironment for regeneration in the CNS. *Neuroscientist* **19,** 195–207 (2013).

Mandillo, S. *et al.* Mice lacking the Parkinson's related GPR37/PAEL receptor show non-motor behavioral phenotypes: age and gender effect. *Genes Brain Behav.* **12,** 465–477 (2013).

Marazziti D, Di Pietro C, Golini E, Mandillo S, La Sala G, Matteoni R, Tocchini-Valentini GP. Precocious cerebellum development and improved motor functions in mice lacking the astrocyte cilium-, patched 1-associated GPR37l1 receptor. Proc Natl Acad Sci U S A 110:16486-91 (2013).

Marcaggi, P., Billups, D. & Attwell, D. The Role of Glial Glutamate Transporters in Maintaining the Independent Operation of Juvenile Mouse Cerebellar Parallel Fibre Synapses. *J Physiol* **552,** 89–107 (2003).

Marchetti, L., Klein, M., Schlett, K., Pfizenmaier, K. & Eisel, U. L. M. Tumor necrosis factor (TNF)-mediated neuroprotection against glutamate-induced excitotoxicity is enhanced by N-methyl-D-aspartate receptor activation. Essential role of a TNF receptor 2-mediated phosphatidylinositol 3-kinase-dependent NF-kappa B pathway. *J. Biol. Chem.* **279,** 32869–32881 (2004).

Marien, M. R., Colpaert, F. C. & Rosenquist, A. C. Noradrenergic mechanisms in neurodegenerative diseases: a theory. *Brain Res. Brain Res. Rev.* **45,** 38–78 (2004).

Mashimo, M. et al. Inositol 1,4,5-trisphosphate signaling maintains the activity of glutamate uptake in Bergmann glia. Eur. J. Neurosci. **32**, 1668–1677 (2010).

Matos, M. *et al.* Adenosine A2A receptors modulate glutamate uptake in cultured astrocytes and gliosomes. *Glia* **60,** 702–716 (2012).

McCoy, K., Gyoneva, S., Vellano, C.P., Smrcka, A.V., Traynelis, F., Hepler, J.R. Protease-Activated Receptor 1 (PAR1) coupling to $G_{q/11}$ but not to $G_{i/o}$ or $G_{12/13}$is mediated by discrete amino acids within the receptor second intracellular loop. *Cell Signal*. **24**(6): 1351–1360 (2012).

McLean, J. & Waterhouse, B. D. Noradrenergic modulation of cat area 17 neuronal responses to moving visual stimuli. *Brain Res.* **667,** 83–97 (1994).

Meme, W., Vandecasteele, M., Giaume, C. & Venance, L. Electrical coupling between hippocampal astrocytes in rat brain slices. *Neurosci. Res.* **63,** 236–243 (2009).

Meunier, C. N. J. *et al.* D-Serine and Glycine Differentially Control Neurotransmission during Visual Cortex Critical Period. *PLoS ONE* **11,** e0151233 (2016).

Meyer RC, Giddens MM, Schaefer SA, Hall RA. GPR37 and GPR37L1 are receptors for the neuroprotective and glioprotective factors prosaptide and prosaposin. Proc Natl Acad Sci U S A 110:9529-34 (2013).

Meyer, R. C., Giddens, M. M., Coleman, B. M. & Hall, R. A. The protective role of prosaposin and its receptors in the nervous system. *Brain Res.* **1585,** 1–12 (2014).

Min KD, Asakura M, Liao Y, Nakamaru K, Okazaki H, Takahashi T, Fujimoto K, Ito S, Takahashi A, Asanuma H and others. Identification of genes related to heart failure using global gene expression profiling of human failing myocardium. Biochem Biophys Res Commun **393**:55-60 (2010).

Misasi, R. *et al.* Prosaposin: a new player in cell death prevention of U937 monocytic cells. prosaposin prevents cell apoptosis by activation of extracellular signal-regulated kinases (ERKs) and sphingosine kinase. *Exp. Cell Res.* **298,** 38–47 (2004).

Moreau, K. et al. PICALM modulates autophagy activity and tau accumulation. Nat. Commun. **5**, 4998 (2014).

Morishita, M. *et al.* Temporal changes in prosaposin expression in the rat dentate gyrus after birth. *PLoS ONE* **9,** e95883 (2014).

Morita F, Wen TC, Tanaka J, Hata R, Desaki J, Sato K, Nakata K, Ma YJ, Sakanaka M. Protective effect of a prosaposin-derived, 18-mer peptide on slowly progressive neuronal degeneration after brief ischaemia. J Cereb Blood Flow Metab **21**:1295-302 (2001).

Mothet, J.-P. *et al*. Glutamate receptor activation triggers a calcium-dependent and SNARE protein-dependent release of the gliotransmitter D-serine. *Proc. Natl. Acad. Sci. USA* **102**,5606–5611 (2005)

Mulligan, S.J. & MacVicar, B.A. Calcium transients in astrocyte endfeet cause cerebrovascular constrictions. Nature **431**, 195–199 (2004).

Murphy-Royal, C. et al. Surface diffusion of astrocytic glutamate transporters shapes synaptic transmission. Nat. Neurosci. **18**, 219–226 (2015).

Nabeka, H. *et al.* A prosaposin-derived Peptide alleviates kainic Acid-induced brain injury. *PLoS ONE* **10,** e0126856 (2015).

Nabeka, H. *et al.* Prosaposin overexpression following kainic acid-induced neurotoxicity. *PLoS ONE* **9,** e110534 (2014).

Nalepa, I., Kreiner, G., Bielawski, A., Rafa-Zabłocka, K. & Roman, A. α1-Adrenergic receptor subtypes in the central nervous system: insights from genetically engineered mouse models. *Pharmacol Rep* **65,** 1489–1497 (2013).

Nedergaard, M. Direct signaling from astrocytes to neurons in cultures of mammalian brain cells. Science **263**, 1768–1771 (1994).

Nett, W.J., Oloff, S.H. & McCarthy, K.D. Hippocampal astrocytes in situ exhibit calcium oscillations that occur independent of neuronal activity. J. Neurophysiol. **87**, 528–537 (2002).

Newman, E.A. Glial cell inhibition of neurons by release of ATP. J. Neurosci. **23**, 1659–1666 (2003).

Newman, E.A. Calcium increases in retinal glial cells evoked by light-induced neuronal activity. *J. Neurosci.* **25**, 5502–5510 (2005)

Newman, E.A. Propagation of intercellular calcium waves in retinal astrocytes and Müller cells. *J. Neurosci.* **21**, 2215–2223 (2001)

Nico, B. & Ribatti, D. Morphofunctional aspects of the blood-brain barrier. *Curr. Drug Metab.* **13,** 50–60 (2012).

Nimmerjahn, A. & Helmchen, F. In vivo labelling of cortical astrocytes with sulforhodamine 101 (SR101). *Cold Spring Harb Protoc* **2012,** 326–334 (2012).

Nimmerjahn, A., Kirchhoff, F., Kerr, J.N. & Helmchen, F. Sulforhodamine 101 as a specific marker of astroglia in the neocortex in vivo. Nat. Methods 1, 31–37 (2004).
Nizar, K. et al. In vivo stimulus-induced vasodilation occurs without IP3 receptor activation and may precede astrocytic calcium increase. J. Neurosci. 33, 8411–8422 (2013).

Oberheim, N.A. et al. Uniquely hominid features of adult human astrocytes. J. Neurosci. 29, 3276–3287 (2009).

Oh, S.J., Han, K.S., Park, H., Woo, D.H., Kim, H.Y., Traynelis, S.F., Lee, C.J. Protease activated receptor 1-induced glutamate release in cultured astrocytes is mediated by Bestrophin-1 channel but not by vesicular exocytosis. *Mol Brain*. **5**:35 (2012)

Olney, J. W. & Sharpe, L. G. Brain lesions in an infant rhesus monkey treated with monsodium glutamate. *Science* **166,** 386–388 (1969).

Orkand RK, Nicholls JG, Kuffler SW. Effect of nerve impulses on the membrane potential of glial cells in the central nervous system of amphibia. *J Neurophysiol.* **29**:788–806 (1966).

Orkand RK. Glial-interstitial fluid exchange. *Ann NY Acad Sci.* **481**:269–272 (1986).

Ozkan, E. D. & Ueda, T. Glutamate transport and storage in synaptic vesicles. *Jpn. J. Pharmacol.* **77,** 1–10 (1998).

Panatier, A. *et al.* Astrocytes are endogenous regulators of basal transmission at central synapses. *Cell* **146,** 785–798 (2011).

Pankratov, Y. & Lalo, U. Role for astroglial α1-adrenoreceptors in gliotransmission and control of synaptic plasticity in the neocortex. Front. Cell. Neurosci. 9, 230 (2015).

Papouin, T. *et al.* Synaptic and extrasynaptic NMDA receptors are gated by different endogenous coagonists. *Cell* **150,** 633–646 (2012).

Park, H. *et al.* High glutamate permeability and distal localization of Best1 channel in CA1 hippocampal astrocyte. *Mol. Brain* **6**, 54 (2013)

Parpura, V. et al. Glutamate-mediated astrocyte-neuron signalling. Nature **369**, 744–747 (1994).

Parri, H.R., Gould, T.M. & Crunelli, V. Spontaneous astrocytic Ca2+ oscillations in situ drive NMDAR-mediated neuronal excitation. Nat. Neurosci. 4, 803–812 (2001).

Parsey, R.V., Matteson, D.R. Ascorbic acid modulation of calcium channels in pancreatic beta cells. *J Gen Physiol*. **102**(3):503-23 (1993)

Pascual, O. et al. Astrocytic purinergic signaling coordinates synaptic networks. Science 310, 113–116 (2005).
Pasti, L., Volterra, A., Pozzan, T. & Carmignoto, G. Intracellular calcium oscillations in astrocytes: a highly plastic, bidirectional form of communication between neurons and astrocytes in situ. J. Neurosci. **17**, 7817–7830 (1997).

Patrushev, I., Gavrilov, N., Turlapov, V. & Semyanov, A. Subcellular location of astrocytic calcium stores favors extrasynaptic neuron-astrocyte communication. Cell Calcium **54**, 343–349 (2013).

Paukert, M. *et al*. Norepinephrine controls astroglial responsiveness to local circuit activity.*Neuron* **82**, 1263–1270 (2014)

Pellerin L, Magistretti PJ. Glutamate uptake into astrocytes stimulates aerobic glycolysis: a mechanism coupling neuronal activity to glucose utilization. *Proc Natl Acad Sci USA.* **91**:10625–10629 (1994).

Perea, G. & Araque, A. Astrocytes potentiate transmitter release at single hippocampal synapses. Science **317**, 1083–1086 (2007).

Perea, G. & Araque, A. Properties of synaptically evoked astrocyte calcium signal reveal synaptic information processing by astrocytes. J. Neurosci. **25**, 2192–2203 (2005).

Perea,G., Yang, A., Boyden, E.S., Sur, M. Optogenetic astrocyte activation modulates response selectivity of visual cortex neurons *in vivo. Nat Commun.* (2013).

Petravicz, J., Boyt, K.M. & McCarthy, K.D. Astrocyte IP3R2-dependent Ca2+ signaling is not a major modulator of neuronal pathways governing behavior. Front. Behav. Neurosci. **8**, 384 (2014).

Petravicz, J., Fiacco, T.A. & McCarthy, K.D. Loss of IP3 receptor-dependent Ca2+ increases in hippocampal astrocytes does not affect baseline CA1 pyramidal neuron synaptic activity. J. Neurosci. 28, 4967–4973 (2008).

Piletz, J. E., Wang, G. & Zhu, H. Cell signaling by imidazoline-1 receptor candidate, IRAS, and the nischarin homologue. *Ann. N. Y. Acad. Sci.* **1009,** 392–399 (2003).

Pinal, C. S. & Tobin, A. J. Uniqueness and redundancy in GABA production. *Perspect Dev Neurobiol* **5,** 109–118 (1998).

Pines, G. & Kanner, B. I. Counterflow of L-glutamate in plasma membrane vesicles and reconstituted preparations from rat brain. *Biochemistry* **29,** 11209–11214 (1990).

Playgin, O., Lalo, U., Verkhratsky, A., Pankratov, Y. Ionotropic NMDA and P2X1/5 receptors mediate synaptically induced Ca2+ signalling in cortical astrocytes. *Cell Calcium*. **48**(4):225-31 (2010)

Porter, J.T. & McCarthy, K.D. Hippocampal astrocytes in situ respond to glutamate released from synaptic terminals. *J. Neurosci.* **16**, 5073–5081 (1996)

Prebil, M., Jensen, J., Zorec, R. & Kreft, M. Astrocytes and energy metabolism. *Arch. Physiol. Biochem.* **117,** 64–69 (2011).

Pryazhnikov, E. & Khiroug, L. Sub-micromolar increase in [Ca2+]i triggers delayed exocytosis of ATP in cultured astrocytes. Glia **56**, 38–49 (2008).

Roberts, E. & Frankel, S. gamma-Aminobutyric acid in brain: its formation from glutamic acid. *J. Biol. Chem.* **187,** 55–63 (1950).

Roberts, P. J. & Watkins, J. C. Structural requirements for the inhibition for L-glutamate uptake by glia and nerve endings. *Brain Res.* **85,** 120–125 (1975).

Robinson, M. B. & Jackson, J. G. Astroglial glutamate transporters coordinate excitatory signaling and brain energetics. *Neurochem. Int.* (2016).

Rosenberg, D. *et al.* Neuronal D-serine and glycine release via the Asc-1 transporter regulates NMDA receptor-dependent synaptic activity. *J. Neurosci.* **33,** 3533–3544 (2013).

Rossi, D. J., Oshima, T. & Attwell, D. Glutamate release in severe brain ischaemia is mainly by reversed uptake. *Nature* **403,** 316–321 (2000).

Rothstein, J. D. *et al.* Knockout of glutamate transporters reveals a major role for astroglial transport in excitotoxicity and clearance of glutamate. *Neuron* **16,** 675–686 (1996).

Sahlender, D.A., Savtchouk, I. & Volterra, A. What do we know about gliotransmitter release from astrocytes? Philos. Trans. R. Soc. Lond. B Biol. Sci. 369, 20130592 (2014).

Salánki, J. Physiology of Non-Excitable Cells: *Proceedings of the 28th International Congress of Physiological Sciences, Budapest, 1980*. (Elsevier, 2013).

Salgado, H., Köhr, G. & Treviño, M. Noradrenergic 'tone' determines dichotomous control of cortical spike-timing-dependent plasticity. *Sci Rep* **2,** 417 (2012).

Salgado, H., Trevino, M., Atzori, M. Layer- and area-specific actions of norepinephrine on cortical synaptic transmission. *Brain Res*. (2016).

Salt, T. E. Modulation of NMDA receptor-mediated responses by glycine and D-serine in the rat thalamus in vivo. *Brain Res.* **481**, 403–406 (1989).

Sano A, Matsuda S, Wen TC, Kotani Y, Kondoh K, Ueno S, Kakimoto Y, Yoshimura H, Sakanaka M. Protection by prosaposin against ischaemia-induced learning disability and neuronal loss. Biochem Biophys Res Commun **204**:994-1000 (1994).

Sarantis, M. & Attwell, D. Glutamate uptake in mammalian retinal glia is voltage- and potassium-dependent. *Brain Res.* **516,** 322–325 (1990).

Sarantis, M., Everett, K. & Attwell, D. A presynaptic action of glutamate at the cone output synapse. *Nature* **332,** 451–453 (1988).

Schnell, C., Negm, M., Driehaus, J., Scheller, A. & Hülsmann, S. Norepinephrine-induced calcium signaling in astrocytes in the respiratory network of the ventrolateral medulla. *Respir Physiol Neurobiol* **226,** 18–23 (2016).

Schousboe A. Transport and metabolism of glutamate and GABA in neurons and glial cells. *Int Rev Neurobiol* **22**, 1-45 (1981).

Schummers, J., Yu, H. & Sur, M. Tuned responses of astrocytes and their influence on hemodynamic signals in the visual cortex. Science 320, 1638–1643 (2008).

Schurr A, West CA, et al. Lactate-supported synaptic function in the rat hippocampal slice preparation. *Science.* **240**:1326–1328 (1988).

Serrano, A., Haddjeri, N., Lacaille, J.-C. & Robitaille, R. GABAergic network activation of glial cells underlies hippocampal heterosynaptic depression. J. Neurosci. 26, 5370–5382 (2006).

Shashidharan, P. *et al.* Immunohistochemical localization of the neuron-specific glutamate transporter EAAC1 (EAAT3) in rat brain and spinal cord revealed by a novel monoclonal antibody. *Brain Res.* **773,** 139–148 (1997).

Shelton, M.K. & McCarthy, K.D. Hippocampal astrocytes exhibit Ca2+-elevating muscarinic cholinergic and histaminergic receptors in situ. J. Neurochem. **74**, 555–563 (2000).

Sher, P. K. & Hu, S. X. Increased glutamate uptake and glutamine synthetase activity in neuronal cell cultures surviving chronic hypoxia. *Glia* **3,** 350–357 (1990).

Shigetomi, E., Bowser, D.N., Sofroniew, M.V. & Khakh, B.S. Two forms of astrocyte calcium excitability have distinct effects on NMDA receptor-mediated slow inward currents in pyramidal neurons. J. Neurosci. **28**, 6659–6663 (2008).

Shigetomi, E., Kracun, S., Sofroniew, M.V. & Khakh, B.S. A genetically targeted optical sensor to monitor calcium signals in astrocyte processes. Nat. Neurosci. **13**, 759–766 (2010).

Shigetomi, E., Patel, S., Kakh, B.S. Probing the Complexities of Astrocyte Calcium Signaling. *Trends Cell Biol*. **26**(4):300-12 (2016).

Shigetomi, E., Tong, X., Kwan, K.Y., Corey, D.P. & Khakh, B.S. TRPA1 channels regulate astrocyte resting calcium and inhibitory synapse efficacy through GAT-3. *Nat. Neurosci.* **15**,70–80 (2012)

Shimamoto, K. *et al.* DL-threo-beta-benzyloxyaspartate, a potent blocker of excitatory amino acid transporters. *Mol. Pharmacol.* **53,** 195–201 (1998).

Shleper, M., Kartvelishvily, E. & Wolosker, H. D-serine is the dominant endogenous coagonist for NMDA receptor neurotoxicity in organotypic hippocampal slices. *J. Neurosci.* **25,** 9413–9417 (2005).

Sibille, J., Zapata, J., Teillon, J. & Rouach, N. Astroglial calcium signaling displays short-term plasticity and adjusts synaptic efficacy. Front. Cell. Neurosci. 9, 189 (2015).

Sluse, F. E. Mitochondrial metabolite carrier family, topology, structure and functional properties: an overview. *Acta Biochim. Pol.* **43,** 349–360 (1996).

Smith NJ. Drug Discovery Opportunities at the Endothelin B Receptor-Related Orphan G Protein-Coupled Receptors, GPR37 and GPR37L1. Front Pharmacol **6**:275 (2015).

Srinivasan, R. *et al.* Ca(2+) signaling in astrocytes from Ip3r2(-/-) mice in brain slices and during startle responses in vivo. *Nat. Neurosci.* **18,** 708–717 (2015).

Stanimirovic, D. B., Ball, R. & Durkin, J. P. Stimulation of glutamate uptake and Na,K-ATPase activity in rat astrocytes exposed to ischaemia-like insults. *Glia* **19,** 123–134 (1997).

Stellwagen, D. & Malenka, R. C. Synaptic scaling mediated by glial TNF-α. *Nature* **440,** 1054–1059 (2006).

Subbarao, K. V. & Hertz, L. Noradrenaline induced stimulation of oxidative metabolism in astrocytes but not in neurons in primary cultures. *Brain Res.* **527,** 346–349 (1990).

Sun, W. et al. Glutamate-dependent neuroglial calcium signaling differs between young and adult brain. Science **339**, 197–200 (2013).

Sun, Z., Chang, C.-H. & Ernsberger, P. Identification of IRAS/Nischarin as an I1-imidazoline receptor in PC12 rat pheochromocytoma cells. *J. Neurochem.* **101,** 99–108 (2007).

Sutherland, M. L., Delaney, T. A. & Noebels, J. L. Molecular characterization of a high-affinity mouse glutamate transporter. *Gene* **162,** 271–274 (1995).

Sutin, J. & Shao, Y. Resting and reactive astrocytes express adrenergic receptors in the adult rat brain. *Brain Res. Bull.* **29,** 277–284 (1992).

Szatkowski, M., Barbour, B. & Attwell, D. The potassium-dependence of excitatory amino acid transport: resolution of a paradox. *Brain Res.* **555,** 343–345 (1991).

Szatkowski, M., Barbour, B. & Attwell, D. Non-vesicular release of glutamate from glial cells by reversed electrogenic glutamate uptake. *Nature* **348,** 443–446 (1990).

Takano, T. et al. Astrocyte-mediated control of cerebral blood flow. Nat. Neurosci. **9**, 260–267 (2006).

Takano, T. et al. Receptor-mediated glutamate release from volume sensitive channels in astrocytes. Proc. Natl. Acad. Sci. USA **102**, 16466–16471 (2005).

Takata, N. et al. Astrocyte calcium signaling transforms cholinergic modulation to cortical plasticity in vivo. J. Neurosci. **31**, 18155–18165 (2011).

Tanaka, J., Ichikawa, R., Watanabe, M., Tanaka, K. & Inoue, Y. Extra-junctional localization of glutamate transporter EAAT4 at excitatory Purkinje cell synapses. *Neuroreport* **8,** 2461–2464 (1997).

Tanaka, K. *et al.* Epilepsy and exacerbation of brain injury in mice lacking the glutamate transporter GLT-1. *Science* **276,** 1699–1702 (1997).

Tang, F. *et al.* Lactate-mediated glia-neuronal signalling in the mammalian brain. *Nat Commun* **5,** 3284 (2014).

Teschemacher, A. G., Gourine, A. V. & Kasparov, S. A Role for Astrocytes in Sensing the Brain Microenvironment and Neuro-Metabolic Integration. *Neurochem. Res.* **40,** 2386–2393 (2015).

Teschemacher, A.G., Spyer, K.M., Deisseroth, K., Kasparov, S. Astrocytes Control Breathing Through pH-Dependent Release of ATP. *Science*. **329**(5991): 571-575 (2010).

Thase, M. E. & Denko, T. Pharmacotherapy of mood disorders. *Annu Rev Clin Psychol* **4,** 53–91 (2008).

Thrane, A.S. et al. General anesthesia selectively disrupts astrocyte calcium signaling in the awake mouse cortex. Proc. Natl. Acad. Sci. USA **109**, 18974–18979 (2012).

Todorovic, S. M. & Jevtovic-Todorovic, V. T-type voltage-gated calcium channels as targets for the development of novel pain therapies. *Br J Pharmacol* **163,** 484–495 (2011).

Torp, R. *et al.* Differential expression of two glial glutamate transporters in the rat brain: an in situ hybridization study. *Eur. J. Neurosci.* **6,** 936–942 (1994).

Trombley, P.Q., Westbrook, G.L. Voltage-gated currents in identified rat olfactory receptor neurons. *J Neurosci*. **11**(2): 435-444 (1991).

Underhill, S. M., Wheeler, D. S. & Amara, S. G. Differential Regulation of Two Isoforms of the Glial Glutamate Transporter EAAT2 by DLG1 and CaMKII. *J. Neurosci.* **35,** 5260–5270 (2015).

Utsunomiya-Tate, N., Endou, H. & Kanai, Y. Cloning and functional characterization of a system ASC-like Na+-dependent neutral amino acid transporter. *J. Biol. Chem.* **271,** 14883–14890 (1996).

Valdenaire O, Giller T, Breu V, Ardati A, Schweizer A, Richards JG. A new family of orphan G protein-coupled receptors predominantly expressed in the brain. FEBS Lett **424**:193-6 (1998).

Volterra, A. *et al.* The competitive transport inhibitor L-trans-pyrrolidine-2, 4-dicarboxylate triggers excitotoxicity in rat cortical neuron-astrocyte co-cultures via glutamate release rather than uptake inhibition. *Eur. J. Neurosci.* **8,** 2019–2028 (1996).

Vivar, R. *et al.* TGF-β1 prevents simulated ischaemia/reperfusion-induced cardiac fibroblast apoptosis by activation of both canonical and non-canonical signaling pathways. *Biochimica et Biophysica Acta (BBA) - Molecular Basis of Disease* **1832,** 754–762 (2013).

Vornov, J. J. & Coyle, J. T. Enhancement of NMDA receptor-mediated neurotoxicity in the hippocampal slice by depolarization and ischemia. *Brain Res.* **555,** 99–106 (1991).

Vyklický, L., Benveniste, M. & Mayer, M. L. Modulation of N-methyl-D-aspartic acid receptor desensitization by glycine in mouse cultured hippocampal neurones. *J. Physiol. (Lond.)* **428,** 313–331 (1990).

Wadiche, J. I., Arriza, J. L., Amara, S. G. & Kavanaugh, M. P. Kinetics of a human glutamate transporter. *Neuron* **14,** 1019–1027 (1995).

Wang, F. et al. Photolysis of caged Ca2+ but not receptor-mediated Ca2+ signaling triggers astrocytic glutamate release. J. Neurosci. **33**, 17404–17412 (2013).

Watase, K. *et al.* Motor discoordination and increased susceptibility to cerebellar injury in GLAST mutant mice. *Eur. J. Neurosci.* **10,** 976–988 (1998).

Watkins, J. C. l-glutamate as a central neurotransmitter: looking back. *Biochem. Soc. Trans.* **28,** 297–309 (2000).

Wejksza, K. *et al.* Ammonia at pathophysiologically relevant concentrations activates kynurenic acid synthesis in cultured astrocytes and neurons. *Neurotoxicology* **27,** 619–622 (2006).

Westergaard N, Sonnewald U, Schousboe A. Metabolic trafficking between neurons and astrocytes: the glutamate/glutamine cycle revisited. *Dev Neurosci.* **17**:203–211 (1995).

Wheeler, D. *et al.* Tumor necrosis factor-alpha-induced neutral sphingomyelinase-2 modulates synaptic plasticity by controlling the membrane insertion of NMDA receptors. *J. Neurochem.* **109,** 1237–1249 (2009).

Williams, M. A., Li, C., Kash, T. L., Matthews, R. T. & Winder, D. G. Excitatory drive onto dopaminergic neurons in the rostral linear nucleus is enhanced by norepinephrine in an α1 adrenergic receptor-dependent manner. *Neuropharmacology* **86,** 116–124 (2014).

Woo, D.H. et al. TREK-1 and Best1 channels mediate fast and slow glutamate release in astrocytes upon GPCR activation. Cell 151, 25–40 (2012).

Wu, X. *et al.* The expression pattern of Nischarin after lipopolysaccharides (LPS)-induced neuroinflammation in rats brain cortex. *Inflamm. Res.* **62,** 929–940 (2013).Ding, Y. *et al.* Nischarin is differentially expressed in rat brain and regulates neuronal migration. *PLoS ONE* **8,** e54563 (2013).

Wu, X., Kihara, T., Akaike, A., Niidome, T. & Sugimoto, H. PI3K/Akt/mTOR signaling regulates glutamate transporter 1 in astrocytes. *Biochem. Biophys. Res. Commun.* **393,** 514–518 (2010).

Wyss, M. T., Jolivet, R., Buck, A., Magistretti, P. J. & Weber, B. In vivo evidence for lactate as a neuronal energy source. *J. Neurosci.* **31,** 7477–7485 (2011).

Xu, G., Wang, W., Kimelberg, H. K. & Zhou, M. Electrical coupling of astrocytes in rat hippocampal slices under physiological and simulated ischemic conditions. *Glia* **58,** 481–493 (2010).

Yang HJ, Vainshtein A, Maik-Rachline G, Peles E. G protein-coupled receptor 37 is a negative regulator of oligodendrocyte differentiation and myelination. Nat Commun **7**:10884 (2016).

Yang Y, Nishimura I, Imai Y, Takahashi R, Lu B. Parkin suppresses dopaminergic neuron-selective neurotoxicity induced by Pael-R in Drosophila. Neuron **37**:911-24 (2003).

Yang, Y. *et al*. Contribution of astrocytes to hippocampal long-term potentiation through release of D-serine. *Proc. Natl. Acad. Sci. USA* **100**, 15194–15199 (2003)

Yernool, D., Boudker, O., Jin, Y. & Gouaux, E. Structure of a glutamate transporter homologue from Pyrococcus horikoshii. *Nature* **431,** 811–818 (2004).

Yokota N, Uchijima M, Nishizawa S, Namba H, Koide Y. Identification of differentially expressed genes in rat hippocampus after transient global cerebral ischaemia using subtractive cDNA cloning based on polymerase chain reaction. Stroke **32**:168-74 (2001).

Yoneshige, A., Suzuki, K., Kojima, N. & Matsuda, J. Regional expression of prosaposin in the wild-type and saposin D-deficient mouse brain detected by an anti-mouse prosaposin-specific antibody. *Proc Jpn Acad Ser B Phys Biol Sci* **85,** 422–434 (2009).

Yuan, L. & Morales, C. R. Prosaposin sorting is mediated by oligomerization. *Exp. Cell Res.* **317,** 2456–2467 (2011).

Yudkoff M, Zaleska MM, Nissim I, et al. Neuronal glutamine utilization: pathways of nitrogen transfer studied with [15N]glutamine.*J Neurochem.* **53**:632–640 (1989).

Yuen, E. Y. *et al.* Synergistic Regulation of Glutamatergic Transmission by Serotonin and Norepinephrine Reuptake Inhibitors in Prefrontal Cortical Neurons. *J Biol Chem* **289,** 25177–25185 (2014).

Zerangue, N. & Kavanaugh, M. P. Flux coupling in a neuronal glutamate transporter. *Nature* **383,** 634–637 (1996).

Zhang, J. & Abdel-Rahman, A. A. Nischarin as a functional imidazoline (I1) receptor. *FEBS Lett.* **580,** 3070–3074 (2006).

Zhang, J.M. et al. ATP released by astrocytes mediates glutamatergic activitydependent heterosynaptic suppression. Neuron **40**, 971–982 (2003).

Zhang, Y. et al. An RNA-sequencing transcriptome and splicing database of glia, neurons, and vascular cells of the cerebral cortex. J. Neurosci. **34**, 11929–11947 (2014).

Zhang, X.-Y. *et al.* Glycine induces bidirectional modifications in N-methyl-D-aspartate receptor-mediated synaptic responses in hippocampal CA1 neurons. *J. Biol. Chem.* **289,** 31200–31211 (2014).

Zhang, Y. *et al.* Purification and Characterization of Progenitor and Mature Human Astrocytes Reveals Transcriptional and Functional Differences with Mouse. *Neuron* **89,** 37–53 (2016).

Zhou, Y., Wang, X., Tzingounis, A. V., Danbolt, N. C. & Larsson, H. P. EAAT2 (GLT-1; slc1a2) glutamate transporters reconstituted in liposomes argues against heteroexchange being substantially faster than net uptake. *J. Neurosci.* **34,** 13472–13485 (2014).

Zhu, X. & Birnbaumer, L. G protein subunits and the stimulation of phospholipase C by Gs-and Gi-coupled receptors: Lack of receptor selectivity of Galpha(16) and evidence for a synergic interaction between Gbeta gamma and the alpha subunit of a receptor activated G protein. *Proc. Natl. Acad. Sci. U.S.A.* **93,** 2827–2831 (1996).

Zonta, M. et al. Neuron-to-astrocyte signaling is central to the dynamic control of brain microcirculation. Nat. Neurosci. 6, 43–50 (2003).